Glucan Metabolism in *Mycobacterium* and *Streptomyces*

Farzana Yasmin Miah

Thesis submitted to the University of East Anglia
for the degree of Doctor of Philosophy

Department of Biological Chemistry
John Innes Centre
Norwich

June 2014

Date

I certify that the work contained in the thesis submitted by me for the degree of PhD is my own original work, except where due reference is made to the author and has not been submitted by me for a degree at this or any other university.

Signed

Farzana Yasmin Miah

This PhD was sponsored by the Biotechnology and Biological Sciences Research Council.

Acknowledgements

First and foremost I would like to thank my supervisor Stephen Bornemann, who has taught me much about the scientific method during the past four years. I'm very grateful for your constant guidance as well as the fact you have always made time to meticulously look through my written work and offer useful feedback.

I would like to thank Mark Buttner, Keith Chater and Alison Smith for being members of my supervisory committee and for providing useful advice throughout. I would also like to thank collaborators Abdul Rashid, Hendrik Koliwer-Brandl, Rainer Kalscheuer, Martin Rejzek, Rob Field and Dave Lawson for their assistance with certain aspects of this thesis. My thanks also goes to Kim Findlay, Elaine Barclay and Grant Calder at the JIC bioimaging facility for either helping me with or conducting parts of the microscopy associated with this work. I'd like to thank Gerhard Saalbach, Alan Jones and Paul Brett for helping with mass spectrometry. Thank you also to all of the JIC media kitchen staff for saving me countless hours!

I would like to express my gratitude to Karl Syson, Maureen Bibb and Clare Stevenson. I wouldn't have been able to do any of the work in this thesis without having had your help and advice throughout. Thank you for your patience with me in the lab and for always being around to troubleshoot or to answer the stupid questions I often have, I am so grateful to have been taught by you all!

I have been extremely lucky to have had some fantastic people around me for good times both in the lab as well as out. I'd especially like to thank Weslee Glenn, Taneli Mäkinen and Daniel Tromans for their good humour and for being around for a good chinwag. I find your outlooks on life truly inspiring. I'd also like to thank my wonderful office mates Jo Harrison, Inga Kruse, Kat Ignasiak and John Steele for keeping me sane during the writing-up period, as well as Richard Payne for keeping me caffeinated.

Finally, I'd like to thank my family for supporting me regardless of whatever I pursue. Thank you to Mum, Dad and to my siblings, Yasmin, Mamun, Humiun and Habibur for always being there for me.

Abstract

α-Glucans are typically used for carbon storage in bacteria, however, they are also a major component of the mycobacterial capsule. In this context, glucans have been implicated in the evasion of recognition by macrophages. A novel α-glucan synthesis pathway, called the GlgE pathway, is a potential source of the capsular glucan in mycobacteria. The pathway converts the disaccharide trehalose into α-glucan by the action of four enzymes: TreS, Pep2, GlgE and GlgB. Functional redundancy between other glucan synthesis pathways has made characterising the GlgE pathway difficult in mycobacteria. The genes encoding the enzymes of the pathway are found in 14% of sequenced bacterial genomes, suggesting the pathway is relatively wide-spread amongst bacteria. α-Glucans have also been isolated in a number of streptomycetes, which are distant relatives of mycobacteria. In this study *Streptomyces venezuelae* was used to show for the first time that the GlgE pathway is responsible for glucan synthesis *in vivo*, as was predicted by the annotations in the genome. A *ΔglgE* mutant was devoid of α-glucan and instead accumulated α-maltose 1-phosphate, which was associated with a developmental phenotype. The spores produced by the *ΔglgE* strain had normal levels of trehalose and had compromised resistance to abiotic stresses, with the exception of desiccation resistance, which was comparable to wild-type. In this study, another mutant from *S. venezuelae ΔotsA* was also investigated, which was hypothesised to be feeding the substrate trehalose into the GlgE pathway from glucose. However, under normal laboratory growth conditions, no phenotype was observed and the strain was able to accrue α-glucan. Surprisingly, a developmental phenotype arose when *ΔotsA* was grown on a galactose carbon source. This developmental phenotype was associated with the accumulation of GDP-glucose. Recombinant *S. venezuelae* OtsA was produced heterologously and the substrate preference for this enzyme was found to be GDP-glucose, as predicted by the phenotypic study of the *ΔotsA* strain. The crystal structure of *S. venezuelae* OtsA was solved to a resolution of 1.95 Å and the unusual substrate specificity was rationalised by comparison with a solved *Escherichia coli* OtsA structure, which has substrate specificity for UDP-glucose, and a pseudo-glycosyltransferase VldE, which uses GTP during catalysis. Four key resides were identified as being important for the substrate specificity of *S. venezuelae* OtsA: Ser^{345}, Phe^{342}, Glu^{341} and Asp^{340}. Finally, TreS was found to be stereospecific for the α anomer of maltose, the appropriate anomer for Pep2, which confirms the prediction of an α-retaining mechanism.

Abbreviations

µg	Microgram
^{19}F	Fluorine
^{1}H	Proton
Å	Angstrom
ADP	Adenosine triphosphate
AIM	Auto induction media
apr	Apramycin
ATP	Adenosine triphosphate
bp	Base pair
BSA	Bovine serum albumin
BTP	Bis tris propane
carb	Carbenicilin
CFU	Colony forming unit
cml	Chloramphenicol
dH_2O	Distilled water
DLS	Dynamic light scattering
DMSO	Dimethyl sulfoxide
DN	Difco nutrient agar
DNA	Deoxyribonucleic acid
DP	Degree of polymerisation
EDTA	Ethylenediaminetetraacetic acid
FAME	Fatty acid methyl esters
GCMS	Gas chromatography mass spectrometry
gDNA	Genomic deoxyribonucleic acid
GDP	Guanine diphosphate
HEPES	4-(2-Hydroxyethyl)-1-piperazineethanesulfonic acid
hyg	Hygromycin
IPTG	Isopropyl β-D-1-thiogalactopyranoside
kan	Kanamycin
kbp	Kilo base pair
kDa	Kilo Dalton
LB	Lysogeny broth
Lx	Lennox broth
MALDI-TOF MS	Matrix-assisted laser desorption/ionization-time-of-flight mass spectrometry

MES	2-(*N*-morpholino)ethanesulfonic acid
M	Molar
mg	Milligram
MGLP	Methylglucose lipopolysaccharide
mL	Millilitre
MM-+	Minimal media
MOPS	3-(N-morpholino)propanesulphonic acid
MOS	Maltooligosaccharide
mRNA	Messenger ribonucleic acid
Mw	Molecular weight
MYGal	Malt extract-yeast extract-galactose
MYM	Malt extract-yeast extract-maltose
nal	Nalidixic acid
NDP	Nucleoside diphosphate
NMR	Nuclear magnetic resonance
OD	Optical density
PAGE	Polyacrylamide gel electrophoresis
PatAg	Periodic acid-thiocarbohydrazide-silver proteinate
PCR	Polymerase chain reaction
Pd	Polydispersity
PDB	Protein data bank
PEG	Poly ethylene glycol
PI	Propidium iodide
Pi	Phosphate
PIPES	Piperazine-N,N'-bis(2-ethanesulfonic acid)
PNK	T_4-polynucleotide kinase
PPi	Pyrophosphate
RMSD	Root mean square deviation
SAP	Shrimp alkaline phosphatase
SDS	Sodium dodecyl sulphate
SE	Standard error of the mean
SEC	Size exclusion chromatography
SEM	Scanning electron microscopy
SFM	Soya flour + Mannitol
SOB	Super optimal broth

SOC	Super optimal broth with catabolite repression
TE	Tris: EDTA buffer
TEM	Transmission electron microscopy
TLC	Thin layer chromatography
TMSP-d_4	Deuterated trimethylsilyl propanoic acid
Tris	Tris(hydroxymethyl)aminomethane
U	Unit
UDP	Uridine diphosphate
UV	Ultraviolet
v/v	Volume/volume
V_E	Elution volume
w/v	Weight/volume
WGA	Wheat germ agglutinin
WT	Wild-type
λ	Wavelength

List of Figures

Chapter 1: Introduction

Chapter 3: TreS Enzymology

Chapter 4: Pep2 Characterisation

Chapter 5: The GlgE Pathway Produces Glycogen in *Streptomyces venezuelae*

Chapter 7: Discussion and Future Work

List of Tables

Chapter 1: Introduction

This thesis describes studies addressing questions relating to the biosynthesis of complex carbohydrates in bacteria, some of which may have a role in the persistence of human pathogens. The work will initially be placed in the context of the biology of carbohydrates. This will be followed by an introduction relating to certain aspects of carbohydrate metabolism in bacteria.

1.1 Carbohydrates

Carbohydrates play an integral role in all living organisms in which they serve a variety of functions. This ranges from energy transfer, providing structural integrity to regulatory roles (Varki, 1993). Despite their central importance to so many aspects of any organism's life-cycle, there has been little research effort focussed on the study of carbohydrates, compared with DNA and protein. This is in part because they are not directly encoded by the genome and their structures are far more diverse than any other biopolymers. The sheer variety of carbohydrates observed in nature as well as the numerous ways in which they can be connected makes them difficult to characterise and they can vary considerably from organism to organism. Moreover, the enzymes involved in carbohydrate metabolism share considerable amino acid sequence similarity despite having altered substrate specificities and producing different sugars (Cantarel, et al., 2009).

Carbohydrates are defined as a molecule comprising, carbon, hydrogen and oxygen with an empirical formula $C_m(H_2O)_n$. Generally carbohydrates are classified according to their structure as being mono-, di-, oligo- or poly-saccharides. Monosaccharides are individual carbohydrates that cannot be hydrolysed into smaller carbohydrate constituents. Disaccharides comprise two monosaccharides condensed together by a glycosidic bond. Polysaccharides are long chains of monosaccharides bonded by glycosidic linkages.

The variety in monosaccharide building blocks, the arrangement of glycosidic bonding and the different stereochemistry leads to great diversity amongst the carbohydrates. This structural diversity affords functional diversity and this is, in part, why carbohydrates have been adopted into so many different aspects of biology. For example, the polysaccharides cellulose and amylose both comprise thousands of glucose molecules bonded by 1,4-glycosidic linkages. Cellulose contains β-1,4 glycosidic linkages whereas amylose contains α-1,4 glycosidic bonds (Dintzis and Tobin, 1969;

Updegraff, 1969). The β-1,4 glycosidic linkages orient the hydroxyl groups of the glucoses in such a way that hydrogen bonds can form within a linear chain of cellulose as well as between different chains, and this creates a strong rod-like fibre (Marrinan and Mann, 1954). The hydrogen bonding network is lacking in α-1,4 glycosidic-bonded amylose as the glucose units are not correctly orientated to form hydrogen bonds. The different properties of these polymers are reflected in their biological roles. Cellulose is a component of the plant cell wall in which it confers tensile strength and it is the most abundant polymer on the planet (Updegraff, 1969). Amylose is instead used as a constituent of starch which is a storage polymer used to store excess carbon in an inert form (Haworth, et al., 1946). The different properties of these polysaccharides, despite comprising the same constituent monosaccharide, demonstrate that small modifications in the bonding of polysaccharides can lead to very different chemical properties.

In recent years there have been concerted efforts to characterise enzymes involved in carbohydrate synthesis and degradation. The two major classes of enzymes using carbohydrates as substrates are glycoside hydrolases (GHs) and glycosyl transferases (GTs) in the carbohydrate active enzyme (CAZy) database (Cantarel, et al., 2009).

GT enzymes typically catalyse the formation of glycosidic bonds by combining an activated sugar donor with a specific acceptor (Cantarel, et al., 2009). As such they can form oligosaccharides and polysaccharides when a saccharide acceptor is used (Cabib and Leloir, 1958). Some GT enzymes can instead transfer a sugar donor onto a non-saccharide acceptors, such as protein or lipids, to yield glycoconjugants (Choi, et al., 2010). Despite a whole suite of different products made by GT enzymes and the high substrate specificity observed for individual GTs, only three distinct structural folds are known (Breton, et al., 2006). The major folds within this class of enzymes are GT-A and GT-B however, a GT_{51} fold has also been identified in the structure of a peptidoglycan glycosyl transferases (Breton, et al., 2006; Lovering, et al., 2007). The enzymes proceed either by a single step, inverting mechanism or by a S_Ni mechanism, which is also a single step reaction, that instead leads to the net retention of stereochemistry relative to the substrate (Figure 1.1) (Errey, et al., 2010; Hancock, et al., 2006).

The glycosidic bonds formed by GT enzymes are the most stable bond found in biopolymers from natural sources (Zechel and Withers, 1999). This is exemplified by cellulose which contains glycosidic bonds with a remarkably slow spontaneous rate of hydrolysis, with a half-life of 4.7 million years (Wolfenden, et al., 1998). In spite of this kinetic barrier, GH enzymes are able to catalyse bond cleavage at rates constants up to 1000 s^{-1} (Zechel and Withers, 1999). The hydrolysis reaction either yields a product with a retained anomeric configuration or with an inverted anomeric configuration relative to the substrate (Figure 1.1 and 1.2).

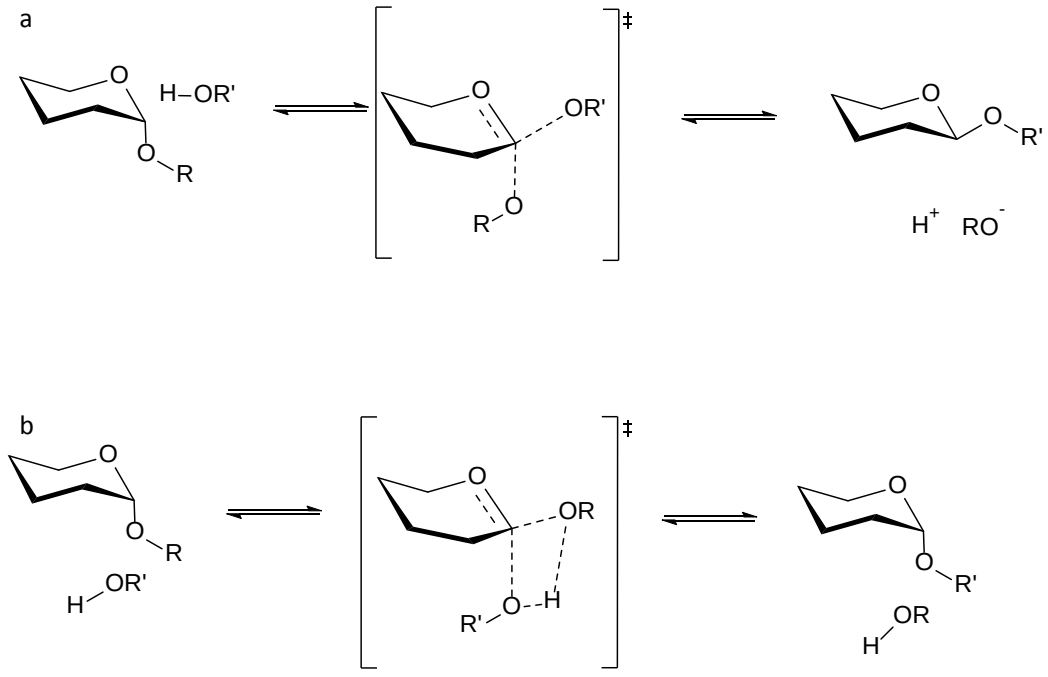

Figure 1.1: Scheme showing transition states of GT enzyme mechanisms
Scheme showing transition states of an inverting S_N2 mechanism (a) and a retaining S_Ni mechanism (b) of GT enzymes. The inverting scheme is applicable to inverting GH enzymes also, where R'= H.

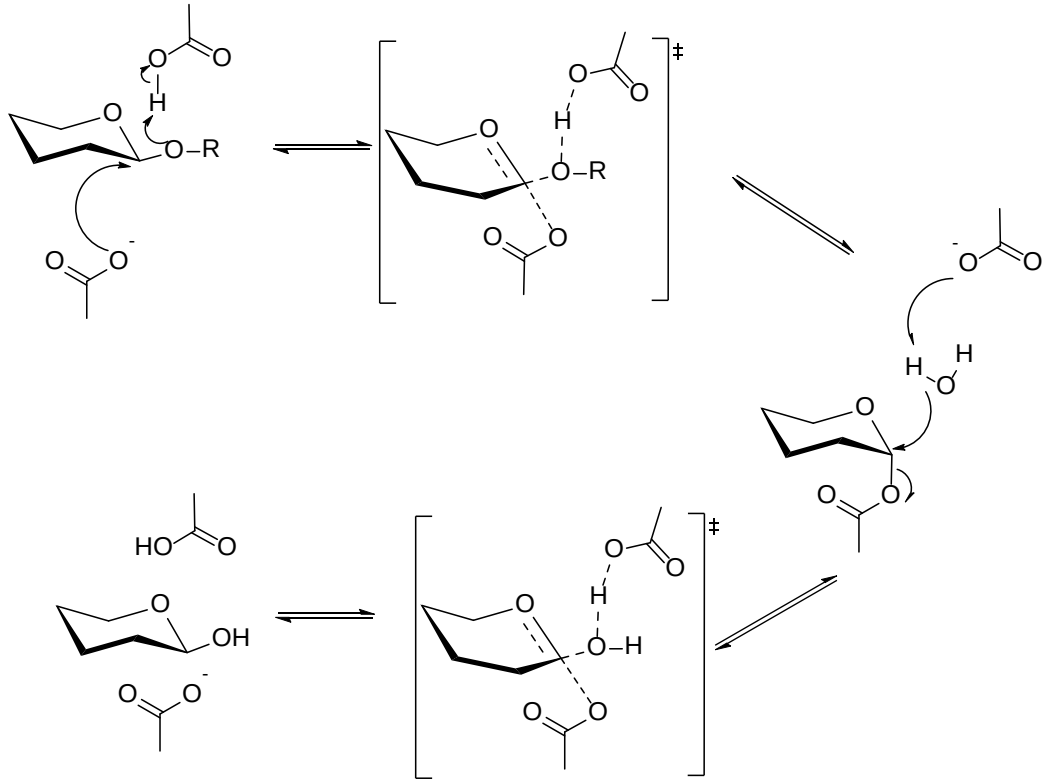

Figure 1.2: General reaction mechanism of a retaining GH enzyme

1.2 Glycogen

The major focus of this thesis is bacterial glycogen metabolism (Figure 1.3). Glycogen is a biopolymer comprising hundreds of thousands of glucose molecules predominantly (~90%) bonded by α-1,4-links with infrequent (~10%) α-1,6-linked branch points (Bell and Young, 1934; Young, 1957). It is a sub-class of glucan, which is defined as a polysaccharide comprising D-glucose substituents. Glycogen is a ubiquitous carbon storage polysaccharide found in bacteria, yeast, fungi, and animals (including humans) (Bell and Young, 1934; Levine, et al., 1953; Northcote, 1953; Rothman and Cabib, 1969). In bacteria, glycogen typically accumulates when growth is limited by a nutrient other than carbon (Montero, et al., 2009). Whilst glycogen is soluble, it is relatively inert and does not significantly affect a cells internal osmotic pressure, which offers a significant advantage over using other mono- or di-saccharides (Wilson, et al., 2010).

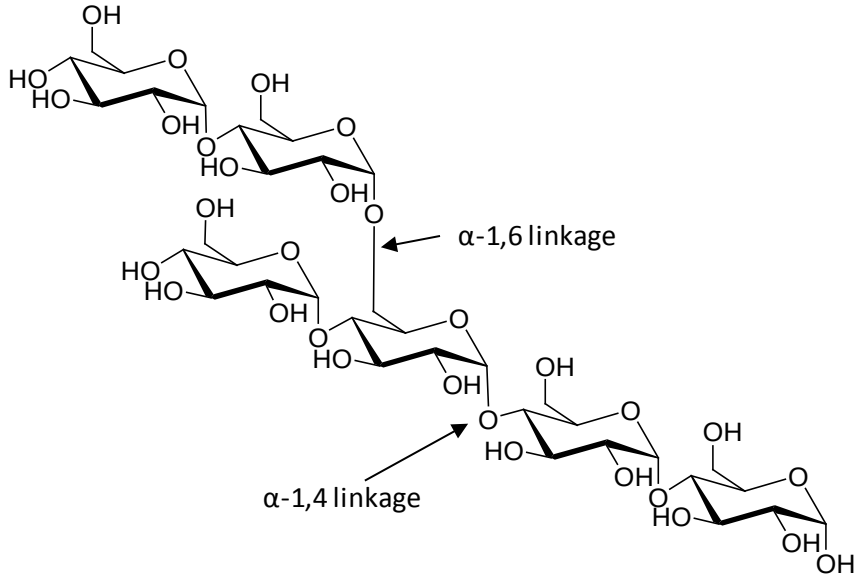

Figure 1.3: Schematic representation of glycogen with the two types of bonding highlighted

There are three known bacterial glucan synthesis pathways: GlgAC, GlgE and Rv3032 (Figure 1.4) (Chandra, et al., 2011). Whilst two of these pathways (GlgE and GlgAC) are known to synthesise glycogen, the third (Rv3032) has only been known to synthesise a glucan polymer, which is ultimately used to produce methylglucose lipopolysaccharides (MGLP) (Figure 1.5) (Chandra, et al., 2011). Glucan is non-essential for the viability of all bacterial species tested and indeed 60% of sequenced bacterial species do not contain any genes encoding the three known glucan synthesis pathways, which suggests that these bacteria need no glucan for survival (Chandra, et al., 2011; Preiss, 1984).

The first known, and best elucidated, pathway is the GlgAC pathway which has been extensively characterised in *Escherichia coli* (Preiss, 1984). The first enzyme of the pathway is a nucleotide diphosphoglucose pyrophosphate pyrophosphorylase (GlgC) that catalyses the formation of adenosine diphosphate (ADP)-glucose from glucose 1-phosphate (Preiss, et al., 1975; Shen and Atkinson, 1970). The ADP-glucose is then used by a glycogen synthase (GlgA), which catalyses a polymerisation reaction to produce an α-1,4-glucan chain (Leloir and Goldemberg, 1962). The final step of the pathway is catalysed by a branching enzyme (GlgB) that introduces α-1,6- linked branch points by transferring a non-reducing-end maltooligosaccharide (MOS) from the 4-position to the 6-position (Larner, 1953). Bioinformatic analysis predicts that this pathway is the most

widely distributed amongst bacterial species, with the genes encoding the pathway present in 32% of sequenced bacteria (Chandra, et al., 2011).

A second route to glucan synthesis is via the MGLP pathway (Figure 1.4) (Jackson, et al., 2007). The presence of this pathway is limited to some actinomycetes, with one example being *Mycobacterium*, and the genes encoding the α-glucan synthesis enzymes of the pathway are present in only 2% of sequenced bacterial genomes (Chandra, et al., 2011). To date, all enzymes involved in producing MGLP are not known, however, the first two steps in the biosynthesis of the oligosaccharide backbone is predicted to lead to the production of a branched glucan (Jackson and Brennan, 2009). Firstly, a glucosyl transferase, Rv3032 (a paralogue of GlgA) is preliminarily thought to use ADP-glucose as well as uridine diphosphoglucose (UDP)-glucose as a donor to synthesise a linear α-1,4-glucan (Kaur, et al., 2009; Stadthagen, et al., 2007). Rv3031 is a predicted to be a branching enzyme that is able to introduce a single α-1,6-branch to produce an α-glucan polysaccharide with a single branch, in a comparable manner to GlgB (Stadthagen, et al., 2007).

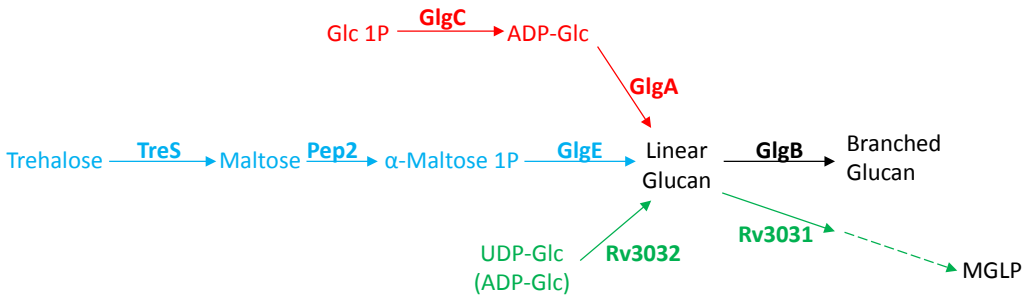

Figure 1.4: Overview of glucan synthesis pathways

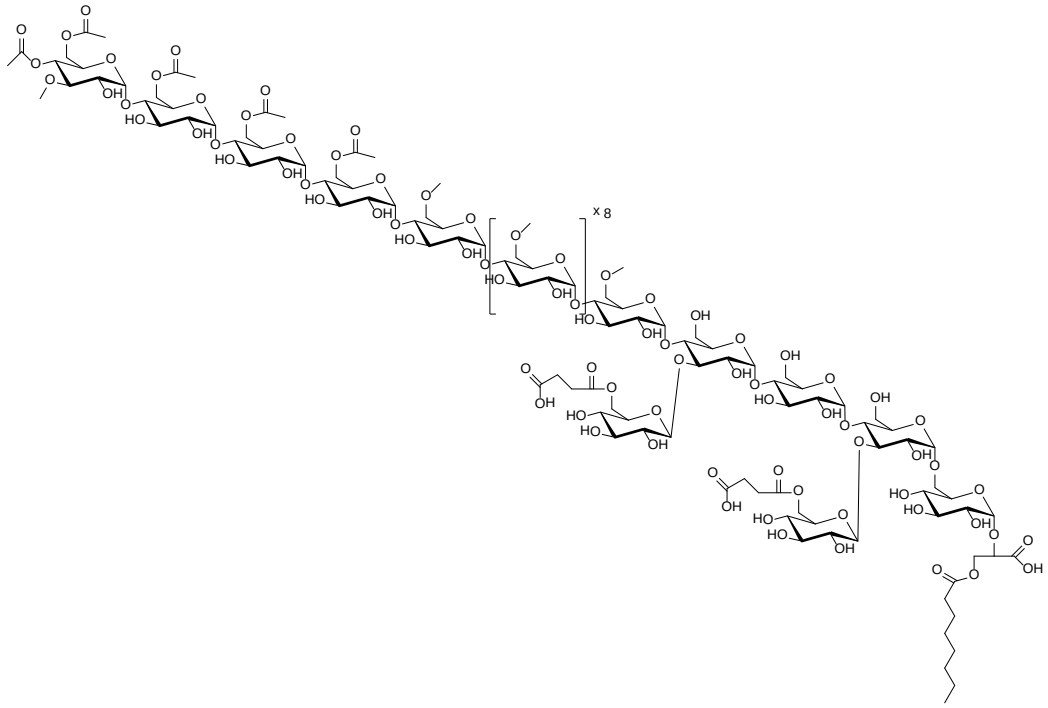

Figure 1.5: Structure of a typical MGLP, which is synthesised by the Rv3032 pathway

The third, and final, known α-glucan synthesis pathway is the GlgE pathway (Figure 1.4) (Elbein, et al., 2010; Kalscheuer, et al., 2010a). The pathway comprises four enzymes, the genes encoding the enzymes are all present in 14% of sequenced bacterial genomes and they are often clustered together in these genomes (Chandra, et al., 2011). The starting substrate of the GlgE pathway is a disaccharide, unlike the GlgAC and Rv3032 pathways. Briefly, trehalose synthase (TreS) is the first enzyme of the pathway and converts trehalose (α-D-glucopyranosyl-(1,1)-α-D-glucopyranoside) to maltose (α-D-glucopyranosyl-(1,4)-D-glucopyranose) (Nishimoto, et al., 1995; Nishimoto, et al., 1996). A maltose kinase (Pep2) subsequently phosphorylates maltose, to form α-maltose 1-phosphate (αM1P), which is added to the non-reducing end of a linear α-glucan chain by a maltosyltransferase (GlgE) (Drepper, et al., 1996; Kalscheuer, et al., 2010a). Finally, GlgB converts the linear α-glucan chain to a branched α-glucan (Larner, 1953). Whilst the individual enzyme activities have been confirmed experimentally, an unequivocal link between the pathway and glucan production *in vivo* has not been demonstrated.

1.3 Enzymes of the GlgE pathway

1.3.1 TreS

TreS is a maltose α-D-glucosylmutase (EC 5.4.99.16) that interconverts maltose and trehalose (Figure 1.6) (Nishimoto, et al., 1995; Pan, et al., 2004). It also displays weak hydrolytic activity (Nishimoto, et al., 1996) and has been observed to slowly hydrolyse glycogen to maltose (Pan, et al., 2008). TreS proceeds via an intramolecular pathway, in which both glucose units from a single molecule of trehalose are used to form a single molecule of maltose and vice versa (Kobayashi, et al., 2003; Koh, et al., 2003; Nishimoto, et al., 1996).

The enzyme belongs to the GH13_33 sub-family according to the CAZy database (Cantarel, et al., 2009; Stam, et al., 2006). Thus, it is predicted to have a $(\beta/\alpha)_8$ barrel fold, defining an active site containing an Asp nucleophile and a Glu proton donor that is expected to catalyse an α-retaining double-displacement reaction mechanism, which will be explored in more detail in subsequent chapters (Figure 1.2). Therefore, the mechanism predicts that TreS should indeed be stereospecific in which it should only interconvert α-maltose and trehalose. From a biological perspective this has implications for flux into the pathway because the second enzyme of the pathway is stereospecific (see 1.3.2) and therefore it is unclear if flux of the GlgE pathway is limited by the slow mutarotation of maltose as there are few known maltose mutarotases in bacteria (Bailey, et al., 1967; Stults, et al., 1987). Crystallography of TreS from two mycobacterial species has confirmed the predicted active site configuration (Caner, et al., 2013; Roy, et al., 2013). Furthermore, the glucosyl-enzyme intermediate involves Asp^{230} in the *Mycobacterium smegmatis* TreS, which supports the mechanistic prediction (Figure 1.2) (Zhang, et al., 2011). Interestingly, crystallography also identified a remote acarbose binding site located 40 Å away from the active site (Caner, et al., 2013).

TreS was initially discovered in *Pimelobacter* sp. R48 but it has been reported in a number of bacteria since, including *Mycobacterium tuberculosis, Pseudomonas syringae* and *Thermus caldophilus* (De Smet, et al., 2000; Freeman, et al., 2010; Koh, et al., 2003; Nishimoto, et al., 1995). Before the discovery of the GlgE pathway, the physiologically relevant reaction of TreS was assumed to be trehalose production from maltose. However, in the context of the GlgE pathway, TreS would be required to

catalyse the reverse reaction and produce maltose from trehalose. Therefore, the role it plays in metabolism is somewhat ambiguous.

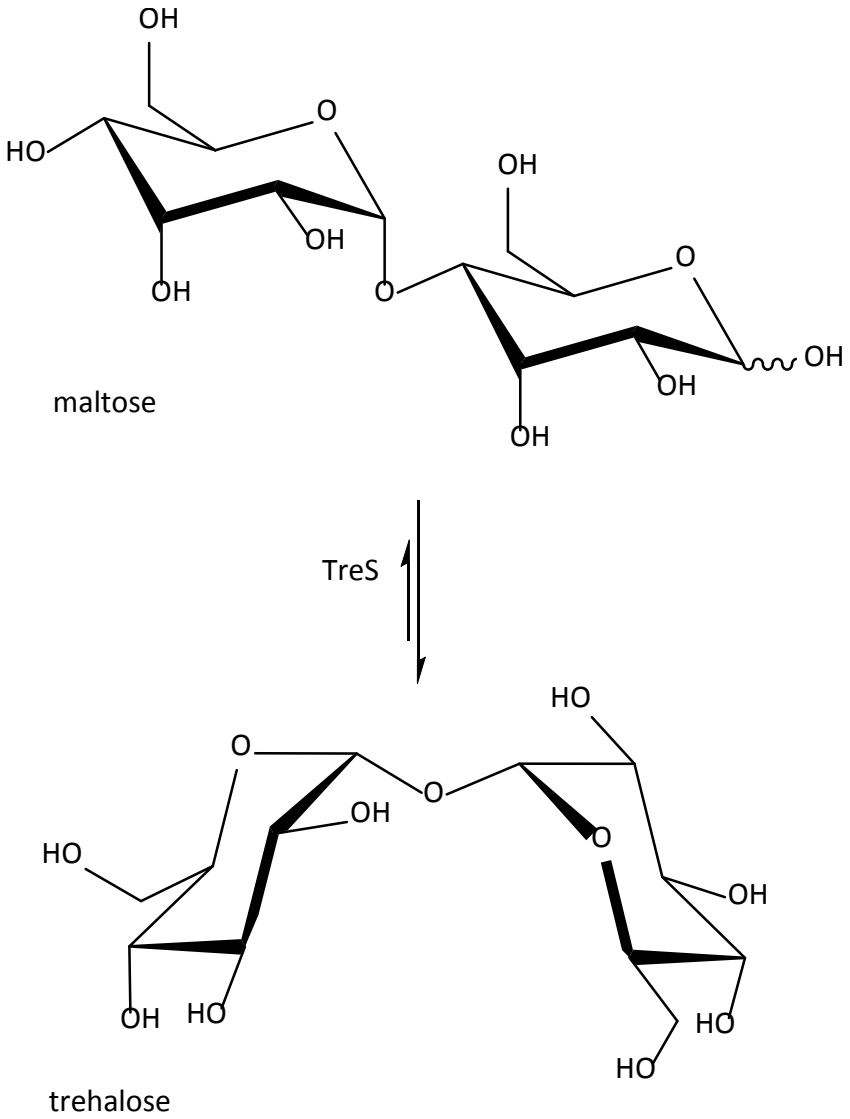

Figure 1.6: Overview of TreS reaction

1.3.2 Pep2

Pep2 (EC 2.7.1.175) is a phosphotransferase that produces αM1P (Figure 1.7) (Drepper, et al., 1996; Niehues, et al., 2003). The gene encoding Pep2 is present in 17% of bacterial genomes (Chandra, et al., 2011) and the Pep2 protein has been characterised from a number of actinomycetes (Jarling, et al., 2004; Mendes, et al., 2010). The physiological role of Pep2 was not immediately apparent prior to the discovery of the GlgE pathway but it is now thought to exclusively function within the GlgE pathway. This is consistent with the finding that the *treS* gene is frequently associated with the *pep2* gene and indeed both protein functions are more often encoded as a single gene fusion than as separate genes in bacterial genomes (Chandra, et al., 2011). Moreover, recent work has shown that TreS and Pep2 proteins from *M. tuberculosis* form a hetero-octameric complex *in vitro* that increases the activity of Pep2 (Roy, et al., 2013).

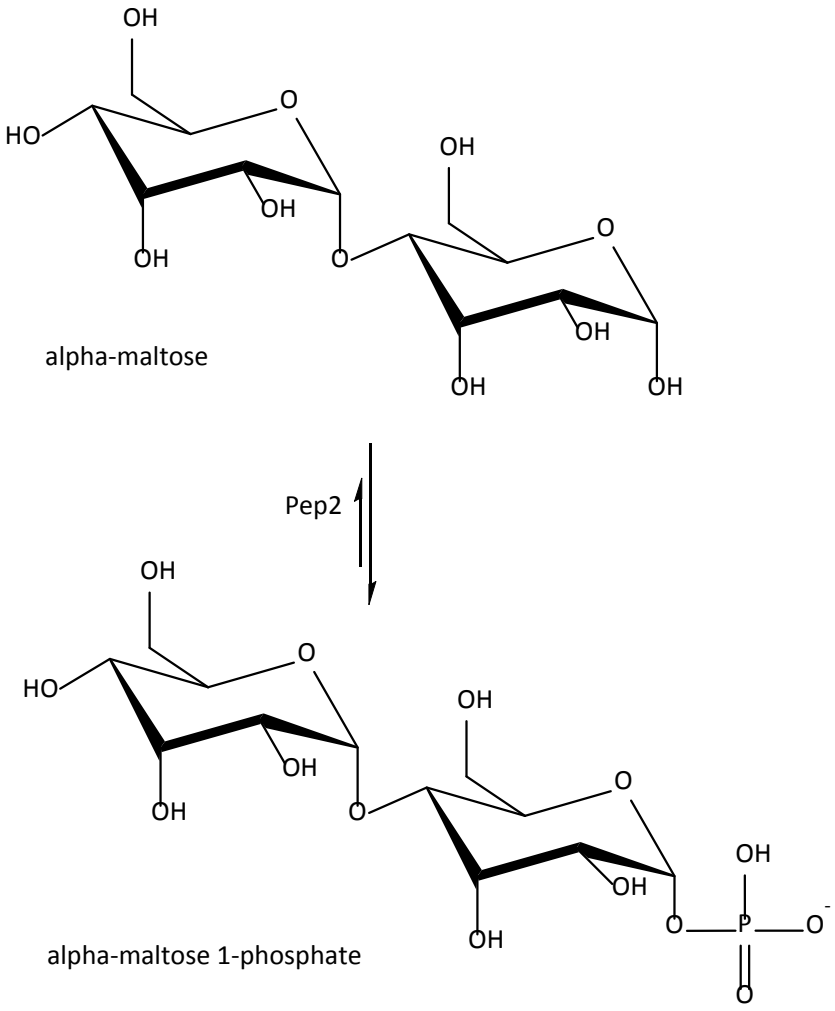

Figure 1.7: Overview of Pep2 reaction

1.3.3 GlgE

The defining enzyme of the pathway is the maltosyl transferase GlgE (EC 2.4.99.16) belonging to the GH13_3 family that also exhibits disproportionation activity of linear α-glucans (Figure 1.8) (Cantarel, et al., 2009; Elbein, et al., 2010; Kalscheuer, et al., 2010a). GlgE transfers maltose from αM1P to the non-reducing end of linear α-glucan via a ping-pong mechanism (Kalscheuer, et al., 2010a). The enzyme requires an α-glucan acceptor with a degree of polymerisation (DP) at least above 4 (Kalscheuer, et al., 2010a). Based on its CAZy family membership allocation, it is predicted to proceed via an α-retaining, two-step, double displacement reaction (Figure 1.2) (Cantarel, et al., 2009). The crystal structure of the apo form of GlgE from *S. coelicolor,* as well as mutein forms of the enzyme bound to deoxy-fluoro-glucosyl intermediates, has revealed how GlgE catalysis occurs (Syson, et al., 2014; Syson, et al., 2011). Small angle X-ray scattering has shown that the overall shape of the outer pocket of *S. coelicolor* GlgE is comparable to *M. tuberculosis* GlgE (Syson, et al., 2014). Moreover, all kinetic and substrate specificity features are identical and they share a conserved donor site according to homology modelling (Syson, et al., 2011). Therefore, the structure of *S. coelicolor* enzyme crystal structure has potential to be used in the rational design of novel *M. tuberculosis* GlgE inhibitors (Syson, et al., 2014).

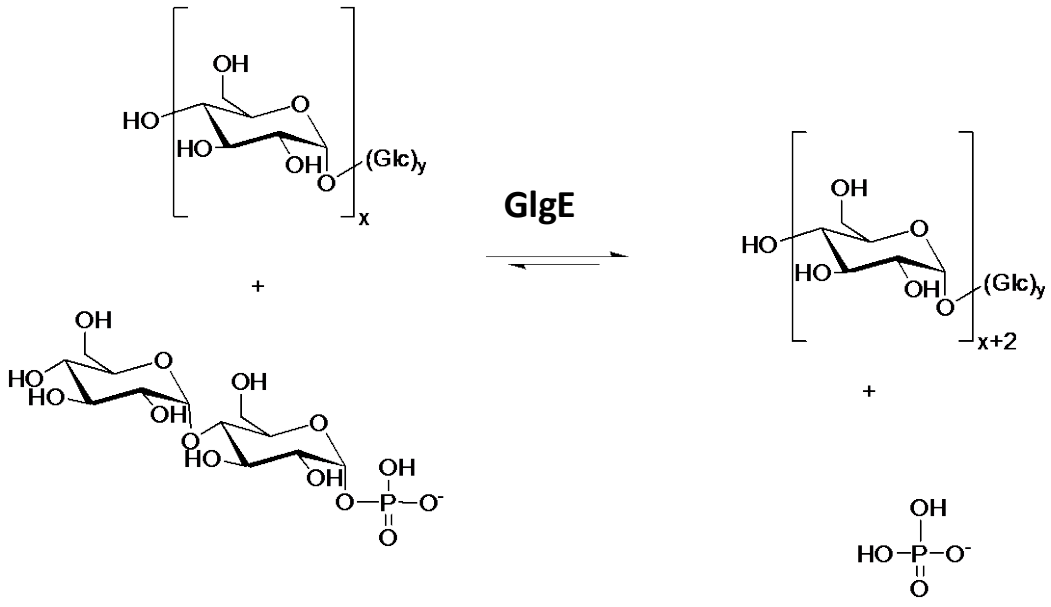

Figure 1.8: Overview of GlgE reaction

1.3.4 GlgB

The final enzyme of the GlgE pathway is GlgB (EC 2.4.1.18), which introduces α-1,6-linked branch points by transferring a non-reducing-end MOS from the 4-position to the 6-position (Figure 1.9) (Lares, et al., 1974). It belongs to the GH 13_9 sub-family, and as with TreS and GlgE, is predicted to proceed via an α-retaining, 2 step, double displacement mechanism (Figure 1.2) (Cantarel, et al., 2009; Stam, et al., 2006). Prior to the discovery of the GlgE pathway, GlgB was thought to be solely involved in classical glycogen synthesis by the GlgAC pathway. However, the *glgB* gene is more frequently associated with the other genes of the GlgE pathway rather than with the genes required for the GlgAC pathway (Chandra, et al., 2011). The crystal structures of several GlgBs have provided insight into the mechanism of catalysis with four domains involved in substrate binding and catalysis (Abad, et al., 2002; Pal, et al., 2010). Furthermore, the potential catalytic triad of Asp^{411}, Glu^{464} and Asp^{532} was identified in the *M. tuberculosis* GlgB, which could carry out general acid catalysis (Pal, et al., 2010). As with GlgE, the structure of this enzyme could help with the design of novel inhibitors (Pal, et al., 2010).

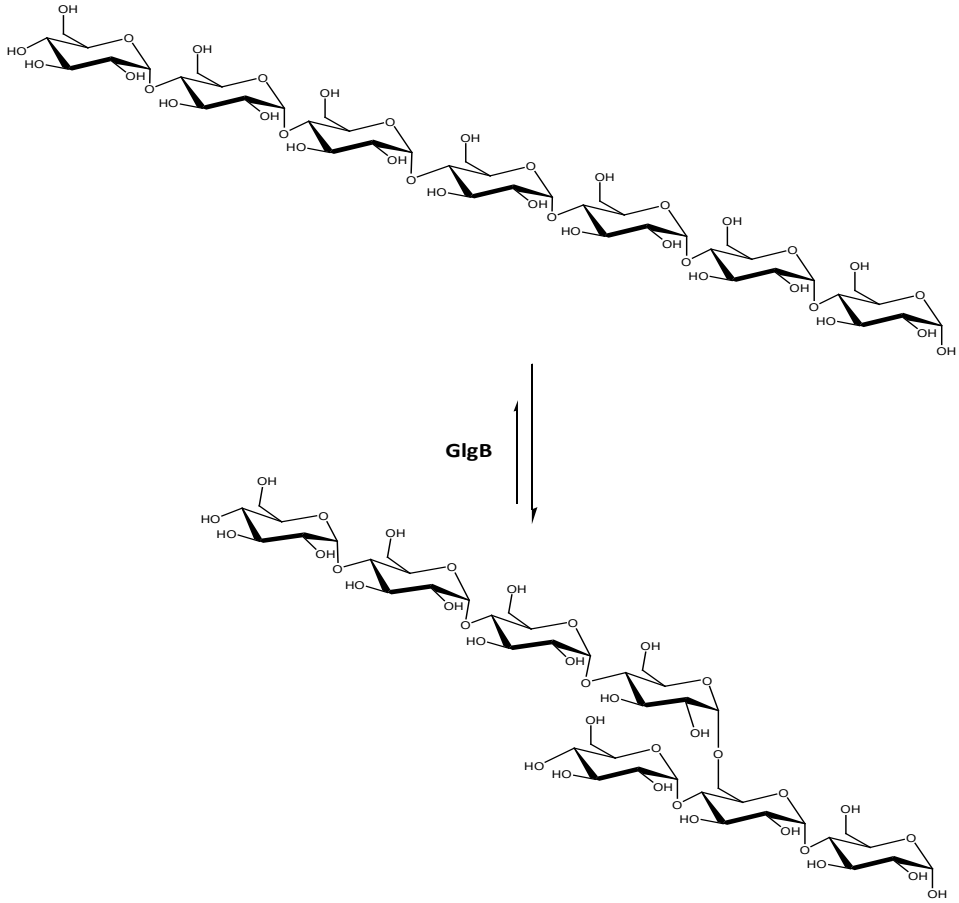

Figure 1.9: Overview of GlgB reaction

1.4 The GlgE pathway in *Mycobacterium*

The GlgE pathway was initially discovered in *M. tuberculosis*, which is the causative agent of the human disease tuberculosis (Dye, 2006; Kalscheuer and Jacobs, 2010). Approximately 2 billion people worldwide are estimated to have asymptomatic latent infections of the bacterium and are at risk of developing the disease (Zumla, et al., 2013). Whilst in up to 90% of these cases active disease will not develop, globally there were 8.7 million new cases of tuberculosis with 1.4 million deaths in 2011 (Zumla, et al., 2013). Treatment of the disease requires a long course of a cocktail containing several antibiotics (Dye, 2006). As the disease symptoms typically subside before the infection is completely eradicated by antibiotics, patients frequently do not complete their treatments, which therefore present a strong selection pressure for multiple-drug resistant strains of *M. tuberculosis* to develop (Zumla, et al., 2013). This has led to the emergence of extensively drug resistant strains in a number of countries across all continents (Zumla, et al., 2013). Consequently there is an urgent need to develop new therapies with novel modes of actions to target *M. tuberculosis* in order to increase the number of therapeutics available.

The gene encoding GlgE was predicted to be essential for the survival of *M. smegmatis* and *M. tuberculosis* (Sassetti, et al., 2003); and accordingly attempts to generate Δ*glgE* in *M. tuberculosis* failed (Kalscheuer, et al., 2010a). However, *ΔglgE* in *M. smegmatis* was only conditionally lethal, with lethality observed when excess trehalose was supplied exogenously in the growth media (Kalscheuer, et al., 2010a). In the absence of GlgE, there is accumulation of the toxic metabolite αM1P (Kalscheuer, et al., 2010a). Therefore, to avoid accumulation of αM1P, chemical genetics was used to generate an inducible *ΔglgE* strain in *M. tuberculosis* (Kalscheuer, et al., 2010a). In addition to being non-viable in a free-living form, the *ΔglgE* strain was unable to colonise mouse tissues and cause pathogenicity (Kalscheuer, et al., 2010a). Thus an inhibitor of GlgE has potential for use in the treatment tuberculosis. The mechanism by which αM1P causes toxicity remains elusive, however, microarray experiments have shown that there are global changes in gene expression upon αM1P accumulation and therefore toxicity is unlikely to be caused by perturbation of a single pathway and/or mechanism (Kalscheuer, et al., 2010a).

GlgE is a particularly attractive drug target because it lacks a human homolog, which minimises the risk of adverse side effects caused by non-specifically disrupting host enzymes (Kalscheuer and Jacobs, 2010; Kalscheuer, et al., 2010a). It is noteworthy that GlgB is also essential for *M. tuberculosis* and therefore it too has potential to be used as a drug target (Sambou, et al., 2008). However, homologues of GlgB exist in humans and therefore any therapies targeting GlgB could be more likely to have adverse side-effects in humans (Kalscheuer, et al., 2010a).

One potential destination of the α-glucan product synthesised by the GlgE pathway is to the capsular layer of *Mycobacterium* (Kalscheuer, et al., 2010a). The capsule is a non-covalently linked structure located in the outermost compartment of the cell envelope (Ortalomagne, et al., 1995; Sani, et al., 2010). It comprises carbohydrates, proteins and small amounts of lipid (Lemassu, et al., 1996; Ortalomagne, et al., 1995).

The capsule plays a key role in pathogenesis as it is the part of the mycobacteria that directly interacts with the host. For example, the capsule enhances interactions made between *Mycobacterium bovis* BCG and macrophages, thereby facilitating infection (Sani, et al., 2010). Several publications have reported that extracellular α-glucans from *M. tuberculosis* are responsible for suppressing recognition within the host and preventing an appropriate immune response being mounted (Gagliardi, et al., 2007; Geurtsen, et al., 2009).

The carbohydrate of the capsule is known to predominantly take the form of an α-glucan, like the products of the GlgE and GlgAC pathways (Dinadayala, et al., 2008; Lemassu and Daffe, 1994; Ortalomagne, et al., 1995). Immunoelectron microscopy has shown that the *M. tuberculosis* TreS is cytosolic and as such the other enzymes of the GlgE pathway are unlikely to be located extracellularly, which suggests the α-glucan will require export to the extracellular space (Vizcaino, et al., 2010). Whilst mycobacteria are known to release active membrane vesicles, α-glucan is absent from such vesicles, which suggests that export is instead taking place via a specific set of transporters (Prados-Rosales, et al., 2011). There are three known pathways that synthesise α-glucan in *Mycobacterium:* GlgAC, GlgE and Rv3032 pathways (Figure 1.10). It remains unclear if one pathway or several pathways are producing α-glucan for the capsular layer as well as contributing to cytosolic glycogen levels (Jackson, et al., 2007; Kalscheuer, et al., 2010a; Sambou, et al., 2008). Exchange of substrates and/or

products between two of these pathways is very likely to occur because the Rv3032 and GlgE pathways are synthetically lethal but the point of cross-talk between these pathways remains unknown (Kalscheuer, et al., 2010a). Mutants in *glgA* and *Rv3032* had major changes in flux balances of extracellular capsular α-glucan and α-glucan levels respectively (Sambou, et al., 2008). Furthermore, the *glgA* mutant produced fewer colonies in a mouse infection model, implying a specific role for α-glucans in the persistent phase infection of mice (Sambou, et al., 2008).

The functional redundancy between these pathways makes it difficult to understand their roles in isolation in *Mycobacterium*. Consequently, understanding the biochemistry of the GlgE pathway, such as characterising the polysaccharide it synthesises, is also difficult in a mycobacterial system.

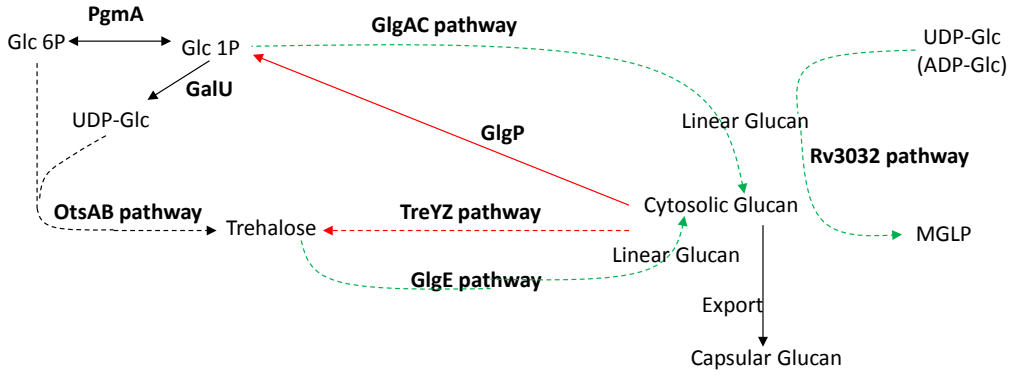

Figure 1.10: Overview of glucan metabolism in *Mycobacterium*
Dashed lines indicate pathways containing multiple enzymes. Green arrows indicate glucan synthesis pathways and the red arrows indicate enzymes/pathways involved in glucan degradation. Glc = glucose, P= phosphate

1.5 Regulation of the GlgE pathway in *Mycobacterium*

The first report of *glgE* came from researchers characterising a temperature sensitive mutant of *M. smegmatis* called SMEG53 (Belanger and Hatfull, 1999). SMEG53 grows like WT under normal culture conditions; however, at temperatures ≥42 °C it ceases to divide and has altered cell wall morphology (Belanger and Hatfull, 1999). The mutation in SMEG53 mapped to a single amino-acid substitution within GlgE (H349Y) (Belanger and Hatfull, 1999). His^{349} is conserved in *S. coelicolor* GlgE and the crystal structure suggests it is located close to a facile lid that allows entry of αM1P into the active site (Syson, et al., 2011). The SMEG53 phenotype is restored to WT by the reintroduction of a non-mutated *glgE* (Belanger and Hatfull, 1999), which suggests that GlgE (H349Y) is a loss of function mutant but the mechanism by which this mutation diminishes GlgE activity remains unclear.

Surprisingly, a WT phenotype is also restored in SMEG53 by the introduction of multiple copies of the *garA* gene (Belanger and Hatfull, 1999). Recently, GlgE has been shown to be negatively regulated by phosphorylation in *M. smegmatis* (Leiba, et al., 2013). The kinase specifically involved in phosphorylation of GlgE is PknB (protein kinase B) (Leiba, et al., 2013). GarA is also a phosphorylation target of PknB. GarA is involved in the regulation of carbon and nitrogen metabolism in other organisms (England, et al., 2009; Ventura, et al., 2013). Therefore, GarA may be acting as a phosphorylation decoy, to prevent phosphorylation and further de-activation of the temperature sensitive GlgE by saturating PknB in the SMEG53 strain, thereby ameliorating the temperature sensitive phenotype (Leiba, et al., 2013).

Together, these observations suggest that mycobacteria are able to regulate accumulation of α-glucan by phosphorylation of GlgE. It is noteworthy that an orthologue of PknB in *S. ceoelicolor* AfsK was also observed to specifically phosphorylate *S. coelicolor* GlgE, suggesting that these regulatory networks may be conserved in at least actinomycetes (Leiba, et al., 2013). Interestingly, this type of regulation contrasts with the allosteric regulation observed in the GlgAC pathway (Preiss, et al., 1983).

1.6 The GlgE pathway in *Streptomyces*

Streptomyces are soil dwelling, multi-cellular colony forming bacteria with distinct developmental stages (Figure 1.11) (Flardh and Buttner, 2009). *Streptomyces* typically produce a diverse array of compounds with anti-microbial activities and over half of antibiotics used by medicine were originally isolated from *Streptomyces* (Kieser, et al., 2000).

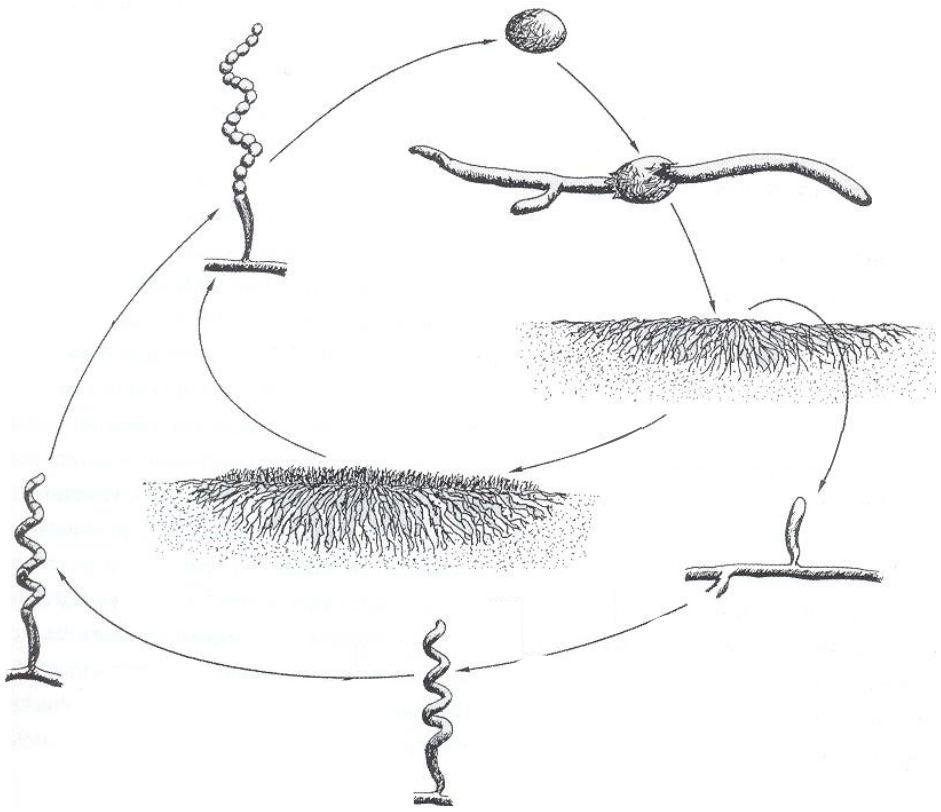

Figure 1.11: Overview of the life-cycle of *Streptomyces*
Adapted from (Kieser, et al., 2000)

Glycogen has been identified in a number of different *Streptomyces* species, including the model streptomycete *S. coelicolor* (Brana, et al., 1980; Braña, et al., 1982; Brana, et al., 1986; Bruton, et al., 1995; Homerova, et al., 1996; Ranade and Vining, 1993; Rueda, et al., 2001). In *S. coelicolor,* glycogen is deposited transiently at the interface between the substrate and aerial hyphae in what is known as phase I glycogen deposition (Plaskitt and Chater, 1995). This is followed by phase II deposition of glycogen in the pre-spore compartments. Phase II deposition is prolonged and qualitative inspection of microscopy images suggests that it is associated with greater glycogen deposition. Ultimately, the mature spores are devoid of glycogen but have high levels (up to 20% of

dry cell weight) of trehalose (Brana, et al., 1986; Ranade and Vining, 1993). Therefore, it has been proposed that glycogen deposition allows localisation of carbon reserves in pre-spores so as to provide a carbon source for trehalose production during spore maturation. This is consistent with the observation in *Streptomyces venezuelae* that gene expression of the sequence encoding the TreZ enzyme (involved in glycogen degradation via the TreYZ pathway) is regulated by a sporulation specific transcription factor (Bush, et al., 2013).

In *S. coelicolor* the genes encoding the GlgE pathway enzymes are all located in the same operon from which they are co-transcribed to produce a polycistronic transcript with three of the genes predicated to be translationally coupled (Schneider, et al., 2000). Unusually *S. coelicolor* has two gene clusters each encoding functional GlgE enzymes (Schneider, et al., 2000). Single disruption mutants of each of the *glgB* genes have shown that each GlgB branches glucans at different phases (Bruton, et al., 1995). Therefore, it suggests that genes from one GlgE operon are responsible for phase I deposition and that genes from the other GlgE operon are required for phase II deposition (Bruton, et al., 1995).

Consistent with this hypothesis is the fact that the two GlgE clusters are under separate developmental control (Plaskitt and Chater, 1995; Schneider, et al., 2000; Yeo and Chater, 2005). The complex morphology of the *S. coelicolor* is mediated by a number of different regulatory genes that are responsible for different developmental stages (Flardh and Buttner, 2009). Two such classes of regulatory genes are *bld* and *whi.* Bld regulatory genes are required for aerial hyphae formation and Whi genes are required for regular septation of aerial hyphae (Flardh and Buttner, 2009). The *bld* genes are required for normal phase I glycogen however, normal phase II glycogen is reliant upon WhiG (a σ^{WhiG} factor for specifying RNA polymerases to initiate sporulation septation) (Plaskitt and Chater, 1995; Yeo and Chater, 2005).

Further investigations on glycogen metabolism *S. coelicolor* are compounded by the fact that the genes encoding the GlgAC pathway are also present. With three glycogen synthesis pathways, genetic studies to generate glycogen deficient mutants are more challenging. Interestingly, another streptomycete, *S. venezuelae,* contains only a single GlgE operon and lacks genes encoding enzymes of the GlgAC and Rv3032 pathways

(Figure 1.12). Glycogen has been reported in *S. venezuelae*; however it is not deposited biphasically as in *S. coelicolor* but instead monophasically during the early stages of sporulation (Ranade and Vining, 1993).

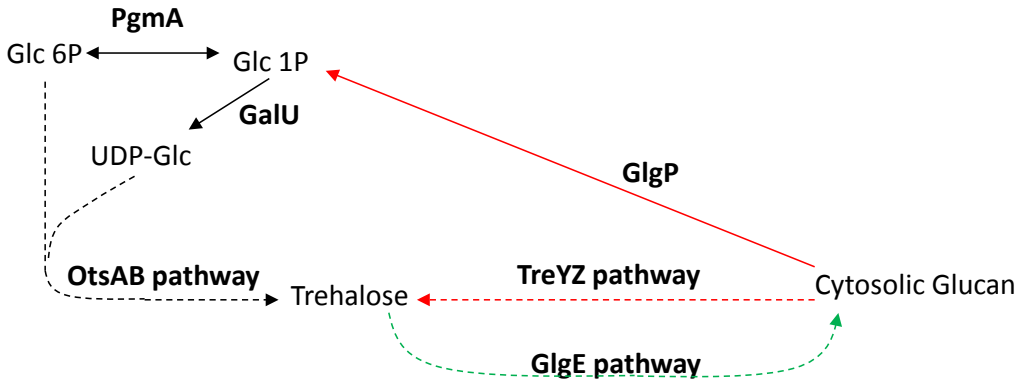

Figure 1.12: Overview of bioinformatic predictions of glucan metabolism in *S. venezuelae*
Dashed lines indicate pathways containing multiple enzymes. Green arrows indicate glucan synthesis pathways and the red arrows indicate enzymes/pathways involved in glucan degradation. Glc = glucose, P= phosphate

1.7 Trehalose synthesis in *Mycobacterium* and *Streptomyces*

In contrast to the other glucan synthesis pathways, a disaccharide (instead of a monosaccharide) trehalose is the initial substrate of the GlgE pathway (Kalscheuer, et al., 2010a). Trehalose is a non-reducing disaccharide that has many roles in biology (Arguelles, 2000; Elbein, et al., 2003; Iturriaga, et al., 2009). For example, it is a precursor for the mycomembrane, trehalose mycolates, which are essential for the growth and virulence of mycobacteria, such as *M. tuberculosis* (Takayama, et al., 2005). Intracellular trehalose levels also increase in response to different stresses in *M. smegmatis,* suggesting that it has a dual function as a stress protectant and has a structural role, which makes it essential for virulence (De Smet, et al., 2000). Trehalose is also present throughout the life-cycle of *Streptomyces*, with maximal accumulation observed in mature spores (McBride and Ensign, 1987). In the spores, trehalose is thought act as a compatible solute, enhancing desiccation tolerance of dormant spores (McBride and Ensign, 1990). Following the onset of germination, trehalose is rapidly hydrolysed to glucose by trehalase, therefore it also acts as a carbon reserve to fuel vegetative growth (McBride and Ensign, 1990).

There are at least three alternate trehalose biosynthetic routes known in bacteria (Figure 1.13) (Iturriaga, et al., 2009). Interestingly, *Mycobacterium* and *Streptomyces* have genes encoding what have to date been considered to be the three most common pathways, perhaps reflecting the critical role trehalose has in these genera (Chandra, et al., 2011; De Smet, et al., 2000).

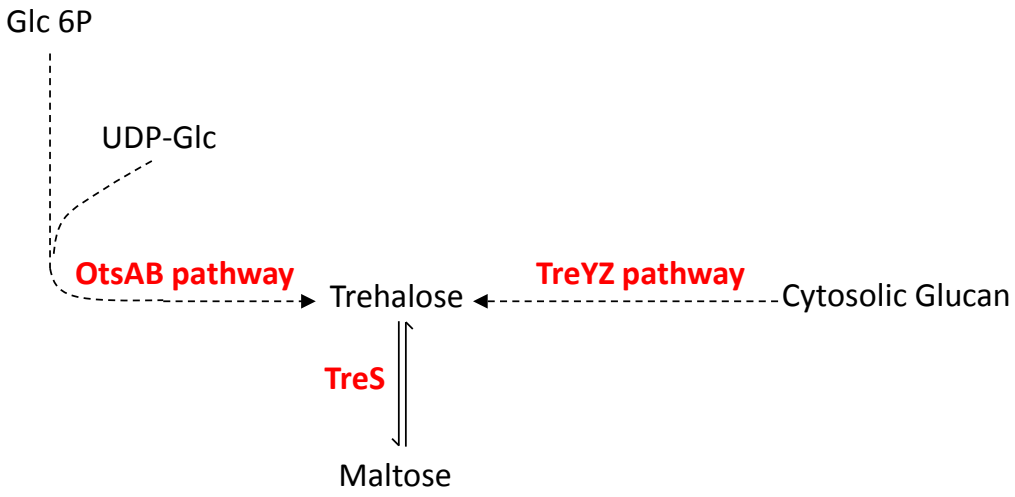

Figure 1.13: Overview of what have been proposed to be trehalose synthesis pathways in bacteria
The most widely distributed pathways associated with trehalose biosynthesis in actinobacteria, reviewed by (Iturriaga, et al., 2009).

The OtsAB pathway synthesises trehalose by condensation of two glucoses, via two enzymes: OtsA (EC 2.4.1.15) and OtsB (EC 3.1.3.12) (Cabib and Leloir, 1958; Matula, et al., 1971). OtsA is classified as a GT20 retaining enzyme and proceeds via an S_Ni reaction mechanism (Figure 1.1a) (Cantarel, et al., 2009; Errey, et al., 2010; Lee, et al., 2011). OtsA condenses glucose 6-phosphate to a nucleoside diphospho glucose (NDP-Glc) to form trehalose 6-phosphate (Cabib and Leloir, 1958). Whilst glucose 6-phosphate is required, the substrate specificity of NDP-glucoses varies between organisms. For example *E. coli* is specific for UDP-glucose, whereas *Streptomyces hygroscopicus* is specific for GDP-glucose (Elbein, 1968; Gibson, et al., 2002). This is followed by dephosphorylation of trehalose 6-phosphate by the phosphatase OtsB to yield trehalose (Matula, et al., 1971).

The TreYZ pathway degrades glycogen and/or glucans into trehalose by a three step process involving the enzymes TreX (EC 3.2.1.33), TreY (EC 5.4.99.15) and TreZ (EC 3.2.1.141) (Maruta, et al., 1996). The first step of the pathway involves de-branching of

α-1,6 branch points of glucans by TreX (Nakayama, et al., 2001). The reducing-end glycosidic bond is then transglycosylated from α-1,4 linkage to a α-1,1 linkage by TreY (Kim, et al., 2000; Maruta, et al., 1996). The terminal α-1,1 bonded disaccharide is subsequently cleaved in a hydrolysis reaction by maltooligosyltrehalose trehalohydrolase TreZ (Kim, et al., 2000).

In vitro experiments have shown that all three pathways could, in principle, operate in *Mycobacterium* (De Smet, et al., 2000). Moreover, genetic experiments appeared to show that all pathways are capable of synthesizing trehalose de novo in *M. smegmatis* (Woodruff, et al., 2004). It is noteworthy that these studies were using non-specified culture media, that could have contained maltose, and therefore interpretations of the results are ambiguous. In contrast, it has been reported that the OtsAB pathway is dominant in trehalose biosynthesis in *M. tuberculosis* (Murphy, et al., 2005). However, in a close relative of mycobacteria *Corynibacterium glutamicum* the TreYZ pathway produces the majority of trehalose (Wolf, et al., 2003). The observed hierarchies will probably be subject to change depending on the nature of the carbon source and therefore it is important to conduct such studies on well-defined media. The presence of several trehalose synthesis pathways is likely to allow organisms to ensure adequate intracellular trehalose supply regardless of the external supplied carbon source.

1.8 Project aims

The main aims of this thesis are threefold:

1. Biochemical characterisation of two of the enzymes of the GlgE pathway, with a view to determining if TreS is stereospecific so as to support the catalytic mechanism by which it undergoes catalysis. Pep2 expression is explored with a view to determining if the enzyme could be combined with TreS *in vitro* to synthesise αM1P.
2. Reverse genetics on *S. venezuelae* to determine experimentally if the GlgE pathway is responsible for glycogen production in this organism and to determine whether *glgE* is essential through αM1P toxicity as well as its overall impact on development of *S. venezuelae*.
3. Reverse genetics and biochemical characterisation of candidate genes that are hypothesised to be either feeding substrate into the GlgE pathway or involved in glycogen degradation in *S. venezuelae*.

Chapter 2: Materials and Methods

2.1 Molecular biology methods

2.1.1 Growth media and supplements

Table 2.1: Constituents of all media used in this study, including supplements

Media	Constituents (g L^{-1})
Lysogeny broth (LB)	(10 agar*), 10 tryptone, 5 yeast extract, 10 NaCl, distilled water (dH_2O)
Lennox (Lx)	(10 agar*), 10 tryptone, 5 yeast extract, 5 NaCl, 1 Glucose, dH_2O
Auto Induction Media (AIM)	10 tryptone, 5 yeast extract, 3.3 $(NH_4)_2SO_4$, 6.8 KH_2PO_4, 7.1 Na_2HPO_4, 0.5 glucose, 2 α-lactose, 0.15 $MgSO_4$, 0.03 ForMedium™ trace elements, dH_2O
Super Optimal Broth with Catabolite Repression (SOC)	20 tryptone, 5 yeast extract, 0.58 NaCl, 3.6 glucose, 0.19 KCl, 2.03 $MgCl_2$, 2.46 $MgSO_4.7H_2O$, dH_2O
Super Optimal Broth (SOB)	20 tryptone, 5 yeast extract, 0.5 NaCl, dH_2O
Malt-Yeast-Maltose (MYM)	(20 agar*), 4 maltose, 4 yeast extract, 10 malt extract, 0.4 mL R2 trace elements, 1:1 dH_2O: JIC borehole H_2O
Malt-Yeast- Galactose (MYGal)	(20 agar*), 4 galactose, 4 yeast extract, 10 malt extract, 0.4 mL R2 trace elements, 1:1 dH_2O: JIC borehole H_2O
Minimal Media‡ (MM)	(10 Lab M agar*),0.5 L-asparagine, 0.5 K_2HPO_4, 0.2 $MgSO_4.7H_2O$, 0.01 $FeSO_4.7H_2O$, dH_2O, pH 7.0
Mannitol Soya Flour (SFM)	(20 Lab M agar*), 20 mannitol, 20 soya flour, JIC borehole H_2O
Difco Nutrient Agar (DN)	2.3 Difco nutrient agar, dH_2O
Minimal Media Iberian Agar‡ (MM-+)	(10 Iberian agar*), 1 $(NH_4)_2SO_4$, 0.5 K_2HPO_4, 0.2 $MgSO_4.7H_2O$, 0.01 $FeSO_4.7H_2O$, dH_2O, pH 7.0
R2 Trace Elements	0.04 $ZnCl_2$, 0.2 $FeCl_3.6H_2O$, 0.01 $CuCl_2.2H_2O$, 0.01 $MnCl_2.4H_2O$, 0.01 $Na_2B_4O_7.10H_2O$, 0.01 $(NH_4)_6 Mo_7O_{24}.4H_2O$, dH_2O

* If solid media was required then agar was added at quantities indicated in parentheses.

‡ Additional carbon sources were added to these media after re-melting the agar, prior to pouring into Petri dishes. The amount added was dependent on the carbon source and varied from 5-10 gL^{-1}.

All media were sterilised by autoclaving at 121 °C, 1.3 bar for 20 min.

2.1.2 Antibiotics

Table 2.2: Antibiotic concentrations used in this study

Antibiotic	Solvent	Final concentration in media ($\mu g.mL^{-1}$)
Apramycin sulphate (apr)	dH_2O	50
Carbenicillin sodium salt (carb)	dH_2O	100
Chloramphenicol (cml)	70% ethanol	25
Hygromycin B (hyg)	dH_2O	50
Kanamycin sulphate (kan)	dH_2O	50
Nalidixic acid sodium salt (nal)	dH_2O, 0.2M NaOH	25

2.1.3 Plasmids

Table 2.3: Plasmids used in this study

Name	Antibiotic resistance and/or relevant genotypes	Source/ reference
pLysS	Cml^R	Invitrogen
pUC57	$Carb^R$	Genscript
pET21a(+)	$Carb^R$	Invitrogen
pIJ773	$Carb^R$, Apr^R, P1-FRT-oriT-aac(3)IV-FRT-P2	JIC,(Gust, et al., 2003)
pIJ790	Cml^R, λ-RED *(gam, bet, exo), araC, rep101^{ts}*	JIC, (Gust, et al., 2003)
pUZ8002	Kan^R, RP4, *tra*	JIC, (Paget, et al., 1999)
pUC19	$Carb^R$	NEB
pMS82	Hyg^R	JIC, (Gregory, et al., 2003)
Supercos1	$Carb^R$, Kan^R	Stratagene

2.1.4 Cosmids

Table 2.4: Cosmids used to generate mutants in this study

Name	Antibiotic resistance	Source
Sv-3-D04	$Carb^R$, Kan^R	JIC
Sv-3-H03	$Carb^R$, Kan^R	JIC
Sv-6-H09	$Carb^R$, Kan^R	JIC
1-H1	$Carb^R$, Kan^R	JIC

2.1.5 Bacterial strains

Table 2.5: Bacterial strains used and generated in this study

Strain	Antibiotic resistance and/or relevant genotypes	Source/ Reference
Streptomyces venezuelae ATCC 10712	wild type (WT)	JIC
Escherichia. coli K-12 DH5α	F– Φ80*lac*ZΔM15 Δ(*lac*ZYA-*arg*F)U169 *rec*A1 *end*A1 *hsd*R17 (rK–, mK+) *pho*A *sup*E44 λ– *thi*-1 *gyr*A96 *rel*A1	Invitrogen
E. coli BL21 (DE3)	F-ompT *hsd*SB (rB- mB-) gal *dcm* (DE3)	Invitrogen
E. coli BL21 (DE3) pLysS	F-ompT *hsd*SB (rB- mB-) gal *dcm* (DE3), pLysS Cml^R	Invitrogen
E. coli soluBL21^{TM} (DE3)	F-ompT *hsd*SB (rB- mB-) gal *dcm* (DE3)*	Genlantis
E. coli BW25113	Δ(*araD-araB*)*567* Δ *lacZ4787*(::*rrnB-4*) *lacIp-4000*(*lacI*^{Q}), l-*rpoS369*(*Am*) *rph-1* Δ(rha*D*-rha*B*)*568 hsdR514*	JIC, (Datsenko and Wanner, 2000)
E. coli ET12567	*dam-, dcm-, hsdM, hsdS, hsdR,* Cml^R, Tet^R	JIC, (Macneil, et al., 1992)
S. venezuelae FM001	*ΔglgE::apr*†	This study
S. venezuelae FM002	*Δpep2::apr*	This study
S. venezuelae FM003	*ΔotsA::apr*	This study
S. venezuelae FM004	*ΔtreS::apr*	This study
S. venezuelae FM005	*ΔtreZ::apr*	This study
S. venezuelae FM006	*ΔglgP::apr*	This study
S. venezuelae FM007	*ΔglgE::apr attB*$_{\Phi BT1}$*::*pMS82	This study
S. venezuelae FM008	*ΔglgE::apr attB*$_{\Phi BT1}$*::glgE-treS*	This study
S. venezuelae FM009	*ΔglgE::apr attB*$_{\Phi BT1}$*::glgE*	This study
S. venezuelae FM010	*Δpep2::apr attB*$_{\Phi BT1}$*::*pMS82	This study
S. venezuelae FM011	*Δpep2::apr attB*$_{\Phi BT1}$*::pep2*	This study
S. venezuelae FM012	*ΔotsA::apr attB*$_{\Phi BT1}$*::*pMS82	This study
S. venezuelae FM013	*ΔotsA::apr attB*$_{\Phi BT1}$*::otsA*	This study

*This strain contains uncharacterised mutations

† This strain is a polar mutant in which the *treS* gene is not translated

2.1.6 Reagents

Table 2.6: Constituents of reagents used in this study

Reagent	Constituents
Plasmid/Cosmid isolation buffer 1 (P1)	50 mM tris(hydroxymethyl)aminomethane) (Tris)-HCl (pH 8.0), 10 mM ethylenediaminetetraacetic acid (EDTA), 100 µg mL^{-1} RNaseA
Plasmid/Cosmid isolation buffer 2 (P2)	1% (w/v) sodium dodecyl sulphate (SDS), 200 mM NaOH
Plasmid/Cosmid isolation buffer 3 (N3)	4.2 M guanidine-HCl, 0.9 M potassium acetate (pH 4.8)
Plasmid/ DNA wash buffer (PE)	10 mM Tris-HCl (pH 7.5), 80% (v/v) ethanol
1 × Tris-acetate-EDTA (TAE) DNA gel running buffer	40 mM Tris (pH 8.0), 20 mM acetic acid, 1 mM EDTA
Streptomyces cell lysis buffer	25 mM Tris (pH 8), 25 mM EDTA (pH 8), 0.3 M sucrose, 50 µg mL^{-1} RNaseA 2 mg mL^{-1} lysozyme
SET buffer	75 mM NaCl, 25 mM EDTA (pH 8), 20 mM Tris (pH 7.5)
DNA re-suspension buffer (TE)	10 mM Tris (pH 7.5), 1 mM EDTA (pH 7.5)
20 × saline sodium citrate (SSC)	3 M NaCl, 300 mM tri-sodium citrate-HCl (pH 7.0)
Denaturation solution	1.5 M NaCl, 0.5 M NaOH
Neutralisation solution	1.5 M NaCl, 0.5 M Tris-HCl (pH 7.5)
Pre-hybridisation buffer	1% (w/v) blocking reagent, 1% (v/v) *N*-lauroylsarcosine, 0.1% (v/v) 20% SDS, 25% (v/v) 20× SSC
Washing solution 1	10% (v/v) 20× SSC, 0.5% (v/v) 20% SDS
Washing solution 2	0.5% (v/v) 20× SSC, 0.5% (v/v) 20% SDS
Detection buffer 1	0.1 M maleic acid (pH 7.5), 0.15 M NaCl
Detection buffer 2	1% (w/v) blocking reagent in detection buffer 1
Detection buffer 3	100 mM Tris-HCl (pH 9.5), 100 mM NaCl
Tbf1	30mM potassium acetate, 100mM KCl, 10mM $CaCl_2$, 50mM $MnCl_2$, 15% (v/v) glycerol
Tbf2	10mM 3-(*N*-morpholino) propanesulfonic acid (MOPS) (pH 6.5), 75mM $CaCl_2$, 10mM KCl, 15% (v/v) glycerol
Buffer A	20 mM Tris-HCl (pH 7.4), 500 mM NaCl, 20 mM imidazole
Buffer B	20 Mm Tris-HCl (pH 7.4), 500 mM NaCl, 500 mM imidazole
Lugols iodine buffer	50 mM Tris-HCl (pH 7.0)

2.1.7 Preparation and transformation of electrocompetent cells

A single colony of *E. coli* was cultured overnight in selective liquid LB with agitation at 37 °C. A 1% (v/v) sample of the overnight culture was used to inoculate fresh selective liquid LB and, when the culture reached an OD_{600nm} of ~0.4, cells were harvested by centrifugation at 3000 × *g* for 5 min at 7 °C. The supernatant was decanted and the cells were gently re-suspended in an equal volume of 10 % (v/v) ice-cold glycerol. The centrifugation step was repeated as above twice and the resulting cell pellet was re-suspended in ~100 µL of 10 % (v/v) ice-cold glycerol.

A 50 µL aliquot of the cell suspension was incubated with 100 ng of DNA for 1 min in an ice-cold 0.2 cm electroporation cuvette (GeneFlow Ltd.). An electric current was applied to the mixture using a GenePulser II (Bio-Rad) set to 200 Ω, 25 µF, 2.5 kV and a time constant of between 4.6-4.8 ms was observed. This was followed by the addition of 750 µL of ice-cold LB and the incubation of the mixture with agitation at 37 or 30 °C (depending on the strain) for 60 min. Successful transformants were identified by spreading the mixture on to selective LB agar and incubating at 37 or 30 °C overnight.

2.1.8 Preparation and transformation of chemically competent cells

A single colony of *E. coli* was cultured overnight in liquid LB with agitation at 37 °C. A 2% (v/v) sample of the overnight culture was used to inoculate fresh liquid LB and, when the culture reached an OD_{600nm} of ~0.6, the culture was left in an ice water bath for 15 min. The cells were then harvested by centrifugation at 5000 × *g* for 5 min at 4 °C. The supernatant was decanted and the cells were gently re-suspended in ice-cold Tbf1 and left on ice for 30 min. After further centrifugation at 5000 × *g* for 5 min at 4 °C, the cells were gently re-suspended in 8 mL Tbf2 and then aliquoted into ice-cold tubes. Aliquots were snap-frozen in liquid N_2 and stored at -80 °C until required.

A thawed 50 µL aliquot of the cell suspension was incubated with 100 ng of DNA for 30 min on ice. The mixture was then subjected to a 30 s heat shock at 42 °C followed by the addition of liquid LB and incubation on ice for 90 s. The mixture was then incubated at 37 °C for 60 min with agitation. Successful transformants were identified by spreading the mixture on to selective LB agar. Any colonies arising after incubation overnight at 37 °C were either used or screened for presence of the plasmid.

2.1.9 Plasmid purification and quantification from *E. coli*

A single colony containing the plasmid of interest was incubated with agitation at 37 °C overnight in selective liquid LB. Cells were harvested by centrifugation at 15000 × *g*, the supernatant was discarded and the plasmid was extracted using QIAprep Spin Miniprep Kit (Qiagen) according to the manufacturers guidelines. Samples were stored at -20 °C. Plasmid concentration was determined using the NanoDrop (NanoDrop®) or by gel electrophoresis (see section 2.1.14).

2.1.10 Cosmid purification and quantification from *E. coli*

A single colony containing the plasmid of interest was incubated with agitation at 37 °C or 30 °C (depending on the strain) overnight in selective liquid LB. Cells contained in 5 mL overnight culture were harvested by centrifugation at 15000 × *g* for 1 min. The pellet was re-suspended in P1, followed by P2, mixed by inversion, and then N3 was added followed by further mixing. The sample was centrifuged as above for 5 min and the supernatant was mixed with 1:1 phenol:chloroform by vortexing for 2 min. After centrifugation, as stated above, the top aqueous layer was combined with 600 µL isopropanol and left on ice for 10 min. Further centrifugation, as stated above, resulted in a pellet of cosmid DNA, which was washed with 70% (v/v) ethanol. The remaining supernatant was removed by air drying and the pellet was re-suspended in dH_2O. Samples were stored at -20 °C. The cosmid was quantified by gel electrophoresis (see section 2.1.14).

2.1.11 Restriction digests

In a typical reaction 2 µL (~150 ng) of purified plasmid DNA was digested by incubation with 5-10 U of restriction enzyme in a 20 µL buffered solution. For cosmids, 5 µL of purified cosmid was used in a 20 µL reaction volume. Samples were incubated at 37 °C for 60 min. The samples were viewed by gel electrophoresis (see section 2.1.14).

2.1.12 Klenow filling of 5′ DNA overhangs

A 100 ng sample of DNA was incubated with 2 U of large fragment polymerase I (Invitrogen) in the appropriate buffer and with 0.08 µM dNTPs. The reaction mixture was left at room temperature for 40 min followed by heat inactivation at 70 °C for 5 min.

2.1.13 Ligation reactions

For blunt end ligations, linearised vectors were de-phosphorylated by 1 U shrimp alkaline phosphatase (SAP) and incubating in a buffered solution at 37 °C for 60 min. This was followed by deactivation of SAP at 65 °C for 15 min. The insert was phosphorylated by 1 U T4 polynucleotide kinase (PNK) in a buffered solution containing 1 mM adenosine triphosphate (ATP). After incubation at 37 °C for 60 min PNK was inactivated at 65 °C for 20 min.

The insert and vector were combined in a molar ratio of 3:1 in a 10 µL reaction volume containing 200 ng total DNA. A 10 µL volume of ligase buffer (Roche) was added and then 1 U of ligase (Roche) was added. Samples were incubated at 23 °C for 10 min and 2 µL of the reaction was used for chemical transformation.

The method used for sticky end ligations was identical to blunt end ligation with the following exceptions: the insert was not phosphorylated and a 1:1 molar ratio of insert and vector was used.

2.1.14 DNA gel electrophoresis

Typically, a 1% (w/v) TAE agarose gel was made to visualise and quantify DNA. Ethidium bromide at a concentration of 1 µg mL^{-1} was added to the molten agarose when the gel was prepared. When the gel solidified, it was transferred to a gel tank containing 1 × TAE buffer.

Typically, 1 × DNA loading dye (Invitrogen) was added to each sample and the samples were then loaded in to wells. A voltage potential of 90 V was applied to the gel so that the DNA would migrate. After 45 min, the gel was removed from the tank and the DNA was visualised by exposing to UV light of a wavelength (λ) of 360 nm. Typically, a 1 kilobase pair (Kbp) DNA ladder (NEB) was used as a standard.

2.1.15 Preparation of digoxygenin (DIG) labelled probe for Southern hybridisation

A 500 ng sample of purified cosmid in a total volume of 15 µL was boiled for 10 min and then stored on ice for 10 min. The sample was centrifuged briefly at 15000 *× g* and 2 µL of 10 × hexanucleotide mixture (vial 5 DNA DIG labelling kit, Roche), 2 µL of 10 × dNTP labelling mixture (vial 6 DNA DIG labelling kit, Roche) and 1 µL of Klenow enzyme (vial 7

DNA DIG labelling kit, Roche) was added to the sample. The sample was mixed by flicking and centrifuged briefly at 15000 × *g* and incubated at 37 °C for 20 h.

2.1.16 Preparation of blot for Southern hybridisation

A 8 µg sample of gDNA in a maximum volume of 43 µL was incubated in a buffered solution with 20-30 U of restriction enzyme overnight at 37 °C. The following day, 1 × loading dye was added to the sample and it was loaded on to a 0.6 % (w/v) agarose gel with a thickness of ~2.5 cm. The gel was run at 45 V for ~7 h. The gel was then stained in 1 µg mL^{-1} ethidium bromide, DNA was visualised under UV light and the gel was de-stained in dH_2O. The gel was soaked in 0.25 M HCl for 20 min, followed by soaking in denaturation buffer for 30 min and then soaked for 30 min in neutralisation buffer.

A nylon Amersham N+ membrane (GE healthcare) was soaked in 2 × SSC. The membrane was placed on top of the gel and capillary blotting was performed overnight. The membrane was then soaked in 2 × SSC and the DNA was cross-linked using a UV-cross-linker (Stratagene). The blot was transferred to a tube containing 20 mL pre-hybridisation buffer and incubated with rotation for 2 h at 68 °C. The DIG-labelled probe was then boiled for 10 min, stored on ice for a further 10 min and 30 mL of ice-cold pre-hybridisation buffer was added. The pre-hybridisation buffer was replaced with hybridisation buffer and incubated overnight with rotation at 68 °C. The blot was then washed twice in washing solution 1 for 5 min. Followed by incubation twice with washing solution 2 for 15 min at 68 °C. Afterwards the blot was incubated in detection buffer 1 for 1 min followed by detection buffer 2 for 60 min. Detection buffer 2 was replaced with detection buffer 2 containing anti-DIG antibodies (15 µL antibodies in 50 mL of buffer) and incubated for 60 min. The blot was then washed for 15 min in detection buffer 1 and transferred to detection buffer 3. Colour solution was prepared by dissolving a SIGMAFAST™ BCIP®/NBT tablet (Sigma) in 10 mL water in the dark. The blot was transferred to a PVC bag containing the colour solution and incubated in the dark until bands were visible.

2.1.17 DNA sequencing

In order to determine the sequence of DNA, a sequencing reaction was carried out. Typically 1 µL of plasmid DNA was mixed with 2 µL 5 × sequencing buffer, 1 µL (v/v) 30% dimethyl sulfoxide (DMSO), 1 µL of 2 µM primer, 4 µL dH_2O and 1 µL Big Dye v3.1

(Life Technologies). The reaction mixture was subjected to the following cycling conditions:

1. 96 °C, 2 min
2. 96 °C, 15 s
3. 50 °C, 10 s
4. 60 °C, 4 min
5. 2 °C, 2 min

Steps 2-4 were repeated 24 times before step 5 was carried out. The samples were submitted for analysis (Eurofins) and the sequences were determined using Chromas2 (Technelysium) software.

2.2 Protein methodologies

2.2.1 Sequence design

The DNA sequence of all genes used for heterologous protein expression in this study were synthesised with optimum codon usage for expression in *E. coli* (Genscript). The sequences were flanked at the 5' end by an Nde I restriction site and a sequence encoding a His_6-tag and a TEV protease cleavage site, and at the 3' end by a Bam HI restriction site (for the exact sequences see Appendix). The genes were supplied in pUC57 vectors.

2.2.2 Protein over-production

All genes were sub-cloned in to a pET-21a (+) (Novagen) vector and heterologously expressed in strains of *E. coli* BL21(DE3) (see table 2.7). Cells containing the expression plasmid were cultured in selective liquid media at 37 °C (see table 2.7). When the cells reached an OD_{600nm} of 0.6, expression was induced by the addition of isopropyl β-D-1-thiogalactopyranoside (IPTG). In some instances the temperature was lowered and additives, like DMSO, were added to aid soluble expression of the protein of interest (see table 2.7). After further incubation, the cells were harvested by centrifugation at 1700 × *g* for 10 min at 4 °C and re-suspended in 30 mL of buffer A containing 6 mg mL^{-1} DNase 1 and a cOmplete™ protease inhibitor cocktail tablet (Roche). The cells were disrupted with a TS Series Benchtop 1.1 kW cell disruptor (Constant Systems Ltd.) at 25 kPSI. The resulting cell lysate was separated from the cell debris by centrifugation at 20000 × *g* for 25 min at 4 °C.

The proteins were purified from cell lysates by application onto a 1 mL FF HisTrap column (GE Healthcare). After subsequent application of 10 column volumes of buffer A, the proteins were eluted with buffer B. Typically the proteins were further purified using a HiLoad 16/600 Superdex 200 size exclusion chromatography column (GE healthcare) equilibrated with different buffers (see table 2.7). Fractions that contained the protein were combined, concentrated and in some cases were solvent exchanged, using an Amicon Ultra-15 centrifugal filter unit with a 30 kDa cut-off (MerckMillipore) and centrifugation at 5000 × *g*. Aliquots of proteins were stored at either 4 or -20 °C.

2.2.3 SDS- polyacrylamide gel electrophoresis (PAGE) of protein samples

Pre-cast 12% (w/v) SDS-PAGE gels (Expedeon Ltd.) were used to determine if the correct sized protein was present in solution. Samples were prepared by the addition of 1 × RunBlue LDS Sample buffer (Expedeon Ltd.) followed by heating at 98 °C for 5 min. Samples were loaded into individual wells, in addition, a molecular weight marker (Expedeon Ltd.) was also added to one of the wells. Gels were run in 1 × SDS running buffer at 200 V for 45 min. The gel was stained with InstantBlue (Expedeon Ltd.) for 20 min.

2.2.4 TEV-protease cleavage of His_6-tag

A 2.5 mg sample of protein in 1 mL was incubated overnight with 100 µL TEV-protease in a buffer of 50 mM Tris, pH 8 and 150 mM NaCl. The following day a final concentration of 30 mM imidazole was added to the reaction and the whole solution was applied onto a FF HisTrap column. The flow-through, containing protein with His_6-tag cleaved, was collected and purity was checked by SDS-PAGE. All of the flow-through was concentrated and solvent exchanged.

2.2.5 Protein concentration determination

Protein concentration was determined either using the Bradford assay (Bradford, 1976) or DirectDetect (MerckMillipore). For the Bradford assay a standard curve was generated by recording the A_{595nm} of solutions with different concentrations of bovine serum albumin (BSA). A 100 µL sample of protein solution was incubated with 200 µL 1:5 Bradford reagent (Bio-Rad) and 700 µL H_2O for 20 min. After incubation the A_{595nm} was measured.

Table 2.7: Culture conditions for all proteins used in this study

Protein name	Source organism	*E. coli* expression strain	Storage temp. (°C)	Storage buffer	Culture conditions				
					Liquid media	Amount (L)	Temp. (°C)	Growth duration (h)	IPTG conc. (mM)
TreS	*Mycobacterium tuberculosis* H37Rv	BL21(DE3) pLysS	- 20	100 mM Na citrate, pH 6.7	Lx	2	37	20	0.5
Pep2	*M. tuberculosis* H37Rv	BL21(DE3)	4	25 mM bistris-propane (BTP), pH 7.5, 50 mM NaCl	AIM	4	18	20	N/A
TreS-Pep2	*Pseudomonas aeruginosa* PAO1	SoluBL21 (DE3)	-20	20 mM HEPES, 150 mM NaCl, pH 7.5	SOC	6	18	20	1+ 0.2% (v/v) DMSO
OtsA	*S. venezuelae* ATCC 10712	SoluBL21 (DE3)	4	5 mM HEPES, 60 mM $MgCl_2$, pH 7.0	LB	3	37	20	1
GalU	*S. venezuelae* ATCC 10712	BL21 (DE3) pLysS	-20	20 mM Tris, 100 mM NaCl, 10 % (v/v) glycerol, pH 8.0	LB	2	28	20	1

2.2.6 Protein identification by matrix-assisted laser desorption/ionization-time-of-flight mass spectrometry (MALDI-TOF MS)

SDS-PAGE gel slices containing the predicted protein of interest were submitted to the JIC proteomics facility. The subsequent procedures were performed by G. Saalbach.

Samples were washed, treated with trypsin, and extracted according to standard procedures adapted from Shevchenko et al. (2007). The resulting peptide solution was spotted onto a Prespotted AnchorChip™ MALDI target plate (PAC plate) (Bruker Daltonics), and the spots were washed with 10 mM ammonium phosphate, 0.1% (v/v) trifluoroacetic acid.

Samples were dried and then analysed by MALDI-TOF MS on a Bruker Ultraflex TOF/TOF. The instrument was calibrated using the pre-spotted standards (ca. 200 laser shots). Samples were analysed using a method optimised for peptide analysis and spectra were summed from ca. 30 x 15 laser shots. Data were processed in FlexAnalysis (Bruker) and submitted for a database search using an in-house Mascot Server 2.2 (Matrixscience), comparing against a Uniprot database with taxonomy set to actinobacteria. For the search criterion, the enzyme was set to trypsin with maximum one missed cleavage using a peptide mass tolerance of 50 ppm. Carbamidomethyl (C) was used as fixed and oxidation (M) as variable modification.

2.2.7 Dynamic light scattering (DLS) of proteins

The oligomeric states of some proteins were determined by DLS (Wyatt Technology). The technique also indicated if proteins had a tendency to aggregate. Samples were passed through a 0.1 µm filter (MerckMillipore) by centrifugation at 12000 × *g*. A 12 µL sample of protein was transferred to a microsampling cell (Wyatt Technology) and 20 scattering measurements were recorded at 20 °C. Data analyses were performed using DYNAMICS V6 software (Wyatt Technology).

2.3 Enzymology methods

2.3.1 Nuclear magnetic resonance (NMR) spectroscopy

Spectra were recorded using a Bruker Avance III 400 spectrometer using standard pulse sequences and a probe temperature of 25 °C at 400 and 376 MHz for proton (^{1}H) solvent-suppressed and fluorine (^{19}F) proton-decoupled spectra, respectively. Chemical shifts are expressed in parts per million (ppm) relative to internal H_2O (4.70 ppm) or $CFCl_3$ (0.00 ppm). Spectra were analysed using Topspin 3.0 (Bruker) and resonances were integrated manually to ensure consistency. NMR spectra associated with trehalose, maltose, maltose 1-phosphate and glucose were assigned using COSY and HSQC experiments, which were consistent with the literature (Usui, et al., 1974).

2.3.2 TreS enzymology

For ^{1}H-NMR spectra, the co-suppression of resonances within 1 ppm of that of solvent was determined with control samples using citrate as an internal standard. A spectrum with solvent suppression of trehalose (10 mM), maltose (10 mM) in 90 mM citrate buffer, pH 6.7, and 10% (v/v) D_2O was compared with that of an identical sample without solvent-suppression after freeze drying and reconstitution in 100% D_2O. The four resonances from the citrate buffer arise from a second order spin system centred on 2.52 ppm that is remote from those of solvent (4.70 ppm) and carbohydrates. Doublet signals associated with α/β-maltose H-1′ (5.32 ppm) and trehalose H-1 (5.10 ppm) gave 89 and 87% of the expected integrals, respectively. Since the ratio of maltose anomers changed as a function of D_2O concentration, it was not possible to directly determine the degree of suppression of the maltose H-1 resonance (5.14 ppm) with confidence. However, since suppression was a function of how close the chemical shift was to that of solvent and the maltose H-1 resonance was between those of maltose H-1′ and trehalose H-1, the maltose H-1 signal was estimated to be 88% of that expected. The double doublet H-2 resonances associated with the β anomers of maltose and glucose (3.19 and 3.15 ppm, respectively) were distant enough from solvent (4.70 ppm) not to be suppressed. The corresponding doublet H-1 resonances of the β anomers (4.57 and 4.56 ppm, respectively) were too significantly supressed, so were not used to quantify reaction products. Thus, resonances associated with trehalose H-1, α/β-maltose H-1′, β-maltose H-2, and β-glucose H-2 were used to

quantify these species. The amount of α-maltose could then be calculated by subtracting the amount of β-maltose from that of α/β-maltose. Although the resonances of the α anomers of maltose and glucose overlapped completely, the concentration of α-glucose could be calculated by subtracting the amount of α-maltose from the combined amounts of the α anomers.

2.3.3 OtsA activity assay

A 0.26 µM sample of OtsA was incubated with 1 mM glucose 6-phosphate, 1 mM nucleotide diphosphate (NDP)-glucose and 1 mM $MgCl_2$ in deuterated buffer at pH 7.0. The reactions with different NDP-glucoses were monitored using solvent suppressed ^{1}H-NMR, as described in section 2.3.2.

Integrals of a doublet of doublet signal associated with H-1 bonded to the anomeric carbon of the glucose molecule of the NDP-glucose (~5.5 ppm) and a doublet signal associated with H-1 of trehalose 6-phosphate (5.10 ppm) were used to determine the substrate to product ratio. Both the doublet of doublet of the NDP-glucose and the doublet of trehalose 6-phosphate represented a single H per molecule. These allowed a percentage conversion to be determined for each selected time-point with different NDP-glucose substrates and therefore the substrate preferences of OtsA.

2.3.4 GalU activity assay

Activity of GalU was monitored by measuring the release of pyrophosphate (PPi) using a malachite green stopped assay. First a standard curve was generated by adding a known concentration of phosphate (Pi) and recording the corresponding A_{630nm} when incubated for 5 min with malachite green. A 2 µM sample of GalU was incubated with 1 U pyrophosphorylase, 1 mM glucose 1-phosphate and 2 mM nucleotide triphosphate (NTP) in a 50 mM MOPS pH 8.0 buffer containing 10 mM $MgCl_2$. Reactions were incubated at 37 °C for 20 min and 10 µL of each assay mixture was quenched with 90 µL of 1 M HCl. The stopped reaction mixture was combined with 700 µL of malachite green and the A_{630nm} was recorded after 5 min. A standard curve was used to determine the PPi released during the reaction. A hierarchy of the substrate preferences of GalU was determined by comparing the Pi released when GalU was incubated with different NTPs.

2.3.5 Pep2-TreS activity assay

A sample of TreS-Pep2 was incubated with 10 mM trehalose, 10 mM $MgCl_2$ and 5 mM ATP in a 20 mM 4-(2-hydroxyethyl)-1-piperazineethanesulfonic acid (HEPES) buffer at pH 7.5 containing 150 mM NaCl. The reaction mixture was incubated at 37 °C and 0.5 µL samples were spotted periodically on silica coated aluminium thin layer chromatography (TLC) plates (MerckMillipore). The TLC plate was run in a 85:20:20:50 acetonitrile:ethylacetate:isopropanol:H_2O solvent system. Spots were visualised by submerging the plate in 80% H_2SO_4 in ethanol followed by charring.

2.3.6 Pep2 activity assay

Samples of Pep2 were incubated with 10 mM maltose, 10 mM $MgCl_2$ and 10 mM ATP in a 25 mM bis-tris propane buffer at pH 7.5 containing 50 mM NaCl. The reaction mixture was incubated at 37 °C and 0.5 µL samples were spotted periodically on silica coated aluminium TLC plates (MerckMillipore) and processed as described in section 2.3.5.

2.4 Protein crystallographic methods

Protein structures were determined in collaboration with C.E.M. Stevenson (JIC), D. M. Lawson (JIC) and scientists at the Diamond Light Source (Oxford).

2.4.1 Crystallisation trials

Protein crystallisation trials were set up in a 96-well MRC plate (Molecular Dimensions) format using the following screens: JCSG-plus (Molecular Dimensions), PACT premier (Molecular Dimensions), Structure (Molecular Dimensions), Morpheus (Molecular Dimensions), ammonium sulphate (Qiagen) and PEG suite (Qiagen). Protein concentrations of between 10-15 mg mL^{-1} were used in each condition. Each reservoir was filled with 50 µL of the screen using the Freedom evo liquid handling robot (Tecan). A 0.3 µL sample of precipitant was subsequently mixed with 0.3 µL protein in a sitting drop format using an OryxNano robot (Douglas Instruments Ltd.). The plates were sealed and stored at 20 °C. Screens were checked regularly using a SMZ800 microscope (Nikon) to monitor physical changes in the drops. Conditions that yielded poor or fragile crystals were optimised further in a 24-well hanging drop format using VDX optimisation plates (Molecular Dimensions) with a reservoir volume of 1 mL and by mixing 1 µL of precipitant with 1 µL protein.

2.4.2 Crystal storage and transport

Crystals were removed from the crystallisation condition using litho-loops (Molecular Dimensions) and, if required, were soaked in cryo-protectant solution comprising the mother liquor with an additional 5% (v/v) glycerol. They were then flash-cooled by plunging into liquid N_2 and stored in unipuck casettes for transport to Diamond Light Source (Didcot, UK) for data collection.

2.4.3 Data collection and processing

X-ray data were collected on the macromolecular crystallography beamlines (i02 and i04-1) or the microfocus beamline (i24), with X-ray diffraction recorded on a Pilatus 2M and 6M detectors (Dectris). Three test images collected at phi = 0°, 45° and 90° were used to determine the quality of diffraction, to estimate the resolution, to establish the crystal symmetry and cell parameters, and to derive a data collection strategy. The resultant datasets were then processed using the *XIA2* expert system (Winter, 2010) and scaled using SCALA (Evans, 2006). A 5% subset of the total number of reflections was set aside in order to determine the free R factor (Kleywegt and Brunger, 1996) during model building and refinement. All subsequent processing was conducted using the CCP4 suite (Winn, et al., 2011).

2.4.4 Molecular replacement, model building and refinement

All structures in this study were solved by molecular replacement using PHASER (McCoy, et al., 2007). Crystal structures of the same enzyme from different organisms were used as the search model and these had between 30-40% amino acid conservation to the target structures. Density modification was carried out using PARROT (Cowtan, 2010) and model building into the maps from PARROT performed with Buccanneer (Cowtan, 2006). Model building was carried out using COOT software (Emsley and Cowtan, 2004) alternating with refinement with REFMAC (Murshudov, et al., 1997).

2.4.5 Structural validation

Validation was carried out throughout to ensure no bias had been introduced during the refinement process. A number of tools within the COOT suite (Emsley and Cowtan, 2004) were utilised, including Ramachandran plots (Ramachandran, et al., 1963),

modelling in molecules of H_2O in extra density regions as well as minor adjustments to the amino acid backbone and side chain angles so that they better represented the observed electron density. Validation was also carried out using MOLPROBITY (Chen, et al., 2010).

2.5 *Streptomyces venezuelae* methods

2.5.1 Generation of *S. venezuelae* mutants

All mutants of *Streptomyces* were generated using PCR targeting via the REDIRECT™ method (Gust, et al., 2003). The method utilises endogenous conjugation and homologous recombination. Primers were designed using the same method as Gust et al., 2003. The primers comprise 2 parts; one part contains sequence flanking the gene of interest and the other part contains sequence complementary to the disruption cassette (Table 2.8). The cassette contains a marker conferring resistance to an antibiotic and the apr resistance cassette was used in this study.

The disruption cassette used as a template for the PCR was generated by double digestion of pIJ773 with Eco RI and Hind III. The cassette was separated from the vector plasmid by gel electrophoresis and the band containing the cassette was gel purified using a QIAquick gel extraction kit (Qiagen) following the manufacturer's protocol. The resulting DNA was tested for absence of circularised plasmid contaminant by transformation. If the transformation yielded no colonies, it indicated that only the linear cassette was present. This was subsequently used as the template for PCR. PCR was performed using Expand High Fidelity Polymerase (Roche) according to the manufacturer's guidelines. The reaction mixture contained 50 pmoles of each primer, 50 ng template DNA, 1 x polymerase buffer, 50 µM of each dNTP, 5% DMSO and 2.5 U polymerase, and was made up to 50 µL using dH_2O. Typically the following cycling conditions were used:

1. 94 °C, 2 min
2. 94 °C, 45 s
3. 50 °C, 45 s
4. 72 °C, 90 s
5. 94 °C, 45 s
6. 55 °C, 45 s
7. 72 °C, 90 s

8. 72 °C, 5 min

Steps 2-4 were repeated 9 times and steps 5-7 were repeated 14 times.

A 4 µL sample of the PCR product was analysed by DNA gel electrophoresis and, if the correct sized product was generated, the remaining product within the reaction mixture was purified with a MiniElute PCR purification kit (Qiagen) according to the manufacturer's guidelines.

A single colony of *E. coli* BW25113/pIJ790 was grown overnight at 30 °C in selective liquid LB. A 1% (v/v) sample of the overnight culture was used to inoculate selective SOB supplemented with 20 mM $MgSO_4$. When OD_{600nm} reached ~0.4, the cells were recovered by centrifugation at 3000 *× g* for 5 min at 7 °C. The cells were then made electrically competent and transformed with an extracted cosmid containing the gene of interest. Successful transformants were screened by culturing colonies overnight to allow the extraction of a sufficient concentration of cosmid, followed by restriction digests and gel electrophoresis. The restriction pattern was compared to the expected pattern. If the two patterns matched, then a sample of the same colony was used to inoculate fresh selective liquid LB. A 1% (v/v) sample was used to inoculate selective SOB containing 10 mM L-arabinose to induce expression of *λ red* genes present on pIJ790. When OD_{600nm} reached ~0.4, the cells were recovered by centrifugation at 3000 *× g* for 5 min at 7 °C. The cells were then made electrically competent and transformed with 100 ng of the extended apr disruption cassette. Successful transformants were screened by extracting the cosmid containing the disruption cassette and testing with restriction enzymes. When a cosmid with a restriction pattern as predicted was found, it was used to transform *E. coli* ET12567/pUZ8002 by electroporation.

Successful transformants were re-cultured in 10 mL selective liquid LB until cells reached an OD_{600nm} of ~0.4. The cells were then harvested by centrifugation at 3000 *× g* for 5 min at 7 °C, washed twice with liquid LB and re-suspended in 0.5 mL liquid LB. They were then mixed with 20 µL WT *S. venezuelae* spores and plated onto SFM agar. Plates were left overnight at room temperature. The plates were subsequently overlaid with 1 mL dH_2O containing 0.5 mg nal and 1.25 mg apr and were stored at 30 °C for 3-4 days. Successful transformants appeared as white colonies and were subjected to 3 further rounds of selective re-streaking and replica plating to test for Apr^R Kan^S. Spore stocks of clonal strains were generated and colony PCR and/or Southern hybridisation

were used to confirm integration of the disruption cassette in the intended region of the genome.

Table 2.8: Primers used to generate mutants in this study

Oligonucleotide name	Sequence (5'- 3')
F: Pep2 ReDirect	AGTCCATTGCGCACCCCGGGGAAAGGACGCGATGCCATGATTCCGG GGATCCGTCGACC
R: Pep2 ReDirect	CGGCTGGGCGGAGGAGCCTGGGGCGGGGGGTGGTGGTCATGTAGG CTGGAGCTGCTTC
F: SVEN_6388	ATGAAACTGACGATTCTCGGAGGCGGCGGGTTCCGGGTGATTCCGG GGATCCGTCGACC
R: SVEN_6388	GGTTCCCCGACGGCCGGAACCCTCGCATCCGCCCGATCATGTAGGCT GGAGCTGCTTC
F 7731 ReDirect	GCGACCGTCCCCGCAGACCGGAGGGTCACCCACATCATGATTCCGGG GATCCGTCGACC
R 7731 ReDirect	CCGTCCCACCCCGGACGTATCCGAACTGACCGGCGGTCATGTAGGCT GGAGCTGCTTC
F: otsA	CGTTTGAGCGTTTACGGGACGGGCTAGGTTCGCCACATGATTCCGGG GATCCGTCGACC
R:otsA	CTGGAGCGGCCCCCACCTCGACAAGGTTCCAGGCGCTCATGTAGGCT GGAGCTGCTTC
F: GlgP	TGGTGCGTCCACTCCGCTCCGTACTCGCCTGCGAAGGTGATTCCGGG GATCCGTCGACC
R: GlgP	CCCTGAGCCGCCCGGGGCCGATCCGAAGGGCGGCCCCTATGTAGGCT GGAGCTGCTTC
F: TreZ	GATGGGGGCGTAGGTCCGTCGACGAGGGGATTTGGCGTGATTCCGG GGATCCGTCGACC
R: TreZ	ATGGCCCTCGTCGAATAGCACGGCCGCGCGGCGGGCTCATGTAGGCT GGAGCTGCTTC
SMD07732 FORWARD	GACCCGCCATCCGAGTGAACGCGGACAGGAGCGGCCATGATTCCGG GGATCCGTCGACC
SMD07732 REVERSE	TGTCCTCGAAGGTGTCGGGGACGGGCTCGTTGACAGTCATGTAGGCT GGAGCTGCTTC
SMD07728 Forward	GCCACACATACCCCCGTACCCCCAGGAGGCACCCCGGTGATTCCGGG GATCCGTCGACC

2.5.2 Preparation of *Streptomyces* genomic deoxyribonucleic acid (gDNA) for PCR

S. venezuelae was cultured overnight in 10 mL liquid MYM and 1.5 mL was harvested by centrifugation at 18000 × *g*. The cell pellet was re-suspended in 500 µL of *Streptomyces* lysis buffer and incubated at 37 °C for 30 min. A 250 µL sample of 2% (v/v) SDS was added to the sample and mixed by vortexing. A 250 µL sample of 1:1 phenol: chloroform was added and mixed by vortexing. Phase separation was reached by centrifugation at 18000 × *g* for 3 min. The top aqueous layer was transferred to another tube and the above process was repeated until little or no white interface was

observed. A 0.1 volume sample of 3 M sodium acetate, pH 4.8, was added to the separated aqueous layer, followed by 1 volume of isopropanol. The mixture was incubated at room temperature for 5 min and a glass Pasteur pipette was used to spool out the visible fragments of gDNA. The gDNA was dipped in 70% (v/v) ethanol and re-dissolved in 500 µL of water by gently flicking the tube. When the gDNA was completely re-dissolved it was stored at 4 °C.

2.5.3 Preparation of *Streptomyces* gDNA for Southern hybridisation

S. venezuelae was cultured overnight in 10 mL liquid MYM and was harvested by centrifugation at 5000 × *g* for 7 min. The cells were washed with 10% (v/v) sucrose and re-suspended in 2 mL SET buffer. A 0.02 mg sample of RNase and 0.8 mg lysozyme were added and the mixture was incubated at 37 °C for 60 min. This was followed by the addition of 1.12 mg of proteinase K and 240 µL of 10% (v/v) SDS and incubating at 55 °C for 2 h with occasional mixing by inversion of the tube. Afterwards, 800 µL of 5 M NaCl was added and the mixture was allowed to cool so that 2 mL chloroform could be added. The mixture was mixed by hand for 30 min at room temperature and subsequently centrifuged at 6000 × *g* for 15 min. The supernatant was combined with 0.6 volumes of isopropanol. After gentle mixing, strands of DNA were visible and were spooled out with a glass Pasteur pipette and dipped in 70% (v/v) ethanol. The DNA was re-suspended in 100 µL TE by gentle flicking and heating to 60 °C. When dissolved the sample was stored at 4 °C.

2.5.4 Generating complemented strains

WT gDNA was extracted and used as a DNA template for PCR. Primers were designed flanking the gene of interest (Table 2.9). The forward primer was selected to be approximately 300 base pairs (bp) upstream of the start codon so as to ensure the endogenous promoter and ribosome binding site were amplified.

PCRs were carried out using either Q5 (NEB) or Phusion (NEB) polymerases using conditions and reagents recommended by the manufacturer. Typically, 4 µL of PCR product was analysed by gel electrophoresis. If the product was the correct size, the remainder of the DNA was purified using QIAquick PCR purification kit (Qiagen) following the manufacturer's guidelines. The PCR product was phosphorylated, ligated to a de-phosphorylated pUC19 vector and the resulting plasmid was transformed into *E. coli* DH5α. Blue-white screening (Vieira and Messing, 1982) was used to select for

transformants containing the circularised vector with insert and the plasmids were sequenced using M13 primers (Table 2.9). If the insert had the same sequence as WT, it was removed from the vector by restriction digestion and purified by gel extraction. The 5' overhangs of the insert were filled using klenow large fragment polymerase I (Invitrogen) and subsequently ligated into a linearised (with Eco RV), de-phosphorylated pMS82 vector and transformed into *E. coli* DH5α. Transformants were screened by extracting the plasmids followed by restriction digestion. If the correct insert was present, then the plasmid was transformed into ET12567/pUZ8002 by electroporation and conjugated with the appropriate mutant strain on SFM agar media. pMS82 confers resistance to hyg, therefore overlays contained nal as well as 1.25 mg hyg and were incubated at 30 °C in the dark. Successful exoconjugants appeared as white colonies and were selectively re-streaked 3 times on DN agar media.

2.5.5 Cell-free extract preparation for ^{1}H-NMR spectroscopy

Spores were counted by plating out a dilution series and counting colony forming units (CFUs). All spore stocks were standardised to 1×10^{9} CFUs and 5 µL was mixed with 70 µL dH_2O and plated on to cellophane discs placed on top of 25 mL MYM-Agar. The spores were distributed evenly throughout the Petri-dish using spreaders (VWR) and left to dry in the flow hood for ~30 min. After incubation for certain times at 30 °C, the cells were scraped off the cellophane disc and placed into a tube. The cells were then dried overnight by freeze-drying. When dry, the cells were powdered using a micro-pestle.

For each sample, 25 mg of dry, powdered *S. venezuelae* were weighed and re-suspended in 800 µL of water by vortexing. The samples were then boiled for 7 min and left to cool on ice. Once cool, the samples were sonicated using a 500 W ultrasonic processor (SONICS®) for 10 cycles of 30 s on and 30 s off at 40% amplitude. The cell debris was pelleted by centrifugation at 18000 *× g* for 30 min at 4 °C. Typically, 540 µL of the cell free extract was transferred to a tube containing 60 µL D_2O and 4 µL deuterated trimethylsilyl propanoic acid (TMSP-d_4).

Table 2.9: Primers used to test mutants and generate complementation plasmids

Oligonucleotide name	Sequence (5'- 3')
7732 Test Forward	CCGCCCTACAAGGGCGGGG
7732 Test Reverse	CGGCGGCAGCCAGAGGCAG
7728 Test Forward	CGGACTGGCTCCCGGTCCC
Test forward 7732	CCCTACAAGGGCGGGGTCT
Test reverse 7732	CAGCCAGAGGCAGTCCACG
7732 Flanking forward	GTCCGGTGTCCGTGCTTGC
7732 Flanking reverse	GTCCCCGTTGCTGTCCTGG
F 7732 complementation plasmid	CTGGTCGACGGATCCGTCC
Complementation treS R	GGGACGGGAGGAAACCGTC
Complementation glgB R	CGGGCTGCCCGAACAGGTG
Internal sequencing TreS	CTGCCTCTGGCTGCCGCCG
Internal sequencing TreS v2	GGAGCGGGCCGGTACCACG
TreS test F	GGAACTCGGCCTCGACTGGC
TreS test R	GGGTGCGCAATGGACTGTCG
SVEN_6388 test F	GGTCTTGCGTCGGGACATGG
SVEN_6388 test R	CCAGAAGGCAGGCGGTGACG
ostA test F far	CGATGGCCGCGACCGGCG
ostA test F close	CGTATACGTACGTTTGAGCG
ostA test R	CCGGTTTTCACGACCTGGCG
TreZ test F	CCTGGGCAACGTCCCGATGG
TreZ test R	CGAACCCGGCGTCTACCTGC
GlgP test F	CCCGGCCATCGGCTGAGACG
GlgP test R	CGGCCGGCATGGACGAGTGC
F GlgP Complement	GTCCATCGTCGACGCGCGC
R GlgP Complement	CTAGCGGAGCAGCACCCCC
F OtsA Complement	GACCGGCCCAAGCCCACCC
R OtsA Complement	TCAGGCGTCGCTCAGCCCC
F TreZ Complement	GTGCCGGAGCCGAAGGGCC
R TreZ Complement	TCAGCCGTCCGTCAGGAGG
F TreS+IR Complement	GGAGCGGCCATGACTGTCAACGAGCCCG
R IR+TreS Complement	GTTGACAGTCATGGCCGCTCCTGTCCGCG
F Internal seq GlgP	CTGCCCGGCGGCCGCAGC
R Internal seq GlgP	GAGGACGGAGAGGTTGAG
Pep2 Comp F	GGTCAGTTCGGATACGTCCG
Pep2 Comp R	GTCATGGGCTGGTGGAGAGG
F M13	GTAAAACGACGGCCAGT
R M13	AACAGCTATGACCATG

2.5.6 Lipid derivitisation and gas chromatography mass spectrometry (GCMS) analysis

Powdered freeze dried cells were prepared as stated in section 2.5.5 and 10 mg of sample was weighed into a glass tube (Agilent Technologies) containing 0.75 mg benzoic acid in methanol. The samples were derivitised by the addition of, 500 µL chloroform and 500 µL 15% (v/v) sulphuric acid in methanol followed by heating at 100 °C for 4 h. After cooling, 1 mL dH_2O was added and the sample was left until phase separation occurred. The lower phase was collected into a separate tube and was used for GCMS analysis.

Analysis was performed on an Agilent GCMS 6890N (Agilent Technologies) by A. Jones (JIC) equipped with a ZB-5HT column (with the dimensions: 30 m by 0.25 mm by 0.10 µm) (Zebron). A 2 µL sample was injected (pulsed splitless, 30 psi for 2 min) on to the column per run and Helium (1 mL min^{-1}) was used as the carrier gas with an inlet temperature of 250 °C, interface temperature of 280 °C, source temperature of 230 °C and a quadrupole temperature of 150 °C. A temperature programme was used as follows: 60 °C for 3.0 min, temperature ramp of 20 °C min^{-1} until 350 °C was reached.

2.5.7 Glycogen quantification with Lugol's iodine

Freeze dried and powdered cells were prepared as previously described and 25 mg were re-suspended in 600 µL Lugols iodine buffer, by vortexing. Samples were boiled for 7 min and then cooled on ice. Once cool, the samples were sonicated using a 500 W ultrasonic processor (SONICS®) for 10 cycles of 30 s on and 30 s off at 40% amplitude. The cell debris was pelleted by centrifugation at 18000 × *g* for 30 min at 4 °C. Typically, 300 µL of the cell-free extract was mixed with 580 µL 50 mM Tris-HCl, pH 7.0 and 120 µL of Lugol's iodine solution (Sigma). The mixture was transferred to a 1.5 mL plastic cuvette (Sarstedt Ltd.) and sealed with parafilm (Slaughter Ltd.) and the colour was allowed to develop for 3 min. Spectra were recorded on a Lambda 25 spectrophotometer (Perkin Elmer) in the region between 900 nm until 400 nm. Sample spectra were analysed using WinLab software (Perkin Elmer).

2.5.8 Spore abiotic stress resistance tests

Spores were harvested by coating a plate with sterilised, acid-washed glass balls. Typically, 500 µL dH_2O was added to 5 spore coated balls, samples were subsequently

sonicated using a 500 W ultrasonic processor (SONICS®) for 4 cycles of 15 s on and 45 s off at 40% amplitude. Samples were then treated with their respective stresses: 0.5 µg lysozyme, sonication, heat shock or desiccation (at a relative humidity of 0% for 8 h). Serial dilutions of the spores were generated before and after stress treatments. A 100 µL sample of each dilution was plated and CFUs were counted after incubation at 30 °C for 1-2 days.

2.6 Microscopy methods

All samples for electron microscopy were prepared for imaging and imaged by either E. Barclay (JIC) or K. Findlay (JIC).

2.6.1 Sample preparation for transmission electron microscopy

Single colonies of *Streptomyces* were cut out of the agar and placed in a solution of 2.5% (v/v) glutaraldehyde in 0.05M sodium cacodylate, pH 7.3, and left overnight to fix the samples (Gordon, et al., 1963). The fixative was washed out by three successive 10 min washes in 0.05 M sodium cacodylate and then the samples were placed in a EM TP machine (Leica, Milton Keynes) to proceed with the remaining steps automatically; post-fixed in 1% (w/v) OsO_4 in 0.05M sodium cacodylate for 60 min at room temperature. This was followed by three 15 min washes in distilled water before beginning the ethanol dehydration series (10%, 20%, 30%, 50%, 70%, and 95% each for a minimum of 30 min, then two changes of 100% ethanol each for 60 min) (Beringer, et al., 1977). Once dehydrated, the samples were gradually infiltrated with LR white resin (London Resin Company, Reading, Berkshire) by successive changes of resin:ethanol mixes for at least 60 min each at room temperature (1:1, 2:1, 3:1) then 100% resin for 16 h and repeated with fresh resin for a further 8 h. The samples were then removed from the EM TP machine and transferred into gelatin capsules filled with LR White resin and placed at 60 ^{o}C for 16 h to polymerise.

The resulting material was sectioned with a diamond knife using a UC6 ultramicrotome (Leica, Milton Keynes). Ultrathin sections of approximately 90 nm were picked up on 200 mesh gold grids which had been coated in pyroxylin and carbon. For contrast staining, the sections were stained with 2% (w/v) uranyl acetate for 60 min and 1% (w/v) lead citrate for 1 min, washed in distilled water and air dried.

The grids were viewed in a FEI Tecnai 20 transmission electron microscope (FEI UK Ltd, Cambridge, UK) at 200 kV and imaged using an AMT XR60 digital camera (Deben, Bury St Edmunds, UK) to record TIF files.

2.6.2 Periodic acid-thiocarbohydrazide-silver proteinate (PATAg) staining of glycogen

Sections of a *Streptomyces* colony were placed onto gold grids coated with pyroxylin and carbon. The grids were inverted onto drops of 1% (v/v) periodic acid for 20 min at room temperature and covered. The grids were washed successively 3 times in dH_2O for 10 s and then a further 3 times in dH_2O for 10 min. The grids were inverted onto 1mL of 0.2% (w/v) thiocarbohydrazide in 20% (v/v) acetic acid and incubated overnight in a sealed tube (Robertson, et al., 1975). The grids were then washed in 10% (v/v) acetic acid 3 times for 10 s followed by 3 times in 10% (v/v) acetic acid for 10 min with gentle shaking. The grids were then washed in 5% (v/v) acetic acid for 10 s followed by washes in 2.5% acetic acid for 10 s. The grids were washed successively 3 times in dH_2O for 10 s and then a further 3 times in dH_2O for 10 min. The grids were inverted on to drops of 1% (w/v) silver proteinate for 30 min in the dark (Robertson, et al., 1975). The grids were washed three times in dH_2O for 10 s followed by 3 washes in dH_2O for 10 min. The grids were viewed as described in section 2.6.1.

2.6.3 Cryo-scanning electron microscopy

Samples of *Streptomyces* were mounted on an aluminium stub using Tissue Tek^R (BDH Laboratory Supplies, Poole, England) containing optimal cutting temperature compound (Agar Scientific Ltd, Essex, UK). The sample was then cryopreserved by placing into liquid N_2 maintained at approximately -210 °C, and transferred to the cryostage of an ALTO 2500 cryotransfer system (Gatan, Oxford, England) attached to a Zeiss Supra 55 VP field emission gun scanning electron microscope (Zeiss SMT, Germany) or the same type of cryo-system on an FEI Nova NanoSEM 450 (FEI, Eindhoven, The Netherlands). Surface frost was sublimated at -95 °C for 3 min. The sample was then transferred to an agar high resolution sputter coater and coated with platinum for 3 min at 10 mA at below -110 °C. Finally, the sample was moved onto the cryostage in the main chamber of the microscope, held at approximately -130°C, viewed at 3.0 kV and digital TIFF files were stored.

2.6.4 Fluorescence light microscopy

Streptomyces was grown at the base of glass cover slips penetrating MYM agar at approximately 45˚ for 5 days at 30 ˚C. The cover slips were left to dry for 10 min in a flow hood and then soaked in 300 µL ice-cold methanol for 1 min, which was rinsed off by dipping in dH_2O. A solution of 25 µg mL^{-1} propidium iodide (PI) (Sigma) and 50 µg mL^{-1} wheat germ agglutinin Alexa Fluor® 488 conjugate (WGA) (Life Technologies) was prepared in dH_2O and 25 µL of the solution was applied to the growth line on the coverslip. The samples were then incubated in the dark for 30 min and excess dye was removed by successively dipping in dH_2O for 20 s. The samples were then blotted dry and 9 µL of 20% (v/v) glycerol was applied to a microscope slide. The coverslip was placed onto the microscope slide and finally nail polish was applied at the edges to ensure the coverslip was secured to the microscope slide. The samples were kept in the dark until viewed with a Nikon Eclipse 600 CCD microscope (Cairn) at × 100 magnification with oil immersion. Photographs were taken by Orca HQ cooled CCD digital camera (Hamamatsu). Digital images were prepared using Image J (NIH) software.

Chapter 3: TreS Enzymology

3.1 Introduction

The first enzyme of the GlgE pathway is trehalose synthase (TreS), which is a maltose α-D-glucosylmutase (EC 5.4.99.16) that interconverts maltose (α-D-glucopyranosyl-(1,4)-D-glucopyranose) and trehalose, with weak hydrolytic activity (α-D-glucopyranosyl-(1,1)-α-D-glucopyranose) (Nishimoto, et al., 1995; Pan, et al., 2004).

TreS is classified in the glycoside hydrolase (GH) 13_33 sub-family (Stam, et al., 2006) according to the carbohydrate active enzyme (CAZy) classification system (Cantarel, et al., 2009). Consequently, it has a $(\beta/\alpha)_8$ fold, defining an active site containing an aspartate (Asp) nucleophile and a glutamate (Glu) proton donor that catalyse an α-retaining double-displacement reaction mechanism (Figure 3.1)(Caner, et al., 2013; Roy, et al., 2013). In support of this mechanism, evidence for the glucosyl-enzyme intermediate involving Asp^{230} in the *Mycobacterium smegmatis* enzyme has been reported (Zhang, et al., 2011). As α,α-trehalose (and no variants with β-configurations) was the only stereoisomer interconverted by TreS (Koh, et al., 2003) it suggests that only α-maltose is used and produced by TreS. Furthermore as TreS proceeds via an α-retaining mechanism, it should be stereospecific for α-maltose.

There were no reports of experimental evidence defining the anomeric configuration of the non-reducing terminus of maltose that TreS produces. The configuration could have consequences for metabolic flux, because the non-enzymatic mutarotation of maltose is so slow that the half-life of anomeric equilibration is of the order of tens of minutes (Bailey, et al., 1967). Moreover, although maltose mutarotase enzymes are known, they have only been detected in higher plants (Bailey, et al., 1967) and *Lactobacillus brevis* (Shirokane and Suzuki, 1995).

The focus of experiments in this chapter was to obtain experimental evidence to define the anomeric configuration of maltose that TreS produces and consumes. Fluorinated maltose analogues were also used as substrates in order to determine if TreS could utilise substrate analogues and to observe if any stereospecificity was retained when these analogues were used.

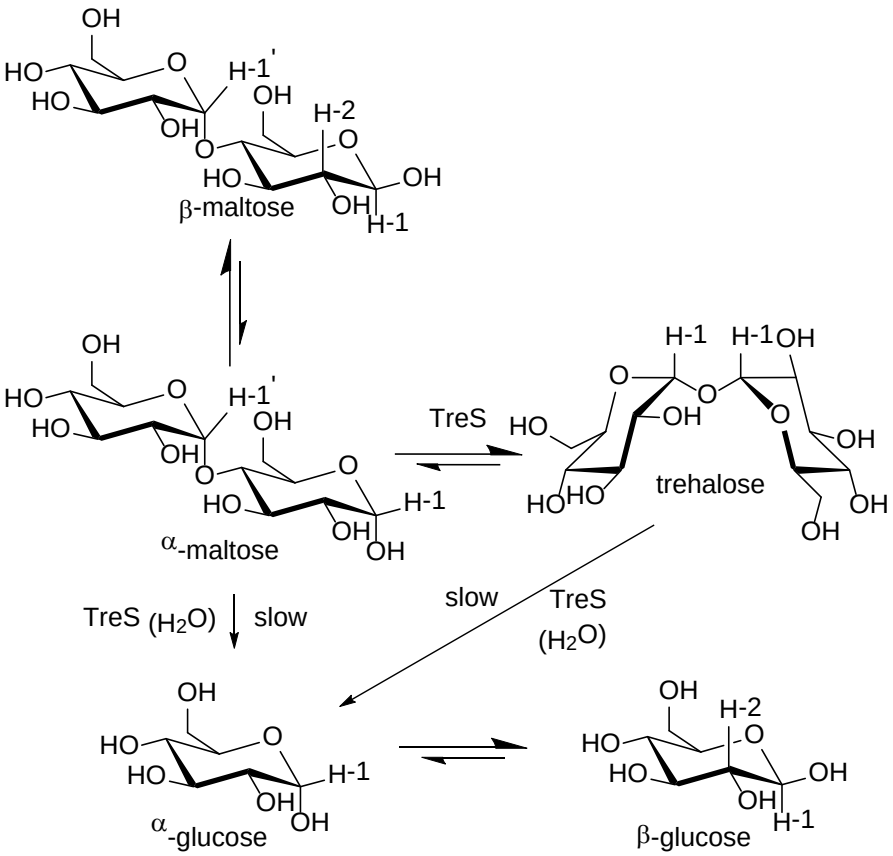

Figure 3.1: Summary of predicted TreS catalysis
The predicted reaction scheme of TreS, indicating that it should interconvert α-maltose and trehalose as well as slowly hydrolyse both substrates into glucose constituents. The labelled protons (Hs) were used to quantify reaction components in this study.

3.2 Heterologous over-production of *Mycobacterium tuberculosis* TreS

3.2.1 Small-scale production trials

A codon-optimised DNA sequence encoding *M. tuberculosis* TreS was synthesised and sub-cloned into an expression vector. Chemical transformation was used to insert the plasmid in to two *Escherichia coli* cell lines optimised for high heterologous protein production; BL21* (DE3) and BL21 (DE3) pLysS. Protein expression was initiated by the addition of isopropyl β-D-1-thiogalactopyranoside (IPTG) when cultures reached an appropriate OD_{600nm}. Protein production was monitored by sodium dodecyl sulphate polyacrylamide gel electrophoresis (SDS-PAGE) (Figure 3.2). Any bands that dramatically increased upon IPTG induction on the gel were deemed as likely to be TreS and therefore were excised and its identity was confirmed by matrix-assisted laser desorption/ionization-time-of-flight mass spectrometry (MALDI-TOF MS).

3.2.2 Large-scale production

As initial protein production yielded soluble TreS, the culture medium was scaled up. TreS was purified from the cell lysate using a HisTrap column (Figure 3.3) and further purified by size exclusion chromatography (SEC) (Figure 3.4a). The SEC chromatogram suggested that TreS formed two oligomeric states in solution, which were stored separately (Figure 3.4b).

3.3 Initial characterisation of TreS

3.3.1 TreS exists as two oligomers in solution

An estimate of the size of oligomers was made based on the elution volume (V_E) of each oligomer by comparison to the V_E of proteins of known masses. This suggested that the larger oligomer was a hexamer (observed size: 427 kDa expected size: 423 kDa) and that the smaller oligomer was a trimer (observed size: 229 kDa; expected size: 211.5 kDa). Dynamic light scattering (DLS) suggested that the larger oligomer may even be a decamer (observed size 691 kDa; expected size 705 kDa) but confirmed that the smaller oligomer was likely to be a trimer (observed size 195 kDa; expected size 211.5 kDa).

The oligomers did not seem to interconvert (data not shown). Analytical ultracentrifugation was attempted to confirm the size of the oligomers but TreS was not sufficiently stable and precipitated during the procedure (data not shown).

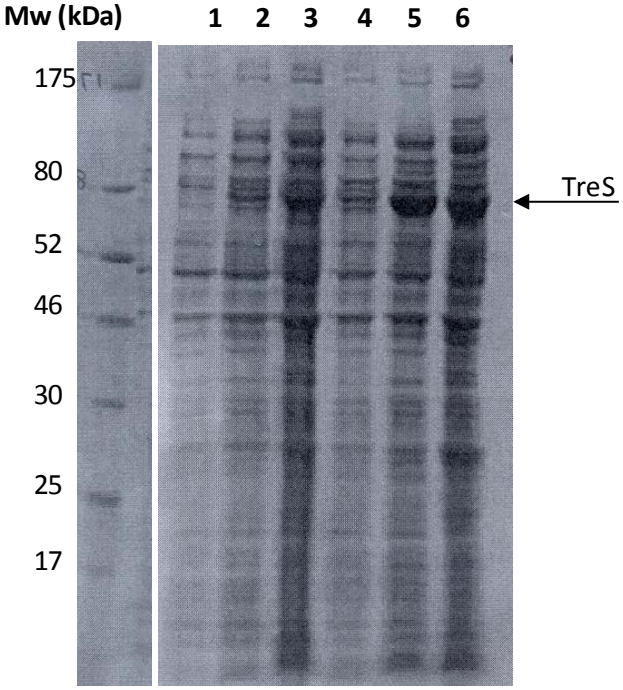

Figure 3.2: Initial TreS expression trials
SDS- PAGE of cell lysates from *E. coli* BL21* (DE3) (lane 1-3) and BL21 (DE3) pLysS (lane 4-6). Lanes 1 and 4 were cell lysates prior to IPTG induction. Lanes 2 and 5 were cell lysates 5 h after induction and lanes 3 and 6 were cell lysates ~17 h after induction. The black arrow indicates the approximate position of TreS (expected size 70.5 kDa).

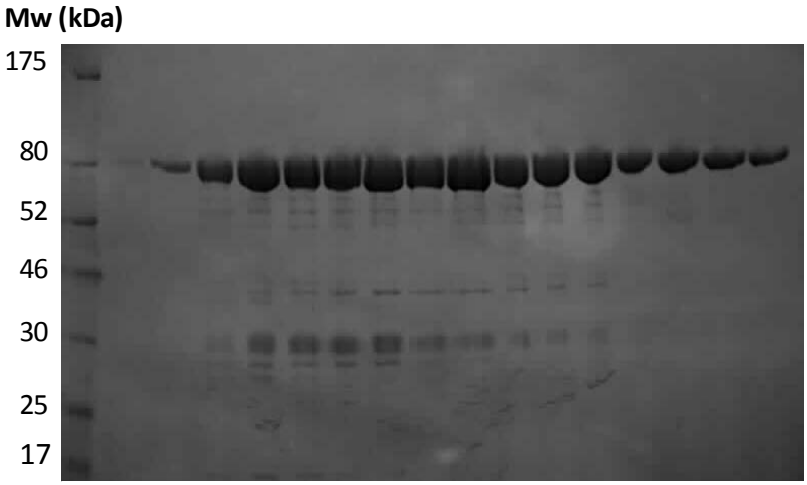

Figure 3.3: Large scale purification of TreS
SDS- PAGE of protein-containing fractions after elution from a HisTrap column.

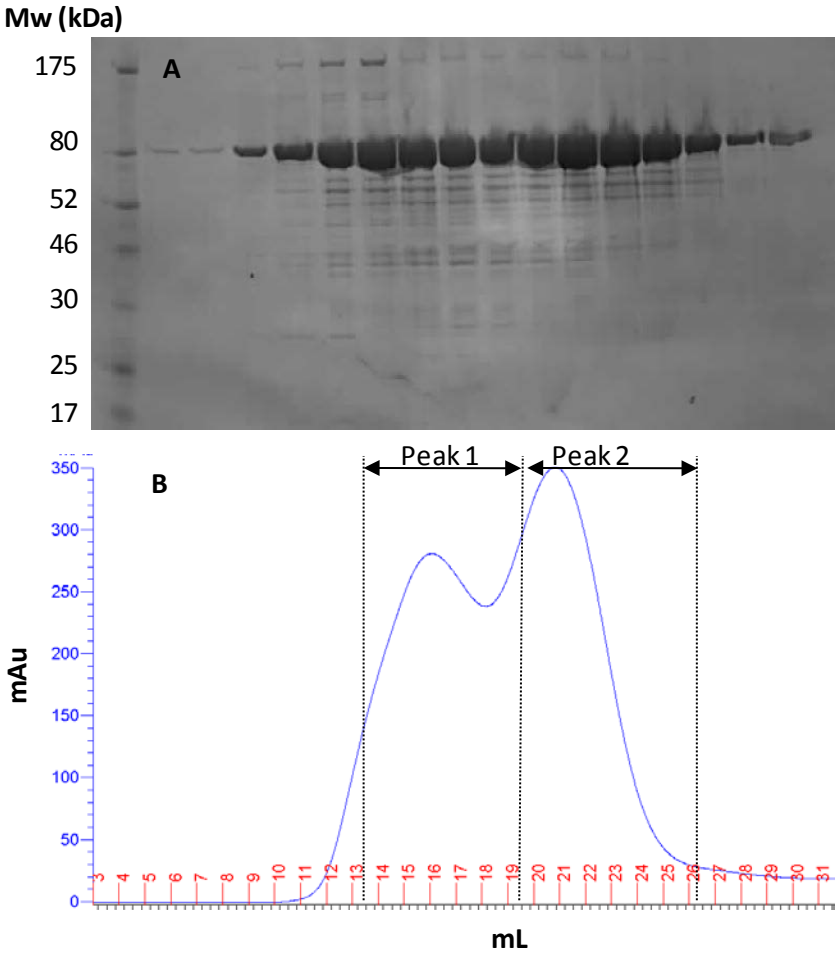

Figure 3.4: Further purification of TreS
(A) SDS-PAGE of protein-containing fractions after elution from a size exclusion chromatography (SEC) column.
(B) SEC (A_{280nm}) chromatogram showing that TreS forms two oligomeric states in solution. Initially, fractions were pooled separately as peak one and peak two.

3.3.2 ^{1}H- NMR spectroscopy can differentiate between the substrates and products of TreS

TreS was known to interconvert trehalose and maltose, but for this study an assay technique that could differentiate between the α and β anomers of maltose was required. Moreover, the assay had to be able to distinguish the disaccharides from glucose, which is a known hydrolysis product of TreS (Nishimoto, et al., 1995; Pan, et al., 2004; Zhang, et al., 2011). NMR spectroscopy was predicted to be one of the few techniques that could be used to distinguish anomers of maltose because it utilises magnetic in-equivalence of the α and β anomers of maltose, it is also non-destructive and so it was possible to take multiple readings of a single TreS reaction. Furthermore, it allowed mixtures to be analysed without chromatography.

A trial experiment monitored by ^{1}H- NMR spectroscopy showed that purified TreS was active and validated this technique for future assays (Figure 3.5). The only challenging aspect regarding the use of this technique was the overlap of resonances associated with α-maltose and α-glucose. However, as resonances associated with β-maltose were resolved from those of β-glucose and there was also a well-defined resonance attributable to the α-1,4 glycosidic bond, it was possible to determine α-maltose concentrations.

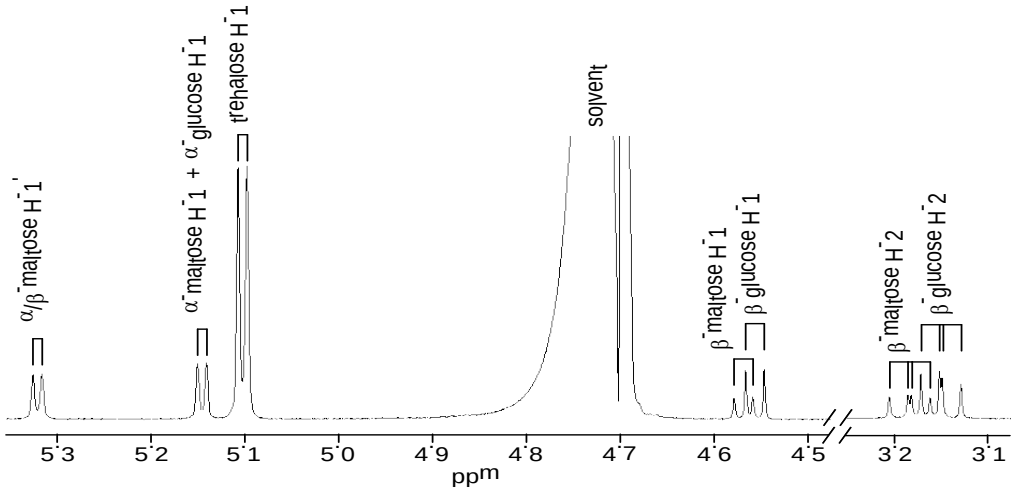

Figure 3.5: ^{1}H-NMR spectroscopy resolves the products and substrates of TreS
A typical ^{1}H-NMR spectrum recorded when 2 µM TreS was incubated with 10 mM maltose for 919 min. Only the regions of the spectrum used to quantify reaction components are shown. For the assignments see materials and methods and figure 3.1.

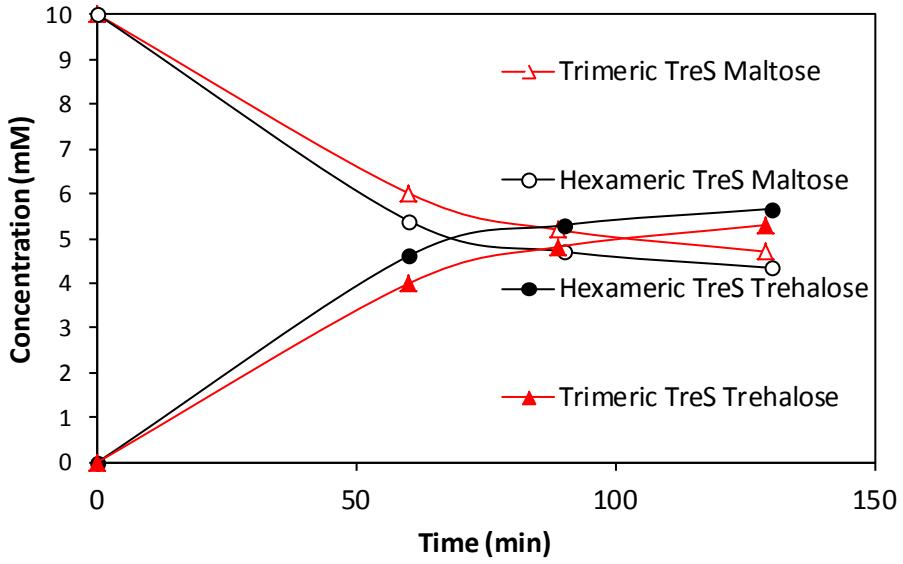

Figure 3.6: Different oligomers of TreS had the same specific activity
TreS at a concentration of 1.75 µM (based on Mw of a single monomer) was incubated with 10 mM maltose and trehalose production was monitored. The rate of conversion was comparable regardless of the oligomer of TreS used in the reaction.

3.3.3 TreS oligomers have similar activity

Time-courses using the same concentration of each TreS oligomer suggested that the two oligomers of TreS had similar specific activities (Figure 3.6). SEC experiments suggested that the oligomers remained discrete and did not inter-convert (data not shown). Consequently, for further enzymology experiments both oligomers were pooled.

3.3.4 Citrate was the optimal buffer for TreS assays

Initial experiments with TreS were performed in a phosphate buffer, which was initially preferred because it does not have any protons and so the ^{1}H-NMR spectra were not affected by the presence of the buffer. However, the rate of mutarotation of glucose increases in the presence of phosphate (Stults, et al., 1987). In order to determine if TreS was stereospecific, it was important to ensure the rate of mutarotation was slow so as to allow the faster TreS enzymatic reaction to be sufficiently distinguishable from relatively slow mutarotation reactions. Initial experiments suggested that, at a phosphate concentration of 145 mM, it was difficult to resolve the two processes occurring. Whilst the concentration of phosphate could have been lowered dramatically, it would have impacted on the buffering capacity of the phosphate and therefore another buffer that operated in the same pH range as phosphate was sought, tris (and bis-tris propane by association) was excluded from this screen because it has been shown to competitively inhibit TreS from *M. smegmatis* (Pan, et al., 2004).

The only buffer tested that had no proton resonances in the same region as that of maltose and trehalose was citrate (Figure 3.7). The rate of maltose mutarotation was much slower than with phosphate and it did not dramatically change as a function of citrate concentration (Figure 3.8).

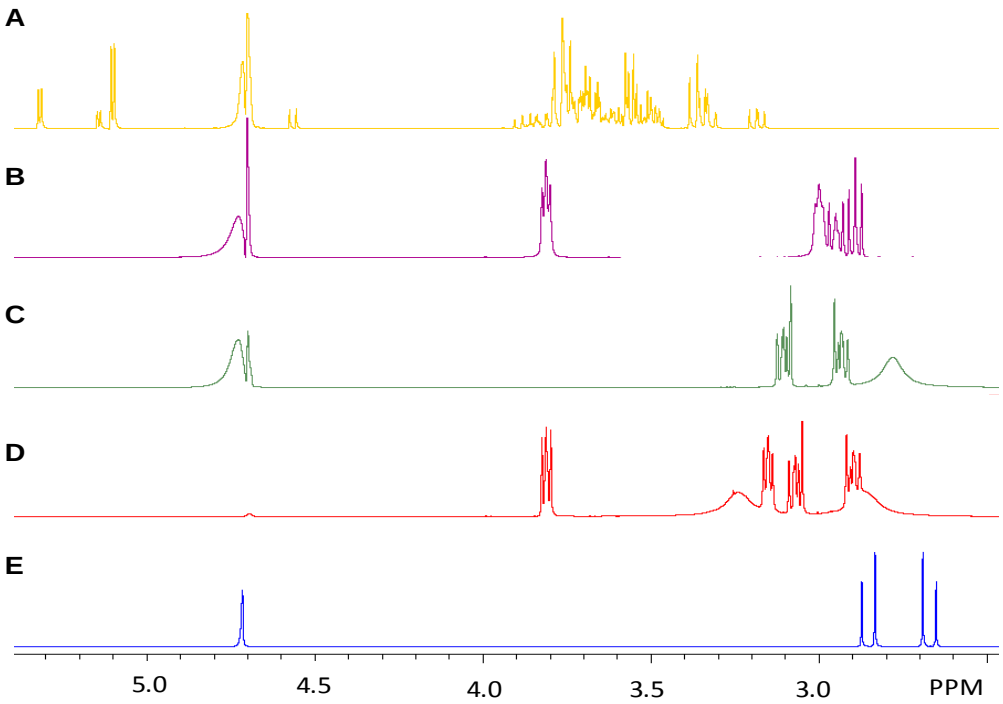

Figure 3.7: Buffer screens showed that citrate buffer was optimal
All samples had a H_2O solvent resonance (4.7 ppm). (A) A spectrum showing all maltose and trehalose resonances. MOPS (B), PIPES (C) and HEPES (D) contained resonances within the maltose and trehalose resonance region but citrate (E) did not.

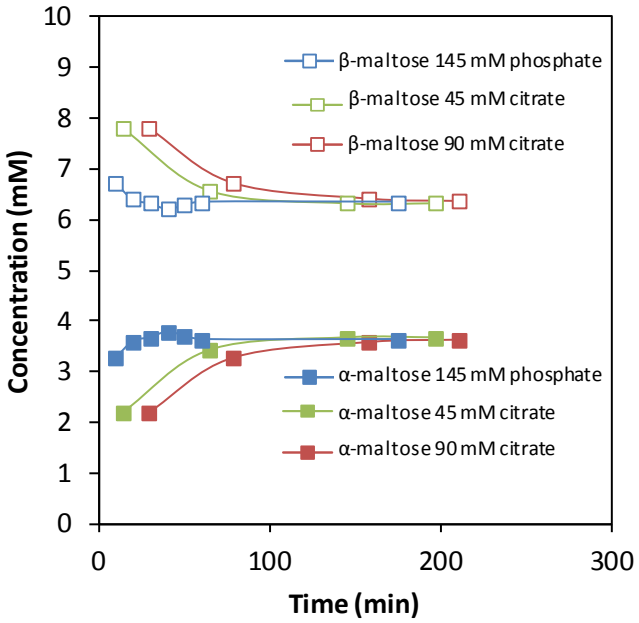

Figure 3.8: Citrate did not accelerate the rate of equilibration between α-maltose and β-maltose
Rates of equilibration with a phosphate buffer were comparable to the rate of catalysis of TreS; therefore it was difficult to distinguish between TreS catalysis and non-enzymatic mutarotation. However, when a citrate buffer was used the rate of mutarotation between α-maltose and β-maltose was much slower and did not increase as a function of citrate concentration.

3.3.5 Solvent suppression correction factors were used

In order to determine the exact concentrations of products and substrates by ^{1}H-NMR spectroscopy it was necessary to determine the area of the integrals and correct for the number of protons each resonance represented. Reaction mixtures contained 10% D_2O to assist spectrum acquisition without significant risk of introducing solvent kinetic and/or equilibrium isotope effects. This necessitated solvent suppression. However, as the resonances of interest were close to the solvent resonance (Figure 3.9), they too were suppressed by solvent suppression. The resonances corresponding to β-maltose H-1 and β-glucose H-1 (Figure 3.1) were not used as they were significantly supressed and instead β-maltose and β-glucose H-2 were used as they were further from the H_2O resonance. Solvent correction factors were determined for trehalose (5.1 ppm) and maltose (5.3 ppm) resonances by comparing integrals in a 100% D_2O non-solvent suppressed sample with 10% D_2O solvent-suppressed sample (Figure 3.9; Table 3.1). The different amounts of D_2O could affect the α-maltose/β-maltose equilibrium position and therefore it was not possible to directly determine the suppression of α-maltose. However, as the resonance was in between the maltose and trehalose resonances, an average of the two resonances was calculated (13.9%) and was used as the suppression correction factor for α-maltose.

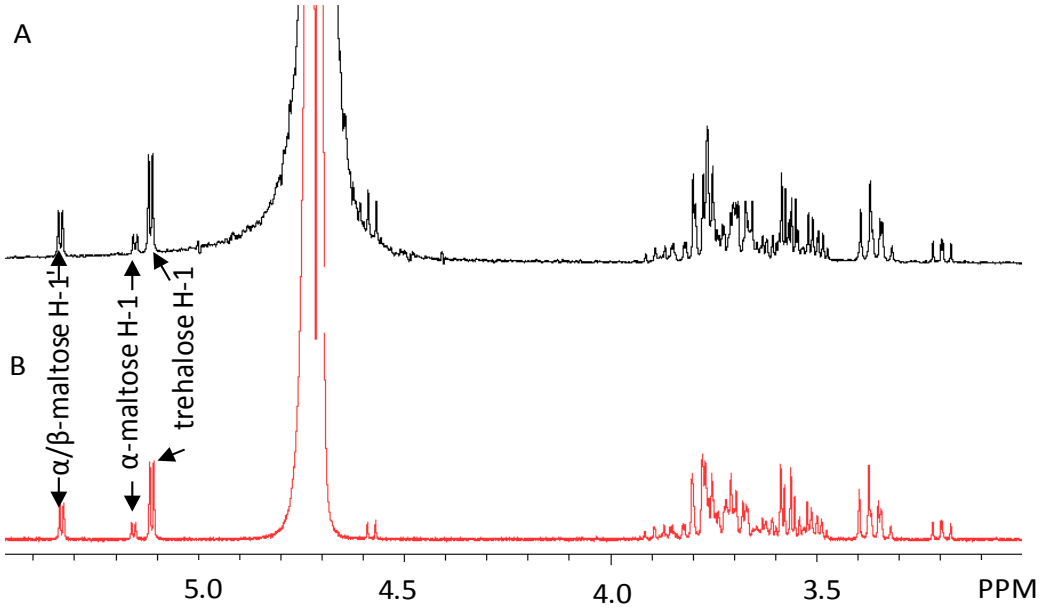

Figure 3.9: Solvent suppression also suppresses resonances used to determine trehalose, maltose and glucose concentrations
Spectra collected using non-solvent suppressed ^{1}H-NMR spectroscopy, containing equal concentrations of trehalose and maltose dissolved in 100% D_2O (A) and solvent suppressed ^{1}H-NMR spectroscopy, containing trehalose and maltose dissolved in 10% D_2O and 90% H_2O (B).

Table 3.1: Solvent suppression factors for trehalose and maltose when citrate resonances were used as an internal standard

Resonance	Integral in 100% D_2O	Integral in 10% D_2O	Difference	% suppression
trehalose H-1	0.61	0.52	0.09	14.9
α/β-maltose H-1'	0.30	0.26	0.04	12.9

3.4 TreS interconverts only the α anomer of maltose

3.4.1 Non-enzymatic mutarotation rate determination

Since anomers mutarotate non-enzymatically, their equilibration upon dissolution of crystalline materials in citrate buffer at 25 °C was monitored using ^{1}H-NMR spectroscopy (Figure 3.10). The rate constants determined, by fitting to a single reversible step reaction, for the mutarotation of α-glucose to β-glucose and the reverse reaction were 0.0316 ± 0.0004 and 0.0192 ± 0.0004 min^{-1} and, for maltose, 0.0286 ± 0.0002 and 0.0187 ± 0.0001 min^{-1}, each respectively (Figure 3.10). These rate constants were consistent with the literature values of 0.027 min^{-1} in 5 mM ethylenediaminetetraacetic acid (EDTA), pH 7.4, at 25 °C (Bailey, et al., 1967) and 0.018 min^{-1} in water at 21 °C (Stults, et al., 1987), and the expected dominance of the β anomers.

3.4.2 TreS produces α-maltose from trehalose

The conversion of trehalose into maltose by TreS in citrate buffer as a function of time was monitored using ^{1}H-NMR spectroscopy (Figure 3.11). The α anomer of maltose was formed 5.4-fold more rapidly than its β anomer, suggesting TreS generates the α anomer. A low level of glucose was also produced through hydrolysis, as observed previously. At longer times, the ratio between trehalose and α/β -maltose was 2.2:1 (at 25 °C and pH 6.7), which is reasonably similar to the equilibrium position of 4.6:1 determined from the free energies of hydrolysis of these disaccharides (at 25 °C and pH 5.65) (Syson, et al., 2011; Tewari and Goldberg, 1991; Tewari, et al., 2008) and of 3.2:1 determined from the kinetics of *M. smegmatis* TreS (Zhang, et al., 2011). The expected equilibrium positions between the anomers of both maltose and glucose were also approached at longer times.

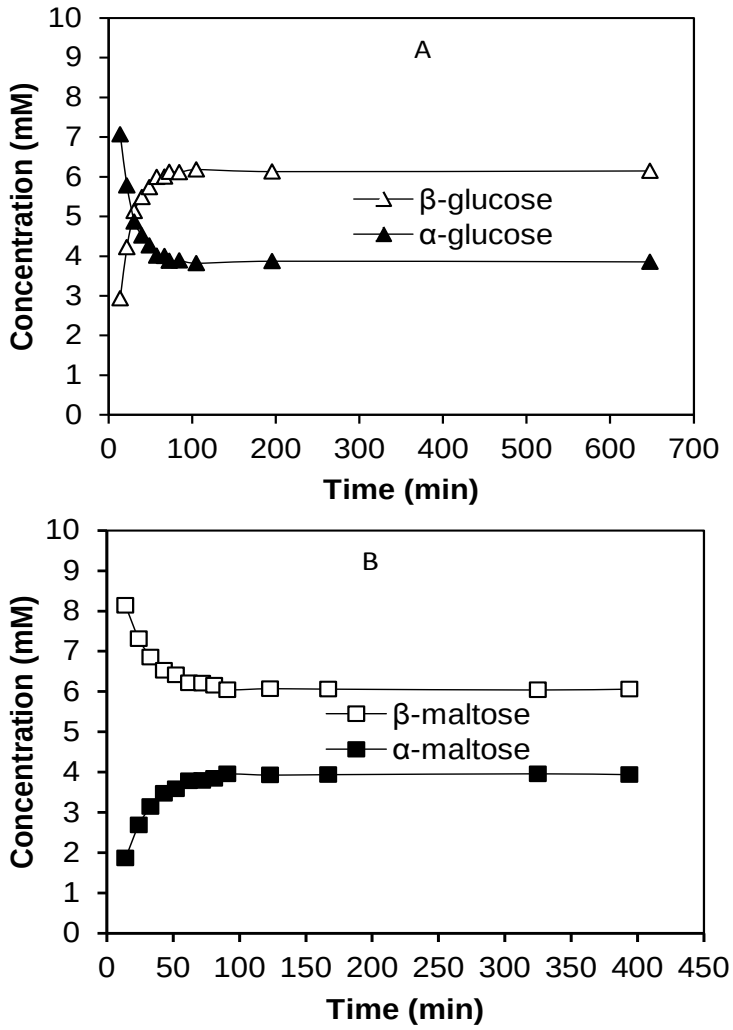

Figure 3.10: Non-enzymatic mutarotation rates of glucose and maltose

(A) Time course of the non-enzymatic mutarotation glucose. The concentrations of each anomer of glucose were determined as a function of time after the dissolution of solid glucose (giving 10 mM in 90 mM citrate buffer, pH 6.7, containing 10% (v/v) D_2O at 25 °C) using ^{1}H-NMR spectroscopy. Fitting of the data gave rate constants of 0.0316 ± 0.0004 and 0.0192 ± 0.0004 min^{-1} for the mutarotation of the α to the β anomer and the reverse reaction, respectively. These values were consistent with not only the literature (0.027 min^{-1} in 5 mM EDTA, pH 7.4, at 25 °C (Bailey et al., 1967) and 0.018 min^{-1} in water at 21 °C (Stults et al., 1987), respectively) but also the expected dominance of the β anomer.

(B) Time course of the non-enzymatic mutarotation of maltose. The concentrations of each anomer of maltose were determined as a function of time after the dissolution of solid maltose (giving 10 mM in 90 mM citrate buffer, pH 6.7, containing 10% (v/v) D_2O at 25 °C) using ^{1}H-NMR spectroscopy. Fitting of the data gave rate constants of 0.0286 ± 0.0002 and 0.0187 ± 0.0001 min^{-1} for the mutarotation of the α to the β anomer and the reverse reaction, respectively, consistent with the literature (0.017 min^{-1} in 5 mM EDTA, pH 7.4, at 25 °C (Bailey et al., 1967) for the reverse reaction) and the expected dominance of the β anomer.

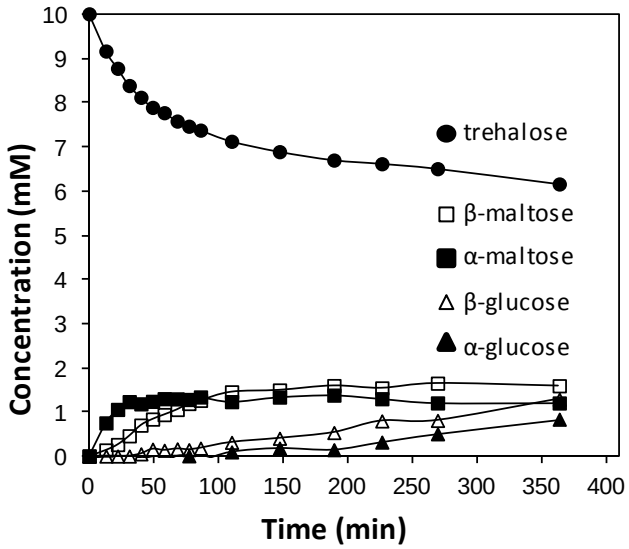

Figure 3.11: TreS produces the α anomer of maltose from trehalose
The conversion of 10 mM trehalose into maltose by 2 µM of TreS according to ^{1}H-NMR spectroscopy. Each component was quantified by signal integration using citrate as an internal standard.

3.4.3 TreS consumed α-maltose to form trehalose

As TreS formed trehalose from pre-equilibrated α/β-maltose (α:β anomeric ratio of 1:1.5), a rapid depletion of α-maltose was immediately apparent (Figure 3.12A). By contrast, the consumption of β-maltose was significantly slower and conformed to a single exponential function (Figure 3.12B) with a rate of 0.019 min^{-1} that was consistent with the rate constant for the mutarotation described above (0.0187 ± 0.0001 min^{-1}). This implied that TreS does not utilize the β anomer. When the experiment was repeated with lower TreS concentrations, the rate of consumption of α-maltose decreased, while that of the β anomer remained similar. Thus, the transient increase in the β/α ratio of the maltose anomers was less pronounced at lower enzyme concentrations (Figure 3.13), providing further evidence that TreS converts only the α anomer of maltose into trehalose, as expected. While the initial formation of glucose through hydrolysis appeared to be more rapid from maltose than trehalose, this most likely reflected the more rapid initial consumption of maltose. This implies the equal probability of either α-maltose or trehalose being hydrolysed based on these data. It is also noteworthy that the α anomer of glucose was produced more rapidly from maltose than its β anomer, suggesting that α-glucose is the product of hydrolysis.

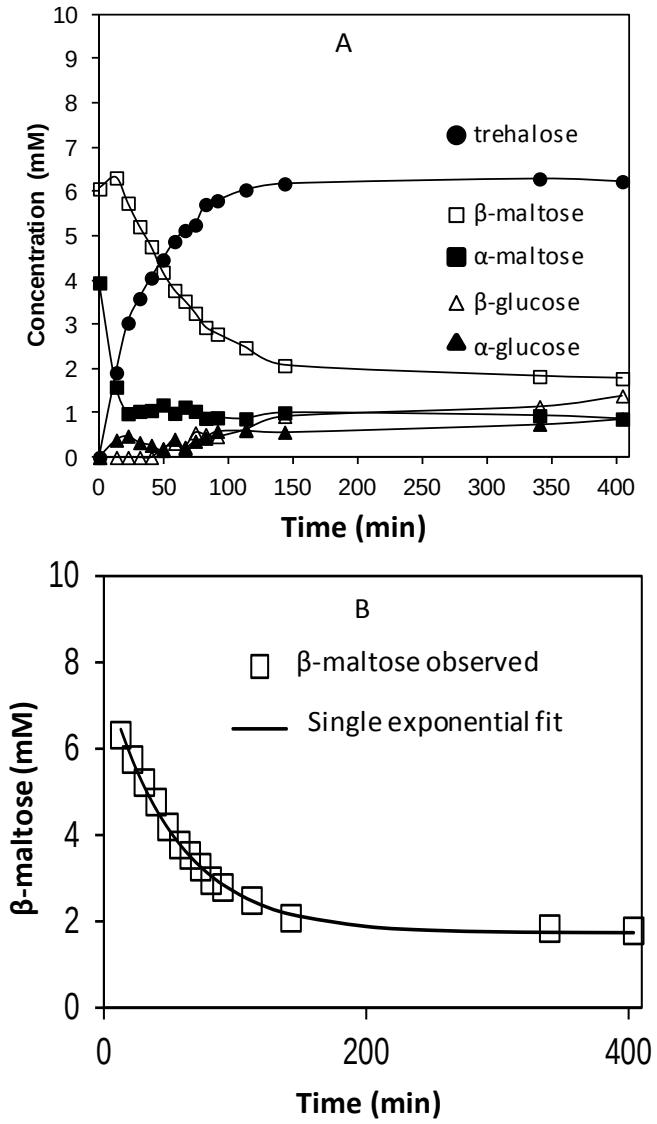

Figure 3.12: TreS converts the α anomer of maltose to trehalose

(A) The conversion of pre-equilibrated 10 mM α/β-maltose into trehalose by 2 µM TreS according to ^{1}H-NMR spectroscopy. TreS was added immediately after the t = 0 data were acquired, resulting in a small and reproducible change in the apparent concentration of starting materials at the second recorded time point. The times taken to produce 2 mM trehalose and consume 50% of the α/β-maltose were 14 and 55 min, respectively.

(B) Fitting of the time course of the depletion of β-maltose during a reaction with α/β-maltose and TreS. The conversion of 10 mM α/β-maltose by 2 µM TreS was monitored using ^{1}H-NMR spectroscopy. Fitting of the data for β-maltose (open squares) to a single exponential (solid line) gave a rate of 0.019 min^{-1}. This was indistinguishable from the rate constant determined for the mutarotation of β-maltose to α-maltose (0.0187 ± 0.0001 min^{-1} shown above).

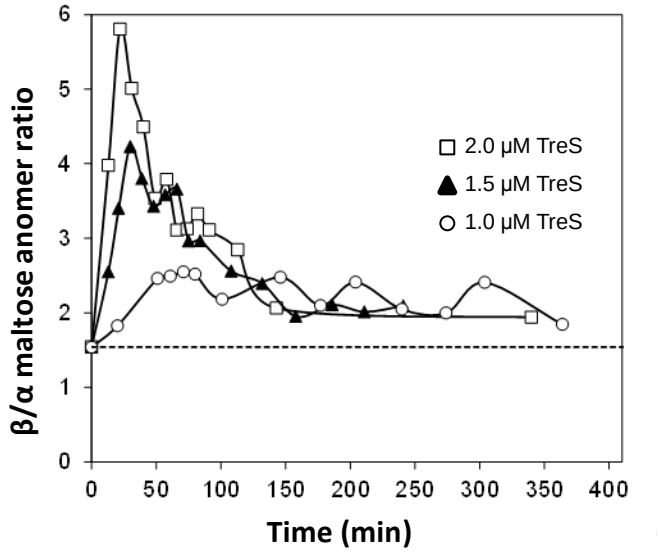

Figure 3.13: β/α-Maltose ratio moves closer to the natural β/α maltose ratio as the reaction proceeds

Time courses of the ratios between the β and α anomers of maltose with different TreS concentrations during the conversion of pre-equilibrated α/β-maltose. The broken line indicates the equilibrium between the two anomers in these conditions in the absence of TreS.

3.5 The specificity of TreS for the α anomer of maltose was retained with deoxyfluoro analogues

Deoxyfluorotrehalose analogues have been shown to label *M. tuberculosis* cells and exhibit weak anti-mycobacterial activity (Backus, et al., 2011). Since *M. tuberculosis* has a trehalose transporter (Kalscheuer, et al., 2010b) and TreS has been reported to utilize 2-fluoro-2-deoxymaltose as a substrate (Zhang, et al., 2011), the ability of TreS to convert 2-, 3-, and 6-deoxyfluoromaltose analogues (Tantanarat, et al., 2012) was monitored using ^{19}F-NMR spectroscopy (Figures 3.14 and 3.16).

The 2-deoxy-2-fluoro and 6-deoxy-6-fluoro compounds were converted to the corresponding deoxyfluorotrehalose analogues ~2-fold and ~180-fold less efficiently than the normal substrate (Figures 3.14A and 3.14C). The hydrolysis of each analogue to the corresponding deoxyfluoroglucose compounds was detected (Figure 3.14), particularly with the 3-fluoro-3-deoxy and 6-fluoro-6-deoxy compounds, with the former being exclusively hydrolysed (Figure 3.14B). The expected concomitant formation of non-fluorinated glucose was detected using ^{1}H-NMR spectroscopy (data not shown). The α anomer was consumed more rapidly than the β anomer with all three analogues (Figure 3.14) consistent with TreS only acting on α anomers. The mutarotation rates of the deoxyfluoro analogues are not known, but fitting the decay of the β anomer of the 2-deoxy-2-fluoro analogue (Figure 3.14A) suggested a rate constant of ~0.004 min^{-1}, an order of magnitude slower than that for maltose.

In order to assess whether fluoro substitution at the three and six positions resulted in poor binding to TreS or slow conversion by TreS, the extent of conversion of 0.52 mM 2-deoxy-2-fluoromaltose was monitored in the presence and absence of 2.1 mM of each of the other two analogues (Figure 3.15). Neither of the analogues gave inhibition, and there may indeed have been a modest stimulation of activity. Given that the K_m for maltose is 8–10 mM with the *M. smegmatis* enzyme (Pan, et al., 2004; Zhang, et al., 2011) and the K_m for the 2-deoxy-2-fluoro analogue would not be expected to be orders of magnitude lower than this, the lack of inhibition is consistent with fluoro substitution at the three and six positions, compromising the ability of maltose analogues to bind to TreS.

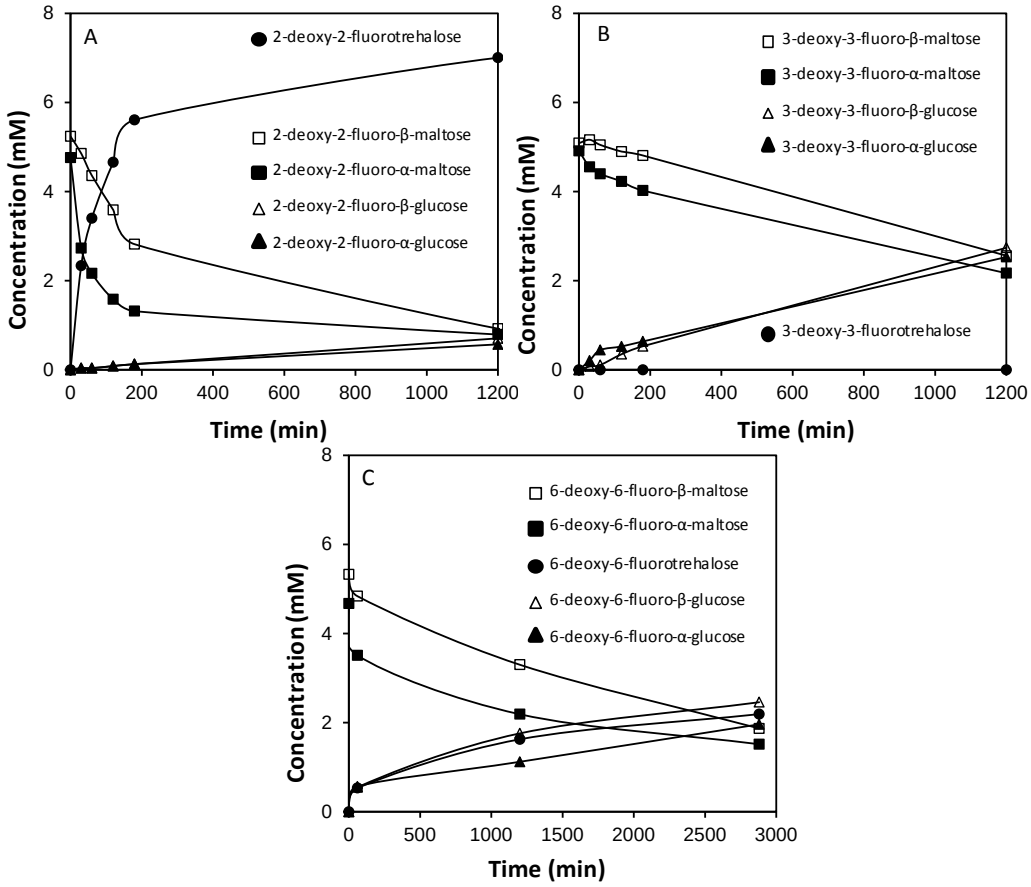

Figure 3.14: TreS Converts the α anomer of deoxyfluoromaltose analogues
These experiments were performed by M. Rejzek.
(A) The conversion of 10 mM pre-equilibrated 2-deoxy-2-fluoro-α/β-maltose by 2 µM of TreS was monitored using ^{19}F-NMR spectroscopy. The times taken to produce 2 mM 2-deoxy-2-fluorotrehalose and consume 50% of the maltose analogue were 25 and 125 min, respectively, both ~2-fold longer than with maltose.
(B) Corresponding data as with 3-deoxy-3-fluoro-α/β-maltose. The time taken to consume 50% of the maltose analogue was 1,100 min, 20-fold longer than with maltose. No 3-deoxy-3-fluorotrehalose was detected.
(C) Corresponding data with 6-deoxy-6-fluoro-α/β-maltose. The times taken to produce 2 mM 6-deoxy-6-fluorotrehalose and consume 50% of the maltose analogue were 2,500 and 1,500 min, respectively, 180- and 27-fold longer than with maltose.

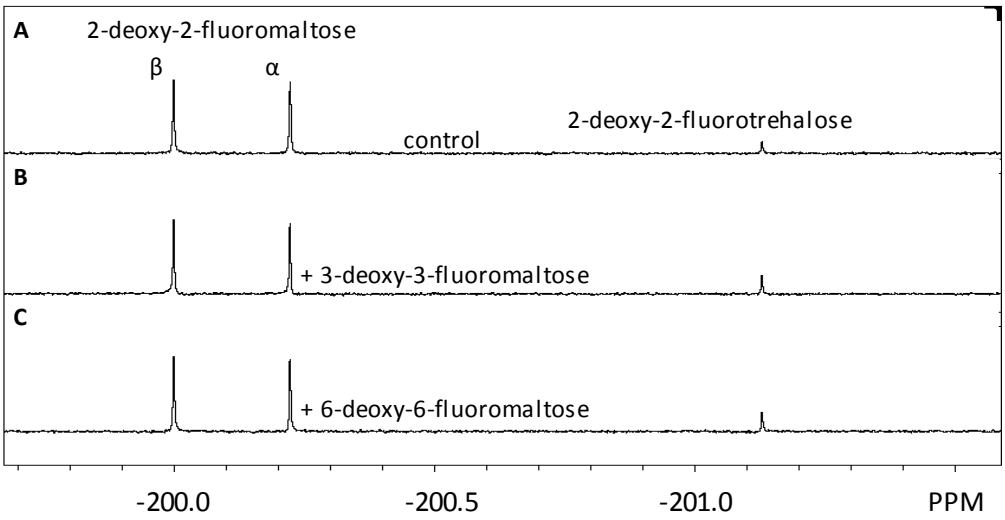

Figure 3.15: Lack of inhibition of the TreS-catalysed conversion of 2-deoxy-2-fluoromaltose to trehalose by either 3-deoxy-3-fluoro or 6-deoxy-6-fluoromaltose according to ^{19}F-NMR spectroscopy

(A) A sample of 0.2 µM TreS was incubated with 0.52 mM 2-deoxy-2 fluoromaltose for 30 min. A relatively short incubation time was used to allow the estimation and comparison of the initial rates of the reactions. A sample of 0.2 µM TreS was incubated with 0.52 mM 2-deoxy-2 fluoromaltose for 30 min pre-incubated with 2.1 mM 3-deoxy-3-fluoromaltose (B) or 6-deoxy-6-fluoromaltose (C).

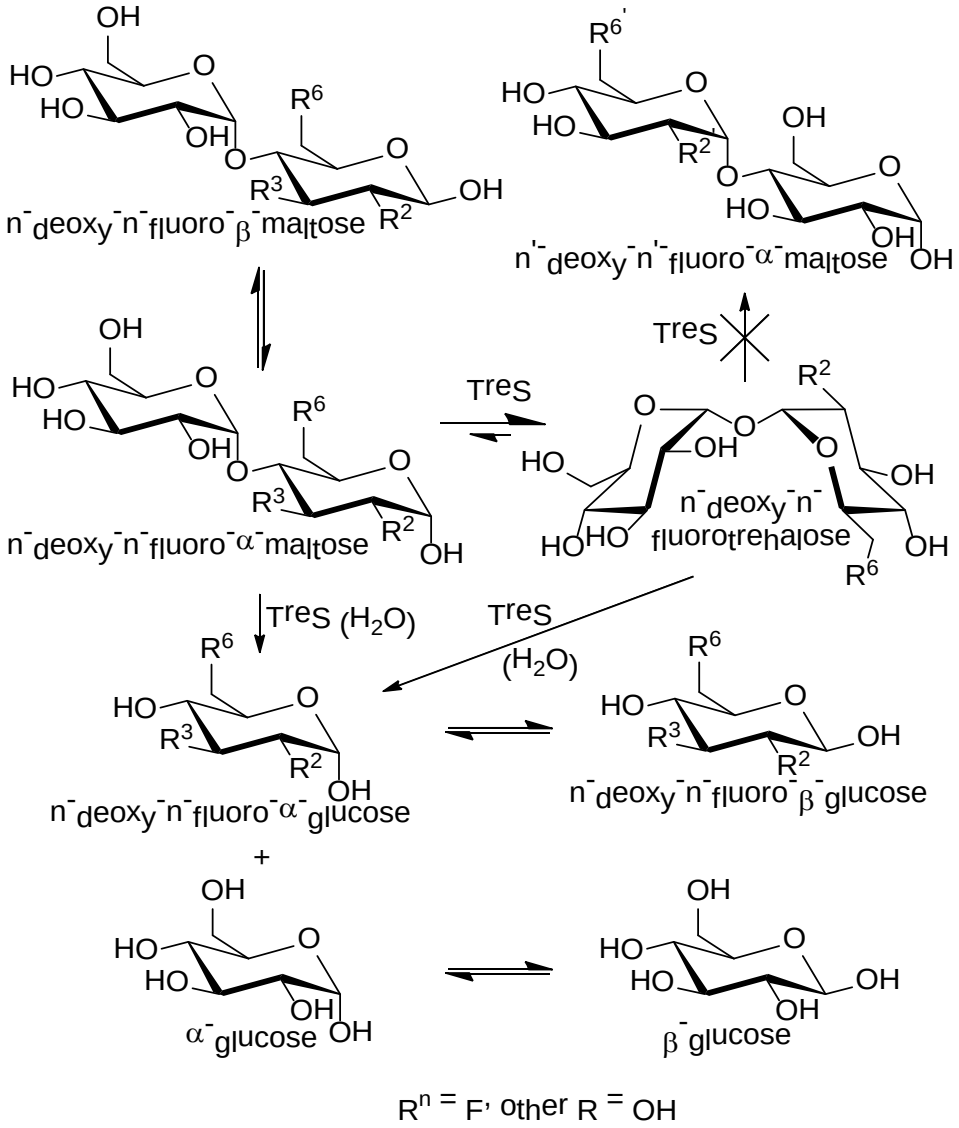

Figure 3.16: Summary of proposed TreS catalysis with deoxyfluoromaltose analogues

3.6 Crystallisation trials of TreS

Attempts were made to crystallise TreS but were unsuccessful. A number of factors were varied such as protein concentration (7.5- 15 $mgmL^{-1}$), buffer constituents, oligomer separation and the His_6-tag was cleaved by TEV protease. Co-crystallisation with glucose was also attempted.

3.7 Discussion

The findings reported in this chapter confirm the mechanistic prediction that TreS is stereospecific. Recent work has demonstrated that TreS is likely to predominantly operate in the direction that produces α-maltose in *Mycobacterium* (Miah, et al., 2013). The findings in this chapter have also highlighted that, in a biological context, the mutarotation between the α and β anomers of maltose and glucose is slow. Moreover, there are no mutarotases in *Mycobacterium* and consequently mutarotation would have to occur non-enzymatically in these bacteria. Therefore, if TreS was non-stereospecific or indeed only used the β anomer of maltose flux into the GlgE pathway could have been limited by the slow rate of mutarotation because the second enzyme of the GlgE pathway, the maltose kinase (Pep2), is stereospecific for α-maltose (Drepper, et al., 1996; Niehues, et al., 2003).

Recently, two crystal structures of TreS from *M. tuberculosis* and *M. smegmatis* have been published (Caner, et al., 2013; Roy, et al., 2013). It is noteworthy that the concentration of protein used for crystallisation was much greater, especially *M. tuberculosis* TreS (80 mg mL^{-1}) but also *M. smegmatis* TreS (20 mg mL^{-1}), than used in this work (Caner, et al., 2013; Roy, et al., 2013). This could potentially be why crystallisation failed in this study because the protein concentration was not sufficiently high for TreS to crystallise as similar crystallisation conditions were used.

Unlike trehalose, the deoxyfluorotrehalose products are asymmetric and might have been converted to the corresponding n'-deoxy-n'-fluoromaltose analogues but were not. This could have been due to the destabilisation of oxocarbenium ion-like transition states associated with these reactions (Withers, et al., 1988). Alternatively, other effects could be involved, such as reduced binding affinities. Indeed, neither of the 3-deoxy-3-fluoro and 6-deoxy-6-fluoromaltose analogues appeared to bind well to the enzyme. The 3-deoxy-3-fluoromaltose was exclusively hydrolysed meaning that 3-

deoxy-3-fluoroglucose was less able than a water molecule to attack the glucosyl-enzyme intermediate. This could be due to changes in the nucleophilicity of 3-deoxy-3-fluoroglucose or more likely due to an inability to orient itself appropriately within the active site.

3.8 Summary

In summary, results in this chapter show definitively that TreS is stereospecific, thereby only catalysing the inter-conversion of the α anomer of maltose and trehalose. This stereospecificity was also retained with maltose analogues.

Chapter 4: Pep2 Characterisation

4.1 Introduction

Maltose kinase activity was initially identified in crude extracts of *Actinoplanes* sp. SN 223/29 (Drepper, et al., 1996). The gene encoding Pep2 was first identified in *Actinoplanes missouriensis* and the gene product was subsequently confirmed as a maltose kinase (Niehues, et al., 2003). Further work has identified the corresponding homologues in *Streptomyces coelicolor* and *Mycobacterium bovis* BCG (Jarling, et al., 2004; Mendes, et al., 2010). A bioinformatic study revealed that 40% of bacterial genomes which contained *treS* also contained *pep2* (also referred to as *mak1*) (Chandra, et al., 2011). Furthermore, in 75% of the genomes containing both *treS* and *pep2*, the genes were fused and predicted to be expressed as a single protein (Chandra, et al., 2011).

Given the close association of the *treS* and *pep2* genes in many bacterial genomes, it seemed possible that there would also be a physical association between the two enzymes. Furthermore, there was no evidence that TreS and Pep2 were able to collectively synthesise α-maltose 1-phosphate (αM1P) from trehalose *in vitro*. There are no commercial sources of αM1P and its chemical synthesis is non-trivial, therefore if this enzyme could be purified easily with high yield there is potential for enzymatic synthesis of αM1P (Syson, et al., 2011).

This focus of this chapter was to express and purify Pep2 from *Mycobacterium tuberculosis* in order to determine if it could be used with TreS to generate αM1P from trehalose. In addition, as the *M. tuberculosis* TreS was not amenable for crystallographic studies, a fusion protein of TreS and Pep2 was expressed and purified for use in crystallisation trials.

4.2 Initial Pep2 production trials

Initial overexpression trials in *Escherichia coli* BL21 Star™ (DE3) did not seem to yield soluble Pep2 (Figure 4.1A). Toxicity tests suggested that Pep2 expression was not toxic for *E. coli* (data not shown) and therefore an alternative expression strain was sought. *E. coli* BL21 (DE3) was chosen becuase Pep2 from *M. bovis* was over-produced in this strain (Mendes, et al., 2010). Whilst cell lysates did not have any bands that clearly increased in intensity upon treatment with isopropyl β-D-1-thiogalactopyranoside

(IPTG), when the cell lysate was passed through a HisTrap column there was a clear protein band that eluted from the column (Figure 4.1B). The band was excised from the gel and the identity of the protein was confirmed by matrix-assisted laser desorption/ionization-time-of-flight mass spectrometry (MALDI-TOF MS).

As the yield of protein was relatively low, culture conditions were further optimised before large-scale production was attempted.

4.3 Large scale production of Pep2 and oligomerisation state

Pep2 was purified from other proteins in the cell lysate by a HisTrap column followed by size exclusion chromatography (SEC) (Figure 4.2).The protein eluted from the SEC column as two separate oligomers. The elution volume of the oligomers was used to estimate their sizes by making comparisons with the elution volumes of proteins of know sizes. The values calculated were consistent with Pep2 eluting as a dimer and monomer. Fractions containing Pep2 were pooled, concentrated and solvent exchanged. Previous work on Pep2 from a related organism suggested that it would aggregate upon a single freeze-thaw cycle; so it was stored at 4 °C (Mendes, et al., 2010).

Dynamic light scattering (DLS) was used to further investigate the oligomeric state of Pep2. It suggested that it existed predominantly as a monomer (observed size 56 kDa; expected size: 51.7 kDa), however over 10% of the total protein mass was attributable to aggregate in the sample, indicating the protein was unstable in solution. The presence of > 5% of the total protein mass as aggregate can adversely affect detection of other oligomers by DLS because it is only capable of accurately determining the size of a monodisperse sample. As the size of the aggregates was much larger (4600 kDa) than any oligomer, the majority of the signal would have been from the aggregate, which would have skewed the signal relating to the size of the oligomers.

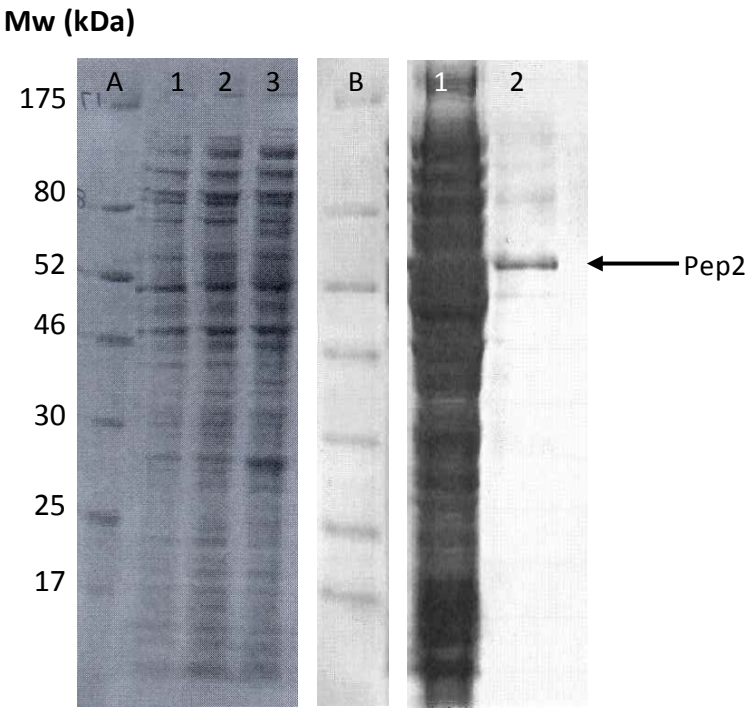

Figure 4.1: Initial Pep2 production trials
(A) SDS-PAGE of cell free extracts of *E. coli* BL21 Star™ (DE3) (lane 1-3). Lane 1 is the cell free extract before induction with IPTG; lane 2 is the cell-free extract 5 h after induction and lanes 3 is the cell-free extract one night after induction. No distinct band corresponding to Pep2 (expected size 52 kDa) was observed.
(B) SDS-PAGE of *E. coli* BL21 (DE3) cell free extracts before (lane 1) and after (lane 2) passing the supernatant through a 0.1 mL HisTrap column. A distinct band was observed after elution with buffer B, suggesting the protein was His_6 -tagged and could be Pep2 (expected size 52 kDa) despite appearing too large when compared to the Mw marker.

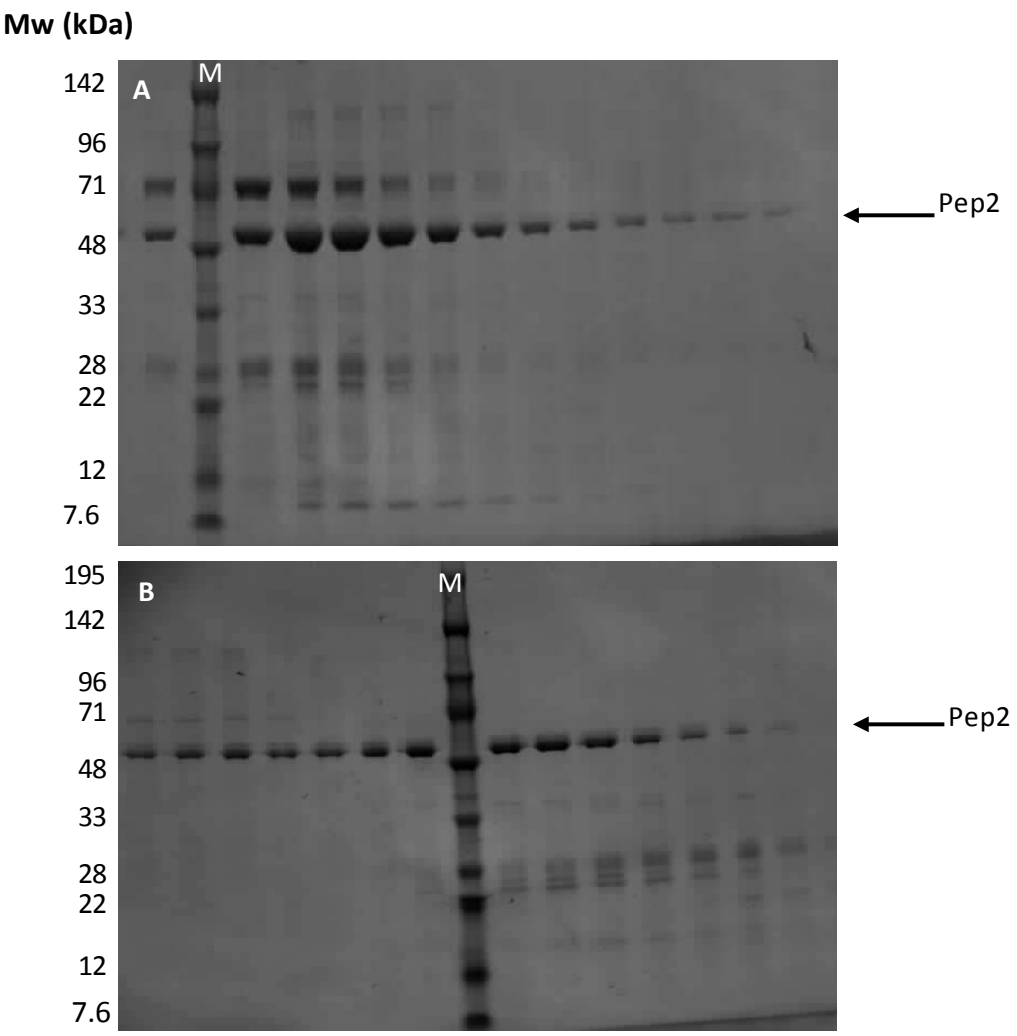

Figure 4.2: Large scale purification of Pep2
(A) SDS-PAGE of protein-containing fractions after elution from a HisTrap column. M= marker
(B) SDS-PAGE of protein-containing fractions after eluting from a size exclusion chromatography (SEC) column. M= marker

4.4 Pep2 activity

Initial activity studies were monitored by thin layer chromatography (TLC) (Figure 4.3). A solvent system that led to differential migrations of maltose and αM1P was used to determine if Pep2 had maltose kinase activity. After 1 h it was evident that there was conversion of maltose into αM1P (Figure 4.3). However, after prolonged incubation a white precipitate was visible in the assay. The white precipitate was only observed when Pep2 was present suggesting that the protein, whilst active, had limited stability in solution at 37 °C.

4.5 TreS and Pep2 might form a physical complex

A sample of TreS was combined with Pep2 in a 1:1 molar ratio and incubated at room temperature. Given that Pep2 seemed to be relatively unstable, the sample was left for 30 min. The mixture was then placed on an analytical SEC column in order to observe if the two proteins had formed a complex with one another. The A_{280nm} showed that two distinct species eluted from the SEC column. When the fractions were viewed by SDS-PAGE it suggested that TreS and Pep2 eluted separately and did not co-elute as would be expected if the two proteins formed a complex (Figure 4.4).

DLS was also used to gain insights in to the possible interaction between the TreS and Pep2. The percentage of total protein mass that was aggregated in the sample was much less (<3%) than was observed when compared to samples containing only Pep2. This suggested that the presence of TreS with Pep2 increased the stability of Pep2 and prevented it from aggregating, supporting the notion of complex formation. The major species detected by DLS closely matched the theoretical size (observed size: 724 kDa; expected size: 733 kDa) of a hetero-hexameric complex comprising 6 subunits each of TreS and Pep2.

Therefore these data, whilst not conclusive, indicated that perhaps TreS stabilised Pep2 by forming a complex with the protein.

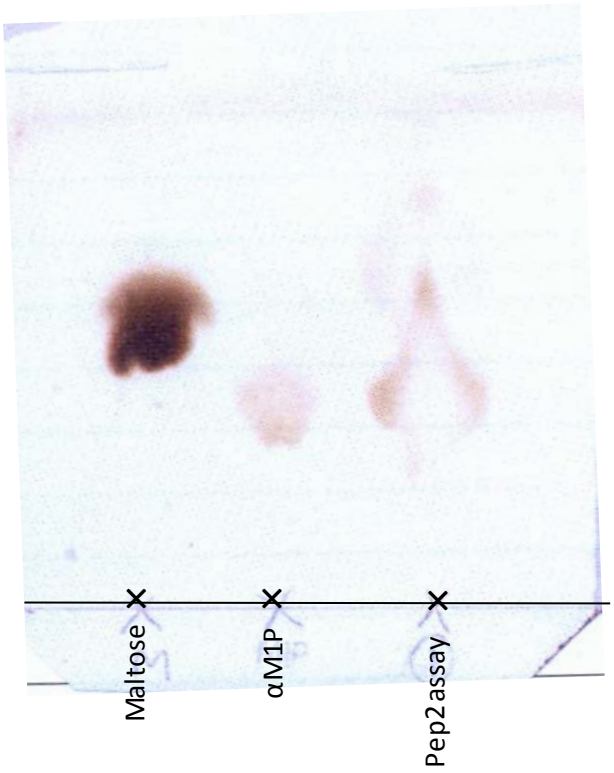

Figure 4.3: Pep2 has maltose kinase activity
A sample of an assay containing Pep2, 10 mM maltose, 10 mM ATP and 10 mM $MgCl_2$ were spotted onto TLC plates after incubation at 37 °C for 1 h. The tear-shaped spots from the assay migrated to the same position as the αM1P and maltose standard implying that Pep2 can produce αM1P.

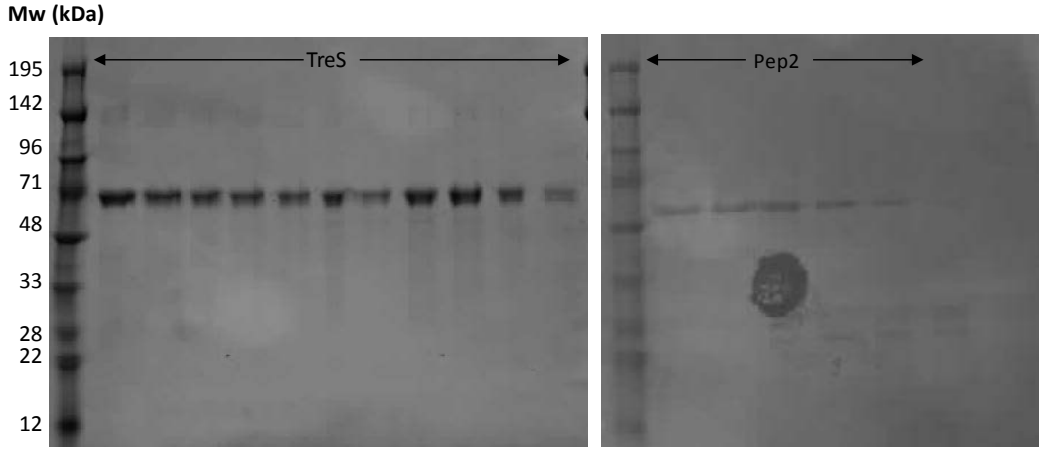

Figure 4.4: TreS and Pep2 do not co-elute from a SEC column
An equimolar solution of TreS and Pep2 was mixed and incubated at room temperature for 30 min. The sample was then injected on to an analytical SEC column to observe if the two proteins co-eluted. Fractions eluting from the column were collected and run on SDS-PAGE. The majority of TreS eluted in earlier fractions and separately from Pep2, which eluted later.

4.6 TreS and Pep2 collectively synthesised αM1P

Enzyme assays were carried out to investigate if TreS and Pep2, at an equimolar concentration and with all the necessary substrates, could synthesise αM1P *in vitro*. TLC suggested that there was production of αM1P under these conditions (Figure 4.5A). This was confirmed by proton nuclear magnetic resonance (^{1}H-NMR) spectroscopy (Figure 4.5B). After prolonged incubation at 37 °C, a white precipitate was visible. As this was also observed in the Pep2 assay, it seems likely that it was Pep2 precipitate.

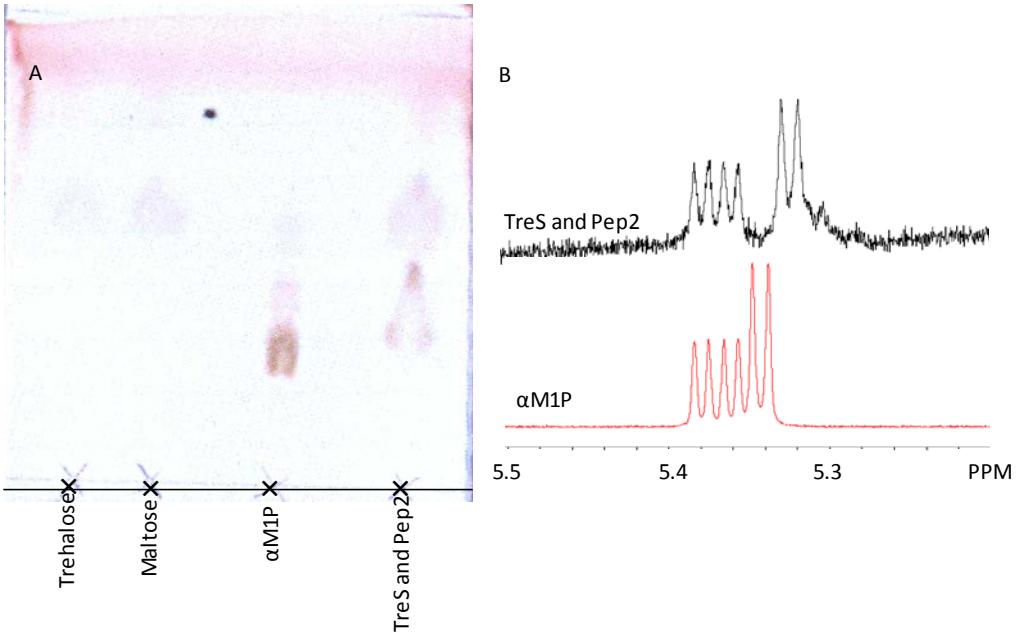

Figure 4.5: TreS and Pep2 convert trehalose into αM1P
(A) A sample of an assay containing 1.5 nM TreS, 1.5 nM Pep2, 10 mM trehalose, 10 mM ATP and 10 mM $MgCl_2$ were spotted onto TLC plates after incubation at 37 °C for 1 h. The tear-shaped spots from the assay migrated to the same position as the αM1P and maltose/trehalose standard which demonstrated that TreS and Pep2 can collectively convert trehalose into αM1P *in vitro*.
(B) The assay was scaled-up and probed by ^{1}H-NMR spectroscopy and resonances matched those for αM1P. A slight shift in the ppm at which the doublet appears was due to the reaction mixture being a different pH to the control αM1P solution.

4.7 Sub-cloning and production trials of TreS-Pep2

A codon-optimised *P .aeruginosa treS-pep2* gene was sub-cloned into a pET21a vector using restriction digestion followed by ligation (Figure 4.6).

Initial small-scale expression trials with *E. coli* BL21 (DE3) seemed to yield large amounts of soluble TreS-Pep2 (Figure 4.7A), which was confirmed by MALDI-TOF mass spectrometry. However, when the condition was scaled-up to 0.5 L there was no significant increase in the amount of TreS-Pep2.

Therefore, more small-scale expression trials of TreS-Pep2 were performed (Figure 4.8). As many conditions initially tested yielded insoluble TreS-Pep2, *E. coli* SoluBL21^{TM} was used because this strain was designed to increase soluble protein expression. Many conditions using *E. coli* SoluBL21^{TM} resulted in soluble TreS-Pep2 (Figure 4.8). The condition yielding greatest levels of soluble TreS-Pep2 was scaled-up and yielded enough protein for further characterisation (Figure 4.9 and 4.10) and possibly crystallography. Aliquots were stored at -20 °C until required.

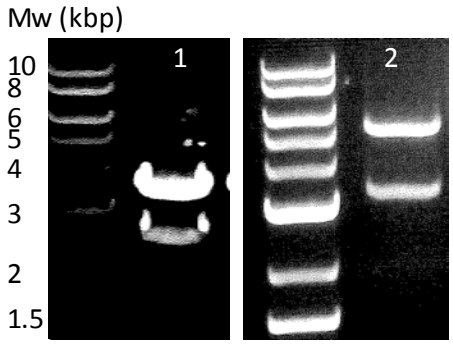

Figure 4.6: Sub-cloning *treS-pep2* into a pET21a expression vector
The *treS-pep2* gene was synthesised (GenScript) for optimal codon usage in *E. coli* and inserted into a pUC57 cloning vector (GenScript). Lane 1 shows that the gene (upper band 3.3 kbp) was excised from the vector (lower band 2.5 kbp) by restriction digestion using NdeI and BamHI. A ligation reaction subsequently fused the gene sequence to a linearised pET21a vector, creating a circularised plasmid suitable for protein expression. *E. coli* DH5α was transformed with the resulting plasmid. Plasmids from successful transformants were purified and subjected to restriction digestion to screen for the correct plasmid. Lane 2 shows the result of a restriction digest of the pET21a vector (upper band 5.5 kbp) containing the full *treS-pep2* gene (lower band 3.3 kbp).

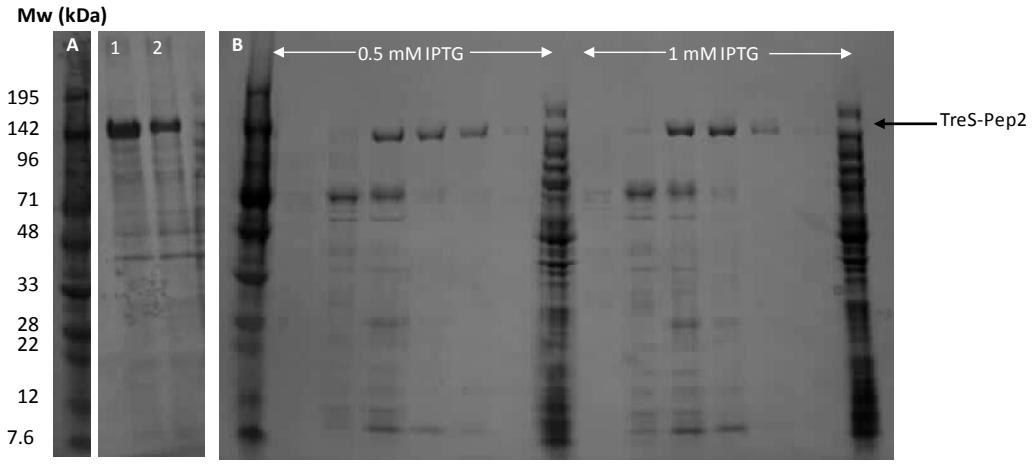

Figure 4.7: Initial expression trials
(A) SDS-PAGE of *E. coli* BL21 (DE3) whole cell fraction (lane 1) and soluble fraction (lane 2) after induction with IPTG and overnight incubation in LB. This suggested that TreS-Pep2 (expected size 125 kDa) was over-expressed in high yields in the soluble fraction.
(B) The above culture was repeated on a 0.5 L scale. Fractions eluted from the column were collected and run on a SDS-PAGE gel. Whilst TreS-Pep2 was observed in the fractions, the protein yield was low.

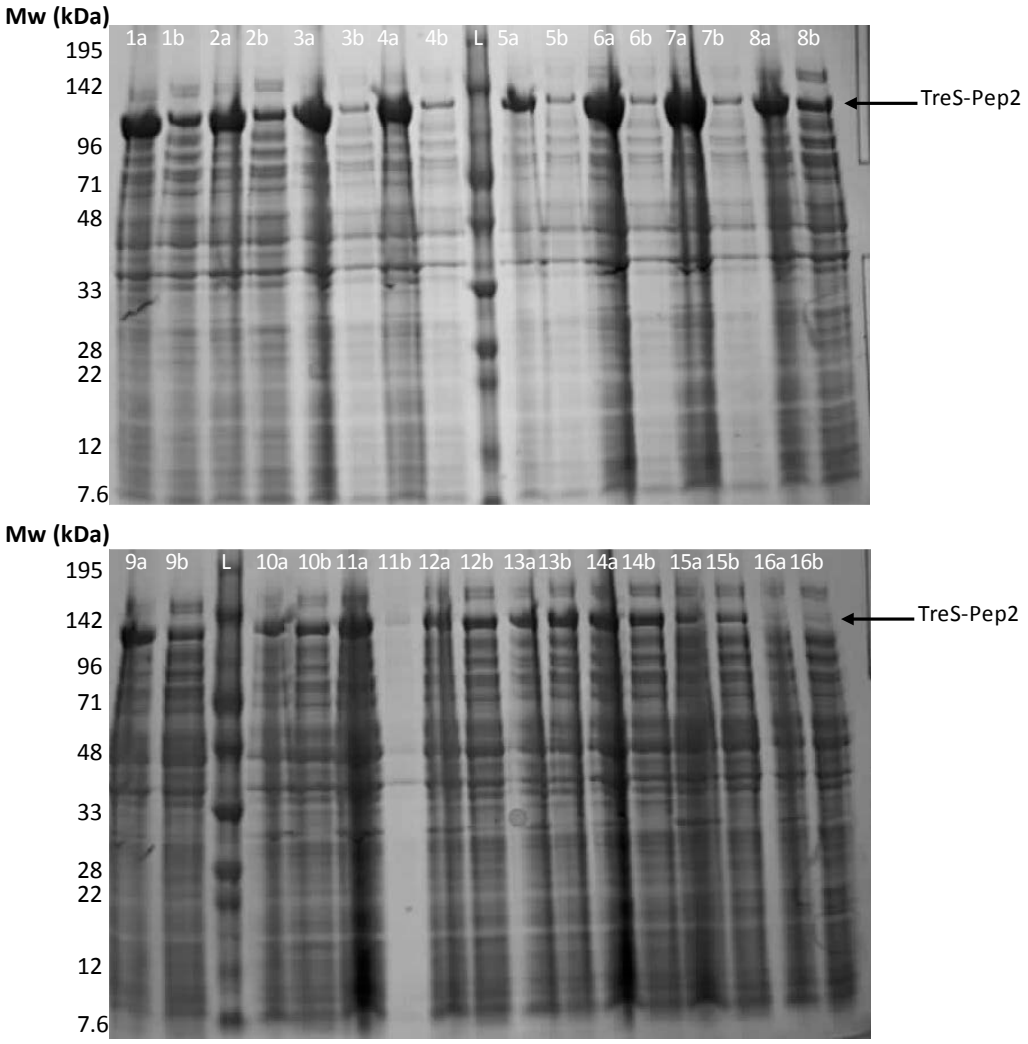

Figure 4.8: TreS-Pep2 further expression trials
SDS-PAGE of whole cell fractions (all lanes labelled a) and soluble fraction (all lanes labelled b) of small scale expression trials using conditions as outlined in Table 4.1. These gels suggested that condition 12 produced the greatest soluble yield of TreS-Pep2 (expected size 125 kDa). L= marker

Table 4.1: Expression trial conditions for TreS-Pep2

Sample Number	***E. coli* strain**	**Liquid media**	**IPTG concentration (mM)**	**DMSO % (v/v)**
1	BL21	LB	2	0
2	BL21	LB	4	0
3	BL21	LB	6	0
4	BL21	LB	1	0.2
5	BL21	LB	1	0.3
6	BL21	LB	1	0.4
7	BL21	SOC	1	0.2
8	BL21	L	1	0.2
9	BL21	AIM	0	0.2
10	SoluBL21	LB	1	0.2
11	SoluBL21	LB	1	0.3
12	SoluBL21	LB	1	0.4
13	SoluBL21	SOC	1	0.2
14	SoluBL21	L	1	0.2
15	SoluBL21	AIM	0	0.2
16	SoluBL21	LB	0	0.2

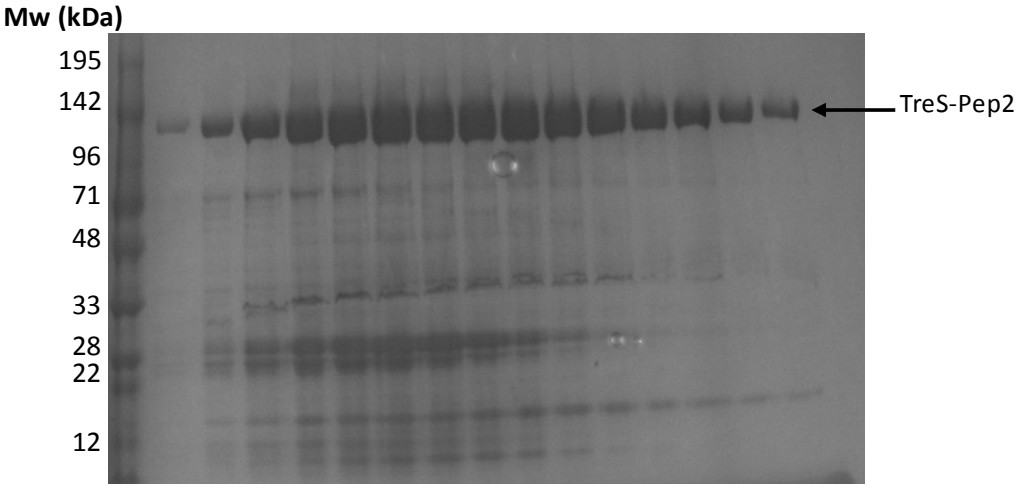

Figure 4.9: Large scale purification of TreS-Pep2
SDS- PAGE of protein-containing fractions after elution from HisTrap column.

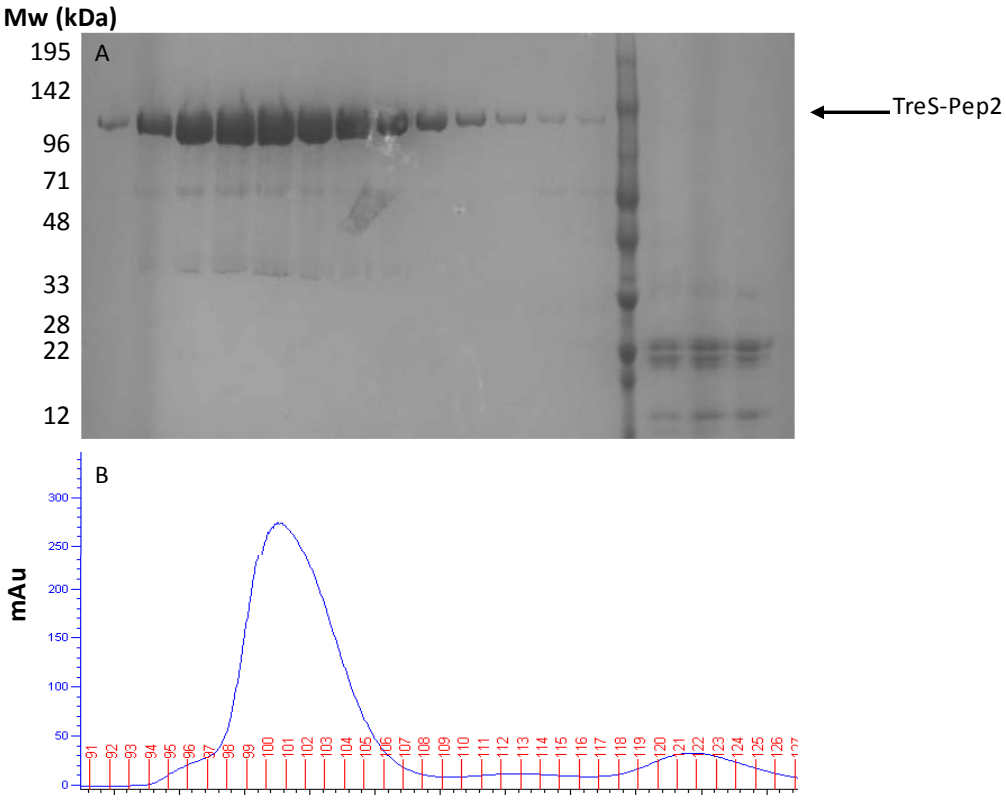

Figure 4.10: SEC suggests that TreS-Pep2 elutes as a pentamer
(A) SDS-PAGE of protein-containing fractions after elution from a SEC coumn.
(B) A_{280nm} chromatogram as TreS-Pep2 (monomeric size 125 kDa) eluted from SEC column showing that it eluted as a single pentamer (expected size 625 kDa; observed size 600 kDa).

4.8 TreS-Pep2 was active but predicted to be disordered and unstable

The A_{280nm} chromatogram as TreS-Pep2 eluted from the SEC column suggested that it eluted as a single pentameric oligomer (Figure 4.10). DLS confirmed the results from the SEC (observed size: 625 kDa; expected size 625 kDa).

Activity assays suggested that the protein was active and could produce αM1P from trehalose (Figure 4.11). There was no visible white precipitate after prolonged incubation, which contrasts to the observations made with TreS and Pep2 from *M. tuberculosis* assays, suggesting the Pep2 is more stable in this enzyme. However, analysis by SEC suggested that the protein was not stable at room temperature for a prolonged period and that it formed aggregates (Figure 4.12). Based on the primary amino acid sequence of TreS-Pep2 it was predicted to have several highly disordered regions (Figure 4.13) (Ward, et al., 2004). Given that TreS-Pep2 was unstable and had many highly disordered regions, crystallisation of this protein was not attempted.

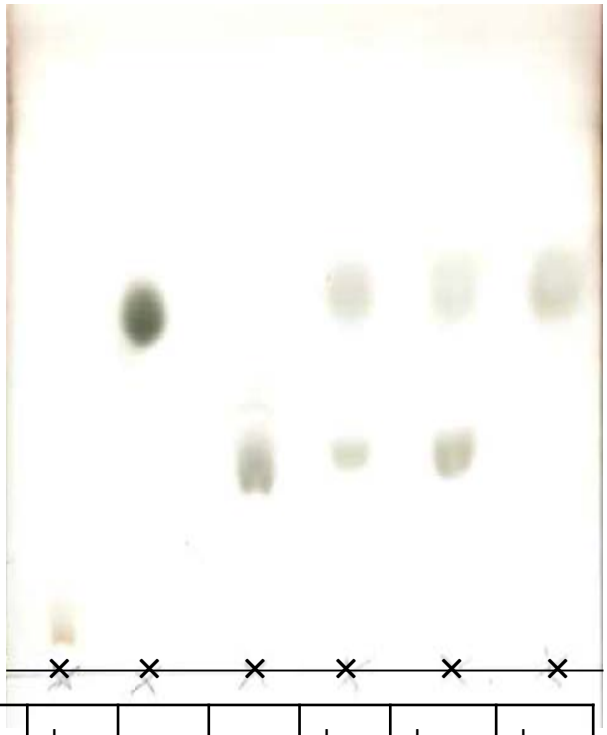

ATP	+	-	-	+	+	+
Trehalose	-	+	-	+	+	+
αM1P	-	-	+	-	-	-
TreS-Pep2	-	-	-	+	+	-

Figure 4.11: TreS -Pep2 converts trehalose into αM1P
Samples of an assay containing TreS-Pep2, 10 mM trehalose, 10 mM ATP and 10 mM $MgCl_2$ were spotted onto TLC plates after incubation at 37 °C for 1 h. The spots from the assay migrated to the same position as the αM1P and trehalose standard, which demonstrated that TreS-Pep2 converts trehalose into αM1P.

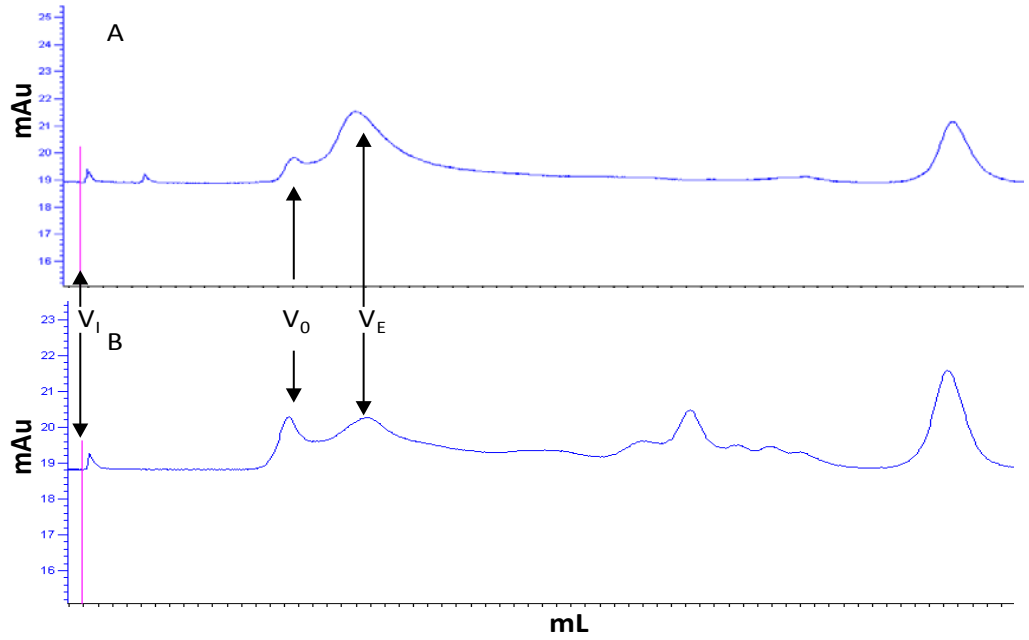

Figure 4.12: TreS-Pep2 formed aggregates

(A) Thawed TreS-Pep2 was injected (V_I) onto and eluted (V_E) from an analytical SEC column.

(B) After incubation for 2.5 h at room temperature, another sample of TreS-Pep2 was injected (V_I) and eluted (V_E) from the analytical SEC column. There was less TreS-Pep2 eluting as a pentamer, and the mAu was approximately half of that observed in 4.12A. There was a concomitant increase in the protein that eluted in the void volume (V_0), suggesting that whilst at room temperature the protein had aggregated. There were also a number of other fragments eluting after the majority of TreS-Pep2. These fragments eluted after the smallest standard that had been used to calibrate this column. The smallest standard used was 12 kDa, which suggested that TreS-Pep2 was broken down by proteolysis into peptide fragments.

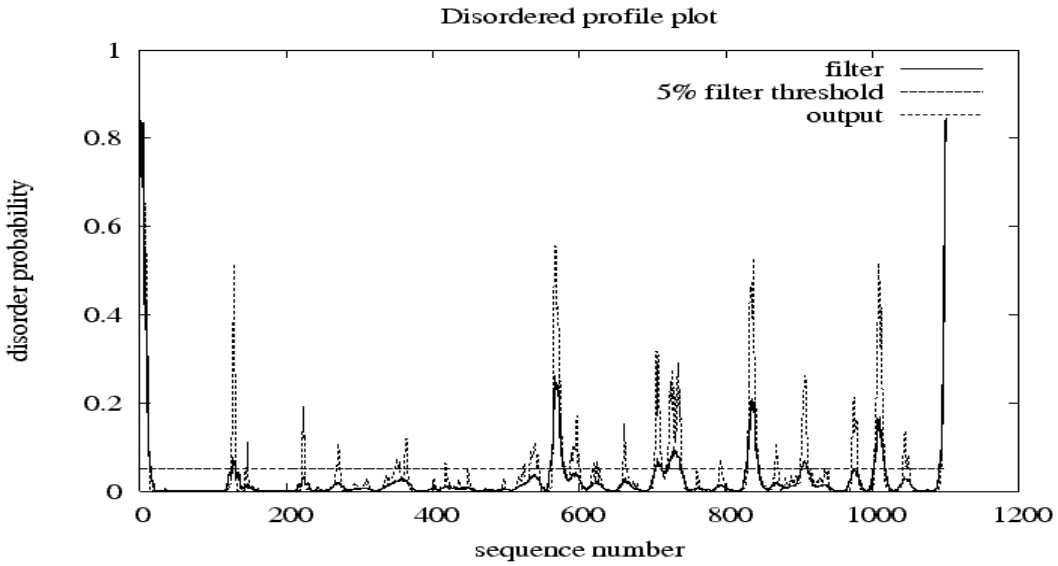

Figure 4.13: Disopred profile for TreS-Pep2 suggested the protein is highly disordered

4.9 Discussion

The focus of this chapter was to characterise the maltose kinase Pep2. Generally, the protein was relatively difficult to purify and had limited stability in assays.

Pep2 was more stable in the presence of TreS. Whilst there was conflicting data for complex formation between the two proteins in vitro, there is recently published evidence that *M. tuberculosis* TreS and Pep2 do form a complex under different experimental conditions (Roy, et al., 2013). Small angle X-ray scattering and analytical ultracentrifugation confirmed that TreS and Pep2 form a hetero-octameric complex in solution (Roy, et al., 2013). This is in the same order magnitude as observed in this study by DLS. The study also presented SEC data to show complex formation (Roy, et al., 2013). A 2:1 molar ratio of Pep2:TreS was used in the published work (Roy, et al., 2013), unlike the 1:1 ratio used in this study, which could be an explanation as to why no conclusive complex formation was observed in this study. Moreover, a different buffering system was employed in the published work, which could have also contributed to the lack of complete complex formation being observed (Roy, et al., 2013).

Attempts to produce the fusion TreS-Pep2 were successful. The fusion protein was also found to be active in vitro. However, the protein was unstable and was subject to proteolysis. This combined with the large pentameric oligomerisation state made it unfavourable for crystallisation.

4.10 Summary

In summary, Pep2 as well as TreS-Pep2 were expressed and purified. These proteins, whilst active, were relatively unstable which made them difficult to characterise. The results are the first demonstration that a TreS-Pep2 fusion protein has activity and is able to synthesise αM1P from trehalose. The TreS-Pep2 protein also has most potential to be used to enzymatically synthesise αM1P as it seemed to have the highest activity that was retained even after the protein was freeze-thawed.

Chapter 5: The GlgE Pathway Produces Glycogen in *Streptomyces venezuelae*

5.1 Introduction

The enzyme encoded by the *glgE* gene is a maltosyl transferase that extends linear α-1,4 glucan chains (Kalscheuer, et al., 2010a). Interestingly, GlgE is essential for the viability of *Mycobacterium tuberculosis* because in its absence there is accumulation of α-maltose 1-phosphate (αM1P), which is toxic for the bacterium (Kalscheuer, et al., 2010a).

There is strong evidence of a functional association between the products of the *treS, pep2, glgE* and *glgB* genes in *M. tuberculosis* (Kalscheuer, et al., 2010a). It has been proposed that the four enzymes collectively synthesise α-glucan and that the GlgE pathway is a novel glucan synthesis pathway (Kalscheuer, et al., 2010a). Bioinformatics has been used to show that all of the genes encoding the enzymes of the GlgE pathway are present in 14% of sequenced bacterial genomes and that all four genes are frequently clustered together (Chandra, et al., 2011). Furthermore, evidence from *Streptomyces coelicolor* suggests that three of the four genes are transcribed as a single polycistronic messenger ribonucleic acid (mRNA) (Schneider, et al., 2000). In summary, there is compelling *in vitro* biochemical and bioinformatic evidence for the existence of a novel α-glucan synthesis pathway.

In *M. tuberculosis* and *Mycobacterium smegmatis* there are at least two other pathways that synthesise glucans (Jackson, et al., 2007; Sambou, et al., 2008). Due to this functional redundancy, genetic evidence proving that the GlgE pathway produces α-glucan *in vivo* in *Mycobacterium* is lacking as this would involve knocking out multiple clusters of genes in a single strain.

Mycobacteria are distant relatives of *Streptomyces,* which are developmentally complex bacteria (Kieser, et al., 2000). Many species of *Streptomyces* accumulate abundant levels of cytosolic glycogen during certain points of their life-cycle (Brana, et al., 1986; Bruton, et al., 1995; Ranade and Vining, 1993; Rueda, et al., 2001). The model organism of *Streptomyces* is *S. coelicolor*, which contains the genes encoding the GlgE pathway (Schneider, et al., 2000). However, the gene cluster is duplicated and the two clusters are under differential developmental control (Plaskitt and Chater, 1995; Yeo and Chater, 2005). Moreover, the organism contains genes encoding GlgA and GlgC, which are involved in a separate glycogen synthesis pathway (Martin, et al., 1997).

Therefore, *S. coelicolor* is not an ideal model to study the GlgE pathway in isolation. *Streptomyces venezuelae* is now emerging as an alternative *Streptomyces* model organism, predominantly because of its ability to develop and sporulate in liquid culture (Ranade and Vining, 1993). Consequently, the full genome sequence is known and, unlike *S. coelicolor*, it contains a single gene cluster encoding the GlgE pathway and it lacks the genes encoding any alternate glycogen synthesis pathways. Therefore *S. venezuelae* was potentially an ideal organism to study the GlgE pathway.

The work presented in this chapter aimed to understand if the GlgE pathway is responsible for glycogen synthesis *in vivo* in *S. venezuelae*. It also aimed to determine if glycogen is essential for the viability of *S. venezuelae* and what impact the absence of glycogen has on the developmental life-cycle of the organism. Finally, this work sought to determine if αM1P is also toxic as observed in other actinomycetes.

5.2 Generation and confirmation of *ΔglgE::apr*

A *ΔglgE::apr* mutation was made following the ReDirect™ protocol (Gust, et al., 2003). Primers were designed according to the protocol suggestions and the formation of the correct polymerase chain reaction (PCR) product was monitored by agarose gel electrophoresis (Figure 5.1). Insertion of the *apr* cassette in place of *glgE* gene in a cosmid was confirmed by restriction digestion of the cosmid followed by agarose gel electrophoresis (Figure 5.1). The mutated cosmid was then transferred into *S. venezuelae* by conjugal transfer and antibiotic selection was used to identify colonies containing the *ΔglgE::apr* mutation. After three further rounds of selective re-streaking from single colonies, spores of the mutant were re-suspended in 20% (v/v) glycerol and stored at -20 °C.

A sample of spores was re-suspended in malt extract-yeast extract-maltose (MYM) liquid medium and incubated overnight at 30 °C with agitation. The cells were harvested and the genomic deoxyribonucleic acid (gDNA) was extracted. The gDNA was used to confirm the mutation by PCR using primers flanking the site of mutation because there was a size difference between the *glgE* and the apramycin *(apr)* genes (Figure 5.2). Southern hybridisation was also used to confirm the mutation as well as to ensure further gene re-arrangements had not occurred during the double cross-over event (Figure 5.2).

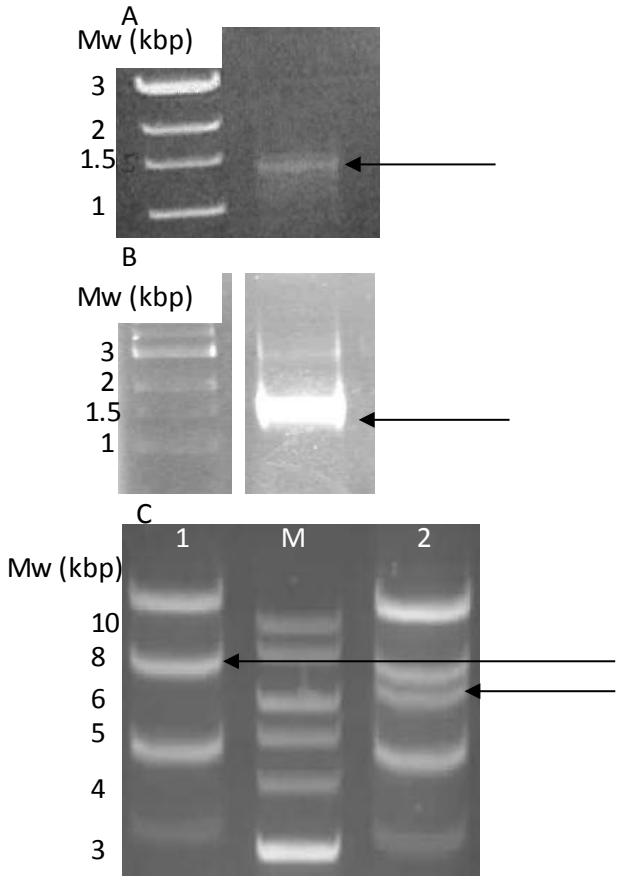

Figure 5.1: The *glgE* gene was replaced with the *acc(3)IV-oriT* cassette in the Sv-3-D04 cosmid

(A) The *acc(3)IV-oriT* cassette (1.4 kbp) was isolated from pIJ773 by restriction digestion with HindIII and EcoRI.

(B) The cassette was used as a template for PCR to generate an *acc(3)IV-oriT* cassette with flanking regions complementary to the flanking regions of *glgE* (1.5 kbp).

(C) *E. coli* BW25113/pIJ790 was transformed with Sv-3-D04 followed by the *glgE* specific *acc(3)IV-oriT* cassette, which replaced *glgE* in Sv-3-D04 by homologous recombination. The cosmid was extracted and digested with MscI (lane 1: WT cosmid; lane 2: Δ*glgE::apr*). A new band emerged (~6.8 kbp) as the cassette was smaller than *glgE*, therefore a doublet in Sv-3-D04 was resolved as 2 separate bands. M=marker

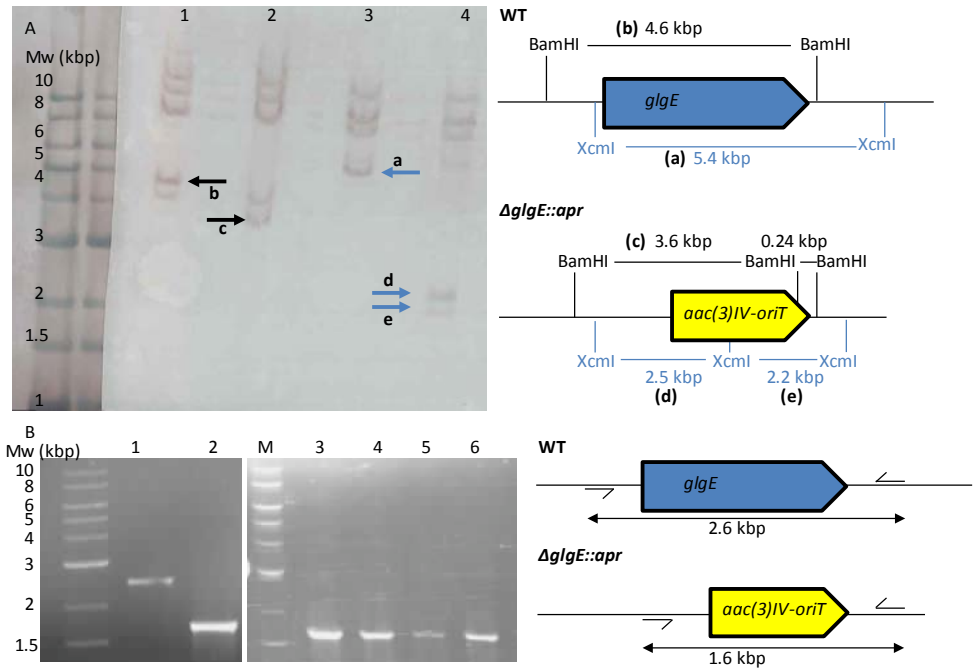

Figure 5.2: Generation of *ΔglgE::apr* was confirmed by Southern hybridisation and PCR analyses

(A) *S. venezuelae* gDNA was extracted and digested with either XcmI or BamHI. For the BamHI digest, one fragment (b) as in wild-type (WT) (lane 1) was expected to form 2 fragments in the *ΔglgE::apr* strain (lane 2), one was visible (C) but the other fragment was too small (0.24 kbp) to be visible. For the XcmI digest, one fragment (a) from WT (lane 3) disappeared and two smaller fragments appeared (d and e) in the *ΔglgE::apr* strain (lane 4), as predicted. The entire Sv-3-D04 cosmid was used as the probe.

(B) *S. venezuelae* gDNA was extracted and used as template for PCR. Primers flanking *glgE* were designed and the PCR product from a reaction in which WT gDNA (lane 1) was used as a template was larger (2.6 kbp) than the product (1.6 kbp) generated from *ΔglgE::apr* gDNA (lanes 2-6) because *glgE* is larger than *aac(3)IV-oriT*. M= Marker.

5.3 Complementation of *ΔglgE::apr*

After the mutant was generated, attempts were made to generate complementation strains. This was to determine if any phenotype observed in the *ΔglgE::apr* mutant could be restored by re-insertion of the *glgE* gene, which would suggest that the mutation was the sole cause of the mutant phenotype.

The *glgE* gene was likely to be translationally coupled to the down-stream *treS* gene and therefore it was not clear if there was a polar effect (Figure 5.5). Sequence analysis suggested that there was a putative ribosome binding sequence within the *glgE* gene upstream of the *treS* gene which might have been required for efficient translation of *treS* (Figure 5.5). Consequently, two complementation plasmids were designed; one contained the endogenous promoter as well as the *glgE* gene and a second additionally contained the *treS* gene. PCR was used to amplify the gene fragments from a wild-type (WT) gDNA template (Figure 5.3). The fragments were cloned into a pUC19 vector and the corresponding plasmids were screened for the correct sized insertion by restriction digestion followed by agarose gel electrophoresis (Figure 5.3). Plasmids that contained the correct sized insert were then sequenced.

When a plasmid containing the correct sequence was identified the gene fragment was sub-cloned into the pMS82 complementation vector (Figure 5.4). The incorporation of the entire fragment into the vector was confirmed using restriction digestion followed by agarose gel electrophoresis. A plasmid containing the correct gene fragment was then used to transform *Escherichia coli* ET12567/pUZ8002. A successful transformant was used to conjugally transfer the complementation plasmid into *ΔglgE::apr* and antibiotic selection was used to screen *ΔglgE::apr* colonies containing the complementation plasmids.

After three rounds of selectively re-streaking from single colonies, the resulting spores were re-suspended in 20 % (v/v) glycerol and stored at -20 °C.

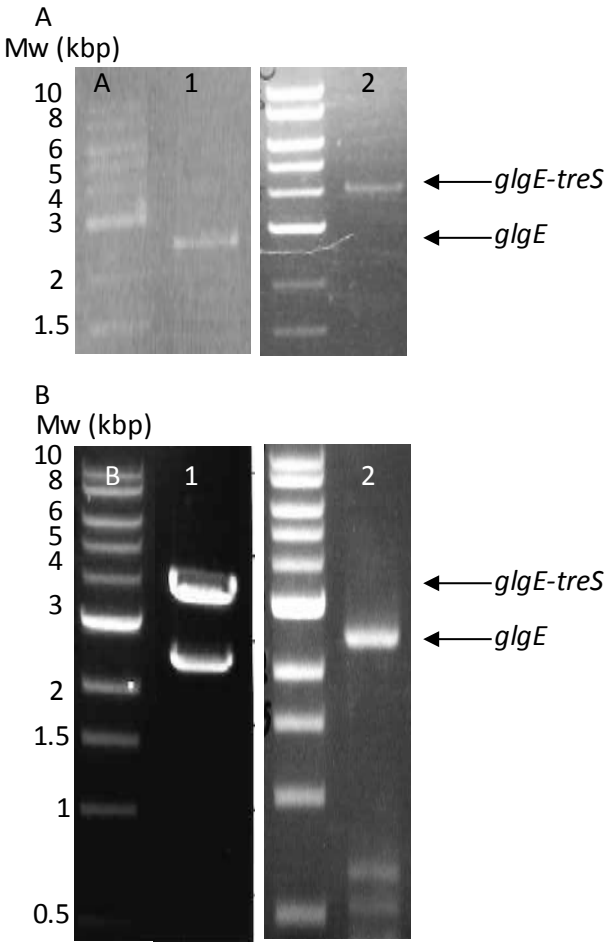

Figure 5.3: Generation of *glgE* and *glgE-treS* fragments by PCR and ligation into pUC19 for sequencing

(A) WT *S. venezuelae* gDNA was extracted and used as a template for PCR. Primers were designed so that the gene as well as the endogenous promoter would be amplified from the gDNA. Fragments corresponding to *glgE* (lane 1, 2.6 kbp) and *glgE-treS* (lane 2, 4 kbp) were generated.

(B) The PCR products were subsequently ligated into a pUC19 vector. The resulting plasmid was used to transform *E. coli* DH5α. Transformants were cultured, and their plasmids were extracted. The plasmids were digested with restriction enzymes (XbaI and EcoRI for *glgE-treS*; XbaI, DdeI and EcoRI for *glgE*)to ensure whole fragments were ligated into the vector (lane 1, *glgE-treS* (upper band; 4 kbp) pUC19 (lower band; 2.7 kbp); lane 2, *glgE* (upper band; 2.5 kbp) pUC19 (lower three bands).

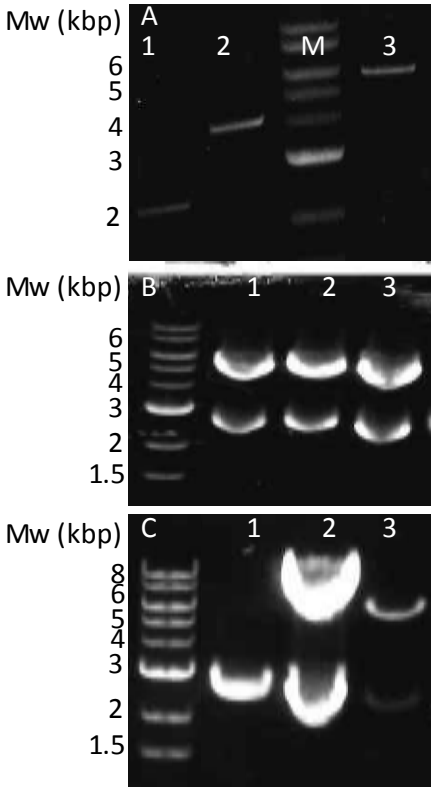

Figure 5.4: Sub-cloning *glgE* and *glgE-treS* fragments into pMS82
(A) Plasmids containing the correct sequence of *glgE* and *glgE-treS* were excised and purified from pUC19 by restriction digestion followed by gel electrophoresis. To ensure the purified sample was free of contaminants, the products were checked by gel electrophoresis (lane 1, *glgE* (2.5 kbp); lane 2, *glgE-treS* (4 kbp)). The pMS82 vector (5.5 kbp) was linearised by restriction digestion with EcoRV (lane 3). M= marker
(B) The *glgE* fragments were ligated to linearised pMS82. The resulting plasmid was used to transform *E. coli* DH5α. Transformants were cultured, and their plasmids were extracted. The plasmids were digested with BglII to ensure *glgE* was ligated into the vector (lane 1-3 clonal strains containing pMS82-*glgE*; expected sizes 2.7 and 5.5 kbp).
(C) As in B above but with *glgE-treS.* Some transformants contained re-circularised vector only (lane 1) and therefore the digest resulted in two bands just below 3 kbp in size. However transformants containing the desired insert (lanes 2 and 3) gave two bands of varying sizes, indicating the additional gene fragment had been ligated into the plasmid (expected sizes 2.7 and 7 kbp).

Figure 5.5: Schematic arrangement of genes encoding enzymes of the GlgE pathway in *S. venezuelae*
The *glgE* and *treS* genes are translationally coupled, sharing a 4 bp atga sequence. Furthermore, there is a putative ribosome binding sequence comprising GGAGG 12 bp upstream of the *treS* start codon, within the *glgE* gene (represented in red). The *pep2* and *glgB* genes, however, are not translationally coupled.

5.4 Polar effects led to no TreS expression in *ΔglgE::apr*

When grown on solid MYM agar, the mutant had a developmentally delayed phenotype (Figure 5.6). The developmental delay was restored when the strain was complemented with either *glgE* or *glgE-treS* (Figure 5.6), suggesting the phenotype was solely due to the absence of the *glgE* gene.

TreS activity was probed in *ΔglgE::apr* by adding trehalose to non-boiled cell extracts and monitoring maltose and trehalose levels as a function of time (Figure 5.7). Whilst there was a decline in trehalose levels with time, it was not clear if there was conversion into maltose because there was also a decline in α-maltose 1-phosphate (αM1P). Therefore, the rise in maltose could have been attributed to either TreS activity or phosphatase activity.

The cell extracts were subsequently incubated with maltose instead to test for TreS activity (Figure 5.8). The results showed that in WT cell extracts trehalose content initially increased, which was followed by a slight decline, most likely due to trehalase activity. However, in the *ΔglgE::apr* mutant only a decline in trehalose levels was observed, which indicated that TreS activity was lacking in the mutant. Therefore, from a genetic perspective, a completely complemented strain required the re-insertion of both *glgE* and *treS* genes.

Sections of WT *S. venezuelae* were stained with periodic acid- thiohydrocarbazide-silver proteinate (PATAg) and visualised with transmission electron microscopy (TEM) (Figure 5.8). This showed that glycogen was found abundantly in pre-spores, as observed in *S. coelicolor* (Figure 5.8) (Bruton, et al., 1995). PATAg staining of the partially complemented strain, which contained only the *glgE* gene showed that it too deposited glycogen in pre-spores, much like WT. This demonstrated that TreS activity was not required for glycogen deposition under typical laboratory growth conditions (Figure 5.8). As the growth medium contained predominantly a maltose carbon source, it seems likely that the maltose is transported directly in to the cytosol, thereby negating the requirement of TreS activity for glycogen production in this organism.

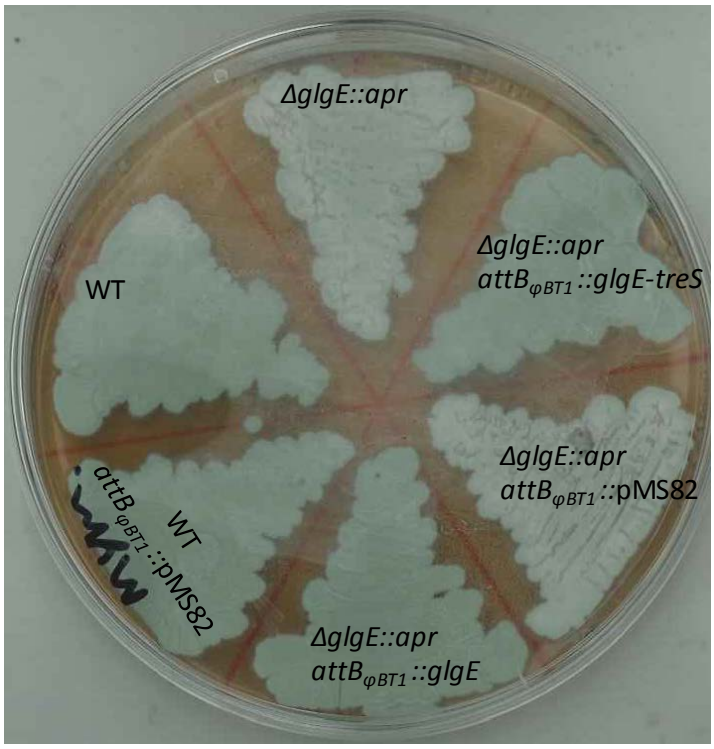

Figure 5.6: Development was delayed in Δ*glgE::apr* and WT-like development was restored by the insertion of *glgE* or *glgE-treS*

Strains of *S. venezuelae* were grown for 2 days, which was sufficient for sporulation of WT (indicated by the green pigmentation of spores, which form at the end of the developmental life-cycle). Development was delayed in Δ*glgE::apr* when compared to WT but was restored by the introduction of either *glgE* or *glgE-treS.*

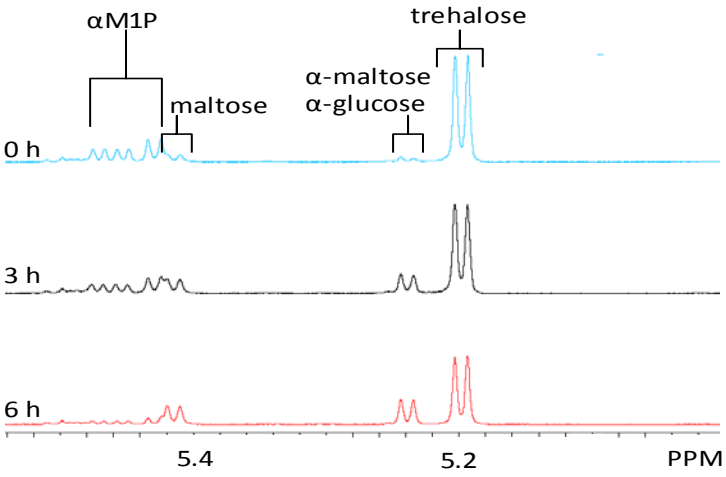

Figure 5.7: TreS activity in Δ*glgE::apr* was unsuccessfully probed by the addition of trehalose

Cell-free extracts of Δ*glgE::apr* were prepared and trehalose (5 mM) was added to the extract. The extracts were monitored by proton nuclear magnetic resonance (^{1}H-NMR) spectroscopy. Whilst there was a noticeable decline in trehalose and increase in maltose as well as glucose, there was also a decline in αM1P and therefore it was unclear if there was TreS activity or not.

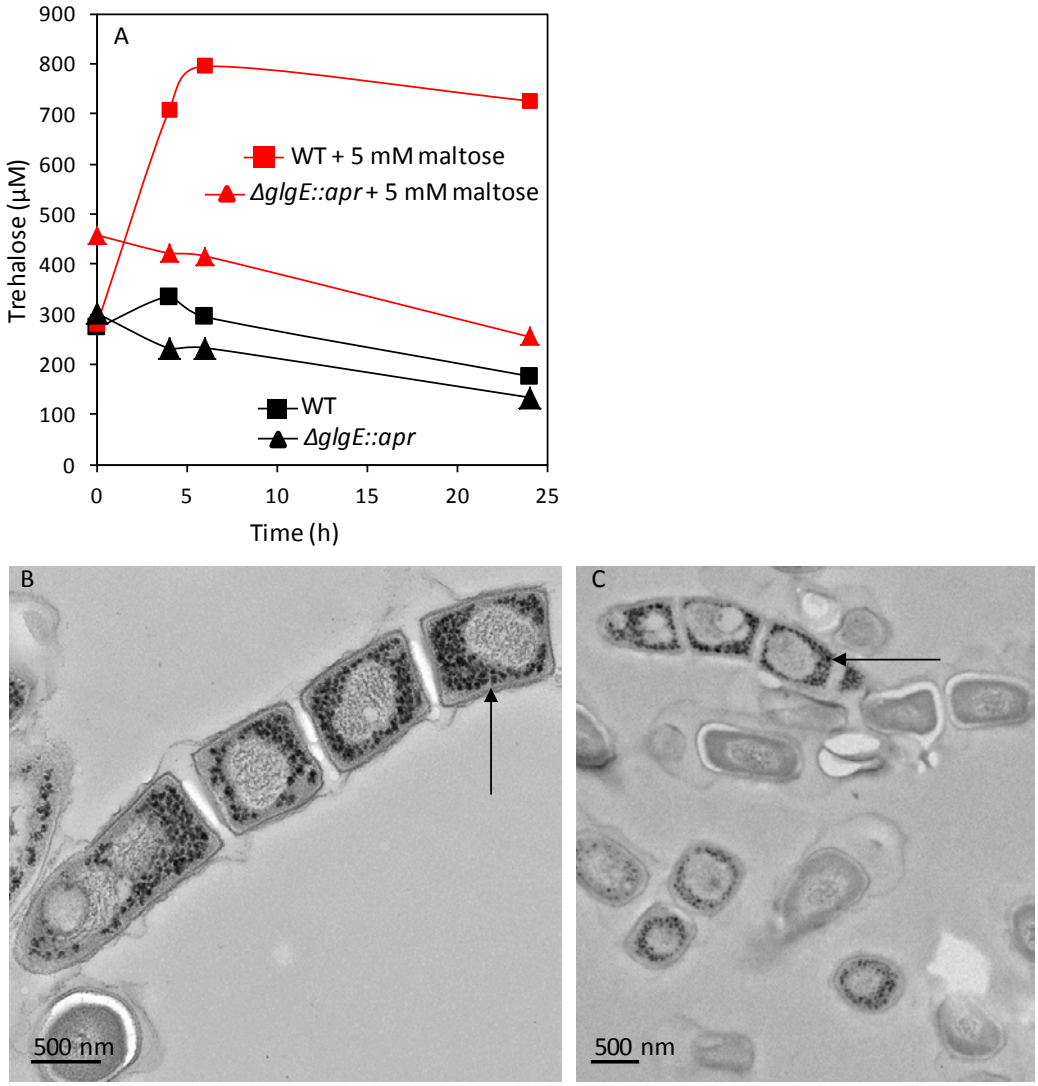

Figure 5.8: There was no detectable TreS activity in Δ*glgE::apr* and it was not required for glycogen synthesis in laboratory growth conditions

(A) Cell-free extracts of Δ*glgE::apr* as well as WT were prepared and maltose (5 mM) was added to the extracts. The extracts were monitored by ^{1}H-NMR spectroscopy. In WT cell-free extracts there was a rapid increase in trehalose levels, suggesting TreS was active and converting α-maltose into trehalose. However, there was no increase in trehalose content in *ΔglgE::apr,* which demonstrated there was no TreS activity within the limits of detection.

(B) PATAg staining of glycogen and visualisation by TEM of WT grown for 5 days showed that glycogen (black granules, highlighted by the arrow) was present in pre-spores. Samples were prepared for microscopy and visualised by K. Findlay and E. Barclay.

(C) PATAg staining of glycogen and visualisation by TEM showed that *ΔglgE::apr attB$_{\varphi BT1}$::glgE* deposited glycogen granules (highlighted by the arrow) like WT. Samples were prepared for microscopy and visualised by K. Findlay or E. Barclay.

5.5 *ΔglgE::apr* had a developmental phenotype and altered metabolism

As mentioned in the previous section, the *ΔglgE::apr* strain had a developmentally delayed phenotype (Figure 5.9). Whilst the strain did sporulate with prolonged incubation, pigmentation was less pronounced when compared to WT and the complemented strain. Furthermore there were consistently fewer spores in the *ΔglgE::apr* strain when compared to WT and complemented strains.

Cell extracts of the *ΔglgE::apr* strain had significant increases in maltose and αM1P levels when compared to WT and the complemented strains throughout their developmental life-cycle (Figure 5.10). The end of the developmental time-course was assumed to be when only trehalose was detected as WT spores are known to contain only trehalose (Ranade and Vining, 1993). Trehalose levels were initially much lower than WT and complemented strains but at the end of the developmental time-course, trehalose levels in *ΔglgE::apr* were similar to WT (Figure 5.10). There was a concomitant decline in αM1P levels, which suggested that the strain re-cycled its carbon stored as αM1P to trehalose (Figure 5.10). Results from non-boiled cell extracts suggested that αM1P was being de-phosphorylated with time (Figure 5.11). This suggested that, in the absence of TreS, a phosphatase was involved in re-cycling carbon to form maltose, which could subsequently be hydrolysed to glucose and then condensed to form trehalose.

The dry cell mass was also recorded for the strains throughout the developmental time-course (Figure 5.12). The results suggested that *ΔglgE::apr* initially accumulated as much mass as WT and complemented strains. However, during later developmental stages *ΔglgE::apr* accumulated significantly less mass than WT and complemented strains (Figure 5.12).

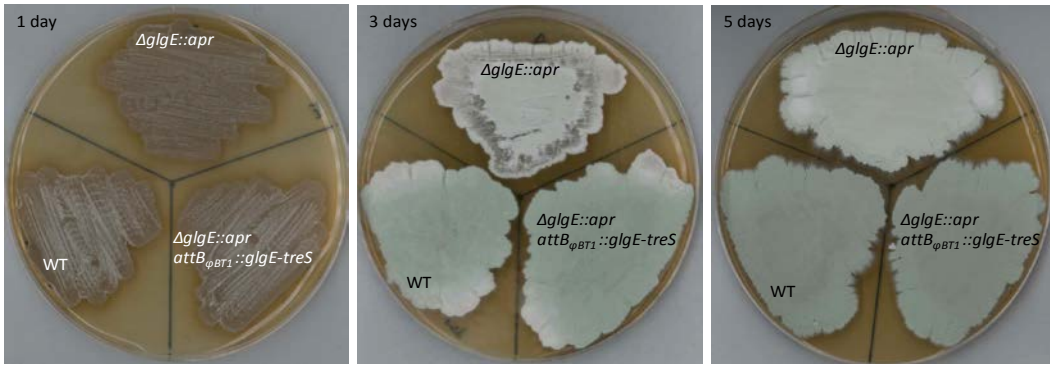

Figure 5.9: Δ*glgE::apr* sporulated after longer periods of incubation but pigmentation was not as pronounced as in the WT or complemented strains

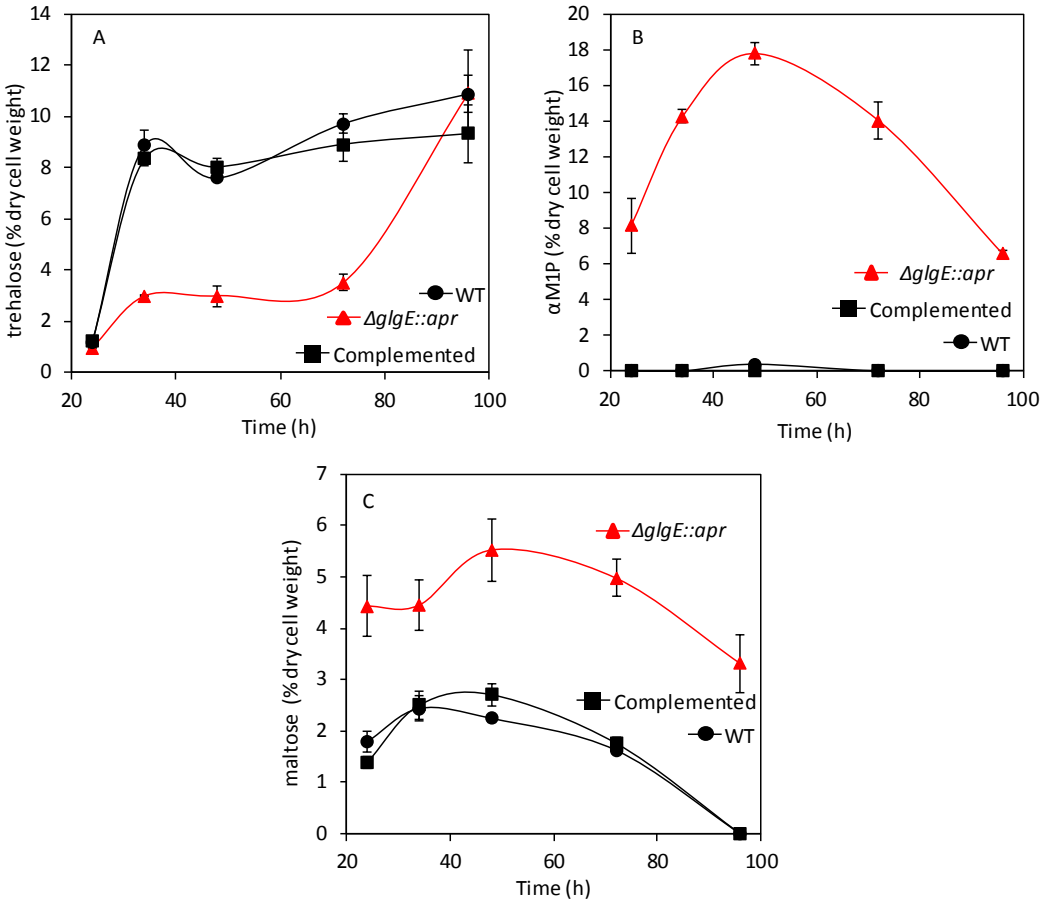

Figure 5.10: Δ*glgE::apr* accumulated large amounts of αM1P and maltose but trehalose levels were the same as in WT at the end of a developmental life-cycle
Error bars are the standard error of the mean (SE) of three observations
(A) Initially, trehalose levels were dramatically lower in Δ*glgE::apr* compared to WT and complemented strains. However, there was a rapid increase in the trehalose content of Δ*glgE::apr* at the end of the developmental life-cycle.
(B) αM1P accumulated in Δ*glgE::apr* but as the life-cycle progressed it declined, which suggested that it was broken down and metabolised.
(C) Maltose levels in Δ*glgE::apr* were approximately twice that of WT and complemented strains.

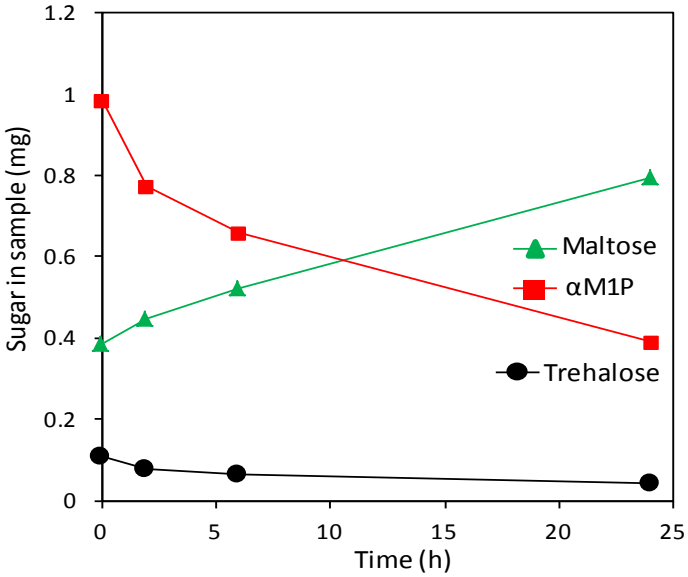

Figure 5.11: αM1P was broken down into maltose by a phosphatase
A non-boiled cell-free extract of Δ*glgE::apr* was probed by ^{1}H-NMR spectroscopy. αM1P was broken down and there was a concomitant increase in maltose levels, suggesting that a phosphatase dephosphorylated αM1P.

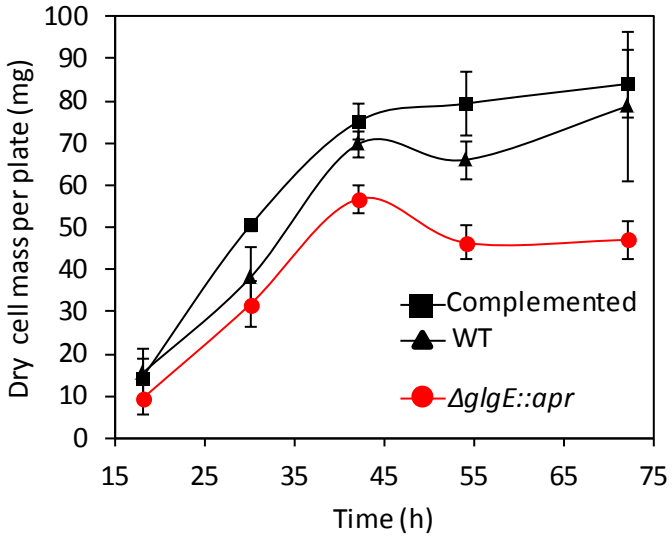

Figure 5.12: Δ*glgE::apr* accumulates less mass
Plates containing MYM-Agar were inoculated with 5 ×10^{6} spores and after set time-points the cell material on the entire plate was scraped off. The samples were subsequently freeze-dried and their masses were recorded. Error bars are the SE of three replicates.

5.6 *ΔglgE::apr* accumulated no glycogen

Samples of WT, complemented and *ΔglgE::apr* strains were prepared for TEM analysis. Samples were stained with PATAg in order to visualise if, and where, glycogen accumulated in colonies. The results suggested that WT and complemented strains accumulated glycogen abundantly in pre-spore compartments (Figures 5.13). Glycogen appeared as electron-dense black granules when stained with PATAg that were each ~50 nm in diameter (Figure 5.13). The mutant strain, however, contained no dark black granules which suggested that it did not accumulate any glycogen (Figure 5.13). This is consistent with the bioinformatic predictions that suggested the GlgE pathway was the only glycogen synthesis pathway in *S. venezuelae*.

Attempts were then made to corroborate the TEM results in a more quantitative fashion. Initial attempts focussed on enzymatic degradation of glycogen into glucose by amyloglucosidases followed by quantification of glucose release, using a modified protocol derived for starch quantification in plants (Smith and Zeeman, 2006). However, the results often suggested that there were equal amounts of glycogen in the WT and *ΔglgE::apr* strains (data not shown). This could be a result of the amyloglucosidase hydrolysing the αM1P in the *ΔglgE::apr* samples, thereby giving a false positive result.

As iodine staining had been routinely used to identify glycogen deficient *E. coli* mutants in high throughput screens (Romeo, et al., 1991; Torija, et al., 2005), this method was subsequently explored. Both WT and mutant strains were grown on a single MYM Agar plate and were then placed in a chamber containing a saturated solution of Lugol's iodine. Unlike *E. coli,* there was no differential staining of the two strains (Figure 5.14) on agar plates. This could have been due to a lack of penetration of the iodine into the aerial hyphae at the surface of *Streptomyces* colonies. However, if the cells were lysed, the cell extracts were differentially stained with Lugol's iodine (Figure 5.14). This suggested that Lugol's iodine could be used to quantify glycogen levels in *S. venezuelae*. The absorbance maxima of cell extract with added Lugol's solution was dependent upon the specific glycogen structure and varied between glycogens isolated from different organisms (Morris, 1946). Therefore, glycogen was extracted from WT *S. venezuelae* to generate a standard curve, using known amounts of dry glucan mass (Figure 5.15). The standard curve was then used to quantify the glycogen levels at

different developmental time-points (Figure 5.16). The results of these assays confirmed that there was no glycogen in the mutant strain at any developmental time-point tested (Figure 5.16). The WT and complemented strains, however, accumulated up to 19% of their dry cell weight as glycogen (Figure 5.16). Interestingly, this matched the maximum αM1P accumulated by the mutant (Figure 5.10), suggesting that it was able to compensate for absence of glycogen by accumulating comparable amounts of αM1P.

A third method was also used to confirm the absence of glycogen in the *ΔglgE::apr* strain. A monoclonal antibody (mAb) raised against glycogen from *M. tuberculosis* recognised glycogen in the cell extract of WT *S. venezuelae* but did not bind to the cell extracts of the *ΔglgE::apr* strain (Figure 5.15) (Baba, 1993).

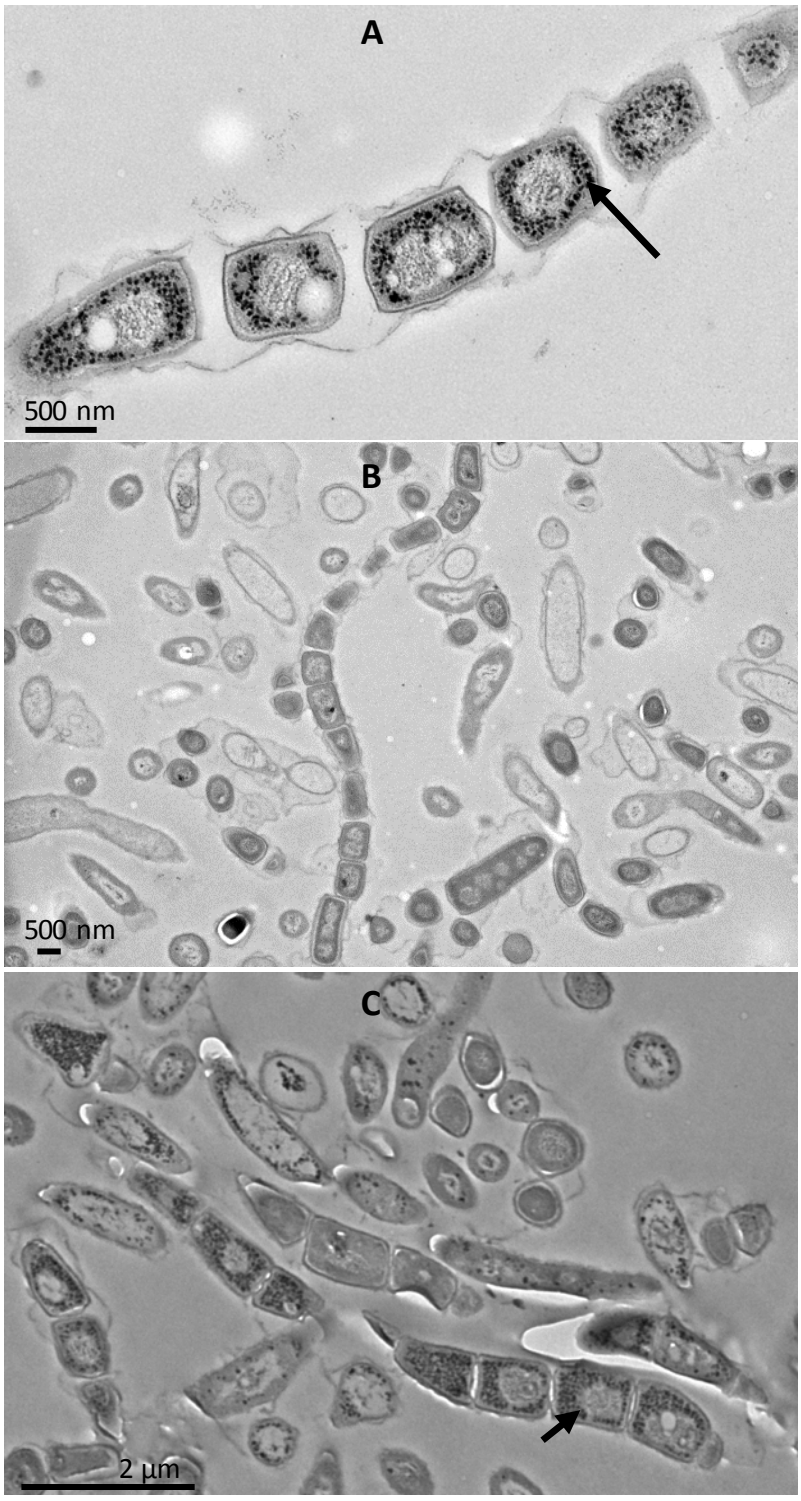

Figure 5.13: WT and complemented *S. venezuelae* accumulated glycogen in pre-spores whereas Δ*glgE::apr* did not

Samples were prepared for imaging and visualised by either K. Findlay or E. Barclay.

PATAg stained sections of *S. venezuelae* grown for 5 days and visualised by TEM suggested that there was glycogen deposited in pre-spore chains of WT (A) and complemented (C) strains, which appeared as black granules highlighted by the black arrows. However, Δ*glgE::apr* had no such black granules (B) in cells at a similar developmental stage, suggesting no glycogen was present in this strain.

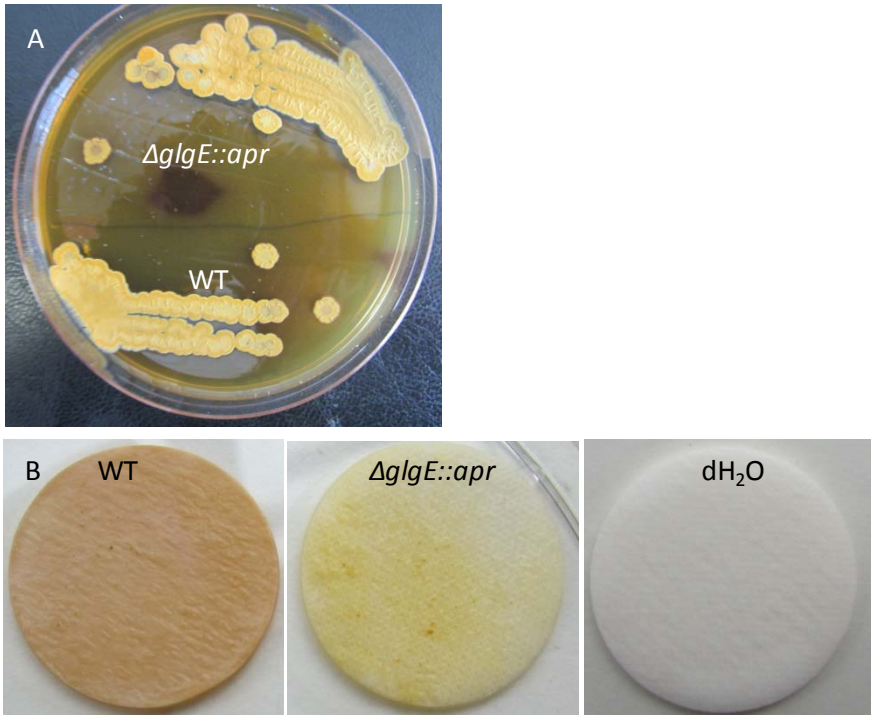

Figure 5.14: Lugol's iodine solution differentially stains cell-free extracts of Δ*glgE::apr* and WT

(A) A plate containing single colonies of WT and Δ*glgE::apr* was placed in a sealed chamber containing Lugol's iodine. The colonies stained yellow and did not differentiate glycogen and non-glycogen containing colonies.

(B) Cell lysates of WT and Δ*glgE::apr* were placed on glass fibre filter paper and placed in a chamber containing a saturating solution of Lugol's iodine. WT stained a brick red/brown colour indicative of glycogen and Δ*glgE::apr* instead stained yellow, much like the whole colonies.

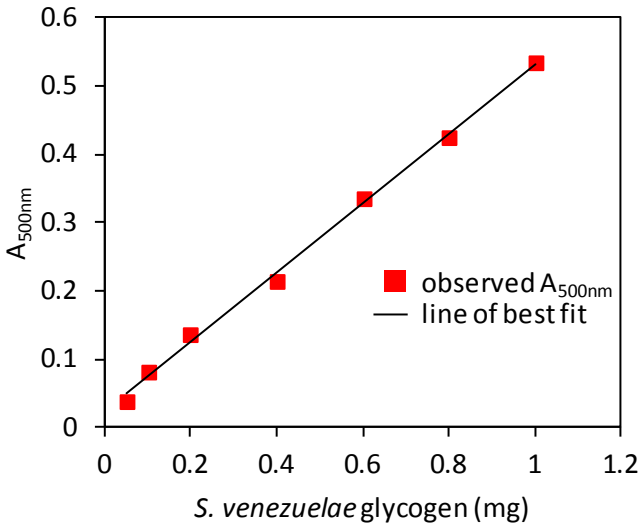

Figure 5.15: Standard curve for Lugol's iodine staining *S. venezuelae* glycogen
Glycogen was extracted from *S. venezuelae,* and known quantities of glycogen were incubated with Lugol's iodine and the A_{500nm} was recorded.

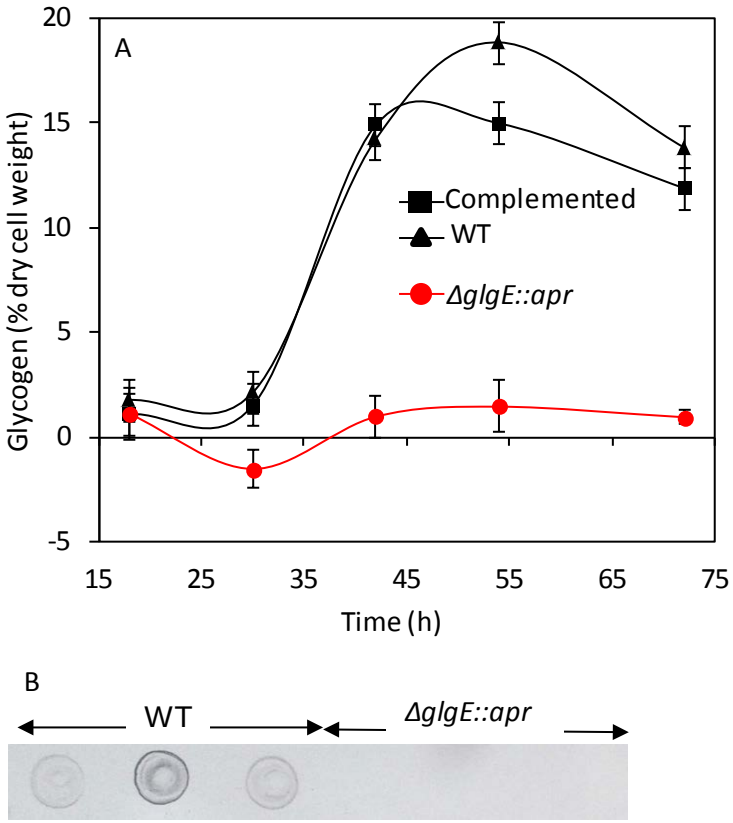

Figure 5.16: Glycogen quantification in *S. venezuelae* strains
(A) Cell-free extracts of *S. venezuelae* strains were incubated with Lugol's iodine and A_{500nm} was recorded, which was used to calculate the glycogen content in the sample. Error bars are the SE of three observations.
(B) Three independent samples of cell-free extracts were treated with a mAb raised against *M. tuberculosis* glycogen and that bound only to WT cell-free extracts. Dot-blot analysis was performed by H. Koliwer Brandl.

5.7 *ΔglgE::apr* produced spores with irregular sizes

It was evident that whilst the *ΔglgE::apr* strain did sporulate, spore pigmentation was less pronounced (Figure 5.9). It was not clear if this was due to fewer spore chains being produced or instead due to reduced spore pigmentation. Therefore, cryo scanning electron microscopy (cryo-SEM) was used to visualise the outer morphology of the spore chains. The images suggested that qualitatively there were comparable amounts of spore chains in all strains (Figure 5.17; K. Findlay personal communication). Therefore, this suggests that there was reduced pigmentation of colonies due to lower levels of spore pigment formation.

Images from cryo-SEM also suggested that although there were abundant spore chains in the mutant strain, the strain frequently produced elongated spores (Figure 5.17). Whilst irregular sized spores were also present occasionally in the WT and complemented strain they were not observed as frequently. Attempts were made to quantitate the numbers of irregular spores by counting all spores in three randomly selected cryo-SEM images of each strain and judging how many had an irregular length. The number of spores present in each image was comparable between every image but ~17% from the mutant strain were irregular in size, which was significantly greater than the WT and complemented strains (Figure 5.18).

5.8 *ΔglgE::apr* spores chromosomal DNA did not condense like WT

Septation in *Streptomyces* spore chains is tightly co-ordinated to DNA replication and condensation (Flardh and Buttner, 2009). Given that irregular septation was observed in the mutant strain, attempts were then made to observe if the condensation and partition of genetic material in spore chains was comparable to WT. All strains were grown on glass coverslips and their cell walls as well as their DNA were stained with wheat germ agglutinin (WGA) and propidium iodide (PI) respectively (Figure 5.19). The samples were viewed with fluorescence microscopy. The images revealed that the mutant strain did not condense its nucleoid DNA like those of WT and complemented strains. In many cases there were several copies of the chromosome in a single elongated spore that was approximately double the normal length in the mutant strain.

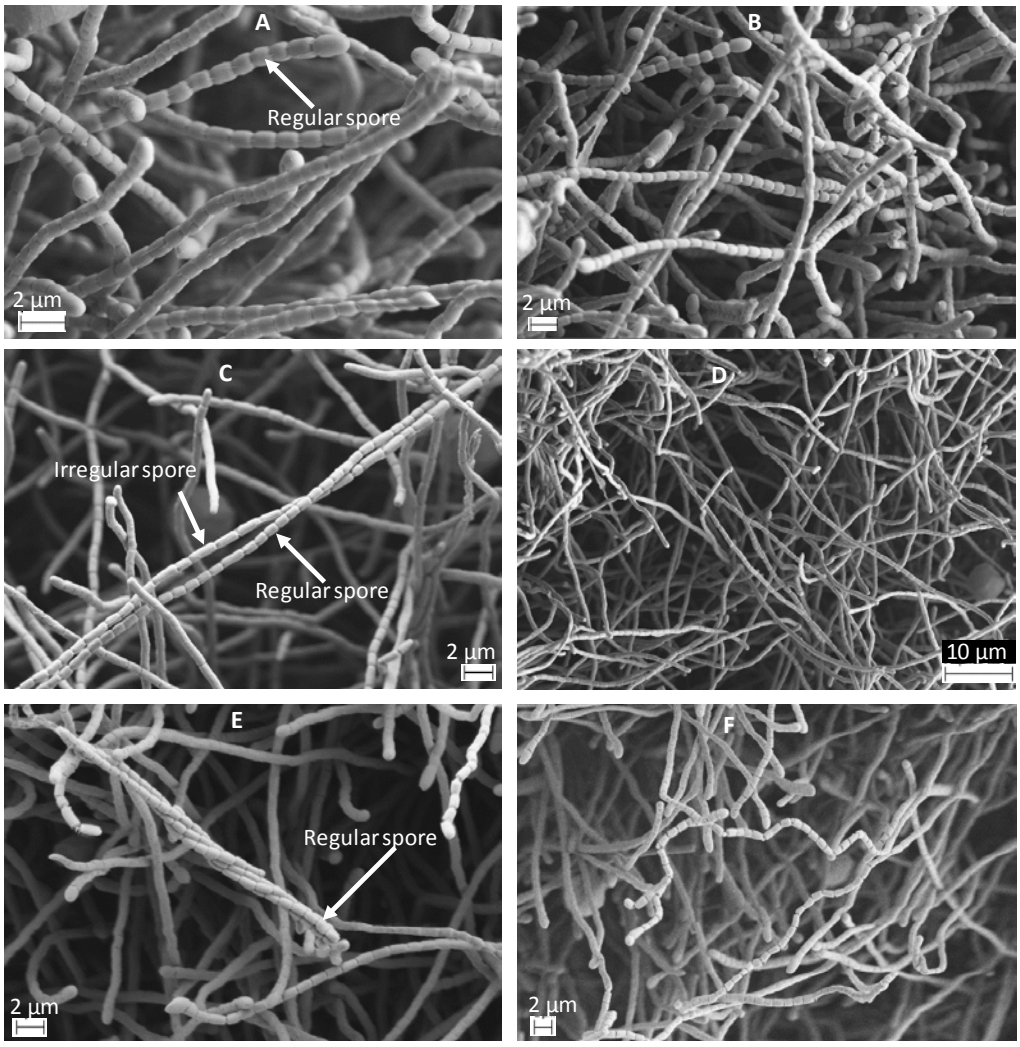

Figure 5.17: *ΔglgE::apr* spores had irregular dimensions when compared to WT and complemented strains

Samples were prepared for imaging and visualised by either K. Findlay or E. Barclay.
Cryo-SEM of *S. venezuelae* strains grown for 7 days showed that spores produced by WT (A and B) and complemented (E and F) strains were predominantly of uniform shape and size. Spores of the *ΔglgE::apr* strain, however, were more frequently irregular. Typically the irregular spores were twice the length of regular spores (C and D).

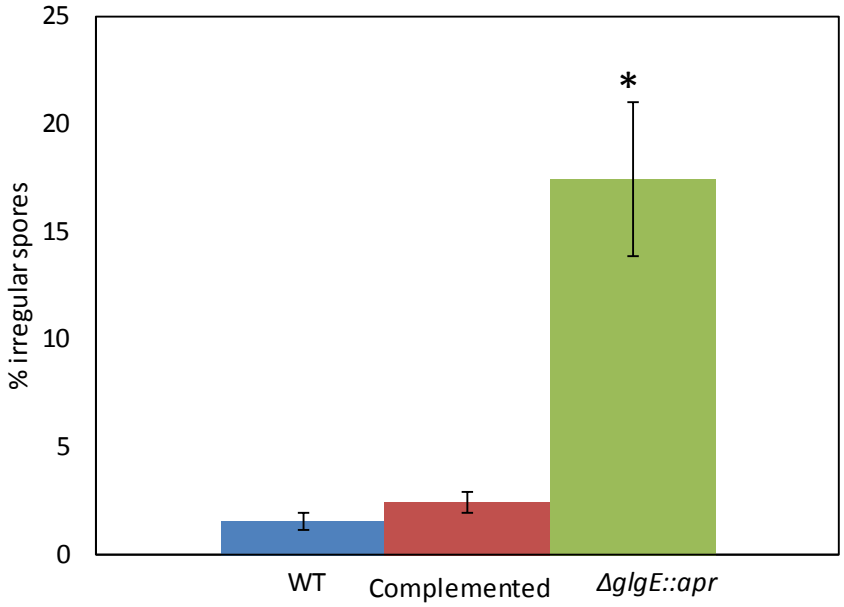

Figure 5.18: Approximately 17 % of Δ*glgE::apr* spores were irregular in size
Spores from three SEM images of each strain were assessed to estimate the percentage of irregular spores. Approximately 100-200 spores were counted in each image.
* = Δ*glgE::apr* was statistically significantly ($p<0.05$) different to WT and complemented strains. Error bars are SE determined for three images.

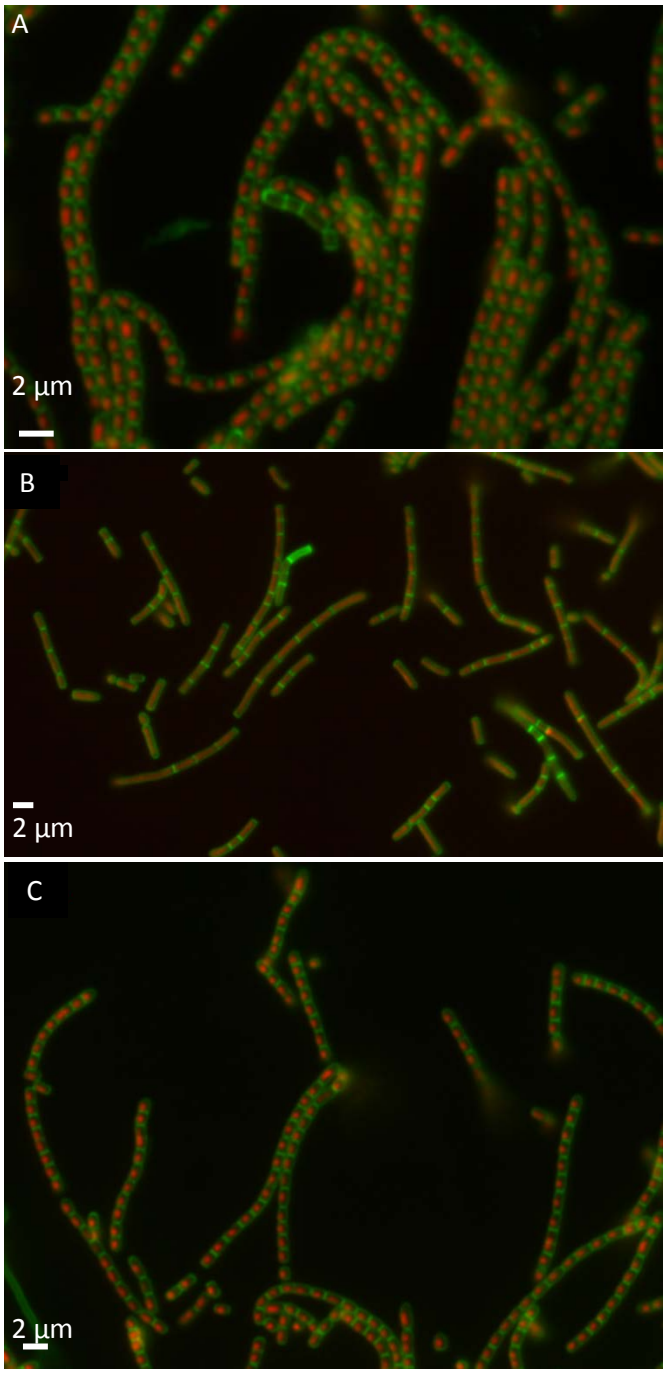

Figure 5.19: Δ*glgE::apr* DNA in pre-spores is diffuse
(A) WT *S. venezuelae* grown for 5 days with nucleic acids stained with PI and cell walls stained with WGA. Spores of uniform size were observed, each containing a single discrete compact nucleoide.
(B) Δ*glgE::apr was* stained as above. Spores were frequently double the normal length and the nucleoides were diffusely distributed throughout the length of the spores.
(C) Complemented strain stained as above appeared to produce spores like those of WT.

5.9 *ΔglgE::apr* spores were less resistant to some abiotic stresses

Given that the spores of the mutant strain were not like WT, their properties were investigated. Resistance to four different abiotic stresses was tested. The spores from the mutant strain were less resistant to lysozyme, heat shock and sonication treatment, suggesting that their cell walls were compromised in some way (Figure 5.20). Interestingly the mutant strain did not have compromised resistance to desiccation stress. Trehalose has been implicated in conferring resistance to desiccation. The metabolite data suggested that trehalose levels in spores were similar to that of WT and complemented strains in the mutant. Therefore, it suggests that as the trehalose content remained the same as WT, *ΔglgE::apr* spores also retained the same ability to survive desiccation stress as WT.

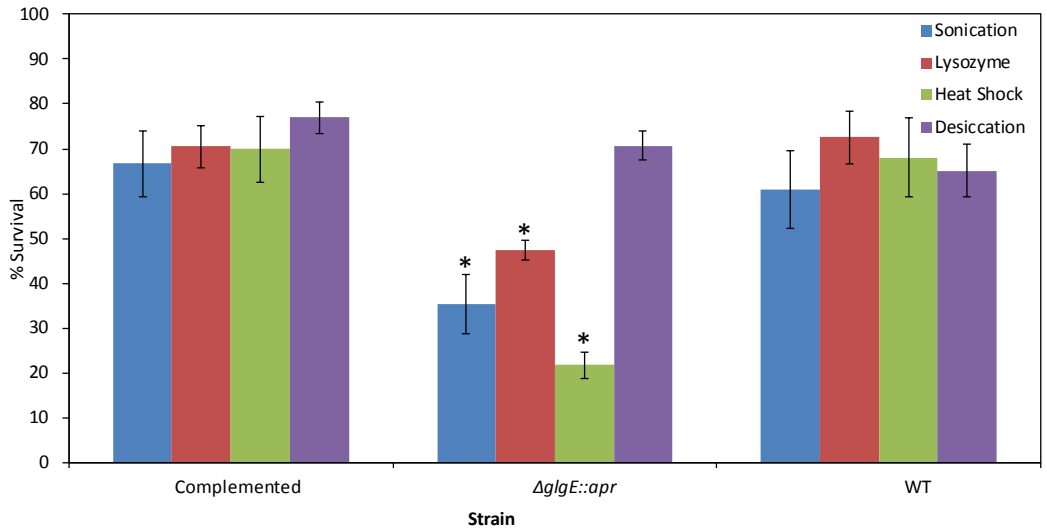

Figure 5.20: Δ*glgE::apr* spores are less resistant to most abiotic stresses with the exception of desiccation stress

Samples of spores were treated with different stresses. An aliquot of spores were taken, prior to treatment, and used to make a serial dilution and plated on to MYM. Colony forming units (CFUs) were counted 1-2 days after the plates were incubated at 30 °C. Survival was determined as a percentage by comparing CFUs before and after treatment.

* = Δ*glgE::apr* was statistically significantly ($p < 0.05$) different to WT and complemented strains as determined by t-tests.

Error bars are SE determined for three replicates, with the exception of sonication, which were of six replicates.

5.10 The phenotype of *ΔglgE::apr* spores was due to accumulation of αM1P

Initially, it was not clear if the phenotype of the mutant was due to the accumulation of αM1P or the absence of glycogen. In order to determine which of the possibilities it could be, an alternative carbon source to maltose was sought. It was hypothesised that by growing the strains on minimal media with different carbon sources it would be possible to have the mutant growing on a carbon source that did not readily allow the *ΔglgE::apr* strain to accumulate αM1P. Growth on a range of different carbon sources was tested (Table 5.1). The most consistent growth and development was observed when maltose was used as the sole carbon source. However, if the duration of incubation was increased, galactose also led to consistent growth and development of WT.

When WT and mutant strains were grown on minimal media with galactose as the carbon source, no developmentally delayed phenotype was observed for the mutant (Figure 5.21). The cell extracts also did not contain any detectable levels of αM1P, suggesting that the developmentally delayed phenotype could be attributable to the build-up of αM1P and not the absence of glycogen.

Cryo-SEM was also used to visualise the spore morphology of the strains when grown on minimal media with either galactose or maltose as the carbon source. This was performed with a view to determining if spore morphology was comparable to WT when the *ΔglgE::apr* strain did not accumulate αM1P. However, unexpectedly, the spore morphology of both WT and the mutant strain was drastically different when grown on galactose (Figure 5.22) and so this question could not be addressed.

Table 5.1: WT *S. venezuelae* growth on different carbon sources

Carbon source	Growth after 9 days on minimal media with iberian agar (MMIA-+)
Maltose	Developed and sporulated
Fructose	Developed and sporulated
Trehalose	Developed
Glycerol	Developed and sporulated
Galactose	Developed and sporulated
Cellobiose	Poor growth
Starch	Poor growth
Sucrose	Poor growth
Lactose	Poor growth

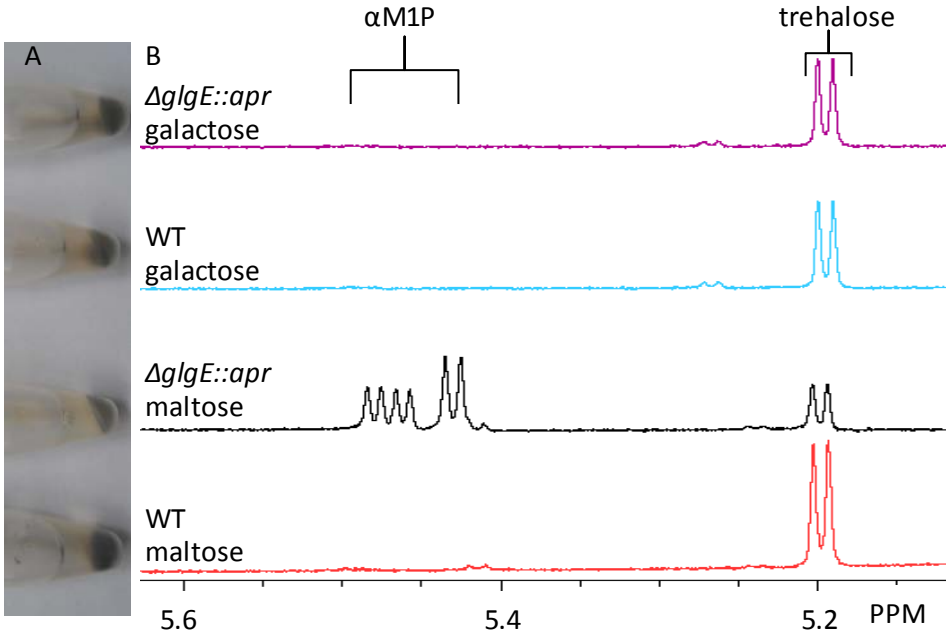

Figure 5.21: Developmental delay was only observed in Δ*glgE::apr* when there is a build-up of αM1P
(A) Cell pellets of strains grown either with maltose or galactose as a carbon source. A phenotype was only visible when *ΔglgE::apr* was grown on maltose. The cell pellet was smaller and had less green pigmentation compared to the other cell pellets.
(B) ^{1}H-NMR spectroscopy of cell-free extracts showed that αM1P was only present in *ΔglgE::apr* when it was grown on maltose, which correlated with the developmentally delayed phenotype.

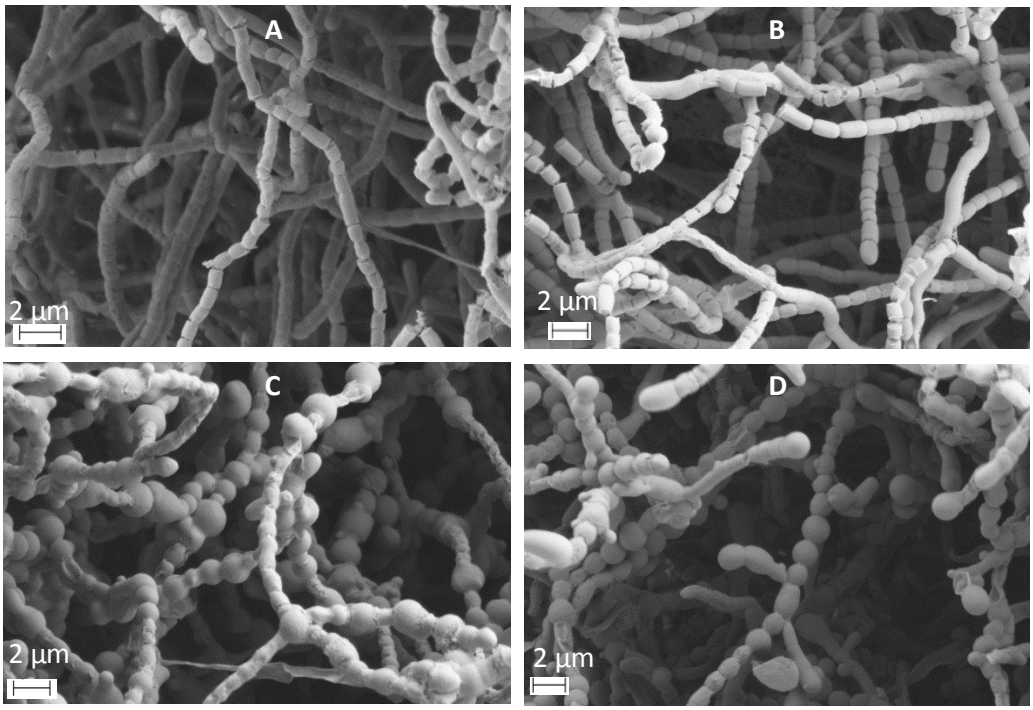

Figure 5.22: Strains grown on different carbon sources had different spore morphologies

Samples were prepared for microscopy and imaged by E. Barclay.

(A) WT *S. venezuelae* was grown for 7 days on MMIA-+ with maltose as a carbon source. Cryo-SEM showed that spores were cylindrical in morphology, as previously observed when WT was grown on MYM.

(B) *ΔglgE::apr* was grown as outlined in A and they had a similar cylindrical shape, as WT.

(C) WT *S. venezuelae* was grown for 9 days on MMIA-+ with galactose as a carbon source. Cryo-SEM showed that spores were spherical, which is different to the spore morphology when WT was grown on MYM.

(D) *ΔglgE::apr* was grown as outlined in C, showed that as with WT the spores were spherical in shape.

5.11 *Δpep2::apr* and the corresponding complementation strain were generated

To further confirm that the developmental delay phenotype was due to αM1P accumulation, a strain lacking the *pep2* gene encoding a maltose kinase was generated. As with the previous mutant, the ReDirect™ protocol was used (Gust, et al., 2003). Replacement of the *pep2* gene with the *apr* cassette in the appropriate cosmid was confirmed by restriction digestion followed by gel electrophoresis (Figure 5.23). After conjugal transfer of the mutated cosmid, *Δpep2::apr* mutants were identified by antibiotic selection. After three rounds of selective re-streaking single colonies, the *Δpep2::apr* strain was allowed to sporulate fully. The mature spores were re-suspended in 20% (v/v) glycerol and stored at -20 °C.

gDNA was extracted from cells that were cultured overnight incubated in MYM medium at 30 °C. The resulting gDNA was used to confirm the mutation by Southern hybridisation as well as indirectly by PCR (Figure 5.24).

WT gDNA was used as a PCR template to amplify the *pep2* gene along with its native promoter. Correct product formation was monitored by gel electrophoresis and the purified PCR product was cloned into a sequencing vector (Figure 5.25) and used to transform *E. coli*. Several positive transformants were screened by colony PCR (Figure 5.25) followed by gel electrophoresis. Plasmid DNA was isolated from any colonies containing the correct sized PCR product and was used for sequencing reactions. A single plasmid containing the correct *pep2* gene sequence was then subjected to restriction digestion. The DNA fragments containing the *pep2* sequence was excised and purified from the vector. It was then sub-cloned into a complementation vector. The incorporation of the entire fragment into the vector was confirmed using restriction digestion followed by gel electrophoresis (Figure 5.25). The plasmid was then used to transform *E. coli* ET12567/pUZ8002. A successful transformant was used to conjugally transfer the complementation plasmid into *Δpep2::apr* and antibiotic selection was used to screen for *S. venezuelae Δpep2::apr* colonies containing the complementation plasmids.

After three rounds of selectively re-streaking from single colonies, the resulting spores were re-suspended in 20 % (v/v) glycerol and stored at -20 °C.

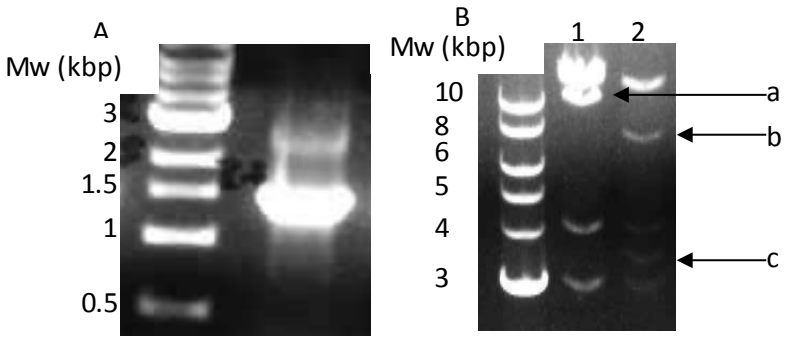

Figure 5.23: The *pep2* gene was replaced with the *acc(3)IV-oriT* cassette in the Sv-3-D04 cosmid

(A) The *acc(3)IV-oriT* cassette (1.4 kbp) was used as a template for PCR to generate a cassette with flanking regions complementary to the flanking regions of *pep2* (1.5 kbp). (B) *E. coli* BW25113/pIJ790 was transformed with Sv-3-D04 followed by the *pep2* specific *acc(3)IV-oriT* cassette, which replaced *pep2* in Sv-3-D04 by homologous recombination. The cosmid was extracted and digested with BglII. A large band (lane 1a: Sv-3-D04 (Δpep2*)*, 11.7 kbp) appeared in place of 2 smaller bands (lane 2b and 2c: Sv-3-D04, 8 and 3.7 kbp respectively) as the cassette was the same size as *pep2*, but had no BglII recognition site.

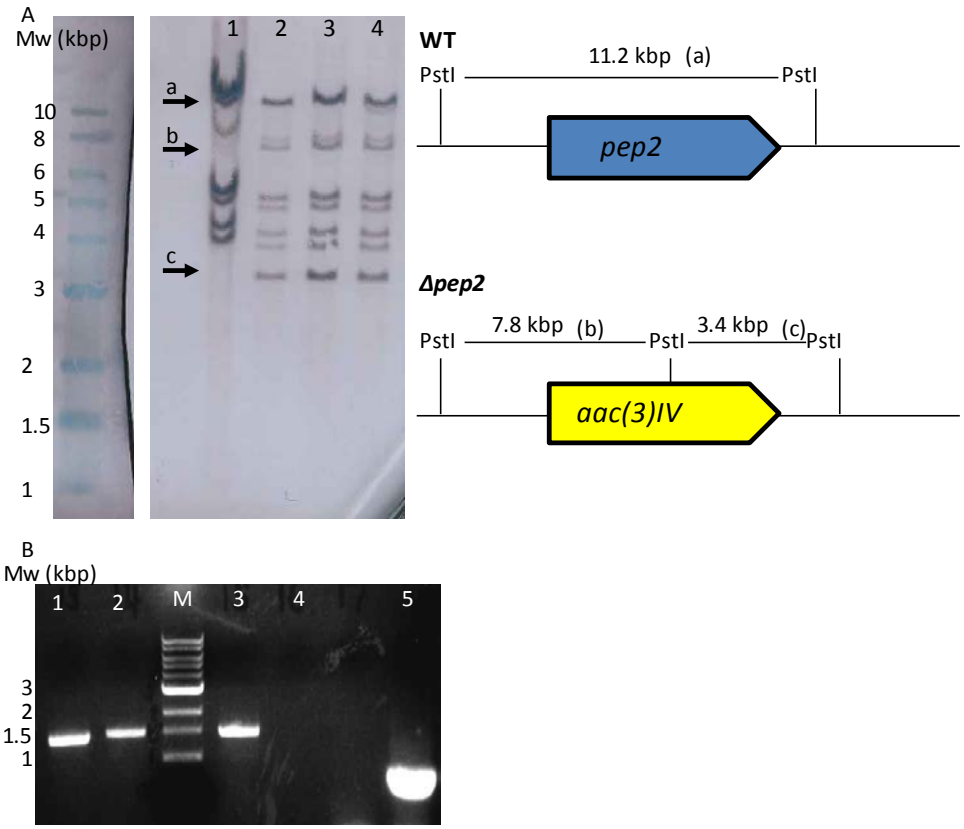

Figure 5.24: The *Δpep2* mutation was confirmed in *S. venezuelae* by PCR and Southern hybridisation

(A) gDNA from WT (lane 1) and three clonal strains of *Δpep2* (lanes 2-4) was extracted and digested with PstI. When probed using the native Sv-3-D04 cosmid, two smaller bands (b (7.8 kbp) and c (3.4 kbp)) in *Δpep2* appeared in place of one large band (a (11.2 kbp)) in WT, as the cassette contained a PstI restriction site whilst *pep2* did not. The entire Sv-3-D04 cosmid was used as the probe.

(B) gDNA was used as a PCR template. PCR reactions were set up using different primers. In lane 1 cassette specific primers were used (expected size 1.4 kbp). In lane 2 a forward primer flanking *pep2* was used with a cassette specific reverse primer (expected size 1.5 kbp). In lane 3 a reverse primer flanking *pep2* was used with a cassette specific forward primer (expected size 1.5 kbp). In lanes 4 and 5 used primers specific for the kanamycin (Kan) resistance cassette, no product was detected when *Δpep2* gDNA was used as the template but a product was observed if the Sv-3-D04 cosmid was used (lane 5, 0.9 kbp) suggesting that a double crossover had occurred.

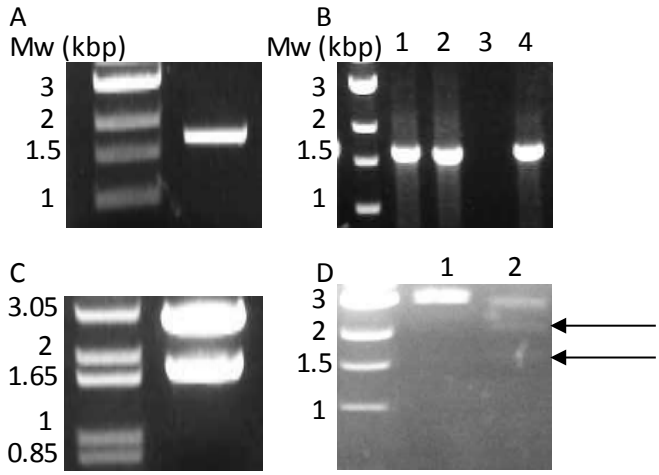

Figure 5.25: A complementation plasmid containing *pep2* was generated
(A) WT gDNA was used as a PCR template and primers were designed to amplify the promoter as well as the *pep2* gene (1.6 kbp).
(B) The product was ligated into a linearised pUC19 vector and used to transform *E. coli* DH5α. Transformants were screened by colony PCR (1.7 kbp). Transformants containing the correct sized product were sequenced.
(C) The *pep2* insert (1.6 kbp) was separated from the pUC19 (2.7 kbp) vector by restriction digestion with EcoRI and SapI followed by gel electrophoresis.
(D) The purified insert was subsequently ligated to an EcoRV linearised pMS82 vector and the plasmid was used to transform E. *coli* DH5α. Plasmids were isolated from successful transformants and screened by restriction digestion with BglII. Lane 1 was the restriction digest from a plasmid containing no insert, which resulted in an unresolved doublet (3 kbp). Lane 2 was the restriction digest from a plasmid containing the *pep2* insert, which yielded a three resolved bands (3, 2.7 and 1.9 kbp)

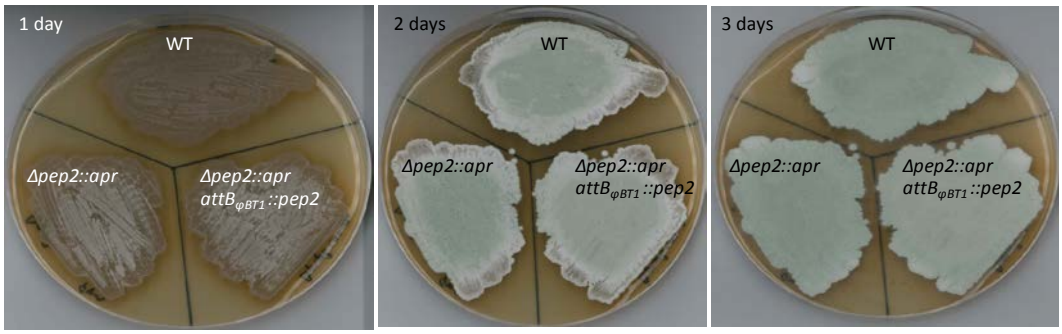

Figure 5.26: *Δpep2::apr* did not display a developmental phenotype

5.12 *Δpep2::apr* did not accumulate glycogen or have a developmental phenotype

When *Δpep2::apr* was grown on solid MYM agar, no developmental phenotype was observed (Figure 5.26). The strain was stained with PATAg, visualised by TEM and the images suggested that the strain had no detectable levels of glycogen (Figure 5.27). The absence of glycogen was confirmed by dot-blot analysis using a glycogen specific mAb (Figure 5.27). The complemented strain contained abundant glycogen in pre-spores, like WT (Figure 5.27).

The morphology of the spores produced by *Δpep2::apr* was also investigated. Cryo-SEM suggested that the strain produced spores comparable to WT that were of consistent dimensions indicating few irregular septation events (Figure 5.28). PI staining followed by fluorescence microscopy suggested that the genetic material of the spores were compacted in to single nucleoids in each pre-spore, as observed with WT (Figure 5.28).

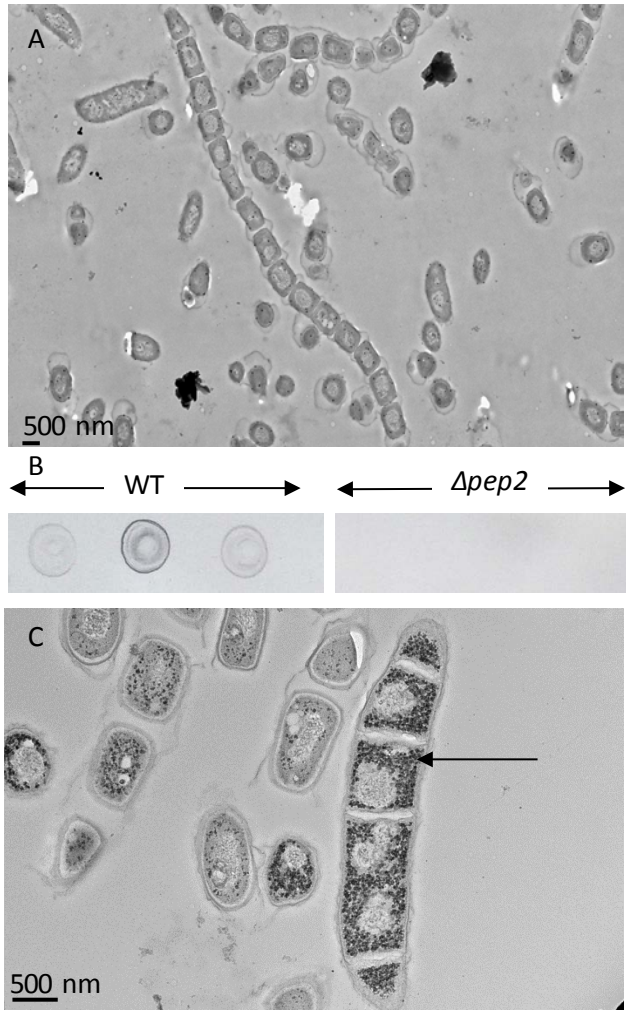

Figure 5.27: *Δpep2::apr* had no glycogen, which was reversed by the insertion of *pep2*
Samples were prepared for microscopy and imaged by E. Barclay; dot blot analysis was performed by H. Koliwer Brandl.
(A) TEM with PATAg staining suggested that glycogen was absent in *Δpep2::apr,* with no dark granules observed in pre-spores.
(B) The absence of glycogen was confirmed in three independent cells extracts of each strain by dot-blot analysis with a mAb raised against *M. tuberculosis* glycogen, which bound to WT cell-free extracts only.
(C) A complemented strain of *Δpep2::apr* containing *pep2* deposited glycogen (highlighted by the black arrow) in pre-spores, like WT.

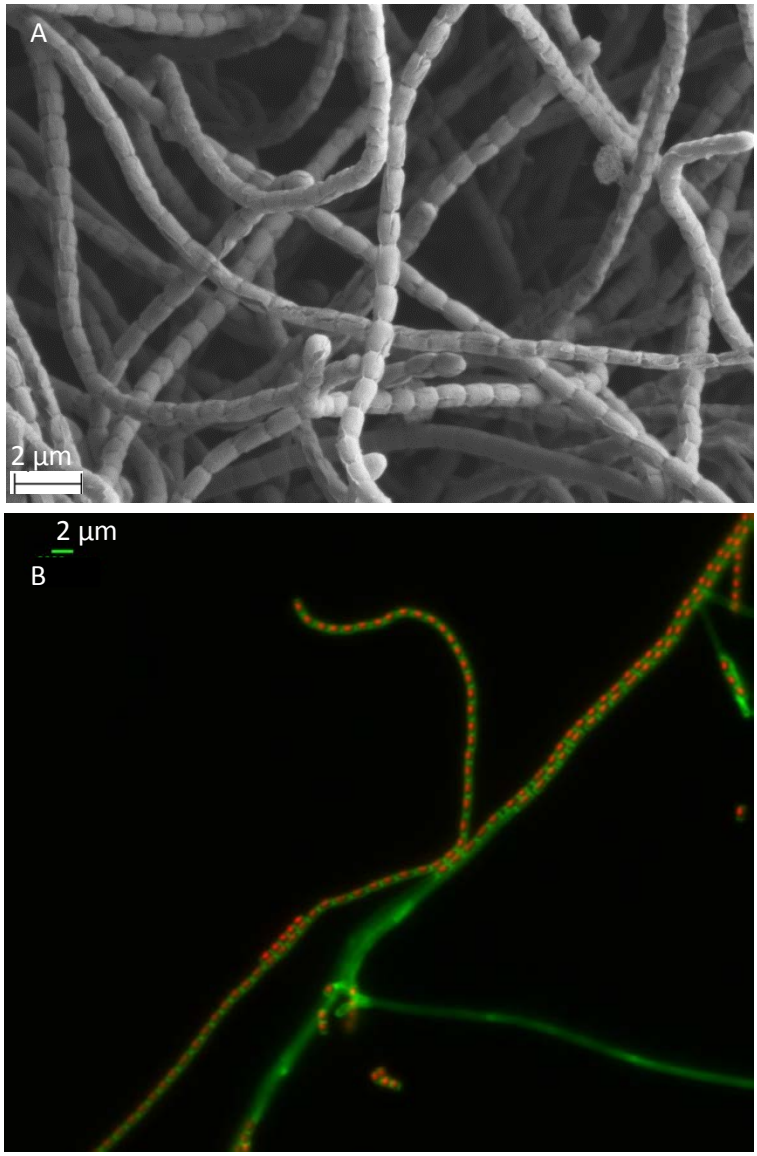

Figure 5.28: Spore morphology of *Δpep2::apr* was like WT
(A) Cryo-SEM of *Δpep2::apr* strain grown for seven days showed that spores produced were of uniform shape and size, as in WT.
(B) A sample of *Δpep2::apr* was grown for five days with nucleic acids stained with PI and cell walls stained with WGA. Spores of uniform size were observed, each containing a single discrete compact nucleoid, like WT.

5.13 *Δpep2::apr* had altered metabolism when compared to the WT strain as well as *ΔglgE::apr*

Sugar content of cell extracts of *Δpep2::apr* was monitored over a developmental time-course (Figure 5.29). The results suggested that sugar metabolism was unlike either the WT or the *ΔglgE::apr* strain. Maltose content was higher in the *Δpep2::apr* strain than in WT but maltose content was similar to that observed in the *ΔglgE::apr* strain. Trehalose content, however, was different in the *Δpep2::apr* when compared to both WT and *ΔglgE::apr* (Figure 5.29). Whilst the trehalose content of *ΔglgE::apr* was like that of WT at the end of the developmental time-course, *Δpep2::apr* had approximately 50% less trehalose in its spores (Figure 5.29). The final ratio between maltose and trehalose (1:6) in the spores of *Δpep2::apr* matched the equilibrium position of recombinant *M. tuberculosis* TreS (see chapter 3) (1:6) and was comparable to the equilibrium determined in recombinant *M. smegmatis* TreS (1:3.2) (Zhang, et al., 2011), which suggests that TreS could be producing the trehalose observed in the *Δpep2::apr* spores.

The cell extracts suggested that *Δpep2::apr* could not store its carbon as αM1P and therefore could not recycle its carbon through αM1P like *ΔglgE::apr* (Figure 5.30). This also confirmed that the developmental phenotype of the *ΔglgE::apr* mutant was solely due to αM1P accumulation. In the absence of glycogen synthesis, it was possible that *Δpep2::apr* was instead channelling its carbon into lipid formation as observed in other bacteria (Wang, et al., 2007). Therefore, the fatty acid methyl ester (FAME) content of *Δpep2::apr* were analysed (Figure 5.31). Preliminary data suggested that whilst the FAME profile and the species present were comparable to WT, there was an approximate 45% increase in the overall FAME content of the *Δpep2::apr* strain as determined by calculating the sum of areas of all species eluting from the GC column (Figure 5.31).

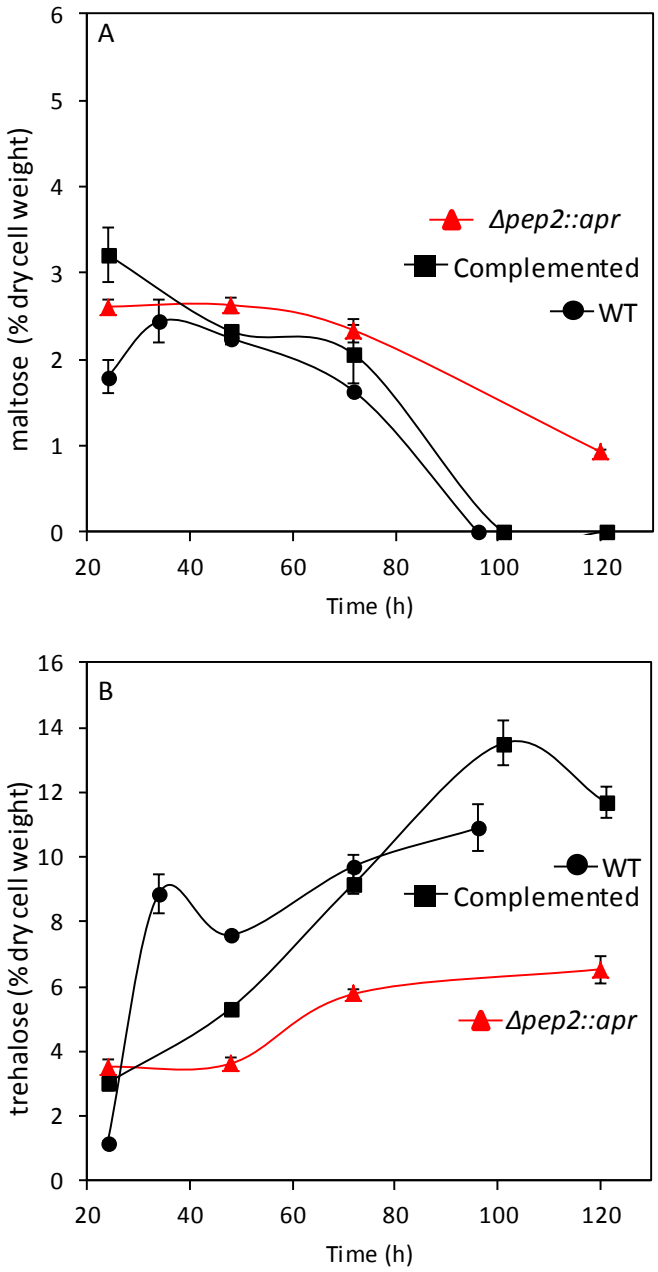

Figure 5.29: *Δpep2* had elevated maltose and decreased trehalose content in cell extracts

Developmental time-courses of *Δpep2::apr,* WT and a complemented strain containing *pep2* suggested that maltose content was increased in *Δpep2* (A) compared to other strains and that trehalose content in spores at the end of the developmental time-point was about half WT and complemented strains (B). Error bars are the SE of three replicates.

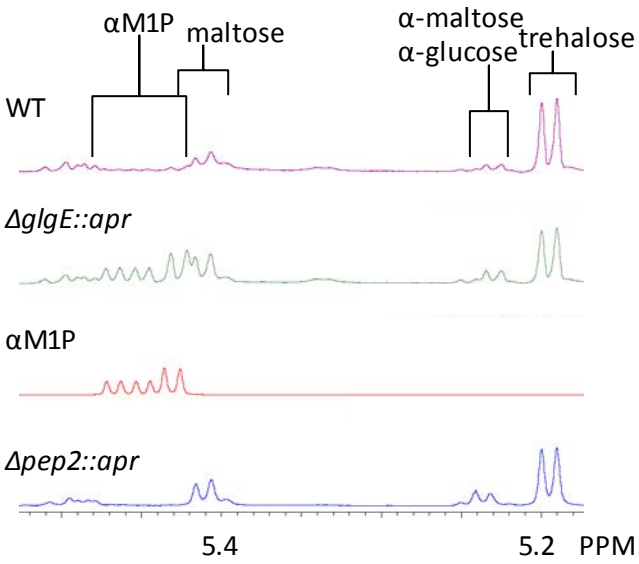

Figure 5.30: There was no build-up of αM1P in *Δpep2::apr*
^{1}H-NMR spectroscopy of cell-free extracts was used to show that no αM1P was deposited in *Δpep2::apr,* unlike *ΔglgE::apr.*

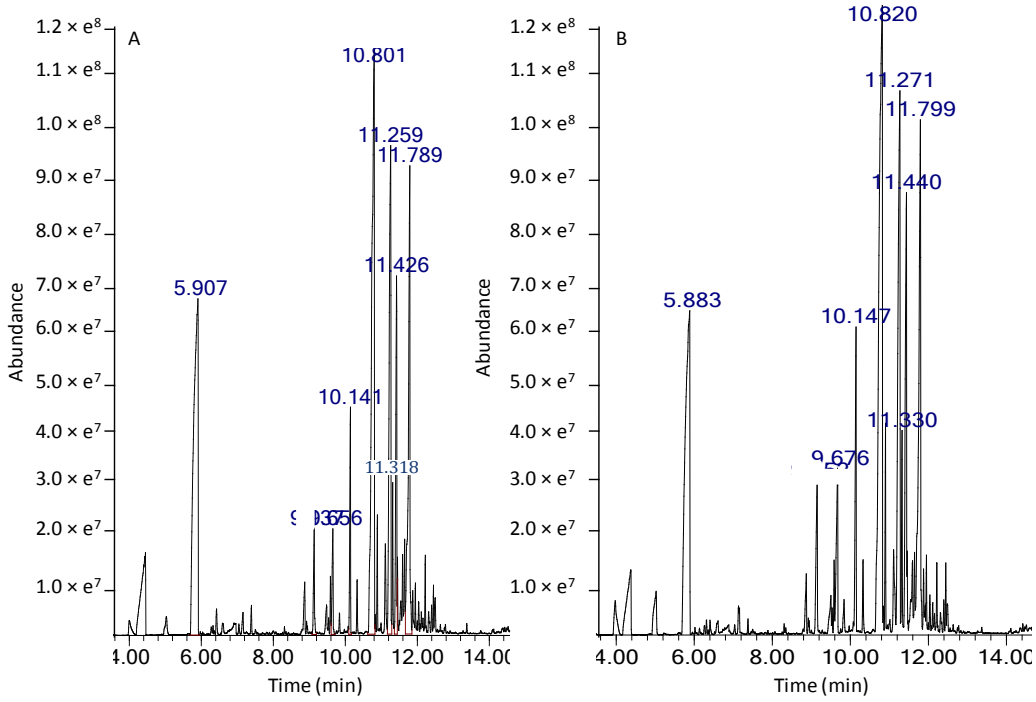

Figure 5.31: There was an increase in the overall FAME content of *Δpep2::apr*
Gas chromatography mass spectrometry (GCMS) profiles of WT (A) and *Δpep2::apr* (B) grown for two days suggested that similar lipids were present in both strains. However, there were increased abundances of a number of the major lipid constituents in the *Δpep2::apr* strain. Methyl ester benzoic acid (elution time= 5.9 min) was used as an internal standard in both samples.

5.14 *ΔtreS::apr, ΔtreZ::apr* and *ΔglgP::apr* mutants were generated and had no developmental phenotype

Further mutants were generated in *S. venezuelae* with a view to determining how they might impact overall metabolism during development. *ΔtreS::apr, ΔtreZ::apr* and *ΔglgP::apr* were all generated using the ReDirect™ protocol (Gust, et al., 2003). Specifically, *ΔtreZ::apr* and *ΔglgP::apr* were generated with a view to understanding which plays a bigger role in glycogen degradation during the sporulation process (Figure 5.32). There was a difference in the size of each targeted gene when compared to the *apr* resistance cassette and therefore PCR could be used to confirm the gene replacements (Figure 5.33).

No developmental phenotype was observed when all strains were grown on solid MYM medium (Figure 5.34). Alternative carbon sources were also used to establish if a developmental phenotype was present on a different carbon source. However, no developmental phenotype was observed on alternate carbon sources (Figure 5.35). It is conceivable that there might be a metabolic phenotype without an associated developmental phenotype, like that observed with *Δpep2::apr*. However, in the absence of a developmental phenotype, these mutants were not further characterised.

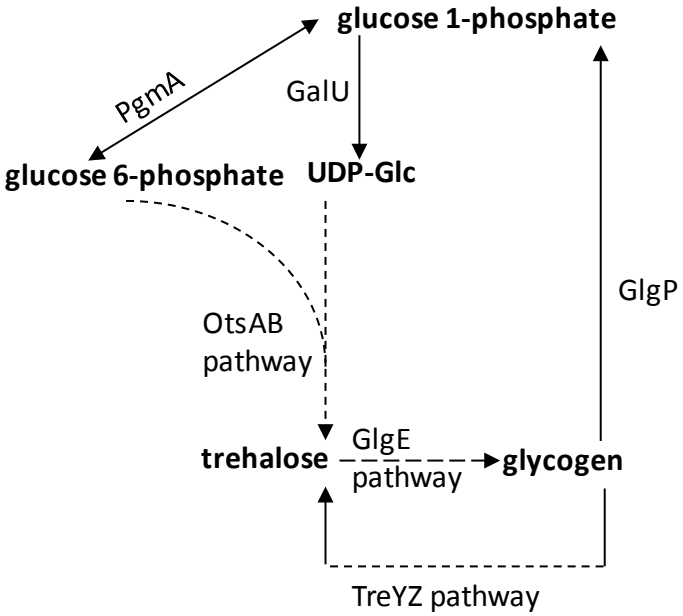

Figure 5.32: Overview of pathways predicted to be involved in glycogen turnover in *S. venezuelae*

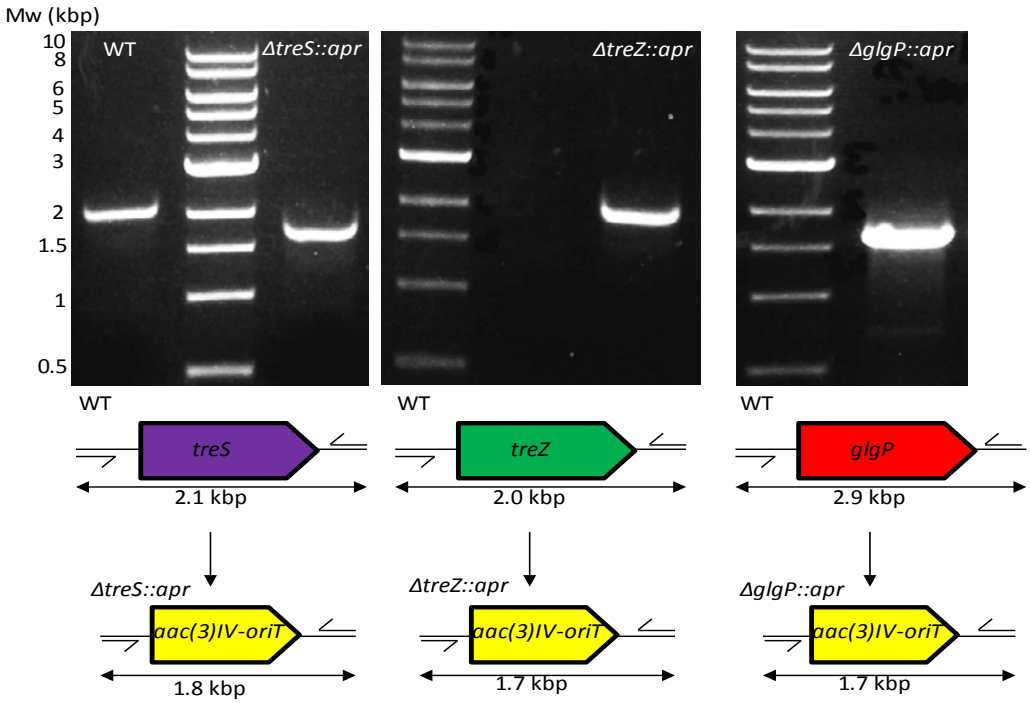

Figure 5.33: *ΔtreS::apr, ΔtreZ::apr* and *ΔglgP::apr* mutants were generated and their mutations were confirmed by PCR

Further strains were generated using ReDirect™ protocol (Gust et al., 2003). gDNA from these strains was extracted and used as a template for PCR using primers that flanked the targeted genes. In all of these mutants the targeted gene was larger than the *aac(3)IV-oriT cassette* and therefore the PCR product was smaller than in WT strains.

Figure 5.34: *ΔtreS::apr, ΔtreZ::apr* and *ΔglgP::apr* strains had no developmental phenotype when grown on MYM
Excess condensation was present on the plate with *ΔtreZ::apr* growing.

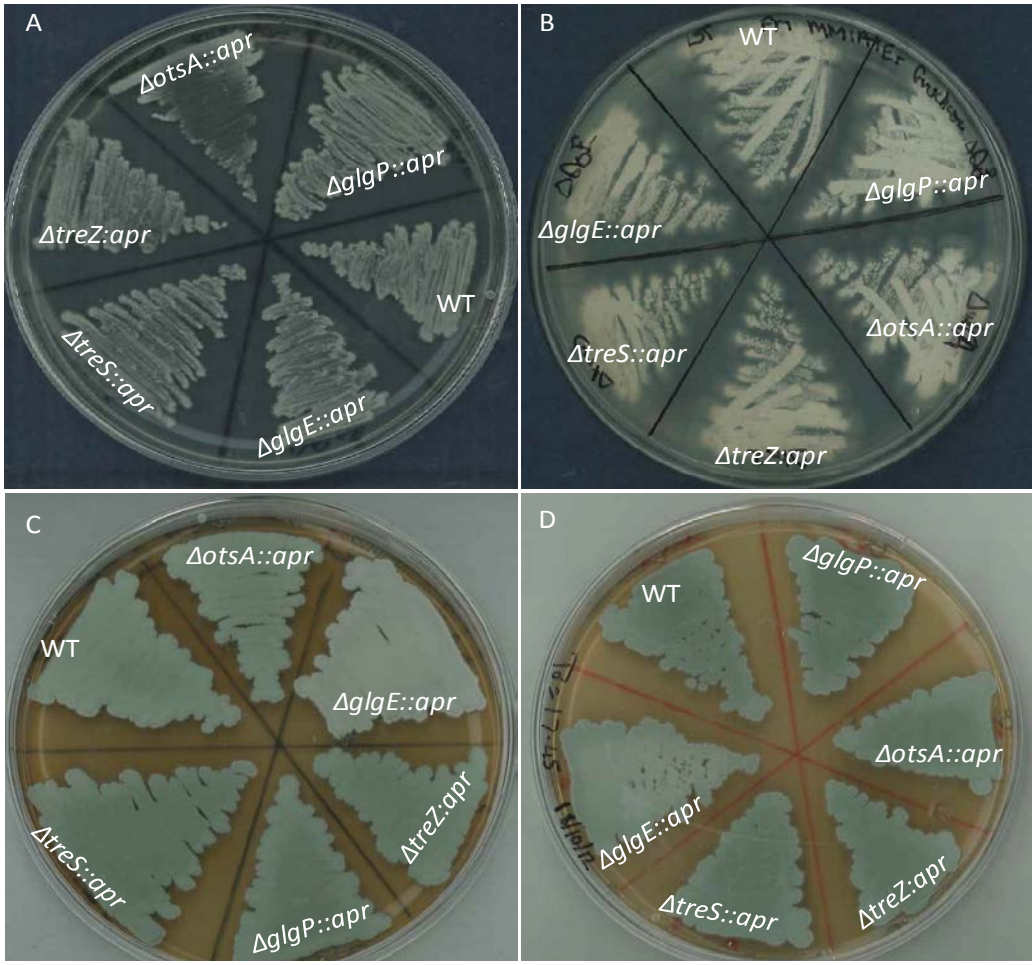

Figure 5.35: *ΔtreS::apr, ΔtreZ::apr* and *ΔglgP::apr* mutants did not have a developmental phenotype on different carbon sources

Strains were grown on minimal media with galactose (A) or fructose (B) as the carbon source, no developmental phenotypes were observed for *ΔtreS::apr, ΔtreZ::apr* and *ΔglgP::apr*. Strains were also grown on MYM agar in which the maltose carbon source was replaced with galactose (C) and fructose (D) and again no developmental phenotype was observed. *ΔotsA::apr* was also grown on these plates, but this mutant will be the focus of chapter 6.

5.15 Discussion

The results presented in this chapter demonstrate that the GlgE pathway is solely responsible for glycogen production in *S. venezuelae.* The results also suggest that in the absence of glycogen production, αM1P can be accumulated instead, which led to equivalent trehalose production in spores. However, there is a fitness consequence to re-cycling carbon in the form of αM1P instead of glycogen such that strains accumulated less mass, had delayed development and produced fewer under-pigmented spores that were less resistant to various stresses. αM1P also adversely affected other processes in the sporulation process such as spore pigment formation and cell wall maturation.

In the absence of glycogen and αM1P there was reduced trehalose in spores. This is consistent with the hypothesis that glycogen deposition in the pre-spore chains allows the organism to relocate its carbon source and use it predominantly for trehalose production for spores.

Furthermore, this work demonstrates that ^{1}H-NMR spectroscopy is a reliable new method to determine sugar content in *Streptomyces* cell extracts. The trehalose content of WT *S. venezuelae* was the same as reported by previous studies (Ranade and Vining, 1993), suggesting that this method is comparable to previous methods for sugar detection. ^{1}H-NMR spectroscopy is preferable to previous methods because it can be used to determine multiple sugars in a single sample and does not rely on enzymic or chemical degradation.

The precise mechanism by which αM1P accumulation leads to developmental delay in *S. venezuelae* remains unclear and further work will need to be carried out to understand the connection. It could be that sequestration of carbon sources as αM1P limits flux of carbon to processes required for the correct development of spores, leading to spores with compromised stress tolerance. Another possibility may be that the organism becomes phosphate limited due to perturbation of cytosolic phosphate levels by a build-up of αM1P. Phosphate is known to be a limiting nutrient in soil environments and *Streptomyces* have developed sophisticated mechanisms to enhance phosphate uptake under such conditions (Sola-Landa, et al., 2003). One response is to increase the expression of phosphatases (Allenby, et al., 2012). Given that αM1P

degradation is dependent on the activity of phosphatases, it could be that the activation of a phosphate starvation response is required in order to break-down αM1P. This would explain the delayed development of the *ΔglgE::apr* strain.

Biochemical characterisation of the *ΔtreS::apr, ΔtreZ::apr* and *ΔglgP::apr* mutants will need to be carried out in order to determine if there are any metabolic phenotypes associated with these mutants.

5.16 Summary

This chapter provides the first evidence that glycogen is non-essential for *Streptomyces.* It also provides the first *in vivo* evidence that the GlgE pathway is responsible for glycogen synthesis. Finally, αM1P accumulation caused developmental delay in *S. venezuelae.* Whilst strains that accumulated αM1P did sporulate, they had impaired resistance to abiotic stresses.

Chapter 6: *Streptomyces venezuelae* OtsA

6.1 Introduction

Glycogen production via the GlgE pathway is dependent on the formation of trehalose from glucose (Figure 6.1). In *S. venezuelae,* the most likely source of this trehalose is via the OtsAB pathway. The pathway involves two enzymes, the first of which is trehalose phosphate synthase (hereinafter referred to as OtsA; EC 2.4.1.15) that condenses a nucleoside diphosphate glucose (NDP-glucose) and glucose 6-phosphate to form trehalose 6-phosphate. The second enzyme of the pathway is trehalose 6-phosphate phosphatase that de-phosphorylates trehalose 6-phosphate to form trehalose.

OtsA is in the glycosyl transferase (GT) 20 family according to the carbohydrate active enzyme (CAZy) classification (Cantarel, et al., 2009; Gibson, et al., 2002). The enzyme proceeds via a S_Ni mechanism that results in the retention of stereochemistry (Errey, et al., 2010) (Figure 6.2). Whilst it is known that OtsA has specificity for glucose 6-phosphate, there are reports from different organisms that it can accept different nucleotide glucose sugars (Gibson, et al., 2002; Pan, et al., 1978). For example, *Escherichia coli* OtsA has substrate specificity for uridine diphosphate glucose (UDP-glucose) (Gibson, et al., 2004). This contrasts to *Mycobacterium smegmatis* OtsA, which has a preference for UDP-glucose and guanosine diphosphate glucose (GDP-glucose) but will accept adenine diphosphate glucose (ADP-glucose) as well as cityidine diphosphate glucose (CDP-gluose) (Pan, et al., 1996; Pan, et al., 1978). Furthermore, *Streptomyces hygroscopicus* OtsA has been reported to exclusively use GDP-glucose (Elbein, 1968). The molecular mechanisms underlying the altered substrate specificity is poorly understood, partly due to the absence of crystallographic data.

There are two other potential trehalose synthesis pathways in *S. venezuelae,* the TreS and TreYZ pathways (Figure 6.1). Recent evidence shows that the net flux of TreS is conversion of trehalose into α-maltose in *Mycobacterium* (Miah, et al., 2013). This means that it is perhaps an unlikely route to trehalose in *S. venezuelae*. The OtsAB pathway produces the majority of trehalose in *Mycobacterium tuberculosis* and it dominates over the TreYZ pathway (Murphy, et al., 2005). However, this hierarchy is not always maintained, even in close relatives of *Mycobacterium*. For example, the TreYZ pathway is the dominant pathway for trehalose synthesis in another actinomycete *Corynebacterium glutamicum* (Wolf, et al., 2003). Therefore, it is not clear if removal of the OtsAB pathway would impact *S. venezuelae* glycogen levels by limiting flux through the GlgE pathway in the pre-spores.

However, it is noteworthy that this bacterium is cultured on a maltose-rich medium and therefore the OtsAB pathway may not be physiologically relevant when grown on maltose. Furthermore, it is not clear if the OtsAB pathway is instead operating to produce trehalose during spore maturation.

Experiments in this chapter sought to determine if OtsA is required for normal development of *S. venezuelae* on a maltose-rich carbon source or indeed other carbon sources. Biochemical characterisation of OtsA was also carried out, with a view to determining the substrate specificity of the OtsA from this organism. Given that *Streptomyces hygroscopicus* OtsA uses GDP-glucose as do other actinomycetes, it suggests that S*. venezuelae* OtsA will also use GDP-glucose. Furthermore, the UDP-glucose pyrophosphorylase (hereinafter referred to as GalU; EC 2.7.7.9) was also characterised with a view to determining if it was responsible for generating the appropriate NDP-glucose substrate for OtsA.

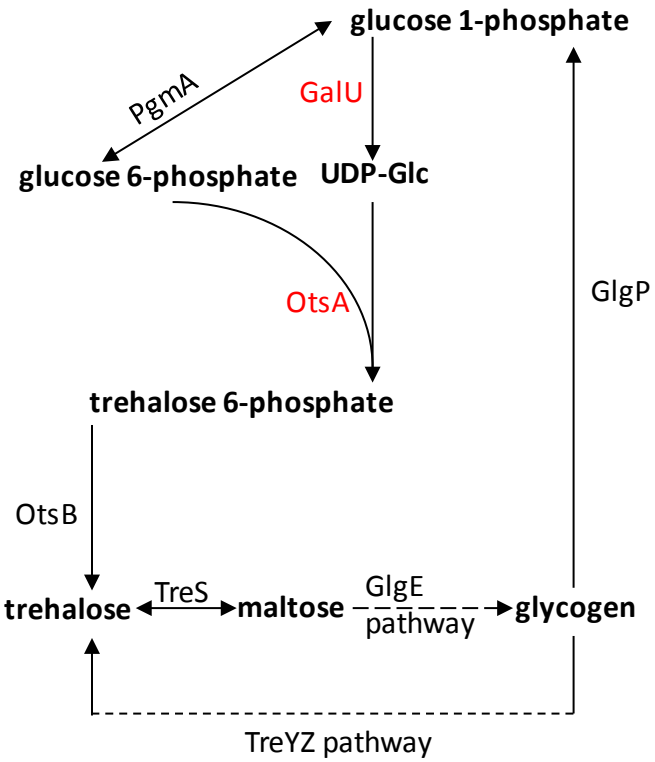

Figure 6.1: Overview of hypothetical glucose and trehalose metabolism in *S .venezuelae*
Enzymes highlighted in red are the focus of experiments in this chapter.

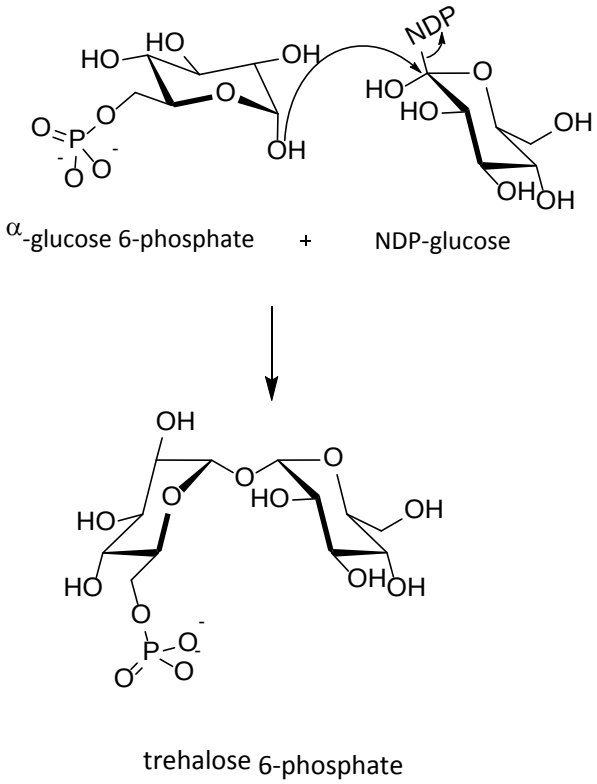

Figure 6.2: OtsA reaction

6.2 A *ΔotsA::apr* strain and a complemented strain was generated

A *ΔotsA::apr* mutation was made following the ReDirect™ protocol (Gust, et al., 2003). The formation of the correct polymerase chain reaction (PCR) product was monitored by agarose gel electrophoresis (Figure 6.3). Insertion of the apramycin (*apr*) cassette in place of *otsA* gene in a cosmid was confirmed by restriction digestion of the cosmid, followed by agarose gel electrophoresis (Figure 6.3). The mutated cosmid was then introduced into *S. venezuelae* by conjugal transfer and antibiotic selection was used to identify colonies containing the *ΔotsA::apr* mutation. After three rounds of selective re-streaking from single colonies, spores of the mutant were harvested and re-suspended in 20 % (v/v) glycerol and then stored at -20 °C until required.

Genomic deoxyribonucleic acid (gDNA) was then extracted and used to confirm the mutation by Southern hybridisation as well as to ensure further gene re-arrangements had not occurred during the double cross-over event (Figure 6.4).

After the mutant was generated, a complementation strain was generated. This was to determine if any phenotype observed in the *ΔotsA::apr* mutant could be restored by re-insertion of the *otsA* gene.

PCR was used to amplify the gene fragment along with the upstream native promoter from a wild-type (WT) gDNA template (Figure 6.5). The fragment was cloned into a pUC19 vector and the corresponding plasmids were screened for the correct sized insertion by colony PCR (Figure 6.5) and then sequenced.

The fully sequenced gene fragment was sub-cloned into the pMS82 complementation vector (Figure 6.5). The incorporation of the entire fragment into the vector was confirmed using restriction digestion followed by agarose gel electrophoresis. A plasmid containing the correct gene fragment was then used to transform *E. coli* ET12567/pUZ8002. A successful transformant was used to conjugally transfer the complementation plasmid into *ΔotsA::apr* and antibiotic selection was used to screen for successful conjugants. After three rounds of selectively re-streaking from single colonies, the resulting spores were re-suspended in 20 % (v/v) glycerol and stored at -20 °C until required.

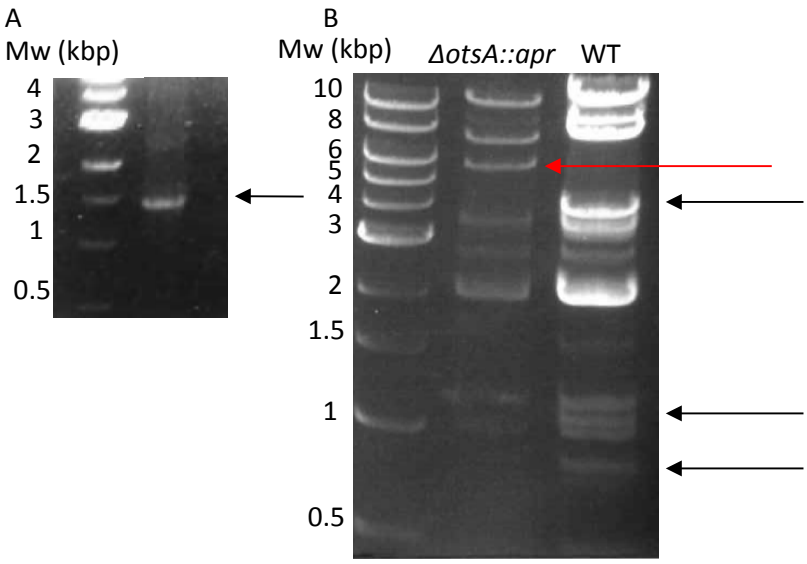

Figure 6.3: The *otsA* gene was replaced with the *acc(3)IV-oriT* cassette in the 1-H1 cosmid
(A) The *acc(3)IV-oriT* cassette was used as a template for PCR to generate a *acc(3)IV-oriT* cassette with flanking regions complementary to the flanking regions of *otsA* (1.5 kbp).
(B) *E. coli* BW25113/pIJ790 was transformed with 1-H1 followed by the linear *otsA* specific *acc(3)IV-oriT* cassette, which replaced *otsA* in 1-H1 by homologous recombination. The cosmid was extracted and digested with NruI. A new band emerged (~6 kbp) as the *otsA* gene contained two NruI cut sites (resulting in 4.1, 1.1 and 0.8 kbp sized fragments; black arrows) whereas the *acc(3)IV-oriT* cassette contained no cut sites. Therefore, the three fragments merged into a single 6 kbp fragment in the *acc(3)IV-oriT* cassette containing cosmid (red arrow).

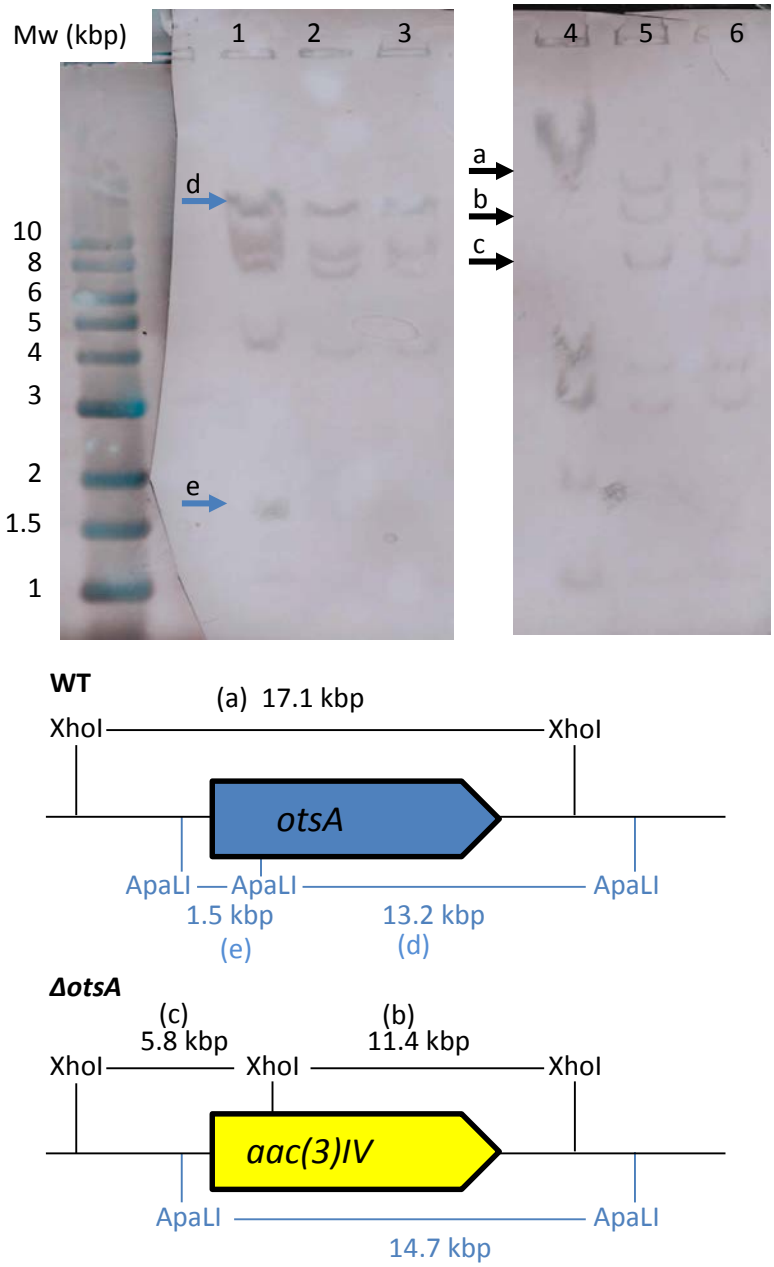

Figure 6.4: The Δ*otsA::apr* was confirmed by Southern hybridisation
S. venezuelae gDNA was extracted and digested with either XhoI or ApaLI. For the XhoI digest, one fragment (band a) as in WT (lane 4) was expected to form two smaller fragments (bands b and c) in the *ΔotsA::apr* strain (lanes 5 and 6). For the ApaLI digest, two fragments (bands d and e) from WT (lane 1) were predicted to form a single larger fragment (14.7 kbp). The resolution of the blot was not sufficient to distinguish 13.2 kbp fragment in WT from the 14.7 kbp fragment in Δ*otsA::apr.* However, the disappearance of the smaller fragment (band e) in Δ*otsA::apr* was clearly visible, suggesting the gene disruption had occurred at the predicted position within the genome. The entire 1-H1 cosmid was used as the probe.

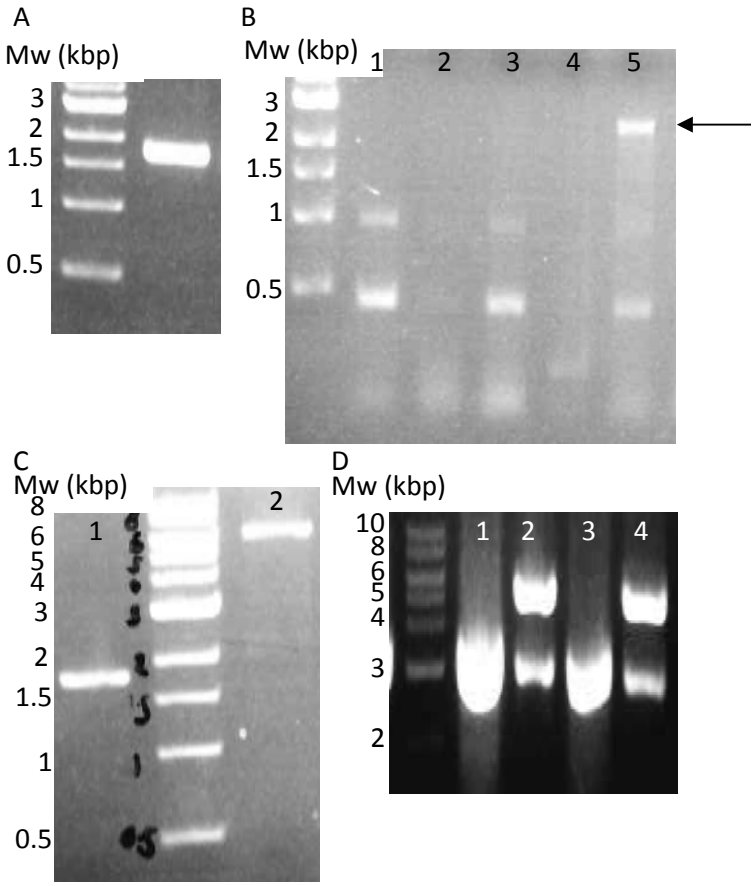

Figure 6.5: A complementation plasmid for the *ΔotsA::apr* strain was generated

(A) WT *S. venezuelae* gDNA was extracted and used as a template for PCR. Primers were designed so that the gene as well as the endogenous promoter would be amplified from the gDNA. A fragment corresponding to *otsA* (1.8 kbp) was generated.

(B) The PCR products were subsequently ligated into a pUC19 vector. The resulting plasmid was used to transform *E. coli* DH5α. Successful transformants were used as template for colony PCR, a number of colonies were screened and any colonies yielding the correct sized PCR product (lane 5; 2 kbp) were sequenced.

(C) A single plasmid containing the correct *otsA* sequence was excised and purified from the pUC19 vector (lane 1) as was linearised pMS82 (lane 2).

(D) To confirm the presence of the *otsA* fragment, plasmids from successful transformants were excised and digested with BglII. Whilst some colonies contained re-circularised pMS82 (lanes 1 and 3), some also contained the *otsA* insert (lanes 2 and 4; expected sizes 3 and 5 kbp).

6.3 *ΔotsA::apr* had no phenotype under normal laboratory growth conditions

When *ΔotsA::apr* was grown on solid malt extract-yeast extract-maltose (MYM) agar, there was no developmental phenotype when grown as a lawn or a as a single colony (Figure 6.6). As MYM media is rich in maltose it seems unlikely that the OtsAB pathway would be required under these growth conditions as the maltose would be imported in, and therefore act downstream of the OtsAB pathway, and subsequently be used to produce glycogen. Therefore, a phenotype would only be expected if *ΔotsA::apr* were grown on a carbon source that made the presence of OtsA necessary for the production of metabolites from trehalose 6-phosphate.

Metabolite analysis suggested that there were increased trehalose levels and contained unexpectedly 4% more trehalose by dry cell weight than WT spores (Figure 6.7). However, the trehalose content of *ΔotsA::apr* was similar to the complemented strain and as they were set up at the same time, unlike WT, it could be due to variations between the amounts of carbon source in the batch of medium used. This suggests that the OtsAB pathway is not the pathway responsible for trehalose production in spores. Maltose levels were also elevated and, during some parts of the life-cycle, the maltose content was double that of WT in the mutant strain (Figure 6.7). However, at the end of the developmental time-point no maltose was detected suggesting that it was not present in spores (Figure 6.7). In general, the metabolic differences were less marked than that of the *ΔglgE::apr* strain (see chapter 5).

Transmission electron microscopy (TEM) suggested that glycogen deposition was still present in the *ΔotsA::apr* strain in pre-spore compartments as observed in WT, which suggests that the OtsAB pathway is not required for glycogen synthesis (Figure 6.8). This is consistent with evidence suggesting that TreS activity was not required for glycogen production, in the presence of maltose, in other mutants of *S. venezuelae* (see chapter 5). There were hints that there may be increased irregular septation events from cryo-scanning electron microscopy (cryo-SEM) images (Figure 6.8). However, this was relatively subtle, varied considerably between different images and was not as obvious as observed previously for the *ΔglgE::apr* strain (see chapter 5).

Figure 6.6: *ΔotsA::apr* had no developmental phenotype when grown on MYM agar medium

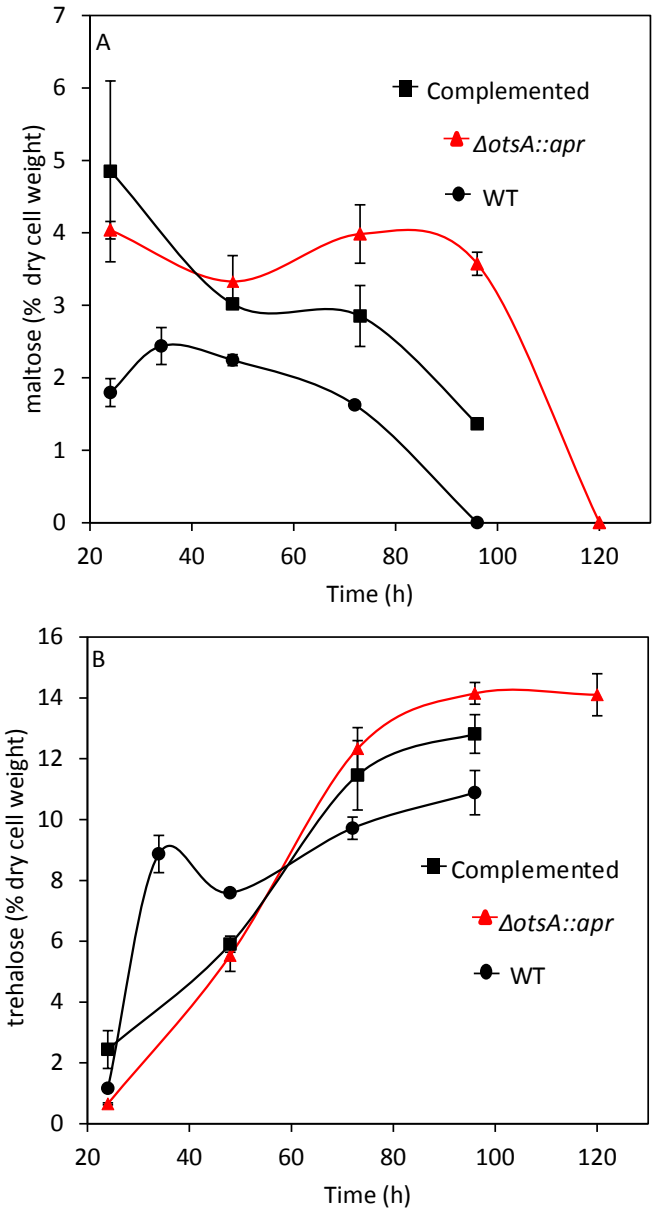

Figure 6.7: *ΔotsA::apr* had slightly elevated trehalose content
Error bars are the standard error of the mean (SE) of three replicates.
(A) *ΔotsA::apr* had elevated maltose content throughout the time course but had no maltose at the end of the developmental life-cycle, like WT.
(B) Initially *ΔotsA::apr* had less trehalose than WT but had elevated trehalose levels at the end of the developmental life-cycle.

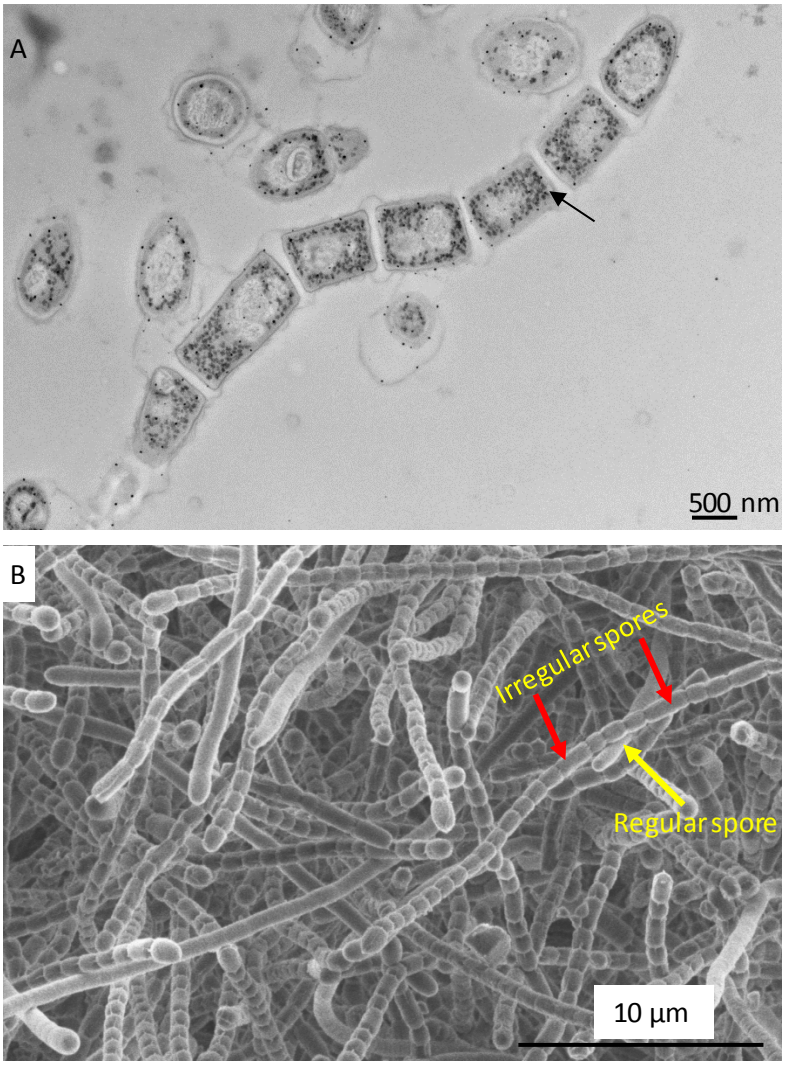

Figure 6.8: *ΔotsA::apr* deposited glycogen and produced spores
Microscopy was performed by E. Barclay or K. Findlay.
(A) *ΔotsA::apr* was not impaired in glycogen synthesis as shown by TEM when the cells were stained with periodic acid-thiocarbohydrazide-silver proteinate (PATAg). Glycogen appeared as deeply staining granules, highlighted by the black arrow.
(B) Cryo-SEM on *ΔotsA::apr* suggested that there might be more spores with irregular septation than in WT.

6.4 *ΔotsA::apr* had delayed development when grown on galactose

As no phenotype was observed on the maltose-rich medium MYM, different carbon sources were used for growth. A monosaccharide carbon source was preferred because it was hypothesised to be more likely that the carbon source would have to be metabolised via the OtsAB pathway to form trehalose and glycogen and thereby making a physical phenotype more likely.

As previously observed with WT, the carbon sources that gave the most consistent growth and development on solid minimal media (MM-+) were galactose and fructose. Therefore, they were the first two carbon sources trialled with *ΔotsA::apr* (Figure 6.9). Whilst there was no phenotype on fructose there was a cell-density dependent growth inhibition phenotype when the *ΔotsA::apr* strain was grown on media containing galactose (Figure 6.9). In regions of high cell density there was limited development whereas at the single colony level there was no obvious difference between WT and the *ΔotsA::apr* strain (Figure 6.10).

Due to this observation, the maltose in MYM was replaced with galactose to determine if there was also a phenotype in complex media that would yield enough cell material for metabolite analysis. A developmental delay was also observed on the malt extract-yeast extract-galactose (MYGal) solid media (Figure 6.11). Whilst the phenotype observed on MYGal was consistent with the phenotype observed on MM-+, it was not identical. On MM-+ the strain did not develop beyond substrate mycelium with increased incubation time (Figure 6.10). However, on MYGal with prolonged incubation time, the strain did develop and eventually sporulated (Figure 6.11).

Images of cryo-SEM of the *ΔotsA::apr* strain grown on MYGal suggested that spore morphology was similar to that of the strain when grown on MYM as well as being comparable to WT (Figure 6.12). Interestingly, spores of *ΔotsA::apr* grown on MYGal had lower trehalose content (5.4% of dry cell weight ± 0.1 SE of three replicates) than the complemented strain (17.9% of dry cell weight ± 0.4 SE of three replicates). This suggests that the OtsAB pathway is in part required to maximise the trehalose content of spores when grown on a galactose carbon source.

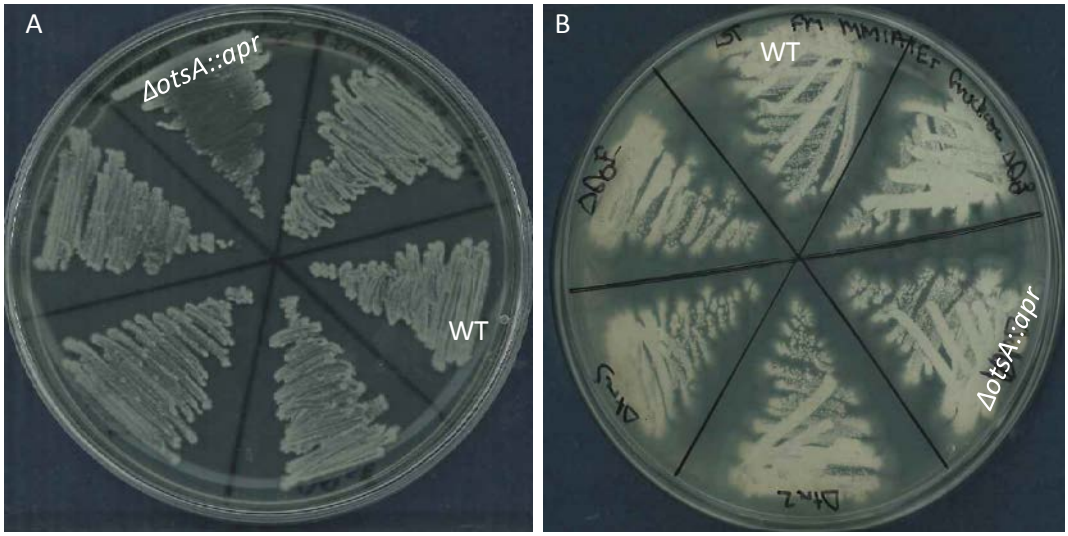

Figure 6.9: *ΔotsA::apr* had a developmental phenotype when grown on galactose but not on fructose

Strains were grown on minimal media containing Iberian agar (MM-+) with galactose (A) or fructose (B) as their carbon sources. There was a cell density dependent developmental phenotype when *ΔotsA::apr* was grown on galactose but not when the strain was grown on fructose.

Figure 6.10: *ΔotsA::apr* had a developmental phenotype when grown on galactose

Strains were grown on MM-+ with galactose as the sole carbon source. After 7 days growth there was an evident developmental delay in the *ΔotsA::apr* strain when compared to WT.

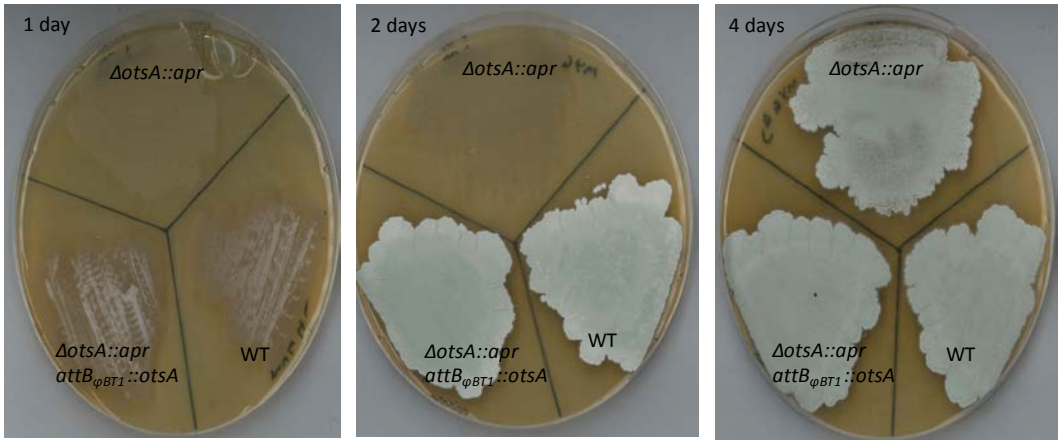

Figure 6.11: *ΔotsA::apr* had a developmental phenotype when grown on complex media containing galactose

Strains were grown on media as with MYM with the exception of maltose in the media was replaced with galactose (MYGal). There was a clear lag in development, but with prolonged incubation the strain did develop and sporulate.

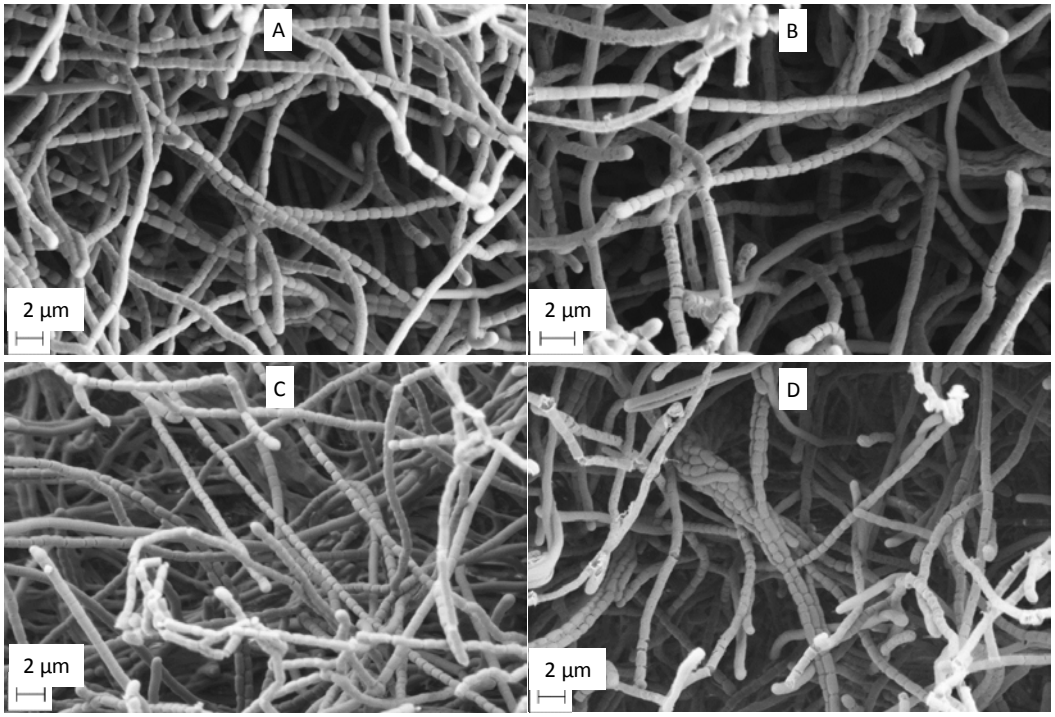

Figure 6.12: *ΔotsA::apr* spore morphology was comparable to WT when grown on complex media containing

Cryo-SEM of WT colonies grown on MYGal containing 4 g L^{-1}(A) and 8 g L^{-1} (B), suggested spores morphologies were comparable to spores developing on MYM. *ΔotsA::apr* spores were also visualised after growth on MYGal containing 4 g L^{-1}(C) and 8 g L^{-1} (D), which suggested that their morphologies were comparable to WT.

6.5 The phenotype of *ΔotsA::apr* was associated with metabolic changes

Galactose is typically metabolised into glucose 1-phosphate and UDP-glucose, which can be fed into central metabolism such as glycolysis by enzymes that make up the Leloir pathway (Holden, et al., 2003) (Figure 6.13). A number of intermediates, most notably galactose 1-phosphate, of the Leloir pathway are known to have adverse effects in different biological systems ranging from humans to yeast (Lai, et al., 2009; Ross, et al., 2004; Zaffanello, et al., 2005). Furthermore, OtsA was hypothesised to be using a product of the Leloir pathway, UDP-glucose, and therefore it was predicted that this sugar was accumulating in cells extracts of *ΔotsA::apr*. The samples were spiked with several sugars and nucleotide sugars hypothesised to be intermediates of the Leloir pathway. Given that a developmental phenotype was only observed when galactose was the primary carbon source, it suggested that the phenotype could be attributable to build-up of a toxic metabolite, as observed with the *ΔglgE::apr* strain (see chapter 5).

To explore this hypothesis further, cell extracts of *ΔotsA::apr* grown on MYGal was compared to *ΔotsA::apr* grown on MYM to identify metabolic differences between the two growth conditions (Figure 6.14). There were two distinct doublet of doublets that were only present when the strain exhibited developmental delay (Figure 6.14). The doublet of doublets appeared in a region of the proton nuclear magnetic resonance (^{1}H-NMR) spectrum which is characteristic of phosphorylated sugars (Figure 6.14). There was, however, an absence of resonances attributable to protons neighbouring any glycosidic bonds, which suggested that the phosphorylated sugars were monosaccharides (Figure 6.14).

As there seemed to be accumulation of phosphorylated sugars, phosphorus NMR (^{31}P-NMR) spectroscopy was also performed with a view to determining if there were also perturbations in phosphate species in cell extracts. There were some distinct changes associated also with phosphorus content (Figure 6.14). The developmentally delayed *ΔotsA::apr* had several additional resonances as well as lacked two resonances observed in *ΔotsA::apr* that developed as WT.

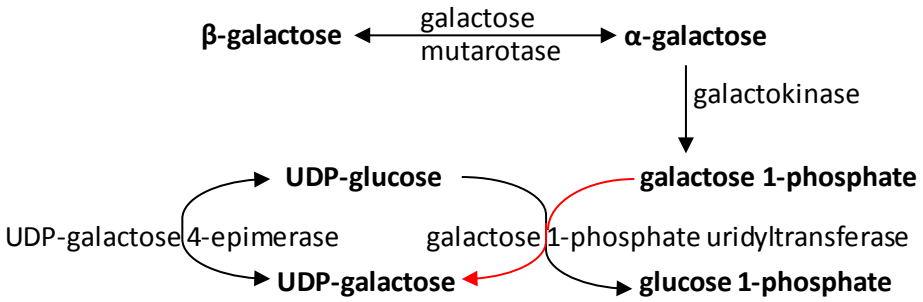

Figure 6.13: Overview of the Leloir pathway
The Leloir pathway converts galactose into activated glucoses which are subsequently used for glycolysis, trehalose and glycogen production.

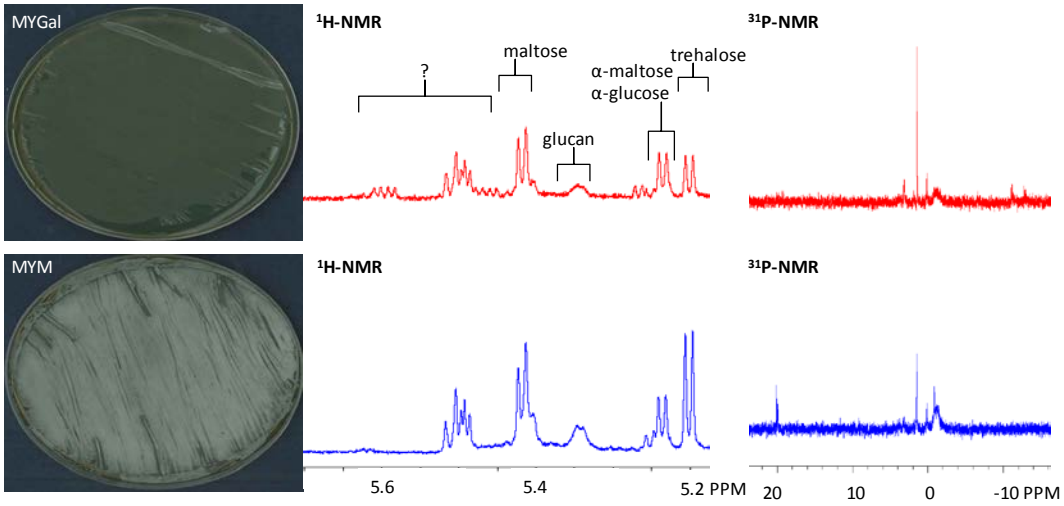

Figure 6.14: The developmental phenotype of *ΔotsA::apr* was associated with several metabolic changes
A sample of non-standardised *ΔotsA::apr* was grown on sterile cellophane discs that were laid on top of either solid MYM or MYGal. After 1.5 days there was a developmental delay when the mutant was grown on MYGal and not MYM. The cell extracts were probed by ^{1}H-NMR and ^{31}P-NMR. The spectra suggested that there were a number of changes in metabolism when *ΔotsA::apr* was grown on the different media. Trehalose resonances were greater when the strain was grown on MYM. New resonances emerged when the strain was grown on MYGal, most noticeably two doublet of doublets at 5.45 and 5.6 ppm in the ^{1}H-NMR and multiple resonances at -10 and 3 ppm in the ^{31}P-NMR. There was also the absence of resonances at 20 ppm in ^{31}P-NMR when the strain was grown on MYGal.

6.6 Developmentally delayed *ΔotsA::apr* accumulated GDP-glucose and glucose 1-phosphate

Attempts were then made to identify the sugars that accumulated when *ΔotsA::apr* displayed a developmental phenotype. This was achieved by spiking cell extracts with known phosphorylated sugars that were thought most likely to accumulate under galactose rich conditions (Figure 6.15). The phosphorylated sugar resonances arise typically at very similar regions of the spectrum and can shift subtly at different pHs. Consequently, it was rationalised that spiking cell extracts with known sugars would circumvent shifts due to pH differences between samples and would be more likely to identify correctly the sugars present in cell extracts.

The most likely candidates were UDP-glucose and glucose 1-phosphate because they are the final products of the Leloir pathway (Frey, 1996) (Figure 6.13). Activated galactose compounds were also used because it was conceivable that some of the intermediates of the Leloir pathway could also have accumulated (Figure 6.15).

One of the species was identified as glucose 1-phosphate, as predicted (Figure 6.15). Surprisingly, however, UDP-glucose did not accumulate (Figure 6.15). The nucleotide sugar was initially identified as ADP-glucose as the doublet of doublet overlapped with the accumulating sugar resonance. However, other resonances downfield of this region did not match resonances associated with ADP-glucose (Figure 6.16). Therefore, other nucleotide sugars were screened and GDP-glucose also overlapped with the doublet of doublets observed in *ΔotsA::apr* as ADP-glucose did. GDP-glucose also matched resonances observed downfield of the doublet of doublets. The presence of these phosphorylated sugars was confirmed by ^{31}P-NMR spectroscopy (data not shown) and corresponded with the extra resonances observed in previous samples (Figure 6.14). This suggested that perhaps either the enzymes of the Leloir pathway in *S. venezuelae* were synthesising GDP-glucose instead of UDP-glucose or that the major substrate of *S. venezuelae* OtsA under physiological conditions is GDP-glucose (Figure 6.15 and 6.16).

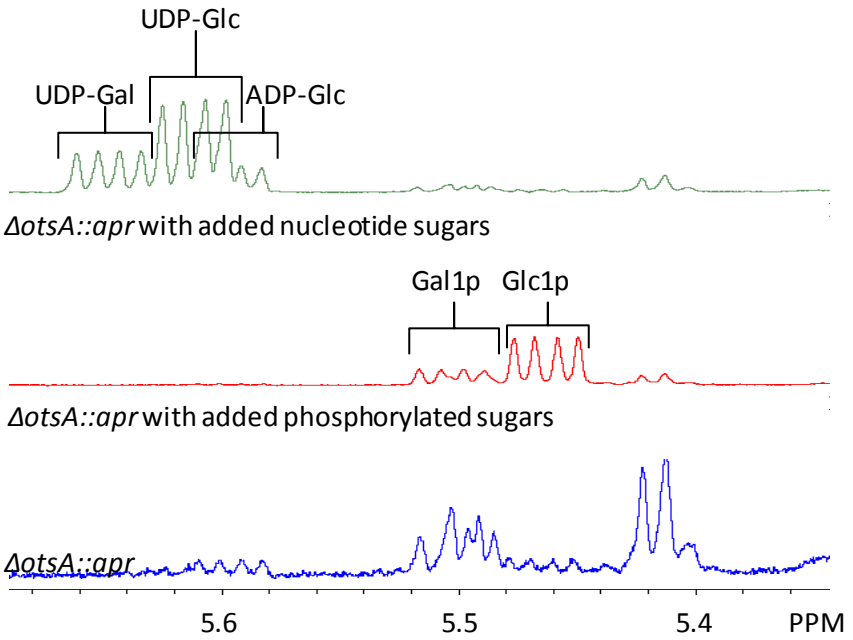

Figure 6.15: Spiking experiments suggested the two doublet of doublets in *ΔotsA::apr* corresponded to ADP-glucose and glucose 1-phosphate
The non-spiked sample *ΔotsA::apr* spectrum was amplified relative to the other two spectra so the location of the doublet of doublets could be observed clearly.

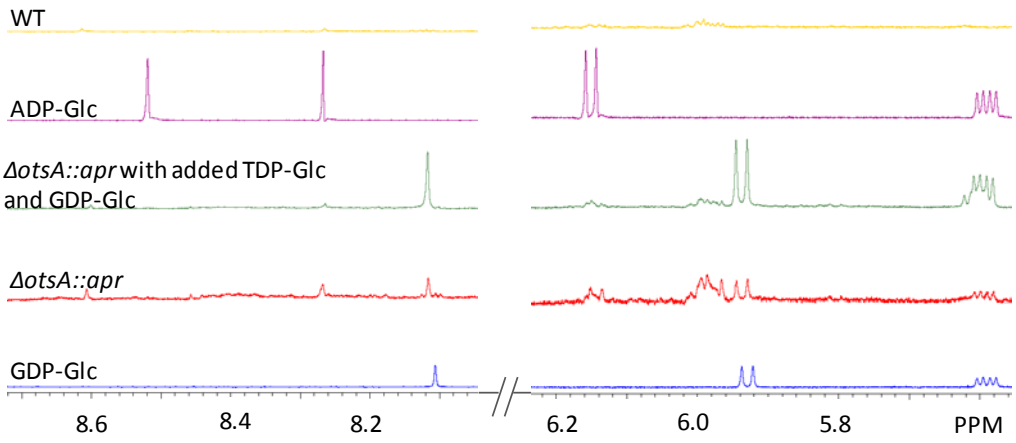

Figure 6.16: Downfield resonances suggested *ΔotsA::apr* was accumulating GDP-glucose and not ADP-glucose
The non-spiked sample *ΔotsA::apr* spectrum was amplified as in the previous figure.

Further attempts were made to correlate build-up of one of these metabolites with the developmental phenotype. The severity of the developmental phenotype was dependent upon the amount of galactose present in the medium (Figure 6.17). Attempts were subsequently made to scale-up and grow *ΔotsA::apr* on separate plates containing different amounts of galactose. However, when this was done using a standardised spore stock of *ΔotsA::apr* using the same concentration of spore inoculum typically used for metabolite analyses, the developmental phenotype was not as pronounced as previously observed (Figure 6.18). There was a subtle developmental phenotype, in which *ΔotsA::apr* would not develop on certain patches only on the plates with increased galactose concentrations (Figure 6.18). In these areas there was substrate mycelia present that had failed to develop (Figure 6.18). Whilst there were also small areas that were devoid of growth on plates containing lower galactose concentrations, these areas were clear indicating no spores were distributed on these areas (Figure 6.18). Nevertheless, the cells were harvested and cell extracts probed. GDP-glucose was only present in *ΔotsA::apr* when grown at the higher galactose concentration (0.6% of dry cell weight ± 0.04 SE). If the spore inoculum was increased four-fold then there was a more severe phenotype observed (Figure 6.19). It is noteworthy that developmental delay was only observed at the periphery of the cellophane disc and that cells with developmental delay had GDP-glucose. Whereas the cells that grew on the centre of the plate developed as WT and did not accumulate GDP-glucose. This also suggests that the cellophane may be acting as a barrier preventing contact with a developmental inhibitor and therefore the phenotype could be a consequence of changes in the growth environment. For example, one contributory factor could be acidification of the nutrient supply and in this context the cellophane could be acting to buffer such fluctuations in pH. The GDP-glucose accumulation was not in the same order of magnitude as α-maltose 1-phosphate (αM1P) build up in *ΔglgE::apr*. Glucose 1-phosphate was present at both galactose concentrations. There were also shifts in phosphate species within the samples and therefore the phenotype could also be attributable to shifts in phosphate pool metabolism.

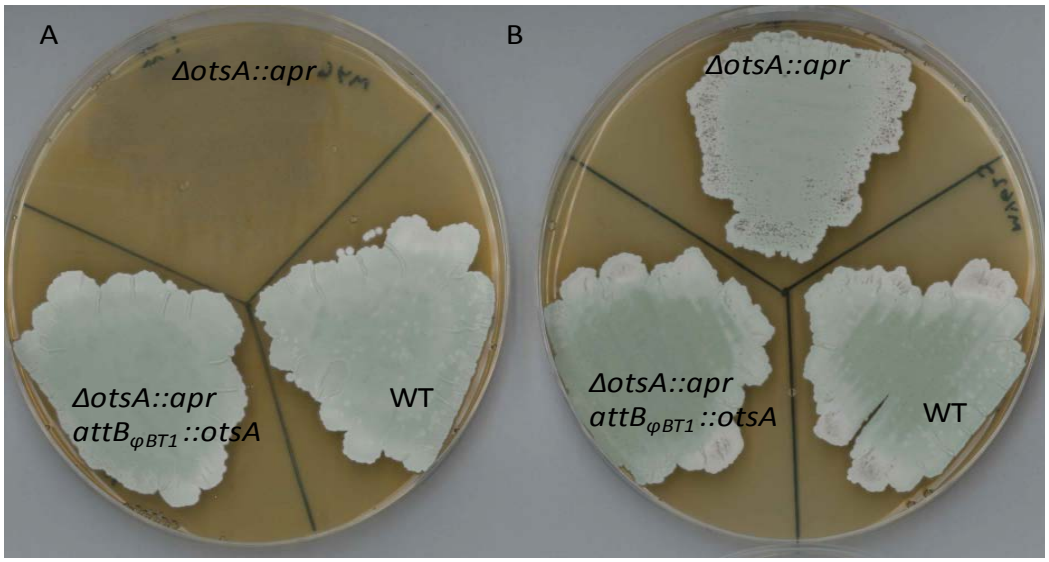

Figure 6.17: The severity of developmental delay of *ΔotsA::apr* correlated with the galactose content of the media

Strains were grown on MYGal media containing 8 g L^{-1} (A) and 4 g L^{-1} (B) galactose for two days. Whilst the WT and complemented strains looked similar when grown on both plates, the *ΔotsA::apr* strain displayed the strongest developmental delay when grown on higher amounts of galactose.

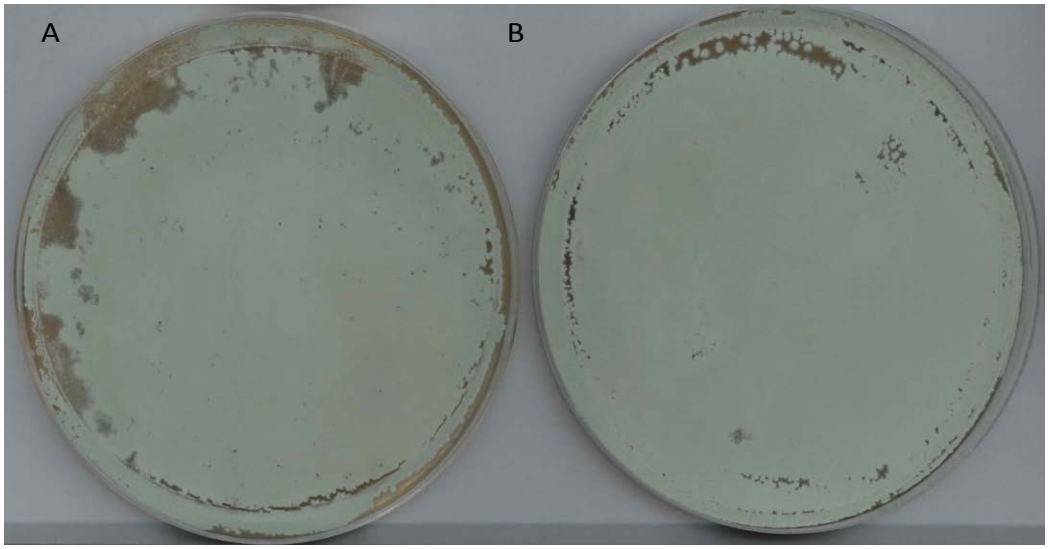

Figure 6.18: The concentration of spore inoculum was too low to observe a differential phenotype

Standardised stocks of *ΔotsA::apr* were grown on MYGal media containing 8 g L^{-1} (A) and 4 g L^{-1} (B) galactose for two days. The spore inoculum was not sufficient to observe as strong phenotype as observed previously. There were, however, regions of growth inhibition only when *ΔotsA::apr* was grown at the higher galactose concentrations.

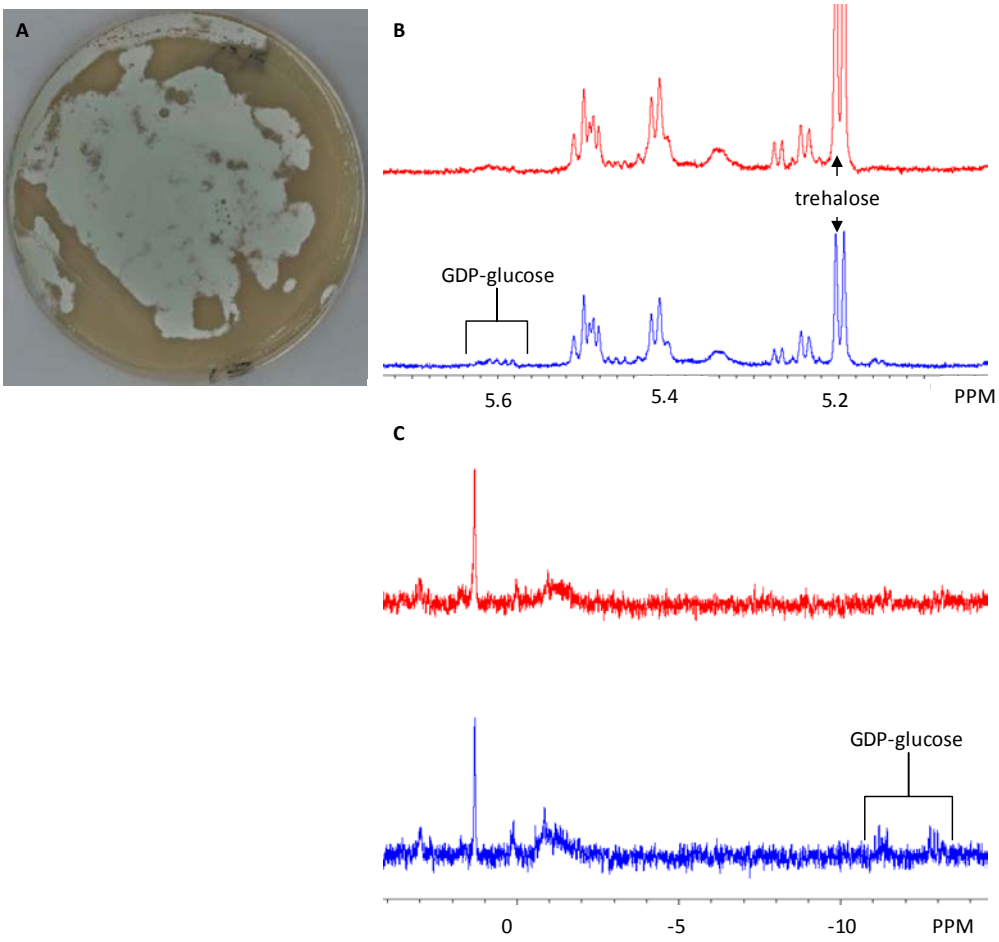

Figure 6.19: The severity of the *ΔotsA::apr* phenotype was enhanced when spore inoculum was increased

The spore inoculum was increased four-fold and around the periphery of the cellophane disc there was a developmental phenotype. The cells were harvested into two separate samples: one contained predominantly developed cells that were as WT (red spectra) and the second contained the cell material that was developmentally delayed (blue spectra). The cell lysates of these two samples were probed with ^{1}H-NMR (B) and ^{31}P-NMR (C). The major difference in sugar content was the presence of GDP-glucose in the developmentally delayed cell material.

6.7 *S. venezuelae* OtsA was heterologously produced in *E. coli*

As the *ΔotsA::apr* strain accumulated GDP-glucose under certain growth conditions, it was hypothesised that GDP-glucose was a major substrate of *S. venezuelae* OtsA. Therefore, a codon-optimised DNA sequence encoding *S. venezuelae* OtsA was synthesised and sub-cloned into an expression vector (Figure 6.20). Chemical transformation was used to insert the plasmid in to three *E. coli* cell lines optimised for high heterologous protein production; BL21 (DE3), SoluBL21 and BL21 (DE3) pLysS. Protein production was initiated by the addition of isopropyl β-D-1-thiogalactopyranoside (IPTG) when cultures reached an OD_{600nm} of 0.6. Protein production was monitored by sodium dodecyl sulphate polyacrylamide gel electrophoresis (SDS-PAGE). Any bands that sharply increased upon IPTG induction on the gel were likely to be OtsA and were excised and the identity of the protein was confirmed by matrix-assisted laser desorption/ionization-time-of-flight mass spectrometry (MALDI-TOF MS).

As initial protein expression yielded soluble OtsA, the volume of culture medium was scaled-up. OtsA was purified from the cell lysate using a HisTrap column (Figure 6.21), further purified by size exclusion chromatography (SEC) and buffer exchanged.

6.8 GDP-glucose is the preferred NDP-glucose substrate for *S. venezuelae* OtsA

Aliquots of 0.26 µM OtsA were incubated with 1 mM each of glucose 6-phosphate and different NDP-glucoses in order to determine the substrate preference of *S. venezuelae* OtsA. Trehalose 6-phosphate production was monitored by ^{1}H-NMR spectroscopy and the conversion rate was determined by comparing integrals of substrate and products. The results showed that OtsA had a strong preference for GDP-glucose, followed by ADP-glucose and slowly consumed UDP-glucose (Table 6.1). The hierarchy of substrate preference is different to the enzyme from *E. coli* (Gibson, et al., 2002). As the two preferred substrates contained purines, it suggested that the active site could be configured to accommodate the larger nucleotides and that there should be structural differences when compared to the *E. coli* enzyme structure, which is highly specific for UDP-glucose (Gibson, et al., 2002)(Figure 6.22).

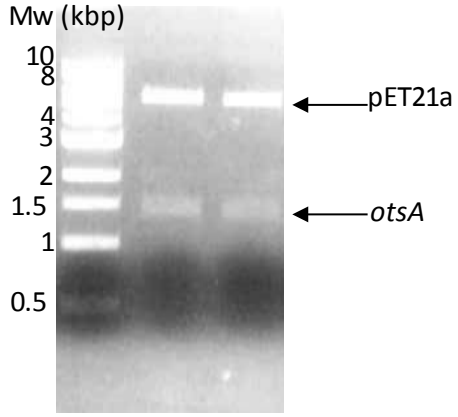

Figure 6.20: Sub-cloning of *S. venezuelae otsA*
The gene encoding *S. venezuelae* OtsA was synthesised with optimal codon usage for expression in *E. coli.* The DNA was excised from a pUC57 vector and sub-cloned into a pET21a vector. Plasmids from successful transformants were screened for the insertion of the whole *otsA* fragment by restriction digestion (expected sizes *otsA*: 1.5 kbp and pET21a: 5.5 kbp).

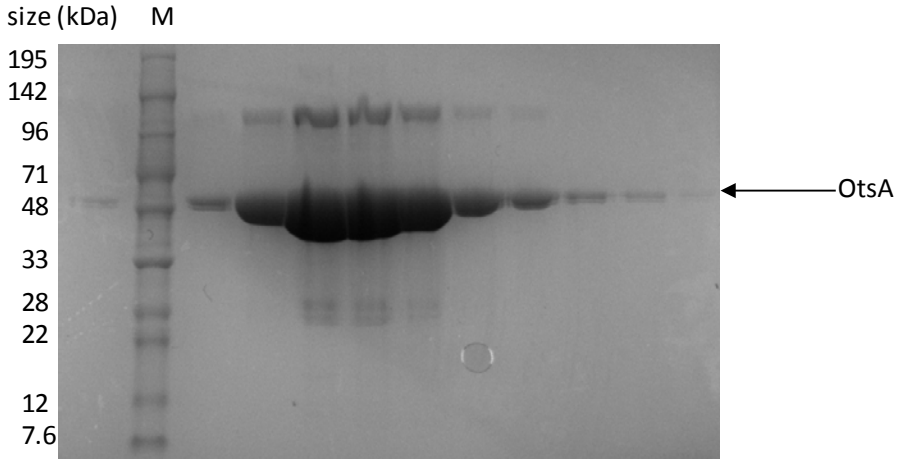

Figure 6.21: Large-scale production of *S. venezuelae* OtsA
E. coli SoluBL21 cells were used for over-production of OtsA. The protein was purified from other proteins in the cell lysate by application onto a HisTrap column. All fractions that eluted from the HisTrap column were run on an SDS-PAGE gel in order to determine which fractions contained OtsA.

Table 6.1: Substrate preferences of OtsA

NDP-glucose	% conversion to product		
	20 min	75 min	90 h
GDP-glucose	100	-	-
ADP-glucose	73	100	-
UDP-glucose	0	0	33

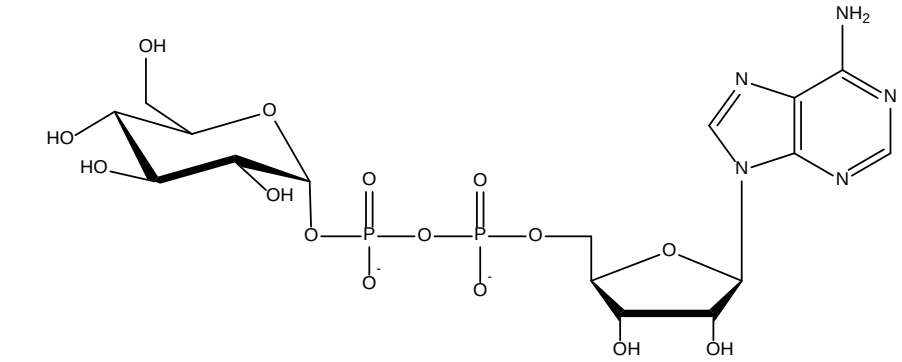

ADP-glucose

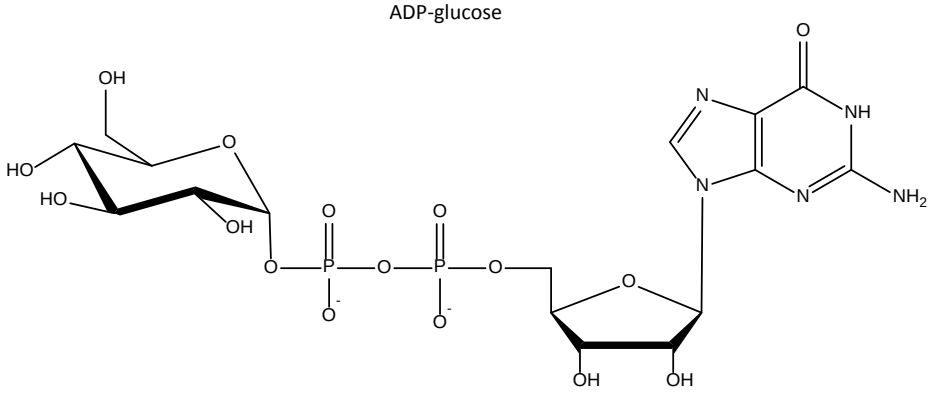

GDP-glucose

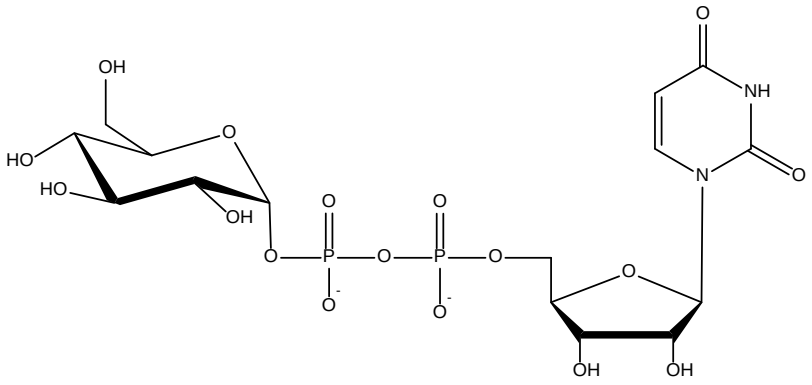

UDP-glucose

Figure 6.22: The structures of different NDP-glucoses

6.9 Structural determination of *S. venezuelae* OtsA

The crystal structure was determined in collaboration with C.E.M. Stevenson, D.M. Lawson and scientists at the Diamond Light Source. Figures were generated with assistance from C.E.M. Stevenson and S. Bornemann.

Purified OtsA was buffer exchanged into 5 mM HEPES, pH 7.0, containing 60 mM $MgCl_2$ and concentrated to 15 mg mL^{-1}. The resulting protein solution was used in crystallisation screens that were set up in a sitting-well format. The crystallisation screens were stored at a constant temperature of 20 °C. Protein crystals appeared in a number of screen conditions after 3 days of incubation. The most promising crystals were mounted onto litho-loops, flash cooled by plunging in liquid nitrogen and subsequently transported to the Diamond Light Source. Cryo-protectant was not necessary for most of the crystals because they were isolated from the Morpheus Screen (Molecular Dimension) in which all screen conditions contain cryo-protectant. One rectangular plate crystal isolated from the Morpheus Screen (Molecular Dimensions) condition B7 (0.12 M ethylene glycols, 0.1 M imidazole and 2-(*N*-morpholino)ethanesulfonic acid (MES), pH 6.5, 30% (v/v) ethylene glycol and PEG 8K) gave the best diffraction (Figure 6.23).

Data were collected from this crystal to 1.95 Å resolution with the data collection statistics reported in Table 6.2. The structure of OtsA was solved by molecular replacement using a model generated from the output of the Phyre2 server (Bennett-Lovsey, et al., 2008). This model was based on the crystal structure of VldE from *Streptomyces hygroscopicus* (PDB accession code 3T5T, Zhang et al., unpublished), with which OtsA shares 31% amino acid sequence identity. The solvent content was calculated using the Matthews program, which suggested that four copies of the OtsA monomer (molecular weight 51,258 Da) were likely to be present in the asymmetric unit, giving a solvent content of 46% (Kantardjieff and Rupp, 2003). A molecular replacement search with the monomer of OtsA was carried out using PHASER and was successful in finding four copies of the monomer per asymmetric unit (McCoy, et al., 2007) (Figure 6.24). After density modification with four-fold averaging in PARROT, BUCCANEER was used and approximately 74% of the residues were built automatically (Cowtan, 2006; Cowtan, 2010). This was then refined using REFMAC, followed by a further iteration of PARROT and BUCCANEER, which resulted in 92% of the residues being built (Cowtan, 2006; Cowtan, 2010; Murshudov, et al., 1997). This model was completed through several iterations of restrained refinement in REFMAC5

(Murshudov, et al., 2011), and manual rebuilding in COOT (Emsley and Cowtan, 2004). The apo model has R_{work} and R_{free} values of 0.202 and 0.231 respectively at 1.95 Å resolution.

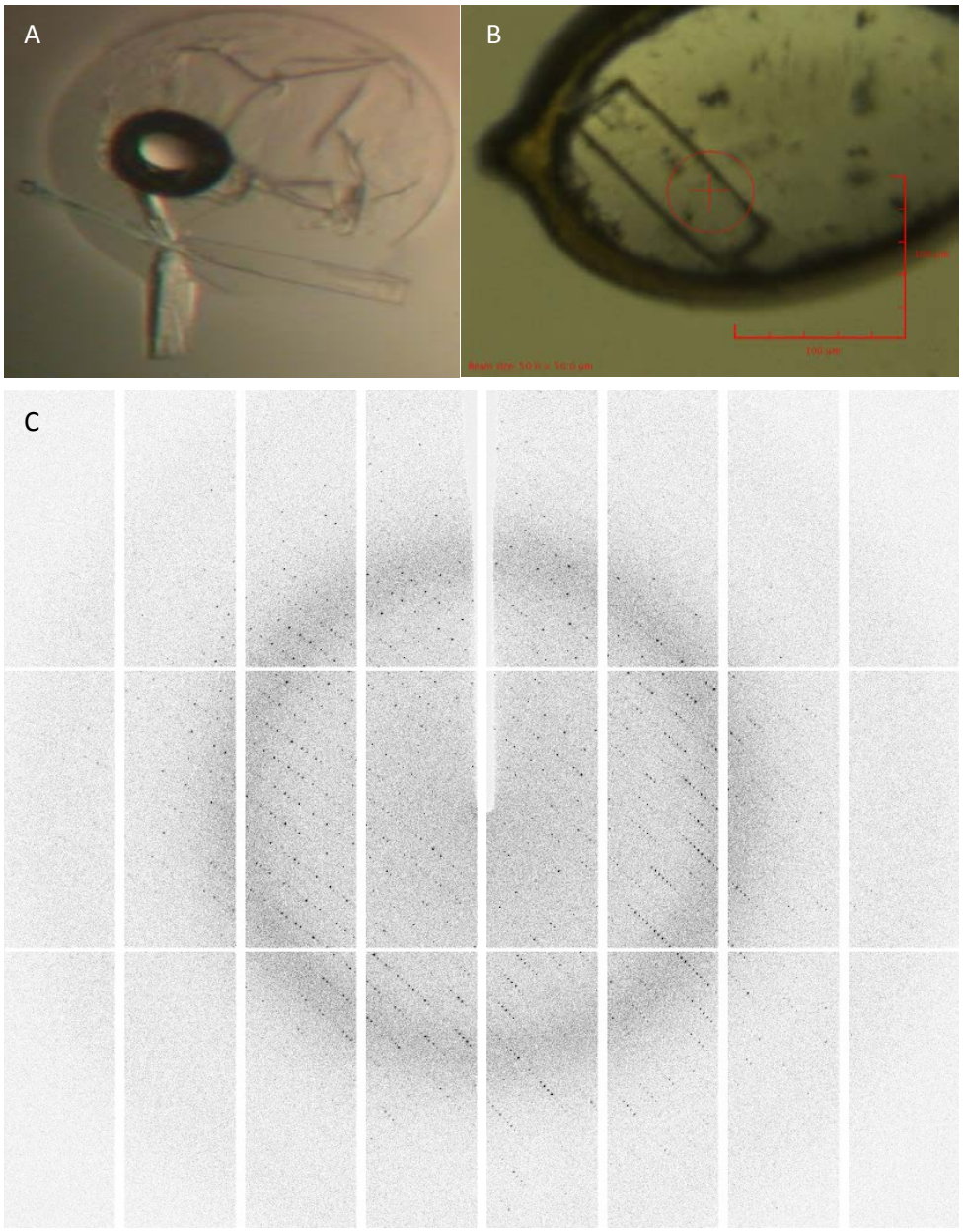

Figure 6.23: OtsA crystals
(A) Initial protein crystallography screens yielded rectangular plate crystals in Morpheus Screen condition B7.
(B) The crystals were positioned within litho loops and sent to the Diamond light source. The X-ray beam was focussed on the region highlighted with +.
(C) The resulting diffraction patterns of the X-rays were recorded.

Table 6.2: Summary of OtsA X-ray data collection

Number of crystals	1
Beamline	I04-1, Diamond Light Source, UK
Detector	Pilatus 2M detector
Space group	$P2_1$
Cell parameters (Å)	a= 41.43, b= 168.40 c= 133.90, β= 97.19
Wavelength (Å)	0.92
Resolution range (Å)	32.64- 1.95
Unique reflections	131515 (9597)
Completeness	99.6 (98.6)
Multiplicity	6.9 (6.2)
R_{merge}[b]	0.092 (0.984)
R_{meas}[c]	0.109 (1.190)
CC½[d]	0.998 (0.661)
Mean I/σ(I)	14.6 (1.6)
Wilson B value (Å^2)	22.102
Refinement	
Resolution range[a] (Å)	364–1.95 (2.0–1.95)
Reflections: working/free[e]	124836/6621
Rwork/ Rfree[a,f]	0.202/0.231 (0.313/0.334)
Ramachandran: favoured/allowed/disallowed[g] (%)	96.8/2.9/0.3
R.m.s. bond distance deviation (Å)	0.010
R.m.s. bond angle deviation (Å)	1.25
No. of protein residues (ranges): chains A/B/C/D	447 (2-18, 23–452)/432 (2-18, 24-29, 43–451)/447 2-18, 23-452)/ 448 (2-18, 23-453)
No. of water molecules/MES/Ethylene glycol molecules	672/4/2
Mean B factors: protein/water/MES/PEG/overall (Å^2)	17.41/40.67/40.87/37.36/18.465

a Figures in parentheses indicate values for the outer resolution shell.

b Rmerge =Phkl Pi|Ii(hkl) hI(hkl)i|/PhklPiIi(hkl).

c Rmeas =Phkl [N/(N 1)]1/2 Pi |Ii(hkl) hI(hkl)i|/Phkl PiIi(hkl), where Ii(hkl) is the ith observation of reflection hkl, hI(hkl)i is the weighted average intensity for all observations i of reflection hkl and N is the number of observations of reflection hkl.

d CC½ is the correlation coefficient between intensities taken from random halves of the dataset.

f The R-factors Rwork and Rfree are calculated as follows: R =P(|Fobs _ Fcalc|)/P|Fobs| _ 100, where Fobs and Fcalc are the observed and calculated structure factor amplitudes, respectively.

g As calculated using MolProbity (Chen, et al., 2010).

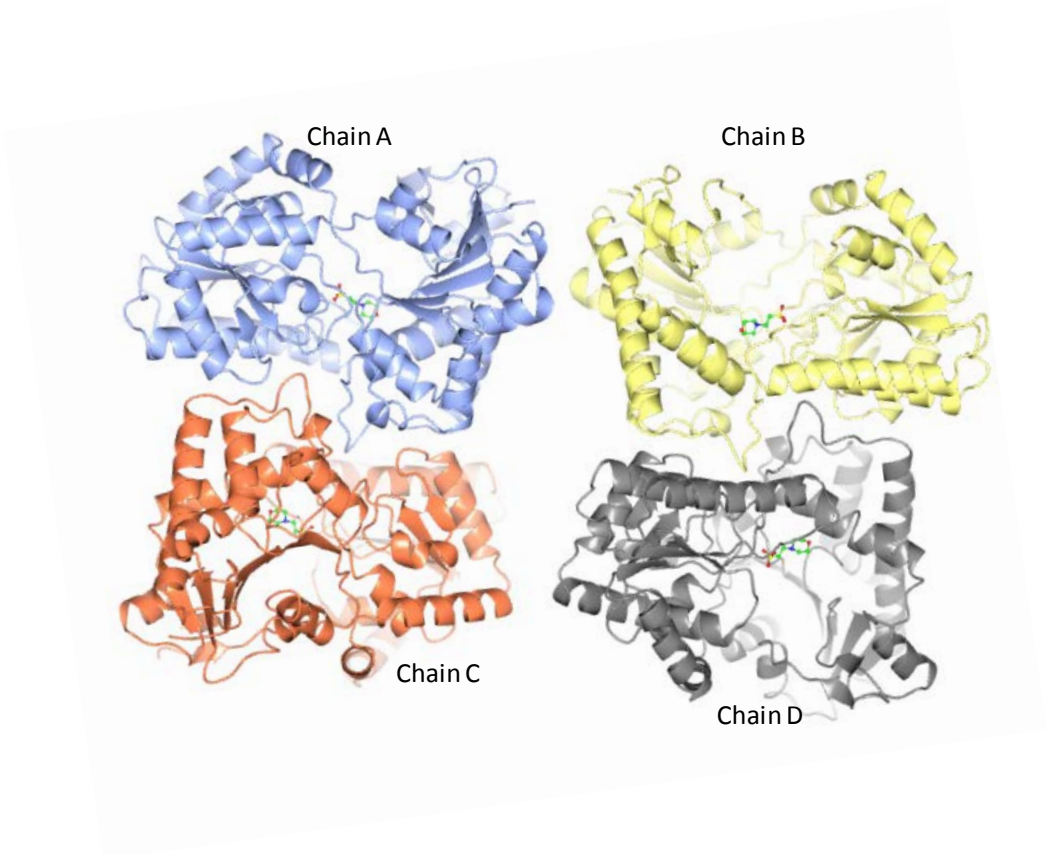

Figure 6.24: *S. venezuelae* OtsA structure
There were four copies of OtsA in the asymmetric unit (labelled chains A-D). There was clear electron density for MES, which was present in the crystallisation condition, in all four sub-units. Figure generated using CCP4mg (McNicholas, et al., 2011).

The solved structure was submitted to the Proteins, Interfaces, Structures and Assemblies (PDBePISA) server to ascertain the most likely biologically relevant oligomer (Krissinel, 2011). The output suggested it was most likely to exist as a dimer, with chains A and C, as well as chains B and D forming dimers with a buried surface area of 1320.5 and 1312.3 $Å^2$ respectively (Figures 6.24 and 6.25). This is consistent with the only deposited structure of OtsA from *E. coli*, which also forms a dimer (Gibson, et al., 2002). Even though both proteins formed dimers it is noteworthy that the dimer interface in each is significantly different (Figure 6.25).

The *S. venezuelae* OtsA monomer comprises twin Rossman-like β/α/β domains in a GT-B configuration. The active site is located in a cleft at the interface between the two domains and there was clear electron density for MES, which was bound within the active site (Figure 6.26). The majority of the amino acids were built into the model, with the exception of a flexible loop comprising residues 29-32 in chain A, this flexible loop is also present in the *E. coli* OtsA. The loop is located in the vicinity of the active site and its positioning suggests that these residues may be involved in gating the active site, which would explain the flexibility of the region (Figure 6.26).

Attempts were then made to co-crystallise *S. venezuelae* OtsA with 1 mM GDP-glucose as well as to soak crystals in a saturated solution containing GDP-glucose. This was pursued in order to determine the structural basis for the altered substrate specificity of the *E. coli* and *S. venezuelae* OtsA enzymes. Co-crystallisations and soaking experiments were carried out and data was collected, but no density was apparent for any ligand.

In the absence of a ligand bound structure, comparisons were made to other structures deposited in the PDB database (www.pdb.org) (Berman, et al., 2000). This was achieved by using the output of the DALI server (Holm and Rosenström, 2010). The most structurally similar entries (in rank order) were a putative glycosyl transferase (RMSD 2.1), VldE (RMSD 2.1) and *E. coli* OtsA (RMSD 2.0). Whilst there were no nucleotide bound ligands to the putative glycosyltransferase, there was a GDP bound VldE structure.

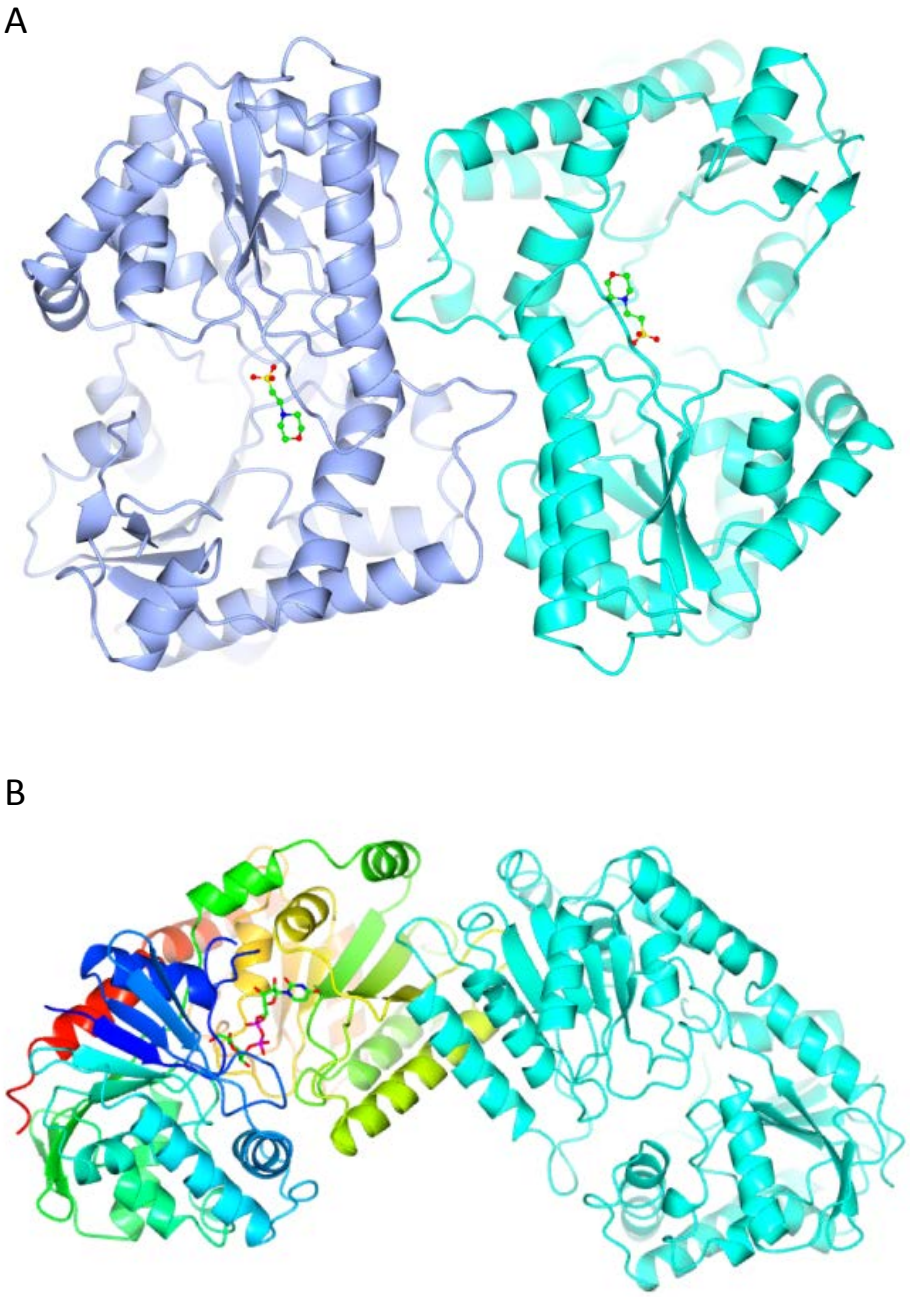

Figure 6.25: OtsA dimers
Both *S. venezuelae* (A) and *E. coli* (B) OtsAs are predicted to form biologically relevant dimers. The dimer interface in these two proteins is, however, very different. Figure generated using CCP4mg (McNicholas, et al., 2011).

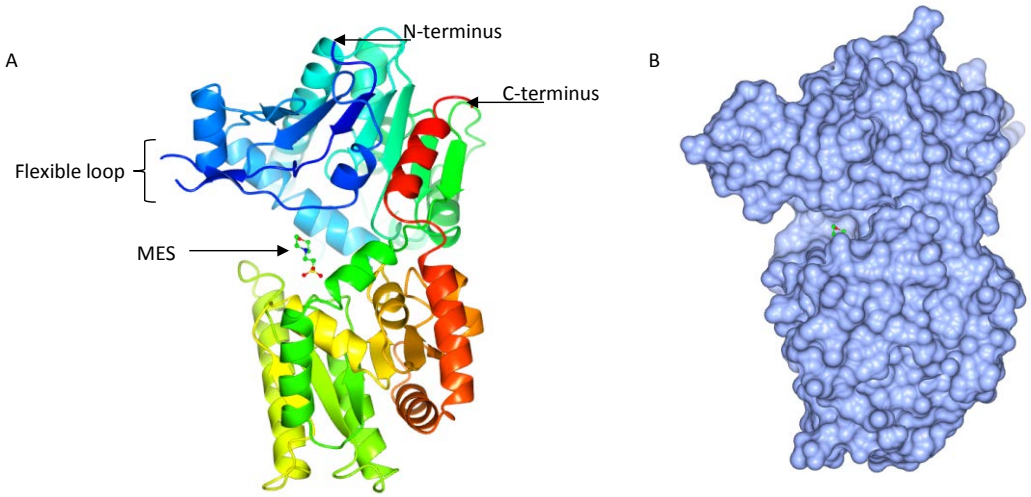

Figure 6.26: OtsA monomer

The overall fold of OtsA represented as a ribbon diagram (A) and space-fill model (B). The active site is located at the interface between the two domains. There was clear electron which suggested that MES was bound in the vicinity of the active site. The space-fill model suggested that the active-site is located within a cleft. Figure generated using CCP4mg (McNicholas, et al., 2011).

VldE is a pseudo-glycosyltransferase isolated originally from *Streptomyces hygroscopicus* that is involved in the biosynthesis of validamycin A that catalyses the formation of a C-N bond instead of a glycosidic bond (Cavalier, et al., 2012). The enzyme mechanism is similar to that of OtsA, in which it uses nucleotide- and phosphate-activated compounds to form a pseudo-disaccharide. Interestingly, VldE uses GDP-valienol that is structurally comparable to GDP-glucose substrate used by OtsA from *S. venezuelae* but not from *E. coli*, which uses UDP-glucose (Cavalier, et al., 2012; Gibson, et al., 2002).

S. venezuelae OtsA shared modest primary sequence identity to *E. coli* OtsA and VldE of 32 and 31% respectively (Figure 6.27). Overlays of the solved structure were performed with the UDP-glucose bound *E. coli* OtsA structure (PDB: 1UQU) as well as the GDP-bound VldE structure (PDB: 4F96) (Figures 6.28 and 6.29). Despite the relatively low primary sequence conservation and the absence of a ligand in *S. venezuelae* OtsA, the overall folds of the monomers were similar, with the exception of an additional β-hairpin motif in VldE, which is not present in either of the OtsAs (Figures 6.28 and 6.29) (Cavalier, et al., 2012). It was also apparent that whilst MES was bound within the active site of *S. venezuelae* OtsA, it was not located at the donor site and so its presence is not relevant to understanding altered substrate specificities (Figures 6.28 and 6.29).

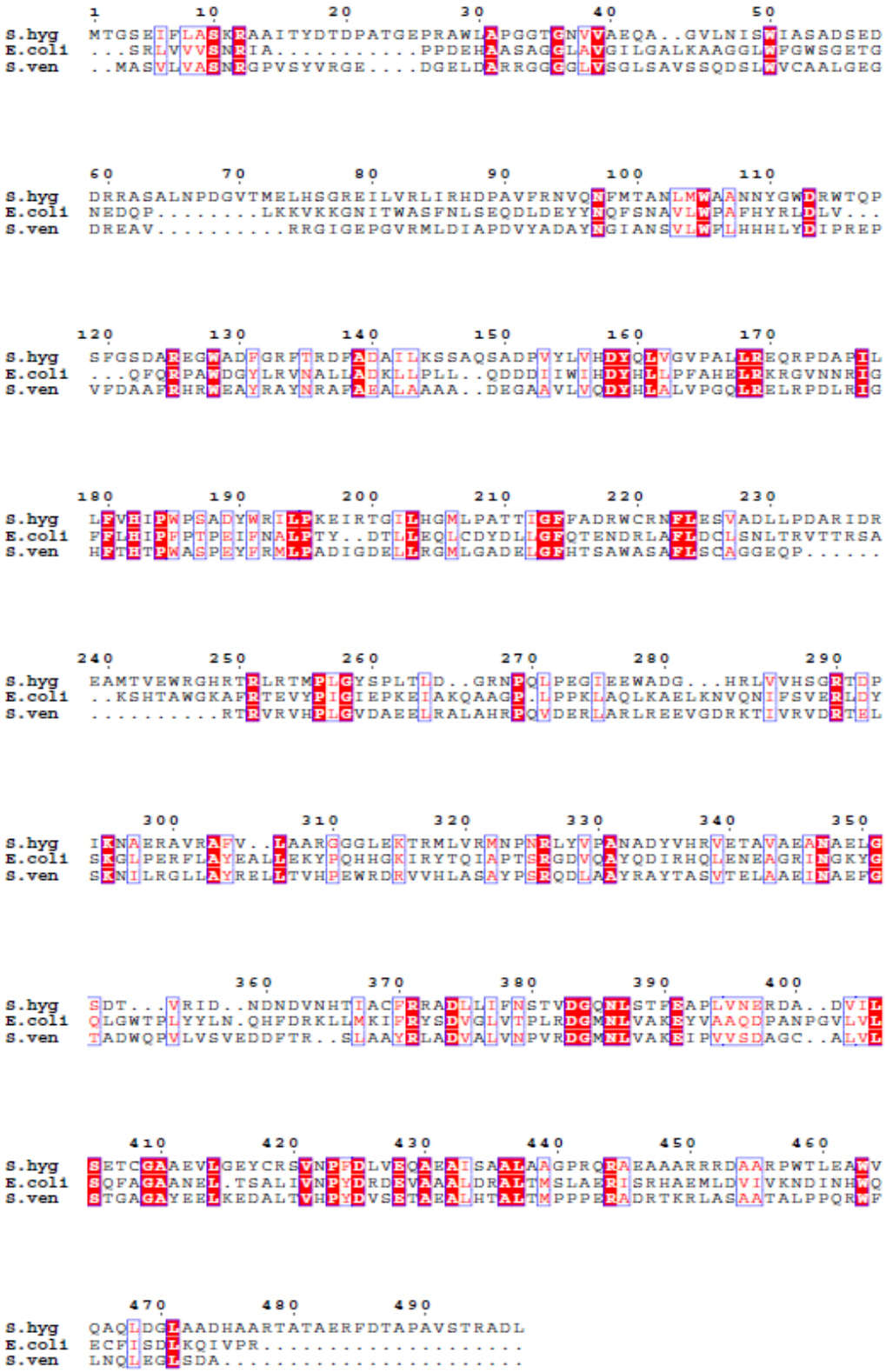

Figure 6.27: Sequence alignments

Sequence alignment of *S. venezuelae* OtsA (S.ven), *E. coli* OtsA (E.coli) and VldE (S.hyg). Residues in red boxes are conserved amongst all three sequences and residues in blue boxes, whilst not conserved, have similar chemical properties in all three sequences. Figure generated using ESPript (Gouet, et al., 2003).

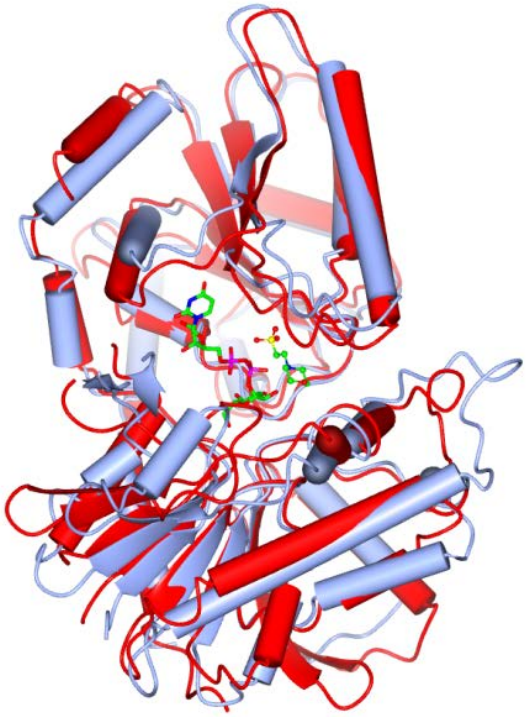

Figure 6.28: Structural overlays of OtsAs
Both A chains of the structures of *E. coli* (red structure) and *S. venezuelae* (blue structure) OtsA were overlaid, the overall fold of both proteins was similar (RMSD: 2.04 Å over 403 residues), despite one being an apo structure and the other being bound to UDP-glucose. Figure generated using CCP4mg (McNicholas, et al., 2011).

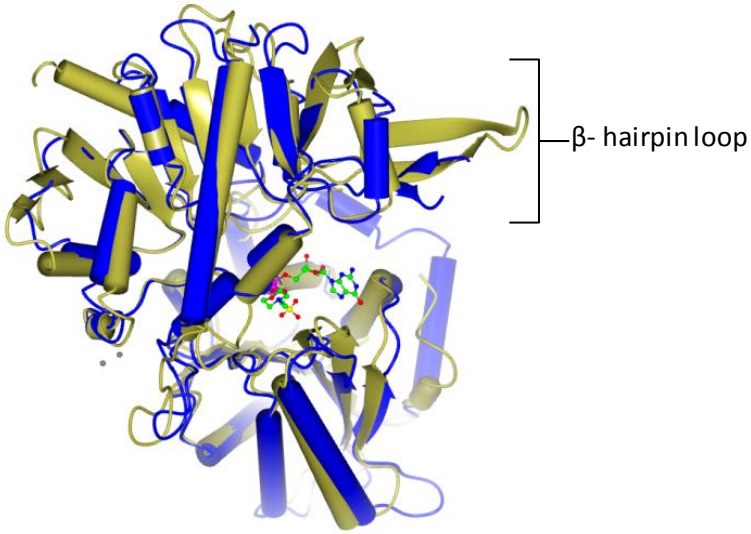

Figure 6.29: Structural overlay of OtsA and VldE
Both A chains from the structures of *S. venezuelae* (blue structure) OtsA and VldE (gold structure) were overlaid, the overall fold of both proteins were similar, with the exception of an extra β-hairpin loop in the VldE structure (RMSD: 1.68 Å over 393 residues), despite one being an apo structure and the other being bound to GDP. Figure generated using CCP4mg (McNicholas, et al., 2011).

As the overall fold of these structures was similar, it allowed informative superpositions to be made of the active site donor region between all three structures (Figure 6.30). The structures were aligned by fixing the positions of the α-carbons of the residues: Arg264, Leu366 and Glu370, which were conserved in all three structures. The overlaid structures suggested that the ligands were bound at similar positions within the donor site, with the phosphate and ribose moieties practically overlapping (Figure 6.30). However, the positioning of the uracil and guanine moieties were markedly different and they were in different planes, suggesting that they were interacting with different residues in each of the structures (Figure 6.30). Moreover, the hydrogen bonding networks and amino acid residues were located at similar positions around the phosphates and ribose sugars but varied considerably at the regions interacting with guanine and uracil (Figure 6.30). The conserved binding of the phosphates and riboses would most likely be required because the mechanisms between these enzymes are conserved. The positioning of the phosphates in particular is important as the phosphate bond to the sugar (or pseudo-sugar in VldE) is cleaved during catalysis.

The interactions between the ligands and amino acid residues were investigated further by generating 2 dimensional (D) representations of their respective nucleotide binding sites (Figure 6.31). As in the 3D depiction, the ribose and phosphate moieties of GDP were predicted to make interactions with the side chain residues of Arg264, Glu370 and Lys269 as well as the backbone residues of Leu366 and Val367 in *S. venezuelae* OtsA (Figure 6.31). These interactions were conserved in all three structures. The guanine moiety of GDP was interacting with the side chain of residues of Ser345 and Asp340 as well as the backbone residue of Glu341 in *S. venezuelae* OtsA, which are all hydrophilic residues. Furthermore, the hydrophobic residue Phe342 secures the guanine in place by potentially stacking above it. The interactions made by *S. venezuelae* OtsA at the guanine moiety closely match the interactions made by VldE, which also interacts with three hydrophilic residues and has a hydrophobic residue positioned above the guanine ring (Figure 6.31) (Cavalier, et al., 2012). This contrasts to the *E. coli* OtsA nucleotide binding site, in which the uracil moiety of UDP only interacts with the backbone of a Phe339 residue (Figure 6.31) (Gibson, et al., 2004). Therefore, there are four key residues that are predicted to be important for *S. venezuelae* OtsA to discriminate for the nucleotide component of GDP-glucose over UDP-glucose.

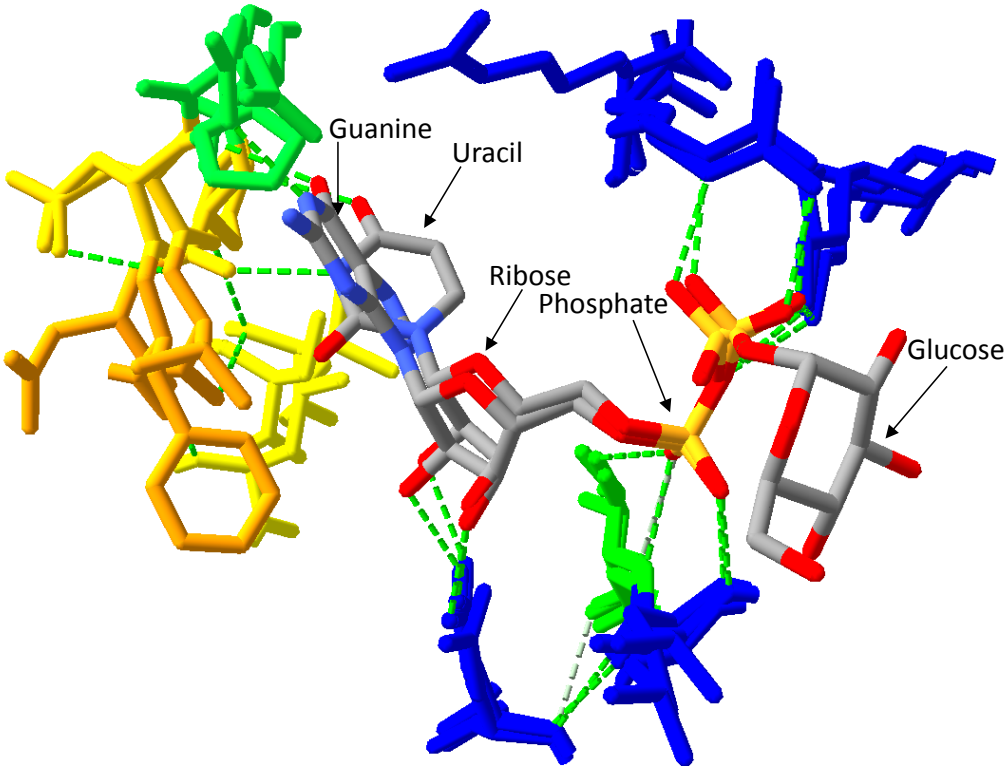

Figure 6.30: Overlay of donor site with ligands

An overlay was performed focussing on the donor site of both OtsA structures and the VldE structure. Both ligands (UDP-glucose and GDP) are shown within the donor site. The amino acid residues are coloured on a graded scale based on sequence conservation. The overlay shows that there is conservation in sequence and space between all of the amino acids interacting with both the phosphate and ribose components of the ligands, as indicated by the blue coloration. However, towards the base region there are considerable deviations between the structures, as indicated by the yellow coloration. The diagram also shows that whilst the ribose and phosphate moieties of the ligands superimpose well, the nucleotide moieties of the ligands are positioned in different planes within the donor site. The uracil base is positioned perpendicular relative to the positioning of the guanine base, which is indicative of different interactions taking place between the residues in the different structures. Image generated using Swiss-PdbViewer (Guex and Peitsch, 1997).

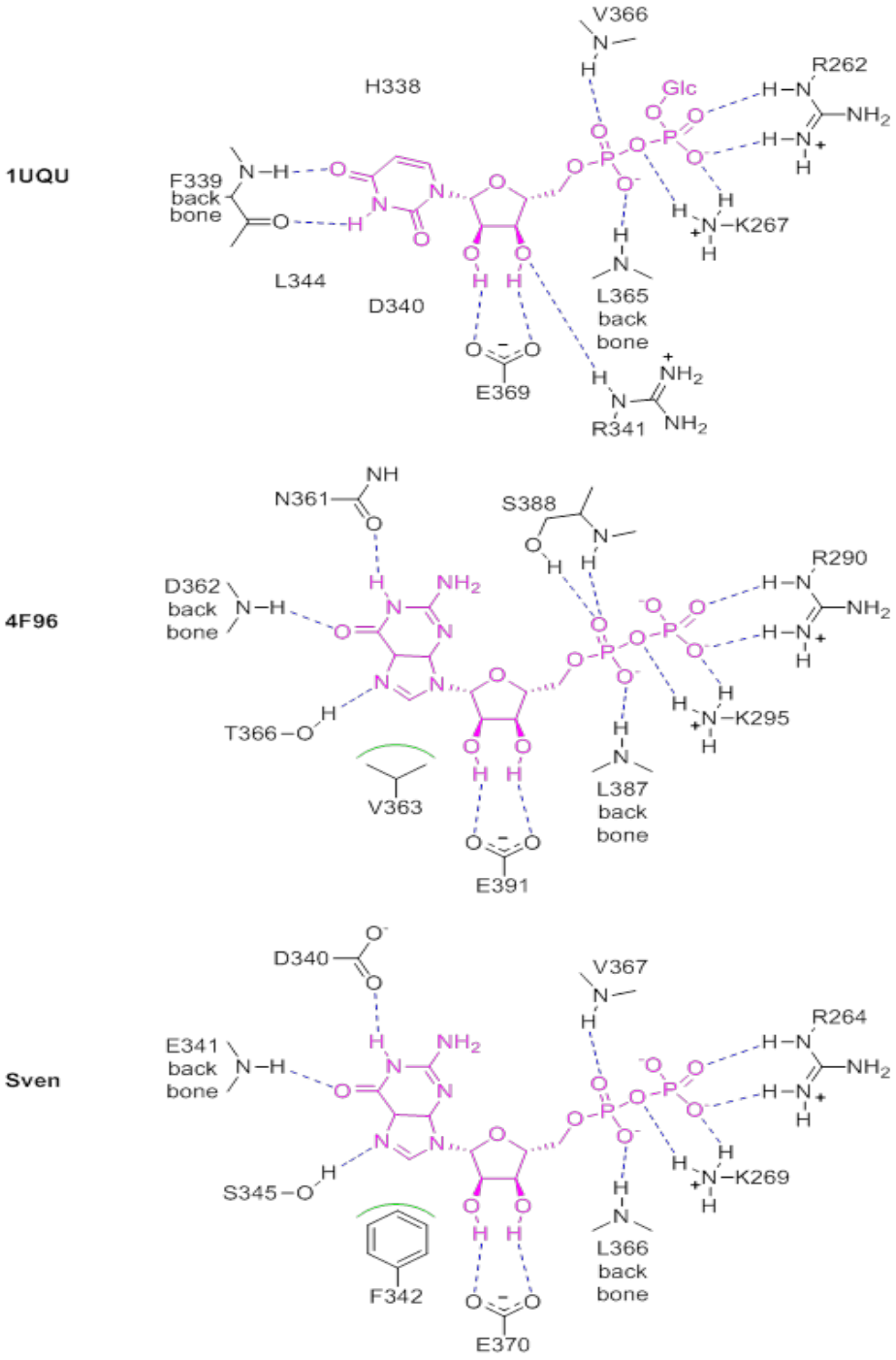

Figure 6.31: 2D representation of the OtsA and VldE nucleotide binding sites
2D representations were generated for *E. coli* OtsA bound to UDP (1UQU), VldE bound to GDP (4F96) and the GDP from VldE was superimposed into *S. venezuelae* OtsA (Sven). The hydrogen bonding networks for all structures are very similar towards the ribose and diphosphate regions of the ligand, with several positively charged side chains interacting with the negative charges on phosphate groups. However, in the GDP-bound structures there are further interactions with amino acid side chains, leading to three hydrogen bonds, which is not possible in the UDP-bound structure as the amino acids present in this region too different.

6.10 *S. venezuelae* GalU was over-produced heterologously in *E. coli*

GalU was hypothesised to be producing the NDP-glucose substrate for OtsA. Given that OtsA uses GDP-glucose, it was hypothesised that GalU could be the source of GDP-glucose. Therefore, GalU was over-produced using the same approach as described previously for OtsA in section 6.7 (Figure 6.32). The only exception was a different strain was used and that the protein was deemed to be of sufficient purity after elution from a HisTrap column and therefore did not require further purification by SEC (Figure 6.33).

6.11 GalU was not able to produce GDP-glucose

Cell extracts of *ΔotsA::apr* indicated that GDP-glucose accumulated. However, the source of GDP-glucose in *S. venezuelae* was unknown and there were no genes annotated in the genome as GDP-glucose synthases or similar. Close homologues of GalU are normally UDP-glucose pyrophosphorylases, which use glucose 1-phosphate and UDP to synthesise UDP-glucose. The enzyme was widely thought to provide UDP-glucose for OtsA.

However, enzyme assays in which 2 mM glucose 1-phosphate was incubated with 2 mM nucleotides suggested that the preferred nucleotides were UTP and dTTP (Table 6.3). Indeed no activity with GTP was observed, which suggests it is not the source of GDP-glucose in *S. venezuelae*. The specific activity for UTP in *S. venezuelae* GalU was several orders of magnitude lower than that of the *S. coelicolor* enzyme (Asencion Diez, et al., 2012). However, this could be in part due to non-optimal assay conditions. Optimisation was not attempted in this study because it was unlikely this would alter substrate specificity.

6.12 *S. venezuelae* GalU was crystallised

Crystallisation of GalU was also attempted in a similar fashion to OtsA using a protein concentration of 13 mg mL^{-1}. Crystals formed after three weeks incubation in the structure screen (Molecular Dimensions) condition F2 (0.2 M ammonium sulphate, 0.1 M sodium cacodylate, pH 6.5, 30% (w/v) PEG 8k) but were too small and fragile to handle, therefore they were used as a seed stock. Optimisations were set up in which the PEG concentration and ammonium sulphate concentration were altered in hanging-drop, vapour diffusion plates. Co-crystallisation was also attempted by the addition of 1 mM of either UTP or glucose 1-phosphate. After several weeks larger plate crystals were present in some of the optimisation screen (Figure 6.34). These crystals were flash-cooled and sent to the Diamond Light Source for data collection. A preliminary data set was

recorded with collection parameters outlined in Table 6.4. As the resolution was relatively poor (3.41 Å) manual structural refinement was not attempted as at this resolution there would have been considerable ambiguity in the density maps.

Co-crystallisation trials were also attempted using a customised screen called the KISS screen. After three weeks incubation, crystals appeared in condition E7 (0.2 M ammonium sulphate, 0.1 M sodium citrate, pH 5, 30% (w/v) PEG 3350) and E8 (0.2 M ammonium sulphate, 0.1 M sodium citrate, pH 5, 35% (w/v) PEG 3350) (Figure 6.34). One of these crystals was sent to the Diamond Light Source for data collection, the data collection parameters are reported in Table 6.5. The resolution at which the data was collected was slightly improved compared to the previous crystal (3.11 Å). However, the space group and the asymmetric unit differed from the previous data set collected.

The solvent content was calculated using the Matthews program, which suggested that 12 copies of the GalU monomer (molecular weight 34,906 Da) were likely to be present in the asymmetric unit, with a solvent content of 68% (Figure 6.35) (Kantardjieff and Rupp, 2003; Matthews, 1968). It is highly unusual to have so many copies of a monomer in a single asymmetric unit. Manual refinement would have been challenging at such a low resolution and therefore was not attempted. However, a model was generated using the non-refined structure to show how the crystal would have packed and this suggested that there were large solvent channels within the crystal. This suggests that the fragility of the crystals could in part be due to the high solvent content of the crystals (Figure 6.35).

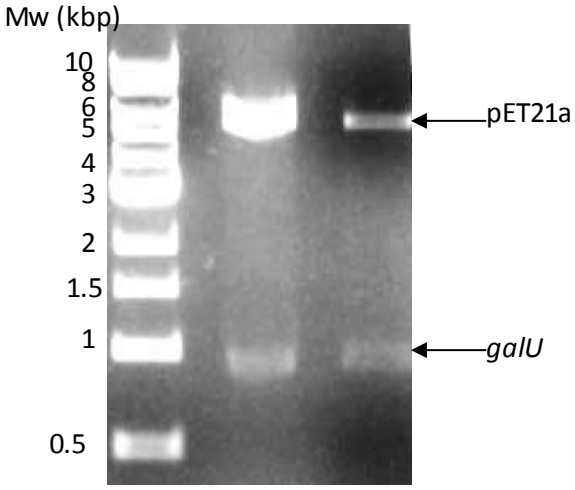

Figure 6.32: Sub-cloning of *S. venezuelae galU*

The gene encoding *S. venezuelae* GalU was synthesised with optimal codon usage for expression in *E. coli.* The sequence was excised from a pUC57 vector and sub-cloned into a pET21a vector. Plasmids from successful transformants were screened for the insertion of the whole galU fragment by restriction digestion (expected sizes *galU*: 0.8 kbp and pET21a: 5.5 kbp).

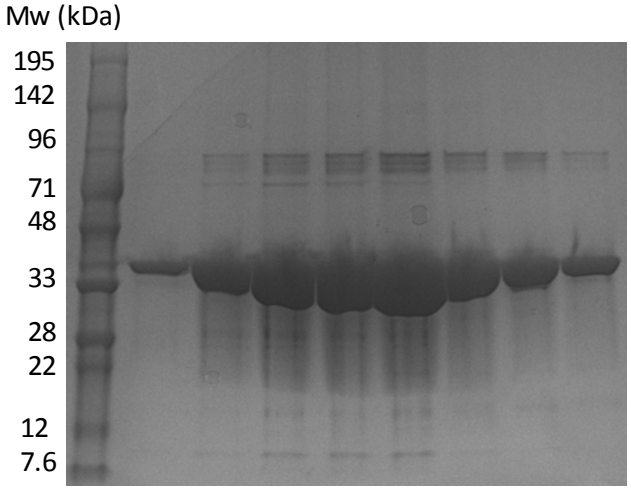

Figure 6.33: Large-scale production of *S. venezuelae* GalU

E. coli BL21 (DE3) pLysS cells were used for over-production of GalU. The protein was purified from other proteins in the cell lysate by application onto a HisTrap column. All fractions that eluted from the HisTrap column were run on an SDS-PAGE gel in order to determine which fractions contained GalU.

Table 6.3: GalU nucleotide preferences

Nucleotide (2 mM)	Specific activity (U mg^{-1})
UTP	0.52
ATP	0.00
GTP	0.03
ITP	-0.01
CTP	0.05
dTTP	0.50

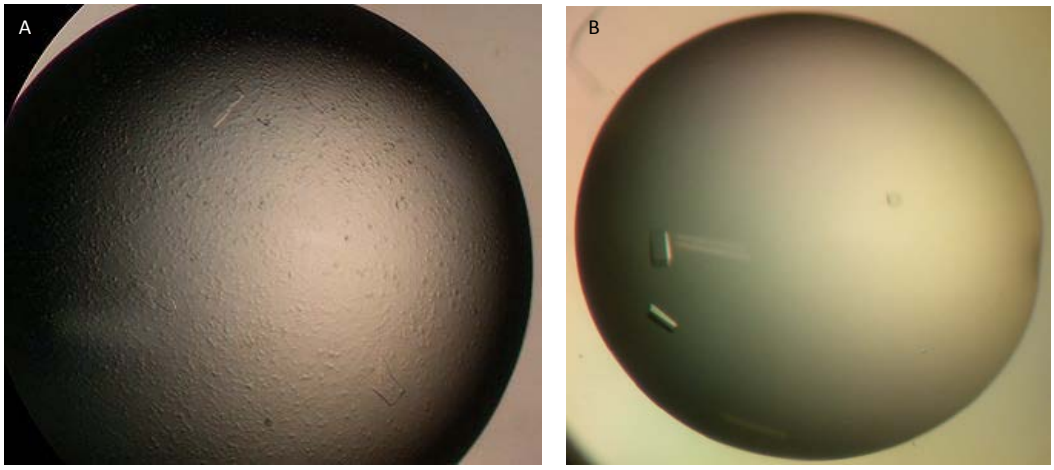

Figure 6.34: GalU crystals
Initial protein crystallography screens yielded delicate plate crystals (A) but cuboids in the KISS screen (B).

Table 6.4: Summary of GalU-1 X-ray data collection

Number of crystals	1
Beamline	I04-1, Diamond Light Source, UK
Detector	Pilatus 2M detector
Space group	$P2_12_12$
Cell parameters (Å)	a= 59.03, b= 91.10, c= 137.20,
Wavelength (Å)	0.92
Resolution range (Å)	75.89-3.41
Unique reflections	10647 (774)
Completeness	99.7 (97.5)
Multiplicity	12.9 (12.5)
R_{merge} [b]	0.217 (1.527)
R_{meas} [c]	0.234 (1.657)
CC½ [d]	0.997 (0.747)
Mean I/σ(I)	11.5 (1.9)
Wilson B value (Å^2)	175.593

a Figures in parentheses indicate values for the outer resolution shell.

b Rmerge =Phkl Pi|Ii(hkl) hI(hkl)i|/PhklPiIi(hkl).

c Rmeas =Phkl [N/(N 1)]1/2 Pi |Ii(hkl) hI(hkl)i|/Phkl PiIi(hkl), where Ii(hkl) is the ith observation of reflection hkl, hI(hkl)i is the weighted average intensity for all observations i of reflection hkl and N is the number of observations of reflection hkl.

d CC½ is the correlation coefficient between intensities taken from random halves of the dataset

Table 6.5: Summary of GalU-2 X-ray data collection

Number of crystals	1
Beamline	I02, Diamond Light Source, UK
Detector	Pilatus 6M detector
Space group	$P2_1$
Cell parameters (Å)	a= 84.25, b= 262.8, c= 147.60, β= 94.04
Wavelength (Å)	0.979
Resolution range (Å)	62.38-3.11
Unique reflections	110507 (8297)
Completeness	96.5 (98.2)
Multiplicity	3.0 (3.0)
R_{merge} [b]	0.095 (0.730)
R_{meas} [c]	0.135 (1.030)
CC½ [d]	0.992 (0.570)
Mean I/σ(I)	10.8 (1.7)
Wilson B value (Å^2)	34.815

a Figures in parentheses indicate values for the outer resolution shell.

b Rmerge =Phkl Pi|Ii(hkl) hI(hkl)i|/PhklPiIi(hkl).

c Rmeas =Phkl [N/(N 1)]1/2 Pi |Ii(hkl) hI(hkl)i|/Phkl PiIi(hkl), where Ii(hkl) is the ith observation of reflection hkl, hI(hkl)i is the weighted average intensity for all observations i of reflection hkl and N is the number of observations of reflection hkl.

d CC½ is the correlation coefficient between intensities taken from random halves of the dataset

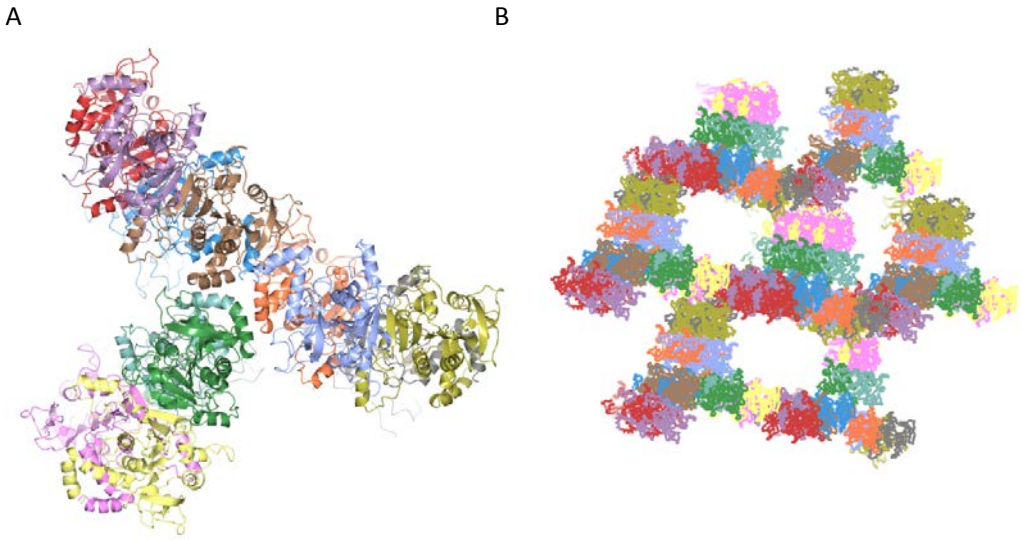

Figure 6.35: GalU crystal packing
A partially solved structural solution to GalU suggested there were at least 12 copies of the GalU monomer in each asymmetrical unit (A) and that the crystal was packed in such a way that there were large solvent channels (B), which would have made the crystals fragile.

6.13 Discussion

Results from this chapter suggest that OtsA is not the major source of trehalose in spores of *S. venezuelae,* when grown on maltose. This suggests that instead the TreYZ pathway is responsible for trehalose production, after the maltose has been converted to glycogen. This is consistent with abundant glycogen observed in the pre-spores, which will be degraded into trehalose by the TreYZ pathway (Figure 6.36). This is also consistent with published data showing that TreZ expression is activated by a transcription factor associated with sporulation in *S. venezuelae* (Bush, et al., 2013). However, it is conceivable that on an alternative carbon source, such as one that did not lead to glycogen deposition in the pre-spores, that the OtsAB pathway may have a greater role in trehalose production. Indeed the *ΔotsA::apr* had reduced trehalose content in its spores compared to the complemented strain when the strains were provided with galactose as a carbon source. In this instance TreS could have been operating to convert α-maltose into trehalose within the pre-spores.

Interestingly, *ΔotsA::apr* has a cell density dependent developmental phenotype when grown on a galactose carbon source. This demonstrates that there is interplay between pathways involved in trehalose synthesis and galactose catabolism and that there are developmental consequences that arise if flux is limited at the point of OtsA. The underlying mechanism by which this leads to a developmental phenotype remains poorly understood. However, the phenotype was associated with alterations in phosphorus metabolism and an accumulation of GDP-glucose, which suggests it could be a result of perturbation of either the phosphate or nucleotide pools. However, some experiments suggested that cellophane was providing some form of protection against an inhibitor of development and so it could also be due to the release of a compound or acidification of the solid media as well. Further work is needed in order to understand the root cause of this phenotype and how cellophane ameliorates the developmental delay.

Biochemical characterisation of *S. venezuelae* OtsA showed that the GDP-glucose build-up was because it is the preferred substrate of OtsA. However, the source of GDP-glucose in *S. venezuelae* remains unknown. There are several putative nucleotide-glucose transporters annotated in the *S. venezuelae* genome. Further bioinformatic analysis twinned with biochemical characterisation of the top candidates should be able to identify the GDP-glucose source. Given that the Leloir pathway is highly conserved from bacteria through to

humans and plants, it seems unlikely that one of the enzymes of the Leloir pathway is synthesising GDP-glucose, but it nevertheless remains a possibility (Frey, 1996).

This study has shown that GalU is not the source of GDP-glucose in *S. venezuelae*. The function of GalU was hypothesised to be providing a substrate for OtsA. However, in light of this evidence, the role GalU plays in carbon metabolism in *S. venezuelae* is now unclear but it is likely to be involved in cell wall proteoglycan biosynthesis. A genetic disruption of *galU* would be useful to determine its potential role in metabolism. Initial characterisation suggested it was orders of magnitude slower than the same enzyme purified from *S. coelicolor* (Asencion Diez, et al., 2012). This may be due to the enzyme being assayed in sub-optimal conditions. Whilst structural studies were pursued, as the enzyme does not have altered substrate specificity, crystallisation of GalU is unlikely to increase scientific understanding of this enzyme as there is already a known structure that has the same substrate specificity (Kim, et al., 2010).

6.14 Summary

In this chapter, an *ΔotsA::apr* knockout was characterised and found to have a developmental phenotype when provided a galactose carbon source. The *S. venezuelae* OtsA was also expressed, purified, characterised and crystallised. It was revealed to have substrate specificity for GDP-glucose. Using crystallography, the key residues underlying this substrate specificity have been identified. This is the first known OtsA structure with a substrate preference for GDP-glucose. GalU was also expressed, purified and characterised and it was found that it does not exhibit substrate specificity like OtsA and it was specific for dTTP and UTP.

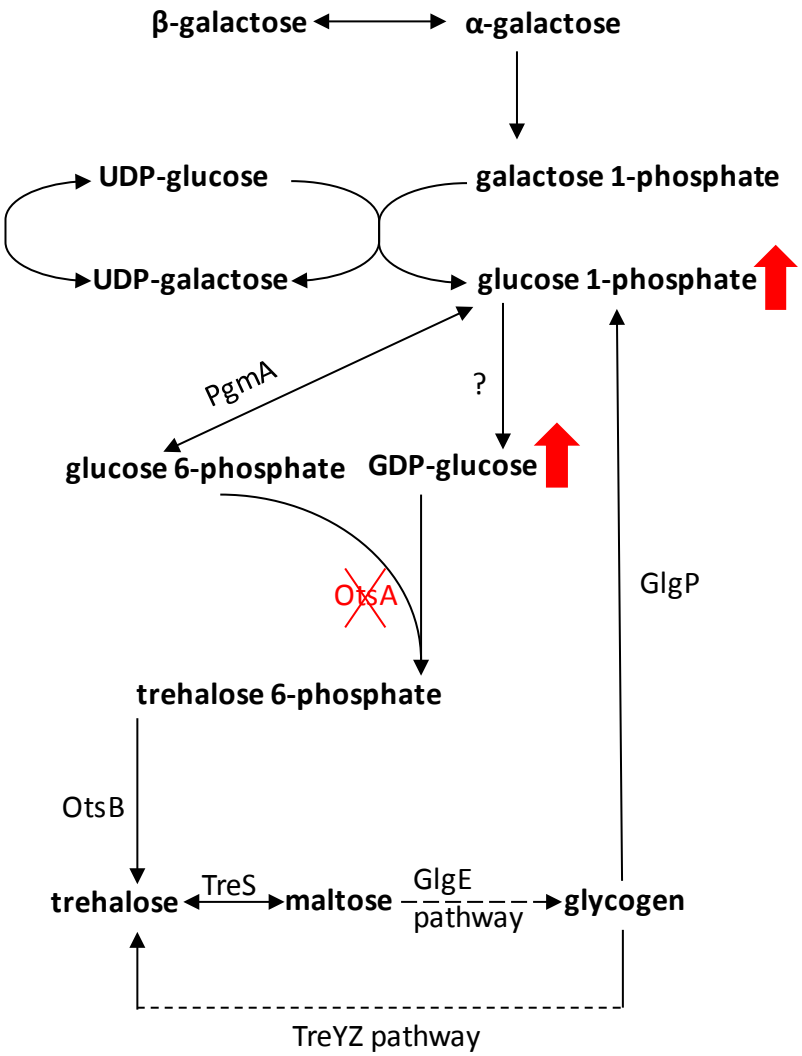

Figure 6.36: Summary of proposed galactose metabolism and glucan metabolism in *S. venezuelae*

Items in red emphasise the altered metabolism of *ΔotsA::apr*.

Chapter 7: Discussion and Future Work

The focus of this thesis was to characterise aspects of the GlgE pathway using enzymology and genetics. A diagrammatic summary of the mutants generated and the proteins characterised in this thesis are shown in figures 7.1 and 7.2 respectively.

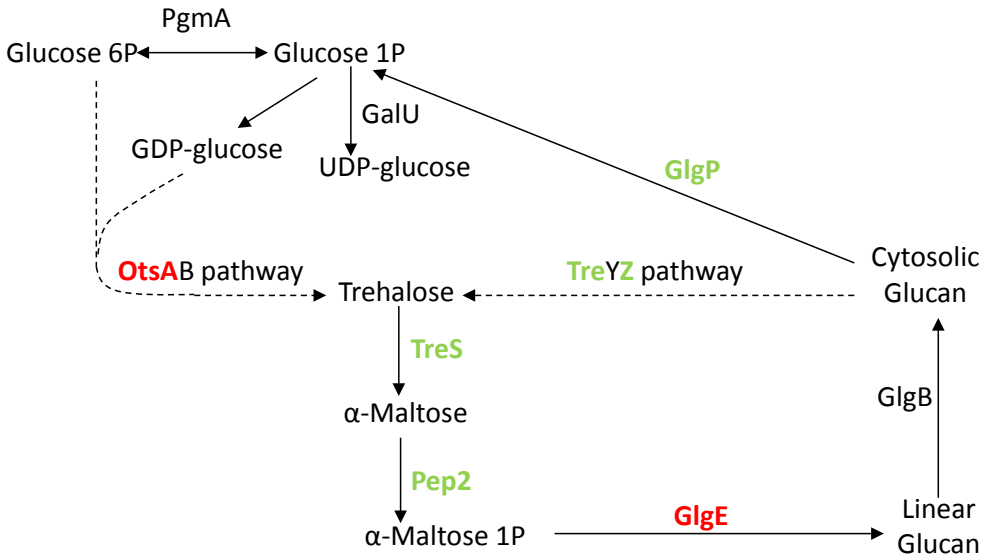

Figure 7.1: Overview of gene disruptions made in *Streptomyces venezuelae* Six gene disruption mutants were generated in this study. Genes encoding the coloured enzymes in the above diagram were disrupted to generate single gene disruptions. Disruptions of the enzymes coloured green had no developmental phenotype, when grown under normal laboratory conditions as well as on some alternative carbon sources. Disruptions of the genes encoding enzymes coloured in red displayed a distinct developmental phenotype.

S. venezuelae was identified as a potential model system to characterise the GlgE pathway because bioinformatics suggested that it contained only a single copy of the GlgE pathway encoding gene cluster and no other glucan synthesis pathways. Therefore, it suggested genetic studies in which single gene deletions could be made in order to ascribe a biological function to the pathway. Mutants generated and characterised in this thesis demonstrate for the first time that the GlgE pathway is solely responsible for glycogen production *in vivo*.

A *Δpep2::apr* strain was generated with a view to determining if glycogen was essential for normal growth and development in *S. venezuelae* and indeed to determine if the GlgE pathway was operating in a biological context. The strain has no developmental phenotype but is devoid of glycogen, there-by confirming that the GlgE pathway operates in a biological context and is solely responsible for glycogen production. The

fact that this strain was viable and has no developmental phenotype suggests that glycogen is non-essential in *S. venezuelae,* which is consistent with findings in *Escherichia coli* (Eydallin, et al., 2007). However, there was a metabolic phenotype in the absence of glycogen as the spores of *Δpep2::apr* had reduced trehalose content. This confirms the long held view that glycogen deposition in the pre-spore chains allows the organism to relocate its carbon reserves for trehalose production in spores (Rueda, et al., 2001). As trehalose has been implicated in conferring resistance to abiotic stresses (Rueda, et al., 2001) and is consumed during germination (McBride and Ensign, 1990), the results suggest that *S. venezuelae* deposits glycogen in the pre-spores to maximise the trehalose content of the spores, which in turn increases the likelihood of spore survival as well as increases the initial nutrient supply upon germination.

In the absence of glycogen synthesis, it was hypothesised that *Δpep2::apr* could channels its carbon into an alternate storage compound, such as lipid, as observed in other bacteria (Wang, et al., 2007). Preliminary results suggested that the *Δpep2::apr* strain accumulated 45% more fatty acid methyl esters (FAME) than WT when grown under the same conditions. This suggests that in the absence of glycogen, carbon flux is channelled into increased synthesis of other metabolites. Other metabolites synthesised by some strains of *S. venezuelae* are the antibiotics chloramphenicol and jadamycin (Yang, et al., 1995). Indeed, chloramphenicol is known to accumulate during the same stages of development as glycogen in *S. venezuelae*, which suggests that there may be competition between the two processes for the same carbon reserves (Ranade and Vining, 1993). Therefore, an avenue to explore in the future would be to determine the impact removal of glycogen synthesis has on antibiotic production in *S. venezuelae*. The type-strain of *S. venezuelae* used in this study produces virtually no antibiotic and therefore it was not feasible to determine if antibiotic production was elevated in the *Δpep2::apr* strain.

A *ΔglgE::apr* strain was generated with a view to understanding if *S. venezuelae* could accrue αM1P and, if so, what the developmental consequences were. The results show that the in the absence of glycogen production in the *ΔglgE::apr* strain, αM1P accumulated instead. This is a surprising finding as *Mycobacterium tuberculosis* is known to be acutely sensitive to αM1P stress (Kalscheuer, et al., 2010a), such that

secondary mutations that suppress αM1P accumulation frequently arise (R. Kalscheuer, unpublished data). In sharp contrast, the *ΔglgE::apr* strain of *S. venezuelae* could accumulate upto 17% of its dry cell weight as αM1P. Whilst αM1P accumulation in *S. venezuelae* causes a delay in development, the organism can relieve itself of the developmental inhibition by degradation of αM1P over the course of its life-cycle. Evidence suggests this occurs by de-phosphorylation of the αM1P into maltose, which happens to be the preferred carbon source of *S. venezuelae.* Whilst the trehalose content of *ΔglgE::apr* spores is not affected, there is a fitness consequence to re-cycling carbon in the form of αM1P instead of glycogen with the strain accumulating less mass, having a delayed development and, producing fewer viable and under-pigmented spores that were less resistant to various abiotic stresses. However, it also suggests that the carbon is being used for other purposes as well, such as growth and cell wall maturation and growth in general because the *ΔglgE::apr* spores were less resistant to lysozyme treatment, heat shock and sonication.

The mechanisms that lead to αM1P-induced toxicity or delayed development in *M. tuberculosis* and *S. venezuelae,* respectively, remain unclear and further work is needed to understand the precise connection. The effects of αM1P accumulation could be organism-specific, but there may also be some conserved pathways that are adversely affected by αM1P accumulation. Microarray studies in *M. tuberculosis* suggest no single mechanism, but rather a suite of pleiotropic affects that occur upon αM1P accumulation (Kalscheuer, et al., 2010a). The pleiotropic affects could be a consequence of accumulating such high amounts of a phosphorylated sugar, which is unlikely to be chemically and osmotically inert like glycogen. Microarray studies could also be employed to understand how αM1P delays development in *S. venezuelae*. These would necessitate characterisation of *ΔglgE::apr* grown in liquid media conditions yet to be studied. However, the metabolic phenotype should be comparable to the phenotype observed on solid media as the preferred carbon source in liquid media is also maltose, which would also lead to accumulation of αM1P. Given that a phosphatase is required to re-cycle αM1P, a hypothesis that seems most likely is that the organism becomes phosphate-limited due to the perturbation of cytosolic phosphate levels when αM1P accumulates. This in turn would lead to increased gene expression of genes associated with phosphate scavenging. One known response to phosphate limitation is to increase the gene expression of phosphatases (Allenby, et al.,

2012). Therefore, it could be that the activation of a phosphate starvation response is required to de-phosphorylate αM1P.

Other mutants outside of the GlgE pathway were also generated in this study. Whilst these genes were not encoding enzymes of the GlgE pathway, they were either hypothesised to be encoding enzymes that were feeding substrate into the pathway (OtsA) or instead were involved in recycling glycogen (TreZ and GlgP). Results from the *ΔotsA::apr* mutant suggest that OtsA is not required for trehalose deposition in spores when grown on a maltose carbon source, which is consistent with it functioning to convert glucose to trehalose to be fed into the GlgE pathway. This suggests that instead the TreYZ pathway is responsible for trehalose production, when grown on a maltose carbon source. This is consistent with abundant glycogen observed in the pre-spores, which could be degraded into trehalose by the TreYZ pathway. This is also consistent with published data showing that TreZ expression is activated by a transcription factor associated with sporulation in *S. venezuelae* (Bush, et al., 2013). Based on results from the characterisation of the *ΔotsA::apr* strain, it suggests that *ΔtreZ::apr* should be more impaired in glycogen re-cycling than the *ΔglgP::apr* strain because it seems that the TreYZ pathway is the major glycogen re-cycling pathway. However, it is conceivable that these genes can compensate for the absence of the other gene in the mutants and therefore it could be that neither are impaired in glycogen re-cycling and so a double knockout of both genes may be required. Biochemical characterisation of the *ΔtreZ::apr* and *ΔglgP::apr* mutants generated in this study would determine if either have a metabolic phenotype and to confirm the observed hierarchy in *S. venezuelae*.

All of the mutants of *S. venezuelae* were grown on different carbon sources with a view to determining if any phenotypes were dependent on the carbon source. Interestingly, *ΔotsA::apr* has a cell density-dependent developmental phenotype when grown on a galactose carbon source. This demonstrates that there is interplay between pathways involved in trehalose synthesis and galactose catabolism and that there are developmental consequences that arise if flux is limited at the point of OtsA. The underlying mechanism by which this leads to a developmental phenotype remains poorly understood. However, the phenotype is associated with alterations in phosphorus metabolism and there is also accumulation of guanosine diphosphate (GDP)-glucose, which suggests the phenotype could be a result of perturbation of

either the phosphate or nucleotide pools. Further work is needed to understand if the phenotype is caused by build-up of a specific metabolite as reported in other organisms (Zaffanello, et al., 2005). It is noteworthy that there is no evidence that the strain was accumulating any phosphorylated galactose compounds, which are frequently associated with disease in other organisms (Frey, 1996; Zaffanello, et al., 2005). It would be worthwhile to test if a WT phenotype could be restored with the additional exogenous phosphate in order to determine if the phenotype is due to phosphate limitation. Moreover, the pH of the surrounding media could also be tested to observe if the regions of developmental delay is due to acidification of the surrounding area.

Characterisation of the metabolic phenotypes of the mutants generated in this study was facilitated by using a new method to determine sugar content in *Streptomyces* cell extracts; namely proton nuclear magnetic resonance (^{1}H-NMR) spectroscopy. The trehalose content of WT *S. venezuelae* spores were comparable to those reported in previous studies (observed: 11%; published: 12%) (Ranade and Vining, 1993), which validated the technique. ^{1}H-NMR spectroscopy is preferable to previous methods because it can be used to determine multiple sugars in a single sample of cell extract that do not require purification and do not rely on downstream enzymic or chemical degradation.

^{1}H-NMR spectroscopy has also been routinely used in this study to characterise enzymes of the GlgE pathway as well as enzymes feeding into the pathway. An overview of the enzymes characterised in this study is given in Figure 7.2.

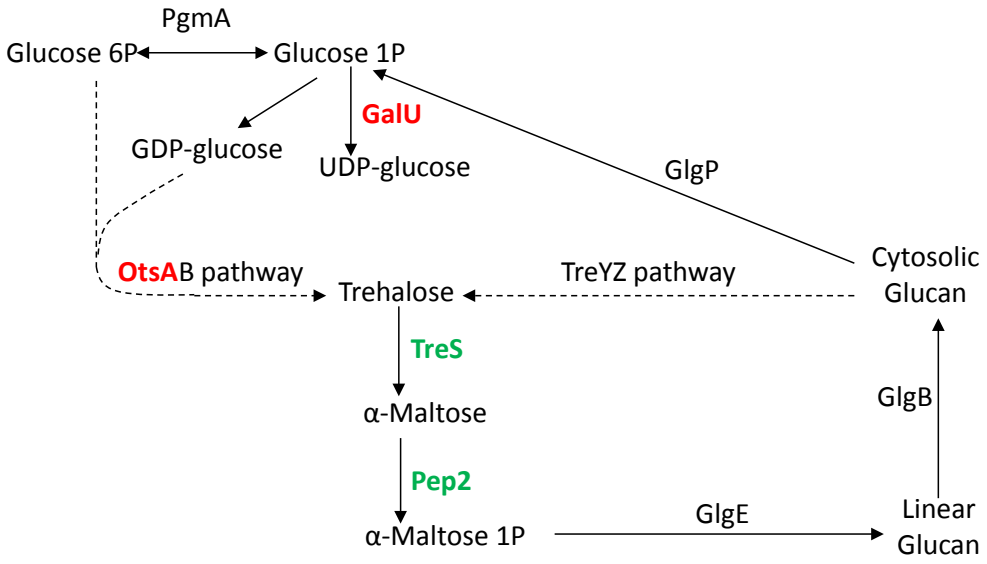

Figure 7.2: Overview of enzymes characterised in this study
Five enzymes originating from *S. venezuelae* (coloured red), *M. tuberculosis* (coloured green) and *Pseudomonas aeriginosa* (also coloured green) were characterised in this study.

The most notable finding relating to the enzymology component of this study is that the first enzyme of the GlgE pathway, TreS, is stereospecific, which confirms the α-retaining mechanistic prediction. TreS enzymology showed that TreS only uses and produces α-maltose, which is also the case with deoxyfluoro-maltose analogues. It is now possible to propose schemes defining the anomeric configurations and origins of all species associated with the TreS-catalysed reactions studied (Figure 3.1). This finding also had biological significance because TreS operates in the direction of α-maltose synthesis in *M. tuberculosis* and *M. smegmatis* (Miah, et al., 2013). As TreS produces the correct anomer for Pep2, the second enzyme of the GlgE pathway, flux through the pathway is not limited by the relatively slow chemical mutarotation of maltose, which would be the case if TreS produced an anomeric mixture of α and β-maltose or just β-maltose (Niehues, et al., 2003).

TreS is hypothesised to sterically capture the glucose molecule such that it liberates a glucose molecule but also transiently excludes access to the active site. Therefore, exogenously supplied glucose is not incorporated into the products of TreS (Koh, et al., 2003; Nishimoto, et al., 1996; Zhang, et al., 2011). Thus, TreS catalyses an isomerisation, whereby the non-covalently captured glucose molecule must rotate within an enclosed active site. This study has established that this glucose molecule

retains its α-configuration regardless of whether it goes on to produce normal disaccharide products or is instead released during the hydrolytic side reaction. Although two crystal structures of TreS from *Mycobacterium* are known, they do not have any relevant ligands bound at the active site (Caner, et al., 2013; Roy, et al., 2013). Further co-crystallisations of TreS may help identify the key residues involved in the proposed steric capture as well as rationalise the rotation of the free glucose whilst trapped within the active site. Furthermore, the structure could be used to design site-directed muteins with compromised steric capture capabilities that would instead lead to the release of the free glucose.

Collectively, these findings on the flux through TreS have implications for the design and efficacy of inhibitors as well as imaging agents that target either trehalose mycolate or α-glucan biosynthetic pathways (Backus, et al., 2011; Swarts, et al., 2012). It is now much clearer that the enzymes of the OtsAB and TreYZ pathways need to be targeted to affect trehalose mycolate production and that TreS should instead be targeted if α-glucan biosynthesis is the therapeutic target. Furthermore, substrate analogues can now be designed as pro-drugs for a given pathway that avoid de-toxification by competing pathways. For example, when targeting the synthesis of essential trehalose mycolates (Backus, et al., 2011; Swarts, et al., 2012), it would be beneficial if trehalose analogues were not turned-over and de-activated by TreS, which tolerates small modifications of its substrates. However, when targeting GlgE or GlgB (Kalscheuer and Jacobs, 2010), there is the challenge of a trehalose analog being tolerated by not only TreS but also the trehalose importer (Kalscheuer, et al., 2010b) and maltose kinase.

Labelling of the *M. smegmatis* capsule by using a 4-azido trehalose analogue was TreS-dependent (Swarts, et al., 2012). This observation implies that perhaps there is tolerance of this analogue in each step of the biosynthesis of capsular α-glucan rather than trehalose mycolates. Whilst unlikely, the labelling could also be a consequence of the weak hydrolytic activity of TreS rather than its isomerase activity and therefore 4-azido trehalose may not be tolerated by all the enzymes involved in capsular α-glucan synthesis. Further work should seek to explore this by feeding the 4-azido analogue, in the first instance, to TreS to determine if TreS isomerises or hydrolyses the compound. If TreS can isomerise the 4-azido trehalose, then the compound should subsequently be

fed collectively to all of the enzymes of the GlgE pathway *in vitro* to determine if a labelled α-glucan is synthesised. Furthermore, the azido-labelled product of *in vivo* feeding studies could be purified and characterised.

In the majority of cases the *pep2* and *treS* genes were often fused and expressed as a single gene product. However, there were no reports of whether these gene products were functional and if they were able to synthesise αM1P from trehalose. Therefore, *P. aeruginosa* TreS-Pep2 was partially characterised in this study. The fusion protein was initially difficult to over-produce in *E. coli*, in part due to its large (125 kDa) size and it frequently accumulated in insoluble fractions of the cell. However, using an *E. coli* SoluBL21 strain that was optimised for soluble protein expression, soluble TreS-Pep2 was produced. In solution it was a single oligomeric state that was a pentamer. Due to its large size, oligomeric state and tendency to aggregate, attempts were not made to crystallise this protein. Nevertheless, the protein is able to convert trehalose into αM1P and activity is retained after freeze-thaw cycles. This is the first demonstration that a TreS-Pep2 fusion protein can produce αM1P from trehalose. Whilst this enzyme may not be optimal for crystallography studies, it has potential to be used for αM1P synthesis. The enzyme could also be used for substrate-tolerance studies with trehalose substrate analogues.

Pep2 from *M. tuberculosis* was also partially characterised, with a view to determining an enzymic route to synthesise αM1P as the chemical synthesis route is non-trivial. As with TreS-Pep2, this protein was not very stable. A relatively low yield of soluble Pep2 was eventually obtained, it had limited stability in assays, and it would precipitate with prolonged incubation. Buffer conditions may not have been optimal as recent work has biophysically characterised Pep2 in complex with TreS from the same mycobacterial strain (Roy, et al., 2013). This suggests that it does behave sufficiently well under certain conditions. The stability of the protein is enhanced when it is combined with TreS. Therefore, co-expression with TreS could be attempted to stabilise Pep2 such that it could be further characterised.

The final enzymes characterised in this study were enzymes that were thought to feed into the GlgE pathway in *S. venezuelae.* By characterising the metabolism of *ΔotsA::apr,* it is known that GDP-glucose accumulates in this strain when grown on a galactose

carbon source. This therefore suggested that perhaps the major substrate for OtsA was GDP-glucose. In order to establish if this was the case, this study determined the *in vitro* substrate specificity of this OtsA, which demonstrates that its preferred substrate was indeed GDP-glucose. However, OtsA was also able to use ADP-glucose as a substrate and, to a lesser extent, UDP-glucose. Whilst the *E. coli* OtsA had substrate specificity for only UDP-glucose another OtsA from *M. tuberculosis* is known to accept all NDP-glucoses, with a substrate preference for UDP-glucose, ADP-glucose and GDP-glucose (Pan, et al., 2002). The K_m of each NDP-glucose varied considerably depending on additives present in the conditions and therefore it is not clear from this study which substrate might be the preferred under physiological conditions (Pan, et al., 2002). Other OtsAs from *Rubrobacter xylanophilus* and *Streptomyces hygroscopicus* have been reported to have a substrate preference for GDP-glucose (Elbein, 1968; Nobre, et al., 2008). Therefore, it suggests that GDP-glucose could be the preferred substrates in the majority of actinobacterial OtsAs. Further enzymology on the *S. venezuelae* OtsA should be carried out to estimate the k_{cat} and K_m so that relative catalytic efficiency can be determined.

S. venezuelae OtsA has also been successfully crystallised in this study, this is first known structure of an OtsA that has a substrate preference for GDP-glucose and only the second known structure of OtsA. By comparing the structure to solved *E. coli* OtsA structure, it is apparent that there are different residues involved in binding the different nucleotide moieties of NDP-glucose and that the two OtsA active sites are configured differently to accommodate the different substrates (Gibson, et al., 2004). There is scope to carry out site-directed mutagenesis of the key residues (Ser^{345}, Phe^{342}, Glu^{341} and Asp^{340}) involved in guanosine binding to test if the substrate specificity can be altered to UDP-glucose.

The final enzyme investigated in this study was GalU because it was hypothesised it might have altered substrate specificity such that it was able to produce GDP-glucose. However, it was not able to use GTP to synthesise GDP-glucose and therefore the source of GDP-glucose in *S. venezuelae* remains unknown. Moreover, the role of GalU in central carbon metabolism of *S. venezuelae* is unclear because its major role was assumed to be feeding substrate to OtsA, which is no longer the case in light of evidence presented in this thesis.

Future work could include exogenously supplying cell extracts of the *ΔotsA::apr* with glucose 1-phosphate and GTP to determine if the enzyme responsible for GDP-glucose production catalyses a similar reaction to that of GalU. If so, bioinformatics analysis could then be conducted to identify candidate genes that encode proteins that are similar to GalU in the *S. venezuelae* genome. Biochemical characterisation of the top candidates should then be able to identify the protein responsible for GDP-glucose production in *S. venezuelae*. A genetic disruption of *galU* would also be valuable in order to understand its role in carbon metabolism. Whilst attempts were made to crystallise GalU, given that its substrate preference is the same as observed for other GalU enzymes and there are numerous structures deposited in the protein data bank (Berman, et al., 2000), it is not an avenue worth pursuing.

In summary, this work has developed *S. venezuelae* as a model organism to understand the biochemistry of the GlgE pathway and determined that this pathway operates *in vivo* to produce α-glucan. It has also determined a novel carbon source dependent phenotype in a *ΔotsA* strain that was associated with the build-up of GDP-glucose and rationalised the substrate preference of the OtsA enzyme from *S. venezuelae.* Finally, the study has determined the stereospecificity of TreS.

By validating *S. venezuelae* as a model organism for the GlgE pathway it has allowed the structure of the glucan polymer produced in *S. venezuelae* to be isolated and characterised (A. Rashid, unpublished data). This has also led to the discovery that the glucan polysaccharide produced has a laminate structure, rather than an arboreal structure, which overturns a widely held notion in glycobiology (A. Rashid, unpublished data).

References

Abad, M.C., Binderup, K., Rios-Steiner, J., Arni, R.K., Preiss, J., and Geiger, J.H. (2002). The X-ray crystallographic structure of *Escherichia coli* branching enzyme. J. Biol. Chem. 277, 42164-42170.

Allenby, N.E., Laing, E., Bucca, G., Kierzek, A.M., and Smith, C.P. (2012). Diverse control of metabolism and other cellular processes in *Streptomyces coelicolor* by the PhoP transcription factor: genome-wide identification of *in vivo* targets. Nucleic Acids Res. 40, 9543-9556.

Arguelles, J.C. (2000). Physiological roles of trehalose in bacteria and yeasts: a comparative analysis. Arch. Microbiol. 174, 217-224.

Asencion Diez, M.D., Peiru, S., Demonte, A.M., Gramajo, H., and Iglesias, A.A. (2012). Characterization of recombinant UDP- and ADP-glucose pyrophosphorylases and glycogen synthase to elucidate glucose-1-phosphate partitioning into oligo- and polysaccharides in *Streptomyces coelicolor*. J. Bacteriol. 194, 1485-1493.

Baba, O. (1993). Production of monoclonal antibody that recognizes glycogen and its application for immunohistochemistry. Kokubyo Gakkai Zasshi, 60, 264-287.

Backus, K.M., Boshoff, H.I., Barry, C.S., Boutureira, O., Patel, M.K., D'Hooge, F., Lee, S.S., Via, L.E., Tahlan, K., Barry, C.E., 3rd, et al. (2011). Uptake of unnatural trehalose analogs as a reporter for *Mycobacterium tuberculosis*. Nat. Chem. Biol. 7, 228-235.

Bailey, J.M., Fishman, P.H., and Pentchev, P.G. (1967). Studies on mutarotases .i. purification and properties of a mutarotase from higher plants. J. Biol. Chem. 242, 4263-4269.

Belanger, A.E., and Hatfull, G.F. (1999). Exponential-phase glycogen recycling is essential for growth of *Mycobacterium smegmatis*. J. Bacteriol. 181, 6670-6678.

Bell, D.J., and Young, F.G. (1934). Observations on the chemistry of liver glycogen. J. Biol. Chem. 28, 882-889.

Beringer, J.E., Johnston, A.W.B., and Wells, B. (1977). The isolation of conditional ineffective mutants of *Rhizobium leguminosarum*. J. Gen. Microbiol. 98, 339-343.

Berman, H.M., Westbrook, J., Feng, Z., Gilliland, G., Bhat, T.N., Weissig, H., Shindyalov, I.N., and Bourne, P.E. (2000). The Protein Data Bank. Nucleic Acids Res. 28, 235-242.

Braña, A.F., Manzanal, M.B., and Hardisson, C. (1980). Occurrence of polysaccharide granules in sporulating hyphae of *Streptomyces viridochromogenes*. J. Bacteriol. 144, 1139-1142.

Braña, A.F., Manzanal, M.B., and Hardisson, C. (1982). Characterization of intracellular polysaccharides of *Streptomyces*. Can. J. Microbiol. 28, 1320-1323.

Braña, A.F., Mendez, C., Diaz, L.A., Manzanal, M.B., and Hardisson, C. (1986). Glycogen and trehalose accumulation during colony development in *Streptomyces antibioticus*. J. Gen. Microbiol. 132, 1319-1326.

Breton, C., Šnajdrová, L., Jeanneau, C., Koča, J., and Imberty, A. (2006). Structures and mechanisms of glycosyltransferases. Glycobiology 16, 29R-37R.

Bruton, C.J., Plaskitt, K.A., and Chater, K.F. (1995). Tissue-specific glycogen branching isoenzymes in a multicellular prokaryote, *Streptomyces coelicolor* A3(2). Mol. Microbiol. 18, 89-99.

Bush, M.J., Bibb, M.J., Chandra, G., Findlay, K.C., and Buttner, M.J. (2013). Genes required for aerial growth, cell division, and chromosome segregation are targets of WhiA before sporulation in *Streptomyces venezuelae*. mBio. 4.

Cabib, E., and Leloir, L.F. (1958). The biosynthesis of trehalose phosphate. J. Biol. Chem. 231, 259-275.

Caner, S., Nguyen, N., Aguda, A., Zhang, R., Pan, Y.T., Withers, S.G., and Brayer, G.D. (2013). The structure of the *Mycobacterium smegmatis* trehalose synthase reveals an unusual active site configuration and acarbose-binding mode. Glycobiology 23, 1075-1083.

Cantarel, B.L., Coutinho, P.M., Rancurel, C., Bernard, T., Lombard, V., and Henrissat, B. (2009). The Carbohydrate-Active EnZymes database (CAZy): an expert resource for glycogenomics. Nucleic Acids Res. 37, D233-D238.

Cavalier, M.C., Yim, Y.-S., Asamizu, S., Neau, D., Almabruk, K.H., Mahmud, T., and Lee, Y.-H. (2012). Mechanistic insights into validoxylamine A 7'-phosphate synthesis by VldE using the structure of the entire product complex. PLoS One 7(9), e44934.

Chandra, G., Chater, K.F., and Bornemann, S. (2011). Unexpected and widespread connections between bacterial glycogen and trehalose metabolism. Microbiol. UK. 157, 1565-1572.

Chen, V.B., Arendall, W.B., III, Headd, J.J., Keedy, D.A., Immormino, R.M., Kapral, G.J., Murray, L.W., Richardson, J.S., and Richardson, D.C. (2010). MolProbity: all-atom structure validation for macromolecular crystallography. Acta Crystallogr. D, 66, 12-21.

Choi, K.J., Grass, S., Paek, S., St. Geme, J.W., III, and Yeo, H.-J. (2010). The *Actinobacillus pleuropneumoniae* HMW1C-like glycosyltransferase mediates N-linked glycosylation of the *Haemophilus influenzae* HMW1 adhesin. PLoS One 5, e15888.

Cowtan, K. (2006). The Buccaneer software for automated model building. 1. Tracing protein chains. Acta Crystallogr. D, 62, 1002-1011.

Cowtan, K. (2010). Recent developments in classical density modification. Acta Crystallogr. D, 66, 470-478.

Datsenko, K.A., and Wanner, B.L. (2000). One-step inactivation of chromosomal genes in *Escherichia coli* K-12 using PCR products. Proc. Natl. Acad. Sci. USA. 97, 6640-6645.

De Smet, K.A.L., Weston, A., Brown, I.N., Young, D.B., and Robertson, B.D. (2000). Three pathways for trehalose biosynthesis in mycobacteria. Microbiol. UK. 146, 199-208.

Dinadayala, P., Sambou, T., Daffe, M., and Lemassu, A. (2008). Comparative structural analyses of the alpha-glucan and glycogen from *Mycobacterium bovis*. Glycobiology 18, 502-508.

Dintzis, F.R., and Tobin, R. (1969). Optical rotation of some alpha-1,4-linked glucopyranosides in system H_2O-DMSO and solution conformation of amylose. Biopolymers 7, 581-593.

Drepper, A., Peitzmann, R., and Pape, H. (1996). Maltokinase (ATP:maltose 1-phosphotransferase) from *Actinoplanes* sp: Demonstration of enzyme activity and characterization of the reaction product. FEBS Lett. 388, 177-179.

Dye, C. (2006). Global epidemiology of tuberculosis. Lancet 367, 938-940.

Elbein, A.D. (1968). Trehalose phosphate synthesis in *Streptomyces hygroscopicus*: Purification of guanosine diphosphate D-glucose: D-glucose-6-phosphate 1-glucosyl-transferase. J. Bacteriol. 96, 1623-1631.

Elbein, A.D., Pan, Y.T., Pastuszak, I., and Carroll, D. (2003). New insights on trehalose: a multifunctional molecule. Glycobiology 13, 17R-27R.

Elbein, A.D., Pastuszak, I., Tackett, A.J., Wilson, T., and Pan, Y.T. (2010). Last step in the conversion of trehalose to glycogen: A mycobacterial enzyme that transfers maltose from maltose 1-phosphate to glycogen. J. Biol. Chem. 285, 9803-9812.

Emsley, P., and Cowtan, K. (2004). Coot: model-building tools for molecular graphics. Acta Crystallogr. D, 60, 2126-2132.

England, P., Wehenkel, A., Martins, S., Hoos, S., Andre-Leroux, G., Villarino, A., and Alzari, P.M. (2009). The FHA-containing protein GarA acts as a phosphorylation-dependent molecular switch in mycobacterial signalling. FEBS Lett. 583, 301-307.

Errey, J.C., Lee, S.S., Gibson, R.P., Martinez Fleites, C., Barry, C.S., Jung, P.M., O'Sullivan, A.C., Davis, B.G., and Davies, G.J. (2010). Mechanistic insight into enzymatic glycosyl transfer with retention of configuration through analysis of glycomimetic inhibitors. Angewandte Chem. Int. Edit. 49, 1234-1237.

Evans, P. (2006). Scaling and assessment of data quality. Acta Crystallogr. D, 62, 72-82.

Eydallin, G., Viale, A.M., Morán-Zorzano, M.T., Muñoz, F.J., Montero, M., Baroja-Fernández, E., and Pozueta-Romero, J. (2007). Genome-wide screening of genes affecting glycogen metabolism in *Escherichia coli* K-12. FEBS Lett. 581, 2947-2953.

Flardh, K., and Buttner, M.J. (2009). Streptomyces morphogenetics: dissecting differentiation in a filamentous bacterium. Nature Rev. Microbiol. 7, 36-49.

Freeman, B.C., Chen, C.L., and Beattie, G.A. (2010). Identification of the trehalose biosynthetic loci of *Pseudomonas syringae* and their contribution to fitness in the phyllosphere. Environ. Microbiol. 12, 1486-1497.

Frey, P.A. (1996). The Leloir pathway: a mechanistic imperative for three enzymes to change the stereochemical configuration of a single carbon in galactose. FASEB J. 10, 461-470.

Gagliardi, M.C., Lemassu, A., Teloni, R., Mariotti, S., Sargentini, V., Pardini, M., Daffe, M., and Nisini, R. (2007). Cell wall-associated alpha-glucan is instrumental for *Mycobacterium tuberculosis* to block CD1 molecule expression and disable the function of dendritic cell derived from infected monocyte. Cell Microbiol. 9, 2081-2092.

Geurtsen, J., Chedammi, S., Mesters, J., Cot, M., Driessen, N.N., Sambou, T., Kakutani, R., Ummels, R., Maaskant, J., Takata, H., et al. (2009). Identification of mycobacterial alpha-glucan as a novel ligand for DC-SIGN: involvement of mycobacterial capsular polysaccharides in host immune modulation. J. Immunol. 183, 5221-5231.

Gibson, R.P., Lloyd, R.M., Charnock, S.J., and Davies, G.J. (2002). Characterization of Escherichia coli OtsA, a trehalose-6-phosphate synthase from glycosyltransferase family 20. Acta crystallogr. D, 58, 349-351.

Gibson, R.P., Tarling, C.A., Roberts, S., Withers, S.G., and Davies, G.J. (2004). The donor subsite of trehalose-6-phosphate synthase: binary complexes with UDP-glucose and UDP-2-deoxy-2-fluoro-glucose at 2 Å resolution. J. Biol. Chem. 279, 1950-1955.

Gibson, R.P., Turkenburg, J.P., Charnock, S.J., Lloyd, R., and Davies, G.J. (2002). Insights into trehalose synthesis provided by the structure of the retaining glucosyltransferase OtsA. Chem. Biol. 9, 1337-1346.

Gordon, G.B., Miller, L.R., and Bensch, K.G. (1963). Fixation of tissue culture cells for ultrastructural cytochemistry. Exp. Cell Res. 31, 440-443.

Gouet, P., Robert, X., and Courcelle, E. (2003). ESPript/ENDscript: extracting and rendering sequence and 3D information from atomic structures of proteins. Nucleic Acids Res. 31, 3320-3323.

Gregory, M.A., Till, R., and Smith, M.C.M. (2003). Integration site for *Streptomyces* phage phi BT1 and development of site-specific integrating vectors. J. Bacteriol. 185, 5320-5323.

Guex, N., and Peitsch, M.C. (1997). SWISS-MODEL and the Swiss-PdbViewer: an environment for comparative protein modeling. Electrophoresis 18, 2714-2723.

Gust, B., Challis, G.L., Fowler, K., Kieser, T., and Chater, K.F. (2003). PCR-targeted *Streptomyces* gene replacement identifies a protein domain needed for biosynthesis of the sesquiterpene soil odor geosmin. Proc. Natl. Acad. Sci. USA. 100, 1541-1546.

Hancock, S.M., Vaughan, M.D., and Withers, S.G. (2006). Engineering of glycosidases and glycosyltransferases. Curr Opin Chem Biol 10, 509-519.

Haworth, W.N., Peat, S., and Sagrott, P.E. (1946). A new method for the separation of the amylose and amylopectin components of starch. Nature 157, 19-19.

Holden, H.M., Rayment, I., and Thoden, J.B. (2003). Structure and function of enzymes of the Leloir pathway for galactose metabolism. J. Biol. Chem. 278, 43885-43888.

Holm, L., and Rosenström, P. (2010). Dali server: conservation mapping in 3D. Nucleic Acids Res. 38, W545-W549.

Homerova, D., Benada, O., Kofronova, O., Rezuchova, B., and Kormanec, J. (1996). Disruption of a glycogen-branching enzyme gene, glgB, specifically affects the sporulation-associated phase of glycogen accumulation in *Streptomyces aureofaciens*. Microbiol. UK. 142, 1201-1208.

Iturriaga, G., Suarez, R., and Nova-Franco, B. (2009). Trehalose metabolism: from osmoprotection to signaling. Int. J. Mol. Sci.10, 3793-3810.

Jackson, M., and Brennan, P.J. (2009). Polymethylated polysaccharides from mycobacterium species revisited. J. Biol. Chem. 284, 1949-1953.

Jackson, M., Stadthagen, G., and Gicquel, B. (2007). Long-chain multiple methyl-branched fatty acid-containing lipids of *Mycobacterium tuberculosis*: Biosynthesis, transport, regulation and biological activities. Tuberculosis (Edinb). 87, 78-86.

Jarling, M., Cauvet, T., Grundmeier, M., Kuhnert, K., and Pape, H. (2004). Isolation of *mak1* from *Actinoplanes missouriensis* and evidence that Pep2 from *Streptomyces coelicolor* is a maltokinase. J. Basic Microbiol. 44, 360-373.

Kalscheuer, R., and Jacobs, W.R., Jr. (2010). The significance of GlgE as a new target for tuberculosis. Drug News Perspect. 23, 619-624.

Kalscheuer, R., Syson, K., Veeraraghavan, U., Weinrick, B., Biermann, K.E., Liu, Z., Sacchettini, J.C., Besra, G., Bornemann, S., and Jacobs, W.R. (2010a). Self-poisoning of *Mycobacterium tuberculosis* by targeting GlgE in an alpha-glucan pathway. Nat. Chem. Biol. 6, 376-384.

Kalscheuer, R., Weinrick, B., Veeraraghavan, U., Besra, G.S., and Jacobs, W.R., Jr. (2010b). Trehalose-recycling ABC transporter LpqY-SugA-SugB-SugC is essential for virulence of *Mycobacterium tuberculosis*. Proc. Natl. Acad. Sci. USA. 107, 21761-21766.

Kantardjieff, K.A., and Rupp, B. (2003). Matthews coefficient probabilities: Improved estimates for unit cell contents of proteins, DNA, and protein–nucleic acid complex crystals. Protein Sci. 12, 1865-1871.

Kaur, D., Pham, H., Larrouy-Maumus, G., Rivière, M., Vissa, V., Guerin, M.E., Puzo, G., Brennan, P.J., and Jackson, M. (2009). Initiation of methylglucose lipopolysaccharide biosynthesis in mycobacteria. PLoS One 4, e5447.

Kieser, T., Bibb, M., Buttner, M., Chater, K., and Hopwood, D. (2000). Practical Streptomyces Genetics, John Innes Foundation.

Kim, H., Choi, J., Kim, T., Lokanath, N.K., Ha, S.C., Suh, S.W., Hwang, H.Y., and Kim, K.K. (2010). Structural basis for the reaction mechanism of UDP-glucose pyrophosphorylase. Mol. Cells 29, 397-405.

Kim, Y.H., Kwon, T.K., Park, S., Seo, H.S., Cheong, J.J., Kim, C.H., Kim, J.K., Lee, J.S., and Choi, Y.D. (2000). Trehalose synthesis by sequential reactions of recombinant maltooligosyltrehalose synthase and maltooligosyltrehalose trehalohydrolase from *Brevibacterium helvolum*. Appl. Environ. Microbiol. 66, 4620-4624.

Kleywegt, G.J., and Brunger, A.T. (1996). Checking your imagination: Applications of the free R value. Structure 4, 897-904.

Kobayashi, M., Kubota, M., and Matsuura, Y. (2003). Refined structure and functional implications of trehalose synthase from *Sulfolobus acidocaldarius*. J. Appl. Glycosci. 50, 1-8.

Koh, S., Kim, J., Shin, H.J., Lee, D., Bae, J., Kim, D., and Lee, D.S. (2003). Mechanistic study of the intramolecular conversion of maltose to trehalose by *Thermus caldophilus* GK24 trehalose synthase. Carbohydr. Res. 338, 1339-1343.

Krissinel, E. (2011). Macromolecular complexes in crystals and solutions. Acta Crystallogr. D, 67, 376-385.

Lai, K., Elsas, L.J., and Wierenga, K.J. (2009). Galactose toxicity in animals. IUBMB Life 61, 1063-1074.

Lares, C., Frixon, C., and Creuzets.N. (1974). Characterization and ultrastructure of mutants of *Escherichia coli* deficient in alpha-1,4-glucan-alpha-1,4-glucan 6- glycosyl transferase (branching enzyme). J. Gen. Microbiol. 82, 279-293.

Larner, J. (1953). The action of branching enzymes on outer chains of glycogen. J. Biol. Chem. 202, 491-503.

Lee, S.S., Hong, S.Y., Errey, J.C., Izumi, A., Davies, G.J., and Davis, B.G. (2011). Mechanistic evidence for a front-side, S_Ni-type reaction in a retaining glycosyltransferase. Nat. Chem. Biol. 7, 631-638.

Leiba, J., Syson, K., Baronian, G., Zanella-Cleon, I., Kalscheuer, R., Kremer, L., Bornemann, S., and Molle, V. (2013). *Mycobacterium tuberculosis* maltosyltransferase GlgE, a genetically validated antituberculosis target, is negatively regulated by Ser/Thr phosphorylation. J. Biol. Chem. 288, 16546-16556.

Leloir, L.F., and Goldemberg, S.H. (1962). Glycogen synthase from rat liver. Method. Enzymol. 5, 145-147.

Lemassu, A., and Daffe, M. (1994). Structural features of the exocellular polysaccharides of *Mycobacterium tuberculosis*. Biochem. J. 297, 351-357.

Lemassu, A., OrtaloMagne, A., Bardou, F., Silve, G., Laneelle, M.A., and Daffe, M. (1996). Extracellular and surface-exposed polysaccharides of non-tuberculous mycobacteria. Microbiol. UK. 142, 1513-1520.

Levine, S., Stevenson, H.J.R., Tabor, E.C., Bordner, R.H., and Chambers, L.A. (1953). Glycogen of enteric bacteria J. Bacteriol. 66, 664-670.

Lovering, A.L., de Castro, L.H., Lim, D., and Strynadka, N.C. (2007). Structural insight into the transglycosylation step of bacterial cell-wall biosynthesis. Science 315, 1402-1405.

Macneil, D.J., Gewain, K.M., Ruby, C.L., Dezeny, G., Gibbons, P.H., and Macneil, T. (1992). Analysis of *Streptomyces avermitilis* genes required for avermectin biosynthesis utilizing a novel integration vector. Gene 111, 61-68.

Marrinan, H.J., and Mann, J. (1954). A study by infra-red spectroscopy of hydrogen bonding in cellulose. J. Appl. Chem. 4, 204-211.

Martin, M.C., Schneider, D., Bruton, C.J., Chater, K.F., and Hardisson, C. (1997). A glgC gene essential only for the first of two spatially distinct phases of glycogen synthesis in *Streptomyces coelicolor* A3(2). J. Bacteriol. 179, 7784-7789.

Maruta, K., Hattori, K., Nakada, T., Kubota, M., Sugimoto, T., and Kurimoto, M. (1996). Cloning and sequencing of trehalose biosynthesis genes from *Arthrobacter* sp. Q36. Biochim. Biophys. Acta 1289, 10-13.

Maruta, K., Mitsuzumi, H., Nakada, T., Kubota, M., Chaen, H., Fukuda, S., Sugimoto, T., and Kurimoto, M. (1996). Cloning and sequencing of a cluster of genes encoding novel enzymes of trehalose biosynthesis from thermophilic archaebacterium *Sulfolobus acidocaldarius*. Biochim. Biophys. Acta 1291, 177-181.

Matthews, B.W. (1968). Solvent content of protein crystals. J. Mol. Biol. 33, 491-497.

Matula, M., Mitchell, M., and Elbein, A.D. (1971). Partial purification and properties of a highly specific trehalose phosphate phosphatase from *Mycobacterium smegmatis*. J. Bacteriol. 107, 217-222.

McBride, M.J., and Ensign, J.C. (1987). Metabolism of endogenous trehalose by *Streptomyces griseus* spores and by spores or cells of other actinomycetes. J. Bacteriol. 169, 5002-5007.

McBride, M.J., and Ensign, J.C. (1990). Regulation of trehalose metabolism by *Streptomyces griseus* spores. J. Bacteriol. 172, 3637-3643.

McCoy, A.J., Grosse-Kunstleve, R.W., Adams, P.D., Winn, M.D., Storoni, L.C., and Read, R.J. (2007). Phaser crystallographic software. J. Appl. Cryst. 40, 658-674.

McNicholas, S., Potterton, E., Wilson, K.S., and Noble, M.E.M. (2011). Presenting your structures: the CCP4mg molecular-graphics software. Acta Crystallogr. D, 67, 386-394.

Mendes, V., Maranha, A., Lamosa, P., da Costa, M.S., and Empadinhas, N. (2010). Biochemical characterization of the maltokinase from *Mycobacterium bovis* BCG. BMC Biochem. 11.

Miah, F., Koliwer-Brandl, H., Rejzek, M., Field, R.A., Kalscheuer, R., and Bornemann, S. (2013). Flux through trehalose synthase flows from trehalose to the alpha anomer of maltose in mycobacteria. Chem. Biol. 20, 487-493.

Montero, M., Eydallin, G., Viale, A.M., Almagro, G., Muñoz, F.J., Rahimpour, M., Sesma, M.T., Baroja‐Fernández, E., and Pozueta‐Romero, J. (2009). *Escherichia coli* glycogen metabolism is controlled by the PhoP-PhoQ regulatory system at sub-millimolar environmental Mg^{2+} concentrations, and is highly interconnected with a wide variety of cellular processes. Biochem. J. 424, 129-141.

Morris, D.L. (1946). Colorimetric determination of glycogen: Disadvantages of the Iodine method. J. Biol. Chem. 166,199-203.

Murphy, H.N., Stewart, G.R., Mischenko, V.V., Apt, A.S., Harris, R., McAlister, M.S.B., Driscoll, P.C., Young, D.B., and Robertson, B.D. (2005). The OtsAB pathway is essential for trehalose biosynthesis in *Mycobacterium tuberculosis*. J. Biol. Chem. 280, 14524-14529.

Murshudov, G.N., Vagin, A.A., and Dodson, E.J. (1997). Refinement of macromolecular structures by the maximum-likelihood method. Acta Crystallogr. D, 53, 240-255.

Nakayama, A., Yamamoto, K., and Tabata, S. (2001). Identification of the catalytic residues of bifunctional glycogen debranching enzyme. J. Biol. Chem. 276, 28824-28828.

Niehues, B., Jossek, R., Kramer, U., Koch, A., Jarling, M., Schroder, W., and Pape, H. (2003). Isolation and characterization of maltokinase (ATP : maltose 1-phosphotransferase) from *Actinoplanes missouriensis*. Arch. Microbiol. 180, 233-239.

Nishimoto, T., Nakano, M., Ikegami, S., Chaen, H., Fukuda, S., Sugimoto, T., Kurimoto, M., and Tsujisaka, Y. (1995). Existence of a novel enzyme converting maltose into trehalose. Biosci. Biotechnol. Biochem. 59, 2189-2190.

Nishimoto, T., Nakano, M., Nakada, T., Chaen, H., Fukuda, S., Sugimoto, T., Kurimoto, M., and Tsujisaka, Y. (1996). Purification and properties of a novel enzyme, trehalose synthase, from *Pimelobacter* sp R48. Biosci. Biotechnol. Biochem. 60, 640-644.

Nobre, A., Alarico, S., Fernandes, C., Empadinhas, N., and da Costa, M.S. (2008). A unique combination of genetic systems for the synthesis of trehalose in *Rubrobacter xylanophilus*: properties of a rare actinobacterial TreT. J Bacteriol. 190, 7939-7946.

Northcote, D.H. (1953). The molecular structure and shape of yeast glycogen. Biochem. J. 53, 348-352.

Ortalomagne, A., Dupont, M.A., Lemassu, A., Andersen, A.B., Gounon, P., and Daffe, M. (1995). Molecular composition of the outermost capsular material of the tubercle bacillus. Microbiol. UK. 141, 1609-1620.

Paget, M.S.B., Chamberlin, L., Atrih, A., Foster, S.J., and Buttner, M.J. (1999). Evidence that the extracytoplasmic function sigma factor sigma(E) is required for normal cell wall structure in *Streptomyces coelicolor* A3(2). J. Bacteriol. 181, 204-211.

Pal, K., Kumar, S., Sharma, S., Garg, S.K., Alam, M.S., Xu, H.E., Agrawal, P., and Swaminathan, K. (2010). Crystal structure of full-length *Mycobacterium tuberculosis* H37Rv glycogen branching enzyme insights of N-terminal beta-sandwich in substrate specificity and enzymatic activity. J. Biol. Chem. 285, 20897-20903.

Pan, Y.T., Carroll, J.D., and Elbein, A.D. (2002). Trehalose-phosphate synthase of *Mycobacterium tuberculosis*. Cloning, expression and properties of the recombinant enzyme. Eur. J. Biochem. 269, 6091-6100.

Pan, Y.T., Carroll, J.D., Asano, N., Pastuszak, I., Edavana, V.K., and Elbein, A.D. (2008). Trehalose synthase converts glycogen to trehalose. FEBS J. 275, 3408-3420.

Pan, Y.T., Drake, R.R., and Elbein, A.D. (1996). Trehalose-P synthase of mycobacteria: its substrate specificity is affected by polyanions. Glycobiology 6, 453-461.

Pan, Y.T., Edavana, V.K., Jourdian, W.J., Edmondson, R., Carroll, J.D., Pastuszak, I., and Elbein, A.D. (2004). Trehalose synthase of *Mycobacterium smegmatis* - Purification, cloning, expression, and properties of the enzyme. Eur. J. Biochem. 271, 4259-4269.

Pan, Y.T., Mitchell, M., and Elbein, A.D. (1978). Studies on the trehalose-phosphate synthase of Mycobacterium smegmatis: binding of heparin to the enzyme. Arch. Biochem. Biophys. 186, 392-400.

Plaskitt, K.A., and Chater, K.F. (1995). Influences of developmental genes on localized glycogen deposition in colonies of a mycelial prokaryote, *Streptomyces coelicolor* A3(2) - A possible interface between metabolism and morphogenesis. Phil. Trans. R. Soc. B 347, 105-121.

Prados-Rosales, R., Baena, A., Martinez, L.R., Luque-Garcia, J., Kalscheuer, R., Veeraraghavan, U., Camara, C., Nosanchuk, J.D., Besra, G.S., Chen, B., et al. (2011). Mycobacteria release active membrane vesicles that modulate immune responses in a TLR2-dependent manner in mice. J. Clin. Invest. 121, 1471-1483.

Preiss, J. (1984). Bacterial glycogen synthesis and its regulation. Annu. Rev. Microbiol. 38, 419-458.

Preiss, J., Greenberg, E., and Sabraw, A. (1975). Biosynthesis of bacterial glycogen-Kinetic studies of a glucose 1-phosphate adenyltransferase (EC 2.7.7.27) from a glycogen deficient mutant of *Escherichia coli* B. J. Biol. Chem. 250, 7631-7638.

Preiss, J., Yung, S.-G., and Baecker, P.A. (1983). Regulation of bacterial glycogen synthesis. Mol. Cell. Biochem. 57, 61-80.

Ramachandran, G.N., Ramakrishnan, C., and Sasisekharan, V. (1963). Stereochemistry of polypeptide chain configurations. J. Mol. Biol. 7, 95-99.

Ranade, N., and Vining, L.C. (1993). Accumulation of intracellular carbon reserves in relation to chloramphenicol biosynthesis by *Streptomyces venezuelae*. Can. J. Microbiol. 39, 377-383.

Robertson, J.G., Lyttleton, P., Williamson, K.I., and Batt, R.D. (1975). The effect of fixation procedures on the electron density of polysaccharide granules in *Nocardia coralina*. J. Ultra. Mol. Struct. R. 52, 321-332.

Romeo, T., Moore, J., and Smith, J. (1991). A simple method for cloning genes involved in glucan biosynthesis- isolation of structural and regulatory genes for glycogen synthesis in *Escherichia coli*. Gene 108, 23-29.

Ross, K.L., Davis, C.N., and Fridovich-Keil, J.L. (2004). Differential roles of the Leloir pathway enzymes and metabolites in defining galactose sensitivity in yeast. Molecular Genetics and Metabolism 83, 103-116.

Rothman, L.B., and Cabib, E. (1969). Regulation of glycogen synthesis in intact yeast cell. Biochemistry 8, 3332-3341.

Roy, R., Usha, V., Kermani, A., Scott, D.J., Hyde, E.I., Besra, G.S., Alderwick, L.J., and Futterer, K. (2013). Synthesis of alpha-glucan in mycobacteria involves a hetero-octameric complex of trehalose synthase TreS and Maltokinase Pep2. ACS Chem. Biol. 8, 2245-2255.

Rueda, B., Miguelez, E.M., Hardisson, C., and Manzanal, M.B. (2001). Changes in glycogen and trehalose content of *Streptomyces brasiliensis* hyphae during growth in liquid cultures under sporulating and non-sporulating conditions. FEMS Microbiol. Lett. 194, 181-185.

Sambou, T., Dinadayala, P., Stadthagen, G., Barilone, N., Bordat, Y., Constant, P., Levillain, F., Neyrolles, O., Gicquel, B., Lemassu, A., et al. (2008). Capsular glucan and intracellular glycogen of *Mycobacterium tuberculosis*: biosynthesis and impact on the persistence in mice. Mol. Microbiol. 70, 762-774.

Sani, M., Houben, E.N.G., Geurtsen, J., Pierson, J., de Punder, K., van Zon, M., Wever, B., Piersma, S.R., Jimenez, C.R., Daffe, M., et al. (2010). Direct visualization by cryo-EM of the mycobacterial capsular layer: a labile structure containing ESX-1-secreted proteins. PLoS Pathog. 6. e1000794

Sassetti, C.M., Boyd, D.H., and Rubin, E.J. (2003). Genes required for mycobacterial growth defined by high density mutagenesis. Mol. Microbiol. 48, 77-84.

Schneider, D., Bruton, C.J., and Chater, K.F. (2000). Duplicated gene clusters suggest an interplay of glycogen and trehalose metabolism during sequential stages of aerial mycelium development in *Streptomyces coelicolor* A3(2). Mol. Gen. Genet. 263, 543-553.

Shen, L.C., and Atkinson, D.E. (1970). Regulation of adenosine diphosphate glucose synthase from *Escherichia coli* -interactions of adenylate energy charge and modifier concentrations. J. Biol. Chem. 245, 3996-4000.

Shirokane, Y., and Suzuki, M. (1995). A novel enzyme, maltose 1-epimerase from *Lactobacillus brevis* IFO-3345. FEBS Lett. 367, 177-179.

Smith, A.M., and Zeeman, S.C. (2006). Quantification of starch in plant tissues. Nat. Protoc. 1, 1342-1345.

Sola-Landa, A., Moura, R.S., and Martín, J.F. (2003). The two-component PhoR-PhoP system controls both primary metabolism and secondary metabolite biosynthesis in *Streptomyces lividans*. P. Natl. Acad. Sci. USA. 100, 6133-6138.

Stadthagen, G., Sambou, T., Guerin, M., Barilone, N., Boudou, F., Kordulakova, J., Charles, P., Alzari, P.M., Lemassu, A., Daffe, M., et al. (2007). Genetic basis for the biosynthesis of methylglucose lipopolysaccharides in *Mycobacterium tuberculosis*. J. Biol. Chem. 282, 27270-27276.

Stam, M.R., Danchin, E.G.J., Rancurel, C., Coutinho, P.M., and Henrissat, B. (2006). Dividing the large glycoside hydrolase family 13 into subfamilies: towards improved functional annotations of alpha-amylase-related proteins. Protein Eng. Des. Sel. 19, 555-562.

Stults, C.L., Wade, A.P., and Crouch, S.R. (1987). Immobilized enzyme kinetic study of D-glucose mutarotation by flow injection analysis. Anal. Chem. 59, 2245-2247.

Swarts, B.M., Holsclaw, C.M., Jewett, J.C., Alber, M., Fox, D.M., Siegrist, M.S., Leary, J.A., Kalscheuer, R., and Bertozzi, C.R. (2012). Probing the Mycobacterial Trehalome with Bioorthogonal Chemistry. J. Am. Chem. Soc. 134, 16123-16126.

Syson, K., Stevenson, C.E.M., Rashid, A.M., Saalbach, G., Tang, M., Tuukkanen, A., Svergun, D.I., Withers, S.G., Lawson, D.M., and Bornemann, S. (2014). Structural insight into how *Streptomyces coelicolor* maltosyl transferase GlgE binds alpha-maltose 1-phosphate and forms a maltosyl-enzyme intermediate. Biochemistry 53, 2494-2504.

Syson, K., Stevenson, C.E., Rejzek, M., Fairhurst, S.A., Nair, A., Bruton, C.J., Field, R.A., Chater, K.F., Lawson, D.M., and Bornemann, S. (2011). Structure of *Streptomyces* maltosyltransferase GlgE, a homologue of a genetically validated anti-tuberculosis target. J. Biol. Chem. 286, 38298-38310.

Takayama, K., Wang, C., and Besra, G.S. (2005). Pathway to synthesis and processing of mycolic acids in *Mycobacterium tuberculosis*. Clin. Microbiol. Rev. 18, 81-101.

Tantanarat, K., Rejzek, M., O'Neill, E., Ruzanski, C., Hill, L., Fairhurst, S.A., Limpaseni, T., and Field, R.A. (2012). An expedient enzymatic route to isomeric 2-, 3- and 6-monodeoxy-monofluoro-maltose derivatives. Carbohydr. Res. 358, 12-18.

Tewari, Y.B., and Goldberg, R.N. (1991). Thermodynamics of hydrolysis of disaccharides. Lactulose, alpha-D-melibiose, palatinose, D-trehalose, D-turanose and 3-*O*-beta-D-galactopyranosyl-D-arabinose. Biophys. Chem. 40, 59-67.

Tewari, Y.B., Lang, B.E., Decker, S.R., and Goldberg, R.N. (2008). Thermodynamics of the hydrolysis reactions of 1,4-β-D-xylobiose, 1,4-β-D-xylotriose, D-cellobiose, and D-maltose. J. Chem. Thermodyn. 40, 1517-1526.

Torija, M.J., Novo, M., Lemassu, A., Wilson, W., Roach, P.J., Francois, J., and Parrou, J.L. (2005). Glycogen synthesis in the absence of glycogenin in the yeast *Saccharomyces cerevisiae*. FEBS Lett. 579, 3999-4004.

Updegraff, D.M. (1969). Semimicro determination of cellulose in biological materials. Anal. Biochem. 32, 420-424.

Usui, T., Yokoyama, M., Yamaoka, N., Matsuda, K., Tuzimura, K., Sugiyama, H., and Seto, S. (1974). Proton magnetic resonance spectra of D-gluco-oligosaccharides and D-glucans. Carbohydr. Res. 33, 105-116.

Varki, A. (1993). Biological roles of oligosaccharides: all of the theories are correct. Glycobiology 3, 97-130.

Ventura, M., Rieck, B., Boldrin, F., Degiacomi, G., Bellinzoni, M., Barilone, N., Alzaidi, F., Alzari, P.M., Manganelli, R., and O'Hare, H.M. (2013). GarA is an essential regulator of metabolism in *Mycobacterium tuberculosis*. Mol. Microbiol. 90, 356-366.

Vieira, J., and Messing, J. (1982). The pUC plasmids, an M13mp7-derived system for insertion mutagenesis and sequencing with synthetic universal primers. Gene 19, 259-268.

Vizcaino, C., Restrepo-Montoya, D., Rodriguez, D., Nino, L.F., Ocampo, M., Vanegas, M., Reguero, M.T., Martinez, N.L., Patarroyo, M.E., and Patarroyo, M.A. (2010). Computational prediction and experimental assessment of secreted/surface proteins from *Mycobacterium tuberculosis* H37Rv. PloS Comput. Biol. 6, e1000824.

Wang, C., Saldanha, M., Sheng, X., Shelswell, K.J., Walsh, K.T., Sobral, B.W., and Charles, T.C. (2007). Roles of poly-3-hydroxybutyrate (PHB) and glycogen in symbiosis of *Sinorhizobium meliloti* with *Medicago* sp. Microbiol. 153, 388-398.

Ward, J.J., McGuffin, L.J., Bryson, K., Buxton, B.F., and Jones, D.T. (2004). The DISOPRED server for the prediction of protein disorder. Bioinformatics 20, 2138-2139.

Wilson, W.A., Roach, P.J., Montero, M., Baroja-Fernández, E., Muñoz, F.J., Eydallin, G., Viale, A.M., and Pozueta-Romero, J. (2010). Regulation of glycogen metabolism in yeast and bacteria. FEMS Microbiol. Rev. 34, 952-985.

Winn, M.D., Ballard, C.C., Cowtan, K.D., Dodson, E.J., Emsley, P., Evans, P.R., Keegan, R.M., Krissinel, E.B., Leslie, A.G.W., McCoy, A., et al. (2011). Overview of the CCP4 suite and current developments. Acta Crystallogr. D, 67, 235-242.

Winter, G. (2010). xia2: an expert system for macromolecular crystallography data reduction. J. Appl. Cryst. 43, 186-190.

Withers, S.G., Rupitz, K., and Street, I.P. (1988). 2-Deoxy-2-fluoro-D-glycosyl fluorides- A new class of specific mechanism based glycosidase inhibitors. J. Biol. Chem. 263, 7929-7932.

Wolf, A., Kramer, R., and Morbach, S. (2003). Three pathways for trehalose metabolism in *Corynebacterium glutamicum* ATCC13032 and their significance in response to osmotic stress. Mol. Microbiol. 49, 1119-1134.

Wolfenden, R., Ridgway, C., and Young, G. (1998). Spontaneous hydrolysis of ionized phosphate monoesters and diesters and the proficiencies of phosphatases and phosphodiesterases as catalysts. J. Am. Chem. Soc. 120, 833-834.

Woodruff, P.J., Carlson, B.L., Siridechadilok, B., Pratt, M.R., Senaratne, R.H., Mougous, J.D., Riley, L.W., Williams, S.J., and Bertozzi, C.R. (2004). Trehalose is required for growth of *Mycobacterium smegmatis*. J. Biol. Chem. 279, 28835-28843.

Yang, K., Han, L., and Vining, L.C. (1995). Regulation of jadomycin B production in *Streptomyces venezuelae* ISP5230: involvement of a repressor gene, jadR2. J. Bacteriol. 177, 6111-6117.

Yeo, M., and Chater, K. (2005). The interplay of glycogen metabolism and differentiation provides an insight into the developmental biology of *Streptomyces coelicolor*. Microbiol. UK. 151, 855-861.

Young, F.G. (1957). Claude Bernard and the discovery of glycogen. Brit. Med. J. 1, 1431-1437.

Zaffanello, M., Zamboni, G., Schadewaldt, P., Borgiani, P., and Novelli, G. (2005). Neonatal screening, clinical features and genetic testing for galactosemia. Genet. Med. 7, 211-212.

Zechel, D.L., and Withers, S.G. (1999). Glycosidase mechanisms: anatomy of a finely tuned catalyst. Accounts Chem. Res. 33, 11-18.

Zhang, R., Pan, Y.T., He, S., Lam, M., Brayer, G.D., Elbein, A.D., and Withers, S.G. (2011). Mechanistic analysis of trehalose synthase from *Mycobacterium smegmatis*. J. Biol. Chem. 286, 35601-35609.

Zumla, A., Raviglione, M., Hafner, R., and Fordham von Reyn, C. (2013). Tuberculosis. New Engl. J. Med. 368, 745-755.

Appendix

The DNA sequence of the synthesised genes with optimum codon usage for expression in *Escherichia coli* (Genscript) is shown 5'-3' with the start codon in bold and the first stop codon underlined. It is flanked at the 5' end by an NdeI restriction site and a sequence encoding a His_6 tag and a TEV protease cleavage site, and at the 3' end by a BamHI restriction site.

1) *Streptomyces venezuelae* ATCC 10712 *otsA* gene

CAT**ATG**CATCATCATCATCATCACGAAAATCTGTACTTCCAAGGTGCTTCTGTCCTGGTTGC
TTCTAATCGCGGTCCGGTCTCCTACGTCCGTGGCGAAGATGGTGAACTGGACGCACGTCGCG
GCGGTGGCGGTCTGGTGTCTGGCCTGTCCGCAGTTAGCTCTCAGGACTCCCTGTGGGTGTGC
GCAGCACTGGGTGAAGGTGATCGTGAAGCAGTCCGTCGCGGTATTGGTGAACCGGGCGTGCG
CATGCTGGATATCGCACCGGACGTTTATGCAGATGCTTACAACGGTATTGCGAATTCAGTTC
TGTGGTTTCTGCATCACCATCTGTATGACATCCCGCGTGAACCGGTGTTTGATGCAGCTTTC
CGTCACCGCTGGGAAGCATATCGTGCTTACAACCGTGCATTCGCAGAAGCACTGGCAGCAGC
AGCTGACGAAGGTGCAGCAGTTCTGGTCCAGGATTATCATCTGGCGCTGGTTCCGGGCCAAC
TGCGCGAACTGCGTCCGGATCTGCGCATTGGTCACTTTACCCATACGCCGTGGGCGAGCCCG
GAATACTTCCGTATGCTGCCGGCCGATATCGGTGACGAACTGCTGCGTGGTATGCTGGGTGC
AGATGAACTGGGTTTTCATACCTCAGCTTGGGCATCGGCCTTCCTGAGCTGTGCCGGCGGTG
AACAGCCGCGTACCCGTGTGCGTGTTCACCCGCTGGGTGTGGACGCGGAAGAACTGCGTGCA
CTGGCTCATCGCCCGCAAGTCGATGAACGTCTGGCACGTCTGCGTGAAGAAGTGGGTGACCG
CAAAACCATTGTCCGCGTGGATCGTACGGAACTGTCGAAGAACATCCTGCGTGGTCTGCTGG
CGTATCGCGAACTGCTGACCGTTCACCCGGAATGGCGCGACCGTGTGGTTCATCTGGCGTCT
GCCTACCCGAGTCGTCAGGATCTGGCAGCTTATCGCGCGTACACCGCCTCCGTGACGGAACT
GGCAGCAGAAATTAATGCAGAATTTGGCACCGCTGATTGGCAACCGGTTCTGGTCTCCGTGG
AAGATGACTTCACGCGTTCACTGGCAGCTTATCGCCTGGCAGACGTTGCTCTGGTCAACCCG
GTGCGTGATGGCATGAATCTGGTTGCGAAAGAAATCCCGGTCGTGTCGGATGCAGGTTGCGC
ACTGGTCCTGAGCACCGGTGCAGGTGCTTATGAAGAACTGAAGGAAGACGCCCTGACCGTTC
ACCCGTACGATGTCAGCGAAACGGCGGAAGCCCTGCATACCGCACTGACGATGCCGCCGCCA
GAACGTGCTGATCGTACCAAACGCCTGGCGTCTGCAGCAACGGCACTGCCGCCGCAGCGTTG
GTTTCTGAATCAACTGGAAGGTCTGAGTGATGCGTAATGAGGATCC

2) *Streptomyces venezuelae* ATCC 10712 *galU* gene

CAT**ATG**CATCATCATCACCATCACGAAAATCTGTACTTCCAAGGCAATCAATCATTCCCGCG
TCTGGGTCGCATCTCAAAAGCCGTTATTCCGGCAGCAGGTCTGGGTACCCGTTTTCTGCCGG
CGACCAAAGCCACGCCGAAAGAAATGCTGCCGGTGGTTGACAAACCGGCAATTCAGTATGTC
GTGGAAGAAGCTGTGGCAGCTGGCCTGTCCGATGTTCTGATGATCACGGGTCGTAACAAACG
CCCGCTGGAAGATCATTTCGACCGCAATTATGAACTGGAAGAAGCGCTGAGTCGTAAAGGCG
ATGACGAACGCCTGTCCAAAGTTCAGGAAAGCTCTGATCTGGCCACCATGCACTACGTGCGT
CAAGGTGCACCGCGCGGCCTGGGTCATGCCGTCCTGTGCGCGGCCCCGCACGTTGGCGATCA
GCCGTTTGCGGTGCTGCTGGGTGATGACCTGATTGATCCGCGTGACCCGCTGCTGAGCCGTA
TGGTCGAAGTGCAGGAACGTGAAGGCGGTTCAGTTATTGCCCTGATGGAAGTCGAACCGTCG
CAAATCCATCTGTACGGCTGTGCAGCTGTTGAAGCAACCGTCGATAGCGACGTTGTCAAAGT
GACGGACCTGGTTGAAAAACCGGATGCAGGCGAAGCTCCGTCTAACTATGCAATTATCGGTC
GCTACGTCCTGGACCCGGCGGTGTTTGGCATGCTGCGTGAAACCGAACCGGGTCGCGGCGGT
GAAATTCAGCTGACGGACGCGCTGCAAAAACTGGCCAGTGATGAAAAAATCGGCGGTCCGGT
TCACGGCGTGGTTTTCAAAGGTCGTCGCTATGATACCGGCGACCGTGGTGATTACCTGCGTG
CAATCGTGCGCCTGGCTTGCGAACGTGAAGACCTGGGCCCGGACTTTCGTGCGTGGCTGCGT
CGCTATGTGTCGGAAGAAATGTAATGAGGATCC

3) *Mycobacterium tuberculosis* H37Rv *treS* gene

CAT**ATG**CATCATCATCATCATCATGAAAACCTGTATTTTCAGGGCAACGAAGCGGAACAT
AGCGTGGAACATCCGCCGGTGCAGGGCAGCCATGTGGAAGGCGGCGTGGTGGAACATCCG
GATGCGAAAGATTTTGGCAGCGCGGCGGCGCTGCCGGCAGATCCAACCTGGTTTAAACAT
GCGGTGTTTTATGAAGTGCTGGTGCGTGCATTTTTCGATGCGAGCGCGGATGGCAGCGGC
GATCTGCGTGGCCTGATTGATCGTCTGGATTATCTGCAGTGGCTGGGCATTGATTGCATT
TGGCTGCCGCCGTTTTATGATAGCCCGCTGCGTGATGGTGGATATGATATTCGTGATTTT
TATAAAGTGCTGCCGGAATTTGGCACCGTGGATGATTTTGTGGCGCTGGTGGATGCGGCG
CATCGTCGTGGCATTCGTATTATTACCGATCTGGTGATGAACCATACCAGCGAAAGCCAT
CCGTGGTTTCAGGAAAGCCGTCGTGATCCGGATGGCCCGTATGGCGATTATTATGTGTGG
AGCGATACCAGCGAACGTTATACCGATGCGCGTATTATTTTTGTGGATACCGAAGAAAGC
AACTGGAGCTTTGATCCGGTGCGTCGTCAGTTTTATTGGCATCGTTTCTTTAGCCATCAG
CCGGATCTGAACTATGATAACCCGGCGGTGCAGGAAGCGATGATTGATGTGATTCGTTTT
TGGCTGGGCCTGGGCATTGATGGCTTTCGTCTGGATGCGGTGCCGTATCTGTTTGAACGT
GAAGGCACCAACTGCGAAAACCTGCCGGAAACCCATGCGTTTCTGAAACGTGTGCGTAAA
GTGGTGGATGATGAATTTCCGGGCCGTGTGCTGCTGGCGGAAGCGAACCAGTGGCCGGGC
GATGTGGTGGAATATTTTGGCGATCCGAACACCGGCGGCGATGAATGCCACATGGCGTTT
CATTTTCCGCTGATGCCGCGTATTTTTATGGCGGTGCGTCGTGAAAGCCGTTTTCCGATT
AGCGAAATTATTGCGCAGACCCCGCCGATTCCGGATATGGCGCAGTGGGGCATTTTTCTG
CGTAACCATGATGAACTGACCCTGGAAATGGTGACCGATGAAGAACGTGATTATATGTAT
GCGGAATATGCGAAAGATCCGCGTATGAAAGCGAACGTGGGTATCCGTCGAAGACTGGCG
CCGCTGCTGGATAACGATCGTAACCAGATTGAACTGTTTACCGCGCTGCTGCTGAGCCTG
CCGGGCAGCCCGGTGCTGTATTATGGCGATGAAATTGGCATGGGCGATGTGATTTGGCTG
GGCGATCGTGATGGCGTGCGTATTCCGATGCAGTGGACCCCGGATCGTAACGCGGGCTTT
AGCACCGCGAACCCGGGCCGTCTGTATCTGCCGCCGAGCCAGGACCCAGTGTATGGCTAT
CAGGCGGTGAACGTGGAAGCGCAGCGTGATACCAGCACCAGCCTGCTGAACTTTACCCGT
ACCATGCTGGCGGTGCGTCGAAGACATCCGGCCTTTGCCGTGGGTGCCTTTCAGGAACTG
GGCGGCAGCAACCCGAGCGTGCTGGCGTATGTGCGTCAGGTGGCGGGCGATGATGGCGAT
ACCGTGCTGTGCGTGAACAACCTGAGCCGTTTTCCGCAGCCGATTGAACTGGATCTGCAG
CAGTGGACCAACTATACCCCGGTGGAACTGACCGGCCATGTGGAATTTCCGCGTATTGGC
CAGGTGCCGTATCTGCTGACCCTGCCGGGCCATGGCTTTTATTGGTTTCAGCTGACCACC
CATGAAGTGGGCGCACCTCCAACCTGCGGCGGCGAACGTCGTCTGTAA<u>TAA</u>GGATCC

4) *Mycobacterium tuberculosis* H37Rv *pep2* gene

CAT**ATG**CATCATCATCATCATCATGAAAACCTGTATTTTCAGGGCACCCGTAGCGATACC
CTGGCGACCAAACTGCCGTGGAGCGATTGGCTGAGCCGTCAGCGTTGGTATGCGGGCCGT
AACCGTGAACTGGCGACCGTGAAACCGGGCGTGGTGGTGGCGCTGCGTCATAACCTGGAT
CTGGTGCTGGTGGATGTGACCTATACCGATGGCGCGACCGAACGTTATCAGGTGCTGGTG
GGCTGGGATTTTGAACCGGCGAGCGAATATGGCACCAAAGCGGCGATTGGCGTGGCGGAT
GATCGTACCGGCTTTGATGCGCTGTATGATGTGGCGGGCCCGCAGTTTCTGCTGAGCCTG
ATTGTGAGCAGCGCGGTGTGCGGCACCAGCACCGGCGAAGTGACCTTTACCCGTGAACCG
GATGTGGAACTGCCGTTTGCGGCGCAGCCGCGTGTGTGCGATGCGGAACAGAGCAACACC
AGCGTGATTTTTGATCGTCGTGCGATTCTGAAAGTGTTTCGTCGTGTGAGCAGCGGCATT
AACCCGGATATTGAACTGAACCGTGTGCTGACCCGTGCGGGCAACCCGCATGTGGCGCGT
CTGCTGGGCGCGTATCAGTTTGGCCGTCCGAACCGTAGCCCGACCGATGCGCTGGCGTAT
GCGCTGGGCATGGTGACCGAATATGAAGCGAACGCGGCGGAAGGCTGGGCGATGGCGACC
GCGAGCGTGCGTGATCTGTTTGCGGAAGGCGATCTGTATGCGCATGAAGTGGGCGGCGAT
TTTGCGGGCGAAAGCTATCGTCTGGGTGAAGCCGTGGCCAGCGTGCATGCCACCCTGGCC
GATAGCCTGGGTACCGCCCAGGCGACCTTTCCGGTGGATCGTATGCTGGCGCGTCTGAGC
AGCACCGTGGCGGTGGTGCCGGAACTGCGTGAATATGCGCCGACCATTGAACAGCAGTTT
CAGAAACTGGCGGCGGAAGCGATTACCGTGCAGCGTGTGCATGGCGATCTGCATCTGGGC
CAGGTGCTGCGTACCCCGGAAAGCTGGCTGCTGATTGATTTTGAAGGCGAACCGGGTCAG
CCGCTGGATGAACGTCGTGCCCCGGATAGCCCGCTGCGTGATGTGGCCGGTGTGCTGCGT
AGCTTTGAATATGCGGCGTATGGCCCGCTGGTGGATCAGGCGACCGATAAACAGCTGGCG
GCGCGTGCGCGTGAATGGGTGGAACGTAACCGTGCGGCGTTTTGCGATGGCTATGCGGTG
GCGAGCGGCATTGATCCGCGTGATAGCGCGCTGCTGCTGGGCGCGTATGAACTGGATAAA
GCGGTGTATGAAACCGGCTATGAAACCCGTCATCGTCCGGGCTGGCTGCCGATTCCGCTG
CGTAGCATTGCGCGTCTGACCGCGAGCTAA<u>TAA</u>GGATCC

5) ***Pseudomonas aeruginosa*** **PAO1** ***treS-pep2*** **gene**

CAT**ATG**CATCATCATCATCATCACGAAAATCTGTACTTCCAAGGTGCCCGCCGCGAAAAACC
GGTCTTCCTGAACGACCCGCAGTGGTATAAAGATGCGGTGATTTATCAGGTCCATGTGAAAT
CTTTTTACGATGCGAACAATGACGGCATCGGTGATTTCGCCGGCCTGATTGAAAAACTGGAC
TATATCGCGGATCTGGGTGTTAACACCCTGTGGCTGCTGCCGTTTTACCCGAGCCCGCGTCG
CGATGACGGCTATGATATTGCCCAGTACCGTGGCGTCCATAGCGACTATGGTTCTCTGGCCG
ATGCACGTCGCTTTATCGCTGAAGCACACCGTCGCGGTCTGCGTGTCATTACCGAACTGGTG
ATCAACCATACGTCAGATCAGCACCCGTGGTTCATTCGTGCCCGCCATGCGAAAAAAGGCTC
GCGTGCCCGCGATTATTACGTGTGGAGCGATTCTGACGAAAAATATCAGGGTACCCGTATTA
TCTTTATCGACACCGAACAAAGCAATTGGACGTGGGACCCGGTTGCGCAGCAATATTACTGG
CATCGCTTTTACTCTCACCAGCCGGACCTGAACTTCGATAATCCGCAAGTTCTGCGTGAAGT
GCTGGGCGTTATGCGCTATTGGCTGGACATGGGCGTCGATGGTCTGCGTCTGGACGCGATTC
CGTACCTGATCGAACGCGATGGTACCAGCTCTGAAAACCTGCCGGAAACGCATCAGGTGCTG
AAACGTATTCGCGCGGAACTGGACGCCCACTATCCGGATCGTATGCTGCTGGCCGAAGCAAA
TCAGTGGCCGGAAGATACCCGCCCGTACTTTGGCGGTGAAGACGGCGGTGAAGGCGATGAAT
GCCACATGGCGTTTCACTTCCCGCTGATGCCGCGTATGTATATGGCTATCGCGCAGGAAGAC
CGTTACCCGATTACCGATATCCTGCGCCAGACGCCGGATATTCCGGCAAACTGTCAATGGGC
TATCTTCCTGCGCAATCATGATGAACTGACCCTGGAAATGGTGACGGATGACGAACGTGACT
ATCTGTGGAACCACTACGCAGCAGATCGTCGCGCACGTCTGAATCTGGGTATTCGTCGCCGT
CTGGCACCGCTGGTTGAACGTGATCGCCGTCGCATCGAACTGCTGCATAGTCTGCTGCTGTC
CATGCCGGGTACCCCGACGCTGTATTACGGTGACGAAATTGGCATGGGTGATAACATCTATC
TGGGTGATCGTGACGGTGTGCGTACCCCGATGCAGTGGAGCGTTGACCGTAATGGCGGTTTT
TCGCGCGCTGATCCGGCGAAACTGGTGCTGCCGCCGATTCTGGACCCGCTGTATGGCTACCA
GACGATCAACGTTGAAGCCCAAGCACGTGATCCGCACAGCCTGCTGAATTGGATGCGTCGCC
TGCTGGCAGTGCGTTCTCAGCAAAAAGCTTTCGGCCGCGGTAGTCTGAAAATGCTGGCCCCG
TCCAACCGTCGCATTCTGGCGTACCTGCGTGAATATGCCGAAGGCGAACGCCAGGATAGCAT
CCTGTGCGTTGCAAATCTGTCTCGCGCAGCTCAAGCTGTCGAACTGGATCTGGCCAGTCATG
CCGGTAAAGTTCCGGTCGAAATGATTGGCGGTATGTCCTTTCCGCCGATCGGCGAACTGACC
TATCTGCTGACGCTGCCGCCGTATGGTTTTTACTGGTTCTATCTGGCTGACGCGACCCAGAT
GCCGAGTTGGCACGTTGCAGCAGATGAACGTCTGCCGGAACTGCCGACCCTGGTGGTGAAAC
AGCGTCTGGGCGAACTGCTGCAGGGTGCGTCCCGCAACATTCTGGAAGGCGAAACCCTGCCG
GCATATCTGCCGAAACGTCGCTGGTTTGCTGGCGAAAAGGGTCAGCCGCGTCTGTGTTACAT
TGTGCCGCTGGACGAAGCAGAACCGCGTTGCGCCCTGTGTGAAGTTGAAATCGATGGTCTGC
GCTATCAGCTGCCGCTGGGCTTCCTGGATGCAGACCAGCGCGGTGATTCACTGCCGCAACTG
CTGGCACTGGCACGTCTGCGTCGCGGTCGCAAAGTGGGTCTGCTGACGGATGCAGCTTCGCT
GCCGCTGTTTGCACGTAAAGTCCTGGCTCAGCTGCGCGCTGAAGCGGTGATTGCGCATGGCG
ATGGTGAAATTCAATTCATCCCGGCGGCCGGCCTGGCAGAAATGGATGACATTGCTGATGAA
GACGTTCTGCCGTTTTCAGTCGAACAGTCGAACAGTTCCATCCGTTTCGGCGAACGCATGGT
CCTGAAAGTGCTGCGTAAAATTCTGCCGGGTCTGCATCCGGAAATCGAAGTGGGCGGTTATC
TGACCCGTCACGGTTACCCGGGTATTGCACCGCTGCTGGGTGAAGTTCGTCGCGTCGGCGCC
GATGGTGAACCGCATACCCTGATGATCCTGCAGGGCTATCTGAACAATCAAGGTGACGCATG
GAACTGGACGCTGGATAATCTGGAACGTGCGGTTCGCGACGAAATTAGTGCAGCTTCCGAAG
CGCTGGAAGGCCAGTATGATAGCCTGGCCGAACTGCGTGGTTTTGCGGCCAATCTGGGCGCA
CGCCTGGGTGAAATGCACAGCGTCCTGGCGGGCGAATCTGATGACCCGGCCTTCGGTTCACG
TGAATCGGATGAAGCGAGTGTGCAGGCCTGGGCACTGCGCATTGCGGAACAACTGCGTGAAG
CAGGTAAACGTCTGTCCGAACCGCCGCGTCCGCTGCAGGGTGAAGCAGCTGAACAAGCACGT
CGCCTGCTGGAACGTCTGCCGGCTCTGCTGGAACGCCTGCCGCTGCTGGCACGTCAGGCAGC
CGGCGGTCTGCTGATTCGTGTGCATGGCGATCTGCACCTGGGTCAGGTGCTGATGGTTCAAG
GCGACGCACGCTTTATCGATTTCGAAGGTGAACCGGCGCGTAGTCTGGAAGAACGTCGCCAG
CGCCATTCCCCGATGAAAGACGTCGGCGGTATGCTGCGTAGCTTTGATTATGCAGCTGCGAT
GGTGCTGCGCAATGCCCAGTCAACCGACTCATCGGAACAAGCTGATTCGGCGCGTCGCAAAG
TTGCAATGCGTTATCGCAGCGAAGCCCGTGATGCATTCCTGGCTGGTTACCGTGCAGCAGCT
GCAGGTCTGATGCATGCATGGCACGGTCGTGAAGGTGAAGGTGCAGCACTGGCTCTGGCATG
CCTGGAAAAAGCTGCGTACGAACTGCTGTATGAAGCGGACTACCGCCCGGATTGGCTGGAAG
TCCCGCTGGCTGGTCTGGCTGAACTGACGGAACACCTGCTGAAAGGCAAAAACCGCTAATAA
GGATCC

Publication

Chemistry & Biology
Brief Communication

Flux through Trehalose Synthase Flows from Trehalose to the Alpha Anomer of Maltose in Mycobacteria

Farzana Miah,[1] Hendrik Koliwer-Brandl,[2] Martin Rejzek,[1] Robert A. Field,[1] Rainer Kalscheuer,[2,*] and Stephen Bornemann[1,*]
[1]Department of Biological Chemistry, John Innes Centre, Norwich Research Park, Norwich, Norfolk NR4 7UH, UK
[2]Institute for Medical Microbiology and Hospital Hygiene, Heinrich-Heine-University Düsseldorf, 40225 Düsseldorf, Germany
*Correspondence: rainer.kalscheuer@med.uni-duesseldorf.de (R.K.), stephen.bornemann@jic.ac.uk (S.B.)
http://dx.doi.org/10.1016/j.chembiol.2013.02.014

SUMMARY

Trehalose synthase (TreS) was thought to catalyze flux from maltose to trehalose, a precursor of essential trehalose mycolates in mycobacterial cell walls. However, we now show, using a genetic approach, that TreS is not required for trehalose biosynthesis in *Mycobacterium smegmatis*, whereas two alternative trehalose-biosynthetic pathways (OtsAB and TreYZ) are crucial. Consistent with this direction of flux, trehalose levels in *Mycobacterium tuberculosis* decreased when TreS was overexpressed. In addition, TreS was shown to interconvert the α anomer of maltose and trehalose using ^{1}H and ^{19}F-nuclear magnetic resonance spectroscopies using its normal substrates and deoxyfluoromaltose analogs, with the nonenzymatic mutarotation of α/β-maltose being slow. Therefore, flux through TreS in mycobacteria flows from trehalose to α-maltose, which is the appropriate anomer for maltose kinase of the GlgE α-glucan pathway, which in turn contributes to intracellular and/or capsular polysaccharide biosynthesis.

INTRODUCTION

Trehalose (α-D-glucopyranosyl-(1→1)-α-D-glucopyranoside) is a nonreducing disaccharide that has many roles in biology (Argüelles, 2000; Elbein et al., 2003; Paul et al., 2008). For example, it is a precursor for cell wall trehalose mycolates (Figure 1A) that are essential for the growth and virulence of mycobacteria, such as *Mycobacterium tuberculosis* (Takayama et al., 2005), the causative agent of the globally widespread human disease tuberculosis (Dye, 2006). For this reason, trehalose has attracted attention in the development of imaging agents (Backus et al., 2011; Swarts et al., 2012) and drugs (Lin et al., 2007; Rose et al., 2002; Wang et al., 2004) to help diagnose and treat tuberculosis. It has been widely thought that there are three pathways responsible for the biosynthesis of trehalose in mycobacteria (Figure 1A): the OtsAB, TreYZ, and trehalose synthase (TreS) pathways (Avonce et al., 2006; Elbein et al., 2003). In vitro experiments have shown that all three pathways could, in principle, operate in mycobacteria (De Smet et al., 2000). In addition, genetic experiments appeared to show that all pathways are capable of synthesizing trehalose de novo in the fast-growing avirulent species *Mycobacterium smegmatis* (Woodruff et al., 2004). By contrast, it has been reported that the OtsAB pathway is dominant in trehalose biosynthesis in *Mycobacterium tuberculosis* and that TreS could have a role only in late-stage pathogenesis in infected mice (Murphy et al., 2005). This implies *Mycobacterium smegmatis* is not an appropriate model organism with respect to the metabolism of trehalose in *Mycobacterium tuberculosis*. The picture is complicated further by evidence that only the OtsAB and TreYZ pathways, but not the TreS pathway, appear to be important in the de novo biosynthesis of trehalose and trehalose mycolate formation in the related actinomycete, *Corynebacterium glutamicum* (Tzvetkov et al., 2003; Wolf et al., 2003).

TreS is a maltose α-D-glucosylmutase (EC 5.4.99.16) that interconverts maltose (α-D-glucopyranosyl-(1,4)-D-glucopyranose) and trehalose (Nishimoto et al., 1995; Pan et al., 2004). Therefore, an oft ignored puzzle has been the lack of an obvious and significant source of maltose in a mycobacterium either from its own metabolism or its environment. This is compounded by the lack of a maltose transporter in *Mycobacterium tuberculosis* (Kalscheuer et al., 2010a). However, we recently discovered an alternative route for α-glucan biosynthesis, the GlgE pathway, which is widespread among bacteria and involves the consumption of trehalose by TreS (Chandra et al., 2011; Kalscheuer et al., 2010b). These observations prompt the question as to whether TreS contributes to the biosynthesis of either trehalose mycolate, α-glucans, or both in mycobacteria.

There are no reports of experimental evidence defining the anomeric configuration of maltose that TreS produces. The configuration could have consequences for metabolic flux, because the nonenzymatic mutarotation of maltose is so slow that the half-life of anomeric equilibration is of the order of tens of minutes (Bailey et al., 1967). Furthermore, although maltose mutarotase enzymes are known, they appear to be rare and have only been detected in higher plants (Bailey et al., 1967) and *Lactobacillus brevis* (Shirokane and Suzuki, 1995). TreS is a glycoside hydrolase GH13_3 (Stam et al., 2006) family member according to the CaZy database (Cantarel et al., 2009). Thus, it is predicted to have a $(\beta/\alpha)_8$ fold, defining an active site containing an Asp nucleophile and a Glu proton donor that catalyze an

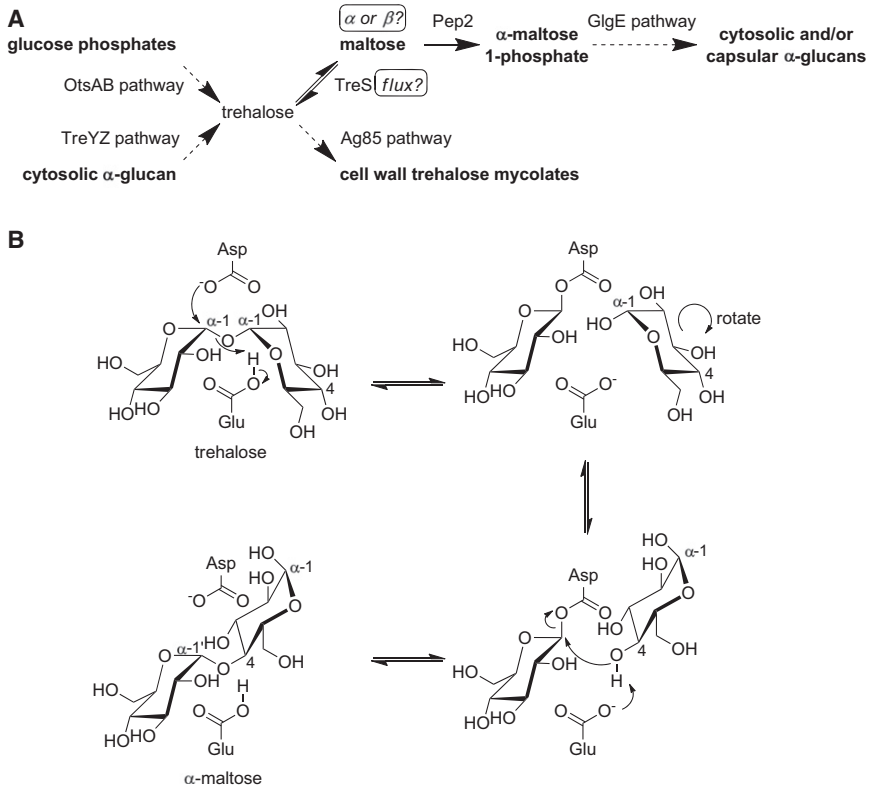

Figure 1. Metabolism of Trehalose in Mycobacteria and Proposed Mechanism of TreS

(A) All known metabolic pathways associated with trehalose in mycobacteria are shown, except for its hydrolysis by trehalase to form glucose as a carbon source for growth (Carroll et al., 2007). The questions addressed by this work are indicated in boxes.

(B) Proposed catalytic mechanism of TreS with the most likely relative orientations of the glucose rings of trehalose and maltose. Hydrolysis would be expected to occur when water attacks the glucosyl-enzyme intermediate, generating a second glucose molecule with an α anomeric configuration.

α-retaining double-displacement reaction mechanism (Figure 1B). In support of this mechanism, evidence for the glucosyl-enzyme intermediate involving Asp230 in the *Mycobacterium smegmatis* enzyme has been reported recently (Zhang et al., 2011). One would therefore predict that α-maltose is utilized and produced by TreS, but evidence to support this notion is currently lacking.

We now show, using a genetic approach, that flux through TreS is from rather than to trehalose in both *Mycobacterium smegmatis* and *Mycobacterium tuberculosis*. Therefore, TreS supplies intermediates for the GlgE α-glucan pathway rather than the trehalose mycolate pathway, both potential targets for imaging agents and therapeutic inhibitors. Furthermore, we show using ^{1}H-nuclear magnetic resonance (NMR) spectroscopy, supported by ^{19}F-NMR spectroscopy and deoxyfluoro substrate analogs, that the appropriate α anomer of maltose is formed for maltose kinase of the GlgE pathway. These findings have implications for the study and targeting of trehalose-dependent pathways in mycobacteria and other bacteria.

RESULTS

Characterization of Trehalose Auxotrophs of *Mycobacterium Smegmatis*

In order to definitively assess the contribution of TreS for the de novo biosynthesis of essential trehalose in mycobacteria, we generated site-specific gene deletion mutants in *Mycobacterium smegmatis* in the three reported trehalose biosynthetic pathways by targeting the genes *treS*, *otsA*, and *treY1-treY2-treZ,* both individually and in combination (Figure S1 available online). Inactivation of *treS* alone or in combination with either *otsA* or *treYZ* did not lead to any detectable growth defect in the absence of exogenous trehalose (Figure 2A). In contrast, we found that not only the Δ*treS*(u)Δ*otsA*(u)Δ*treYZ* triple mutant but also the Δ*otsA*(u)Δ*treYZ* double mutant strictly required trehalose supplementation for growth on solid medium (Figure 2B) and in liquid culture (Figure 2C), despite the double mutant possessing an intact *treS* gene. Supplementation with exogenous trehalose in the μM range was sufficient to support growth of these two trehalose auxotrophs (Figure 2C), showing that TreS does not contribute significantly to the de novo production of trehalose in *Mycobacterium smegmatis*. In the absence of trehalose, exogenous maltose in the mM range could partially restore growth of the Δ*otsA*(u)Δ*treYZ* but not the Δ*treS*(u)Δ*otsA*(u)Δ*treYZ* mutant (Figure 2D). These data indicate that TreS could be capable of synthesizing trehalose in mycobacteria but that the biosynthesis of maltose is severely limited in the growth conditions tested.

TreS Consumes Trehalose in *Mycobacterium Tuberculosis*

In order to assess the direction of flux through TreS in *Mycobacterium tuberculosis*, we analyzed intracellular trehalose levels in *Mycobacterium tuberculosis* wild-type, the Δ*treS* mutant and *treS*-overexpressing strains (Figure 2E). Deletion of *treS* had no influence on the intracellular trehalose concentration, precluding the ability to distinguish between TreS having a role in trehalose formation and consumption. However, the intracellular trehalose level in the *treS*-overexpressing strain was dramatically reduced, which indicates that TreS has a role in the consumption of trehalose in *Mycobacterium tuberculosis*, a direction of flux consistent with that in *Mycobacterium smegmatis*.

TreS Interconverts Trehalose with the α Anomer of Maltose According to ^{1}H-NMR Spectroscopy

With a view to establishing whether TreS interconverts the α anomer of maltose, we explored the use of ^{1}H-NMR spectroscopy. A spectrum of a reaction mixture generated from maltose by TreS allowed each component to be detected (Figure S2A),

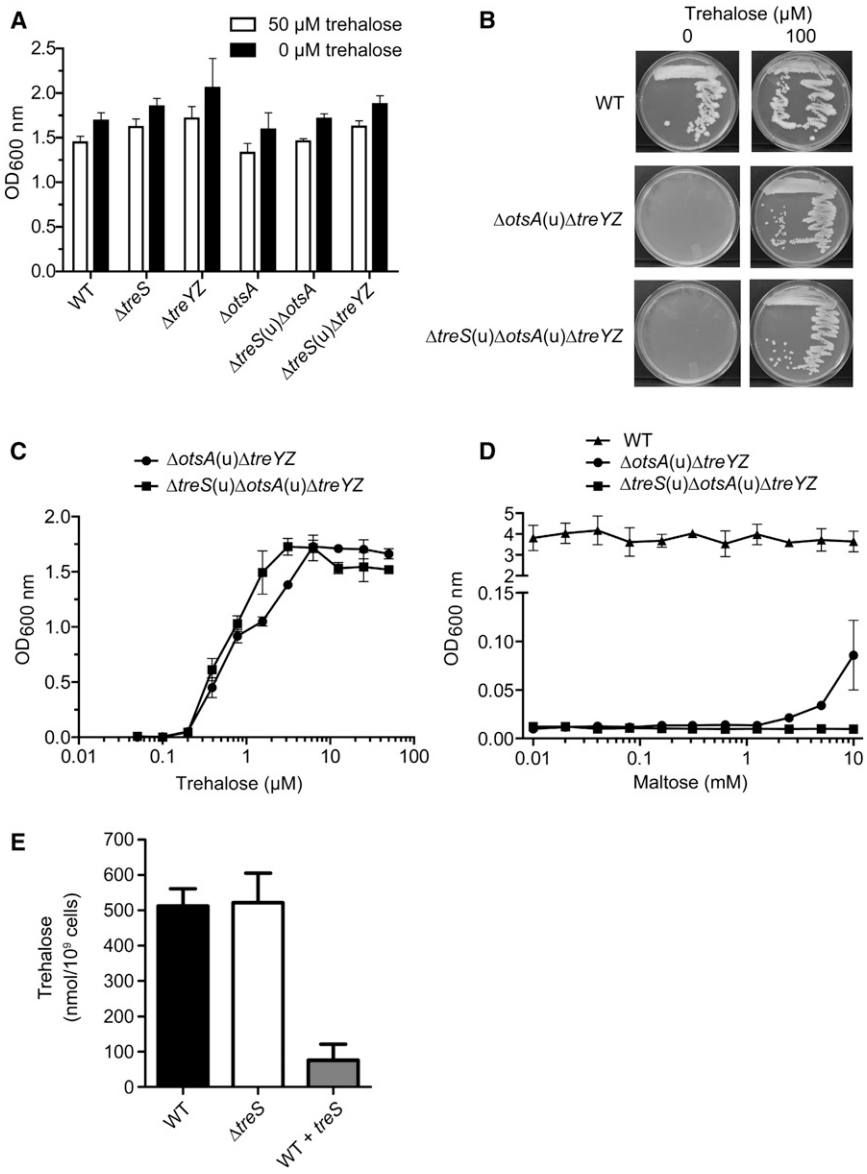

Figure 2. The TreS Pathway Does Not Contribute to the De Novo Biosynthesis of Trehalose in Mycobacteria

(A) Trehalose growth requirements in liquid culture of *Mycobacterium smegmatis* gene deletion mutants (see Figure S1 for how they were generated). Cultures were incubated for 48 hr at 37°C in Middlebrook 7H9 medium containing 0.5% (v/v) glycerol and 10% (v/v) albumin-dextrose-saline (ADS) enrichment containing either 0 or 50 μM trehalose. Values are means of triplicates ± SD.

(B) Trehalose growth requirements on solid media of the trehalose-auxotrophic *Mycobacterium smegmatis* mutants Δ*otsA*(u)Δ*treYZ* and Δ*treS*(u)Δ*otsA*(u)Δ*treYZ*. Cells were cultivated for 72 hr on Middlebrook 7H10 agar containing 0.5% (v/v) glycerol and 10% (v/v) ADS enrichment in the presence or absence of 100 μM trehalose.

(C) Trehalose growth requirements in liquid culture of the trehalose-auxotrophic *Mycobacterium smegmatis* mutants Δ*otsA*(u)Δ*treYZ* and Δ*treS*(u)Δ*otsA*(u)Δ*treYZ*. Growth conditions were essentially as described for (A) with 0–50 μM trehalose.

(D) Maltose supplementation of trehalose auxotrophic *Mycobacterium smegmatis* gene deletion mutants. Growth conditions were essentially as described for (A) without trehalose but with 0–10 mM maltose. Values are means of triplicates ± SD.

(E) Effect of *treS* deficiency and overexpression on intracellular trehalose concentration in *Mycobacterium tuberculosis*. Cultures of *Mycobacterium tuberculosis* H37Rv wild-type, the Δ*treS* mutant and a *treS* overexpressing strain (wild type [WT] + *treS*) were incubated for 14 days in Middlebrook 7H9 medium containing 0.5% (v/v) glycerol and 10% (v/v) oleic acid-albumin-dextrose-catalase enrichment before enzymatically determining trehalose concentrations. Values are means of sextuplicates ± SD.

including glucose, a known product of hydrolysis (Nishimoto et al., 1996; Pan et al., 2004; Zhang et al., 2011), and the anomers of each reducing sugar. Since anomers mutarotate non-enzymatically, their equilibration upon dissolution of crystalline materials in citrate buffer at 25°C was monitored using ^{1}H-NMR spectroscopy (Figure S2B). The rate constants determined for the mutarotation of α-glucose to β-glucose and the reverse reaction were 0.0316 ± 0.0004 and 0.0192 ± 0.0004 min^{-1} and, for maltose, 0.0286 ± 0.0002 and 0.0187 ± 0.0001 min^{-1}, each respectively (Figure S2C). These rate constants were consistent with the literature (Bailey et al., 1967; Stults et al., 1987) and the expected dominance of the β anomers.

The conversion of trehalose into maltose by TreS in citrate buffer as a function of time was monitored using ^{1}H-NMR spectroscopy (Figure 3A). The α anomer of maltose was formed 5.4-fold more rapidly than its β anomer, suggesting TreS generates the α anomer. A low level of glucose was also produced through hydrolysis, as observed previously. At longer times, the ratio between trehalose and α/β-maltose was 2.2:1 (at 25°C and pH 6.7), which is reasonably similar to the equilibrium position of 4.6:1 determined from the free energies of hydrolysis of these disaccharides (at 25°C and pH 5.65) (Syson et al., 2011; Tewari and Goldberg, 1991; Tewari et al., 2008) and of 3.2:1 determined from the kinetics of *Mycobacterium smegmatis* TreS (Zhang et al., 2011). The expected equilibrium positions between the anomers of both maltose and glucose were also approached at longer times.

As TreS formed trehalose from pre-equilibrated α/β-maltose (α:β anomeric ratio of 1:1.5), a rapid depletion of α-maltose was immediately apparent (Figure 3B). By contrast, the consumption of β-maltose was significantly slower and conformed to a single exponential function (Figure S2D) with a rate of 0.019 min^{-1} that was consistent with the rate constant for the mutarotation described above (0.0187 ± 0.0001 min^{-1}). This implied that TreS does not utilize the β anomer. When the experiment was repeated with lower TreS concentrations, the rate of consumption of α-maltose decreased, while that of the β anomer

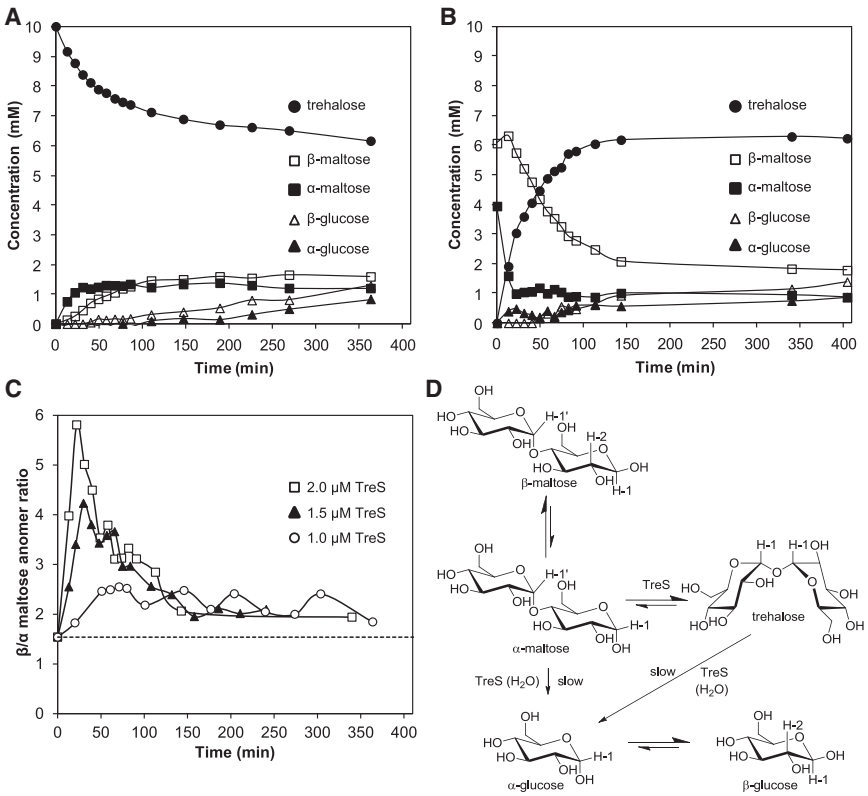

Figure 3. *Mycobacterium Tuberculosis* TreS Interconverts the α Anomer of Maltose

(A) The conversion of trehalose (10 mM) into maltose by TreS (2 μM) according to ^{1}H-NMR spectroscopy (see Figures S2A–S2C for representative spectra and nonenzymic mutarotation controls). Each component was quantified by signal integration using citrate as an internal standard. Reaction mixtures contained 10% D_2O to assist spectrum acquisition without significant risk of introducing solvent kinetic and/or equilibrium isotope effects. This necessitated solvent suppression and the introduction of experimentally determined correction factors for the cosuppression of resonances that were close to the solvent resonance.

(B) The conversion of pre-equilibrated α/β-maltose (10 mM) into trehalose by TreS (2 μM) according to ^{1}H-NMR spectroscopy. Note that enzyme was added immediately after the t = 0 data were acquired, resulting in a small and reproducible change in the apparent concentration of starting materials at the second recorded time point. See Figure S2D for the fit of the β-maltose curve (Hoops et al., 2006). The times taken to produce 2 mM trehalose and consume 50% of the α/β-maltose were 14 and 55 min, respectively.

(C) Time courses of the ratios between the β and α anomers of maltose with different TreS concentrations during the conversion of pre-equilibrated α/β-maltose. The broken line indicates the equilibrium between the two anomers in these conditions.

(D) Proposed reaction scheme to account for TreS-catalyzed reactions. Protons used to quantify components of the reaction mixtures by ^{1}H-NMR spectroscopy (Figure S2A) are indicated.

remained similar. Thus, the transient increase in the β/α ratio of the maltose anomers was less pronounced at lower enzyme concentrations (Figure 3C), providing further evidence that TreS converts only the α anomer of maltose into trehalose, as expected. While the initial formation of glucose through hydrolysis appeared to be more rapid from maltose than trehalose, this most likely reflected the more rapid initial consumption of maltose. This implies the equal probability of either α-maltose or trehalose being hydrolyzed. It is also noteworthy that the α anomer of glucose was produced more rapidly from maltose than its β anomer, suggesting that α-glucose is the product of hydrolysis.

The Specificity of TreS for the α Anomer of Maltose Is Retained with Deoxyfluoro Analogs According to ^{19}F-NMR Spectroscopy

Deoxyfluorotrehalose analogs have been shown to label *Mycobacterium tuberculosis* cells and exhibit weak antimycobacterial activity (Backus et al., 2011). Since *Mycobacterium tuberculosis* has a trehalose transporter (Kalscheuer et al., 2010a) and TreS has been reported to utilize 2-fluoro-2-deoxymaltose as a substrate (Zhang et al., 2011), the ability of TreS to convert 2-, 3-, and 6-deoxyfluoromaltose analogs (Tantanarat et al., 2012) was monitored using ^{19}F-NMR spectroscopy (Figure 4). The 2-deoxy-2-fluoro and 6-deoxy-6-fluoro compounds were converted to the corresponding deoxyfluorotrehalose analogs ~2-fold and ~180-fold less efficiently than the normal substrate (Figures 4A and 4C). The hydrolysis of each analog to the corresponding deoxyfluoroglucose compounds was detected (Figures 4A–4C), particularly with the 3-fluoro-3-deoxy and 6-fluoro-6-deoxy compounds, with the former being exclusively hydrolyzed (Figure 4B). The expected concomitant formation of nonfluorinated glucose was detected using ^{1}H-NMR spectroscopy (data not shown). The α anomer was consumed more rapidly than the β anomer with all three analogs (Figures 4A–4C), consistent with TreS only acting on α anomers. The mutarotation rates of the deoxyfluoro analogs are not known, but fitting the decay of the β anomer of the 2-deoxy-2-fluoro analog (Figure 4A) suggested a rate constant of ~0.004 min^{-1}, an order of magnitude slower than that for maltose.

In order to assess whether fluoro substitution at the three and six positions resulted in poor binding to TreS or slow conversion by TreS, the extent of conversion of 0.52 mM 2-deoxy-2-fluoromaltose was monitored in the presence and absence of 2.1 mM of each of the other two analogs (Figure S3D). Neither of the analogs gave inhibition, and there may indeed have been a modest stimulation of activity. Given that the K_m for maltose is 8–10 mM with the *Mycobacterium smegmatis* enzyme (Pan et al., 2004; Zhang et al., 2011) and the K_m for the 2-deoxy-2-fluoro analog would not be expected to be orders of magnitude lower than this, the lack of inhibition is consistent with fluoro substitution at the three and six positions, compromising the ability of maltose analogs to bind to TreS.

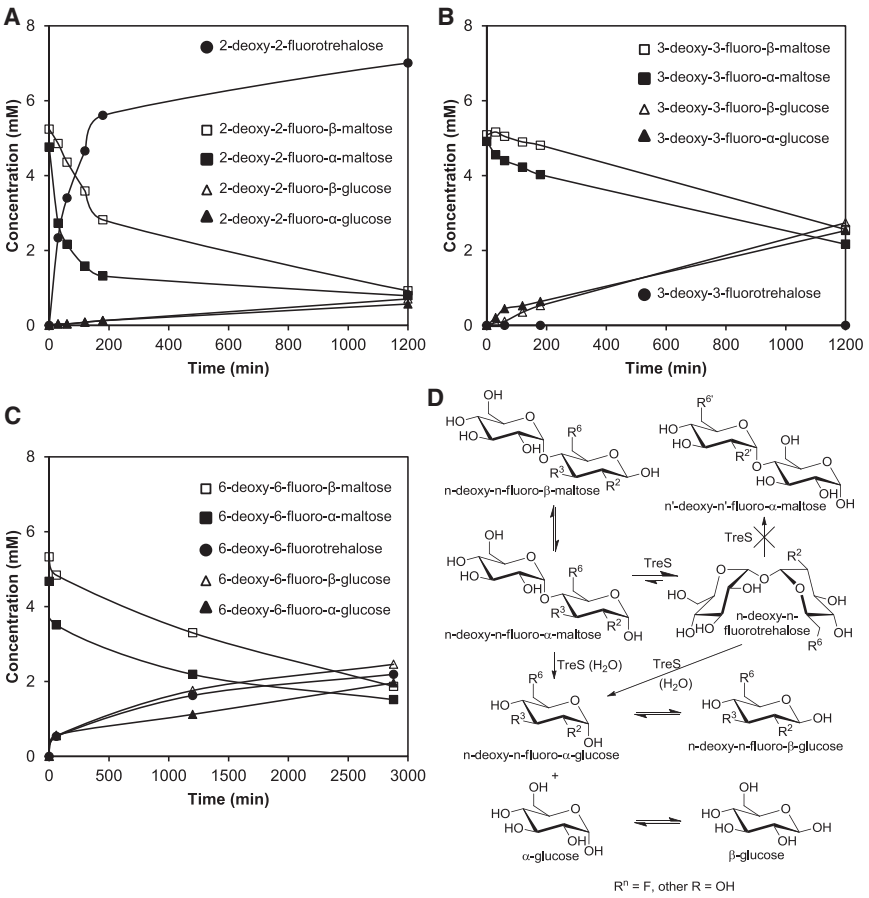

Figure 4. *Mycobacterium Tuberculosis* TreS Converts the α Anomers of Deoxyfluoromaltose Analogs

(A) The conversion of pre-equilibrated 2-deoxy-2-fluoro-α/β-maltose (10 mM) by TreS (2 μM) was monitored using ^{19}F-NMR spectroscopy (see Figure S3A for spectra). The times taken to produce 2 mM 2-deoxy-2-fluorotrehalose and consume 50% of the maltose analog were 25 and 125 min, respectively, both ~2-fold longer than with maltose.

(B) Corresponding data with 3-deoxy-3-fluoro-α/β-maltose (Figure S3B). The time taken to consume 50% of the maltose analog was 1,100 min, 20-fold longer than with maltose. No 3-deoxy-3-fluorotrehalose was detected.

(C) Corresponding data with 6-deoxy-6-fluoro-α/β-maltose (Figure S3C). The times taken to produce 2 mM 6-deoxy-6-fluorotrehalose and consume 50% of the maltose analog were 2,500 and 1,500 min, respectively, 180- and 27-fold longer than with maltose.

(D) Proposed reaction scheme to account for the conversion of deoxyfluoromaltoses by TreS.

DISCUSSION

We have shown that the direction of flux through TreS is from trehalose to maltose and that the source of trehalose is a combination of the OtsAB and TreYZ pathways in *Mycobacterium smegmatis* (Figure 2). The overexpression of TreS led to a decrease in trehalose levels, indicating the same direction of flux in *Mycobacterium tuberculosis*. Thus, TreS appears not to generate trehalose for trehalose mycolate biosynthesis but to convert trehalose into maltose for the GlgE pathway in mycobacteria (Elbein et al., 2010; Kalscheuer et al., 2010b). Although the equilibrium of the TreS-catalyzed reaction is not in line with the direction of flux, the ATP requirement of maltose kinase for the formation of α-maltose 1-phosphate provides most of the driving force through the GlgE pathway, as discussed elsewhere (Syson et al., 2011). Consistent with this, exogenously supplied ^{14}C-labeled trehalose is rapidly and substantially converted to α-maltose 1-phosphate in a *Mycobacterium smegmatis* Δ*glgE* mutant, with maltose only being detected when the *pep2* maltose kinase gene was inactivated (Kalscheuer et al., 2010b). The observed direction of flux contrasts with a previous study in *Mycobacterium smegmatis* (Woodruff et al., 2004). However, the authors did not employ a defined Δ*otsA*Δ*treY* double mutant to study the specific contribution of TreS in the de novo biosynthesis of trehalose but rather a surrogate strain (a Δ*otsA*Δ*treS*Δ*treY* triple mutant with a reconstituted *treS* gene constitutively expressed from an episomal multicopy plasmid) that likely exhibited a much higher *treS* expression level compared with the native gene. Moreover, as nonspecified culture conditions were used, it is unclear whether the medium was devoid of maltose, which might be sufficient to support growth in this genetic context in the absence of trehalose. In any case, our observations are consistent with those of others in *Mycobacterium tuberculosis* (Murphy et al., 2005) and *Corynebacterium glutamicum* (Tzvetkov et al., 2003; Wolf et al., 2003). Thus, we have shown that the metabolism of trehalose in *Mycobacterium smegmatis* is similar to that in *Mycobacterium tuberculosis* after all, allowing *Mycobacterium smegmatis* to be used as a model organism in this context. Furthermore, our *Mycobacterium smegmatis* strains, particularly the strains that are auxotrophic for trehalose, could be used to study the impact of trehalose analogs on specific pathways. It is also intriguing that TreS may be important in late-stage pathogenesis in mice (Murphy et al., 2005), implying a potential role of GlgE pathway-generated cytosolic and/or capsular α-glucan in this process, noting that the latter has been implicated in immune evasion (Sambou et al., 2008).

TreS generates the appropriate α anomer for maltose kinase (Drepper et al., 1996; Mendes et al., 2010) of the GlgE pathway (Kalscheuer et al., 2010b). Thus, the formation of α-maltose 1-phosphate is not limited by the mutarotation of maltose in mycobacteria. This is relevant to many other species, because the *treS* gene coexists with the other genes of the GlgE pathway in 14% of all sequenced bacterial genomes (Chandra et al., 2011). In a further 28% of genomes that possess the *treS* gene, one or more of the other GlgE pathway genes is missing. It is therefore not possible to rule out that flux through TreS favors the conversion of maltose to trehalose in organisms that have access to sufficient cytosolic maltose from intracellular or extracellular sources. If the maltose were generated by an enzyme

such as β-amylase, the mutarotation of β-maltose could become an issue for flux through TreS to trehalose. Indeed, this work highlights that the mutarotation of any given reducing sugar should not be assumed to be fast compared with the metabolism of a specific sugar anomer.

It is now possible to propose schemes defining the anomeric configurations and origins of all species associated with the TreS-catalyzed reactions studied (Figures 3D and 4D). TreS interconverts the α anomer of maltose (Figures 3A–3C) as expected (Figure 1B), and specificity was also retained with deoxyfluoro analogs (Figures 4A–4C). The TreS enzyme is thought to sterically capture the glucose molecule that it liberates (Figure 1B) and transiently exclude access to the active site such that exogenously supplied glucose does not get incorporated into the products of TreS (Koh et al., 2003; Nishimoto et al., 1996; Zhang et al., 2011). Thus, TreS catalyzes an isomerization, whereby the noncovalently captured glucose molecule must rotate within an enclosed active site. We have now established that this glucose molecule retains its α configuration, whether it goes on to produce normal disaccharide products or is released in the hydrolytic side reaction. Therefore, TreS catalyzes the mutarotation of neither maltose nor glucose.

Unlike trehalose, the deoxyfluorotrehalose products are asymmetric and might have been converted to the corresponding n′-deoxy-n′-fluoromaltose analogs but were not (Figure 4D). This could have been due to the destabilization of oxocarbenium ion-like transition states associated with these reactions (Withers et al., 1988). Alternatively, other effects could be involved, such as reduced binding affinities. Indeed, neither of the 3-deoxy-3-fluoro and 6-deoxy-6-fluoromaltose analogs appeared to bind well to the enzyme. That 3-deoxy-3-fluoromaltose was exclusively hydrolyzed means that 3-deoxy-3-fluoroglucose is less able than a water molecule to attack the glucosyl-enzyme intermediate. This could be due to changes in the nucleophilicity of 3-deoxy-3-fluoroglucose or more likely to an inability to orient itself appropriately within the active site.

SIGNIFICANCE

Our findings about the flux through TreS to supply the trehalose mycolate and α-glucan biosynthetic pathways (Figure 1A) have implications for the design and efficacy of inhibitors/imaging agents that target them (Backus et al., 2011; Swarts et al., 2012). It is now much clearer which enzymes need to be targeted to affect either one or both of these pathways. Furthermore, substrate analogs can now be designed as prodrugs for a given pathway that avoid detoxification by competing pathways. For example, when targeting the synthesis of essential trehalose mycolates (Backus et al., 2011; Swarts et al., 2012), it would be an advantage if trehalose analogs were not converted and deactivated by TreS. Indeed, we have observed the limited ability of TreS to tolerate relatively small modifications of its substrates. However, when targeting GlgE or GlgB (Kalscheuer and Jacobs, 2010), there is the challenge of a trehalose analog being tolerated by not only TreS but also the trehalose importer (Kalscheuer et al., 2010a) and maltose kinase. Therefore, the weak inhibition of the growth of *Mycobacterium tuberculosis* by either 2-deoxy-2-fluoro or 6-deoxy-6-fluoromaltose (Backus et al., 2011) could be due to a lack of either import, efficient processing, and/or inhibition of the GlgE/GlgB targets. Interestingly, labeling of *Mycobacterium smegmatis* using a 4-azido analog of trehalose is TreS-dependent (Swarts et al., 2012). This observation implies the tolerance of this analog through each step in the biosynthesis of capsular α-glucan rather than trehalose mycolates. Our work supports this interpretation and also shows that this observation in *Mycobacterium smegmatis* is likely to be relevant to *Mycobacterium tuberculosis*.

EXPERIMENTAL PROCEDURES

All details about the Experimental Procedures used are given in the Supplemental Experimental Procedures.

SUPPLEMENTAL INFORMATION

Supplemental Information includes three figures and Supplemental Experimental Procedures and can be found with this article online at http://dx.doi.org/10.1016/j.chembiol.2013.02.014.

ACKNOWLEDGMENTS

This work was supported by the United Kingdom Biotechnology and Biological Sciences Research Council (Doctoral Training Grant [BB/F017294/1] and Institute Strategic Programme Grant [BB/J004561/1]), the John Innes Foundation, the Strategic Research Fund of the Heinrich-Heine-University Düsseldorf, and the Jürgen Manchot Foundation. We thank Karl Syson for practical assistance and useful discussion, Shirley Fairhurst for assistance with the NMR spectroscopy, and Krit Tantanarat for kindly providing deoxyfluoromaltose analogs.

Received: December 20, 2012
Revised: February 12, 2013
Accepted: February 28, 2013
Published: April 18, 2013

REFERENCES

Argüelles, J.C. (2000). Physiological roles of trehalose in bacteria and yeasts: a comparative analysis. Arch. Microbiol. *174*, 217–224.

Avonce, N., Mendoza-Vargas, A., Morett, E., and Iturriaga, G. (2006). Insights on the evolution of trehalose biosynthesis. BMC Evol. Biol. *6*, 109. http://dx.doi.org/10.1186/1471-2148-1186-1109.

Backus, K.M., Boshoff, H.I., Barry, C.S., Boutureira, O., Patel, M.K., D'Hooge, F., Lee, S.S., Via, L.E., Tahlan, K., Barry, C.E., 3rd, and Davis, B.G. (2011). Uptake of unnatural trehalose analogs as a reporter for *Mycobacterium tuberculosis*. Nat. Chem. Biol. *7*, 228–235.

Bailey, J.M., Fishman, P.H., and Pentchev, P.G. (1967). Studies on mutarotases. I. Purification and properties of a mutarotase from higher plants. J. Biol. Chem. *242*, 4263–4269.

Cantarel, B.L., Coutinho, P.M., Rancurel, C., Bernard, T., Lombard, V., and Henrissat, B. (2009). The Carbohydrate-Active EnZymes database (CAZy): an expert resource for Glycogenomics. Nucleic Acids Res. *37*(Database issue), D233–D238.

Carroll, J.D., Pastuszak, I., Edavana, V.K., Pan, Y.T., and Elbein, A.D. (2007). A novel trehalase from *Mycobacterium smegmatis* - purification, properties, requirements. FEBS J. *274*, 1701–1714.

Chandra, G., Chater, K.F., and Bornemann, S. (2011). Unexpected and widespread connections between bacterial glycogen and trehalose metabolism. Microbiology *157*, 1565–1572.

De Smet, K.A.L., Weston, A., Brown, I.N., Young, D.B., and Robertson, B.D. (2000). Three pathways for trehalose biosynthesis in mycobacteria. Microbiology *146*, 199–208.

Drepper, A., Peitzmann, R., and Pape, H. (1996). Maltokinase (ATP:maltose 1-phosphotransferase) from *Actinoplanes* sp.: demonstration of enzyme activity and characterization of the reaction product. FEBS Lett. *388*, 177–179.

Dye, C. (2006). Global epidemiology of tuberculosis. Lancet *367*, 938–940.

Elbein, A.D., Pan, Y.T., Pastuszak, I., and Carroll, D. (2003). New insights on trehalose: a multifunctional molecule. Glycobiology *13*, 17R–27R.

Elbein, A.D., Pastuszak, I., Tackett, A.J., Wilson, T., and Pan, Y.T. (2010). Last step in the conversion of trehalose to glycogen: a mycobacterial enzyme that transfers maltose from maltose 1-phosphate to glycogen. J. Biol. Chem. *285*, 9803–9812.

Hoops, S., Sahle, S., Gauges, R., Lee, C., Pahle, J., Simus, N., Singhal, M., Xu, L., Mendes, P., and Kummer, U. (2006). COPASI—a COmplex PAthway SImulator. Bioinformatics *22*, 3067–3074.

Kalscheuer, R., and Jacobs, W.R., Jr. (2010). The significance of GlgE as a new target for tuberculosis. Drug News Perspect. *23*, 619–624.

Kalscheuer, R., Weinrick, B., Veeraraghavan, U., Besra, G.S., and Jacobs, W.R., Jr. (2010a). Trehalose-recycling ABC transporter LpqY-SugA-SugB-SugC is essential for virulence of *Mycobacterium tuberculosis*. Proc. Natl. Acad. Sci. USA *107*, 21761–21766.

Kalscheuer, R., Syson, K., Veeraraghavan, U., Weinrick, B., Biermann, K.E., Liu, Z., Sacchettini, J.C., Besra, G., Bornemann, S., and Jacobs, W.R., Jr. (2010b). Self-poisoning of *Mycobacterium tuberculosis* by targeting GlgE in an α-glucan pathway. Nat. Chem. Biol. *6*, 376–384.

Koh, S., Kim, J., Shin, H.J., Lee, D., Bae, J., Kim, D., and Lee, D.S. (2003). Mechanistic study of the intramolecular conversion of maltose to trehalose by *Thermus caldophilus* GK24 trehalose synthase. Carbohydr. Res. *338*, 1339–1343.

Lin, F.L., van Halbeek, H., and Bertozzi, C.R. (2007). Synthesis of mono- and dideoxygenated α,α-trehalose analogs. Carbohydr. Res. *342*, 2014–2030.

Mendes, V., Maranha, A., Lamosa, P., da Costa, M.S., and Empadinhas, N. (2010). Biochemical characterization of the maltokinase from *Mycobacterium bovis* BCG. BMC Biochem. *11*, 21. http://dx.doi.org/10.1186/1471-2091-1111-1121.

Murphy, H.N., Stewart, G.R., Mischenko, V.V., Apt, A.S., Harris, R., McAlister, M.S.B., Driscoll, P.C., Young, D.B., and Robertson, B.D. (2005). The OtsAB pathway is essential for trehalose biosynthesis in *Mycobacterium tuberculosis*. J. Biol. Chem. *280*, 14524–14529.

Nishimoto, T., Nakano, M., Ikegami, S., Chaen, H., Fukuda, S., Sugimoto, T., Kurimoto, M., and Tsujisaka, Y. (1995). Existence of a novel enzyme converting maltose into trehalose. Biosci. Biotechnol. Biochem. *59*, 2189–2190.

Nishimoto, T., Nakano, M., Nakada, T., Chaen, H., Fukuda, S., Sugimoto, T., Kurimoto, M., and Tsujisaka, Y. (1996). Purification and properties of a novel enzyme, trehalose synthase, from *Pimelobacter* sp. R48. Biosci. Biotechnol. Biochem. *60*, 640–644.

Pan, Y.T., Koroth Edavana, V., Jourdian, W.J., Edmondson, R., Carroll, J.D., Pastuszak, I., and Elbein, A.D. (2004). Trehalose synthase of *Mycobacterium smegmatis*: purification, cloning, expression, and properties of the enzyme. Eur. J. Biochem. *271*, 4259–4269.

Paul, M.J., Primavesi, L.F., Jhurreea, D., and Zhang, Y.H. (2008). Trehalose metabolism and signaling. Annu. Rev. Plant Biol. *59*, 417–441.

Rose, J.D., Maddry, J.A., Comber, R.N., Suling, W.J., Wilson, L.N., and Reynolds, R.C. (2002). Synthesis and biological evaluation of trehalose analogs as potential inhibitors of mycobacterial cell wall biosynthesis. Carbohydr. Res. *337*, 105–120.

Sambou, T., Dinadayala, P., Stadthagen, G., Barilone, N., Bordat, Y., Constant, P., Levillain, F., Neyrolles, O., Gicquel, B., Lemassu, A., et al. (2008). Capsular glucan and intracellular glycogen of *Mycobacterium tuberculosis*: biosynthesis and impact on the persistence in mice. Mol. Microbiol. *70*, 762–774.

Shirokane, Y., and Suzuki, M. (1995). A novel enzyme, maltose 1-epimerase from *Lactobacillus brevis* IFO 3345. FEBS Lett. *367*, 177–179.

Stam, M.R., Danchin, E.G.J., Rancurel, C., Coutinho, P.M., and Henrissat, B. (2006). Dividing the large glycoside hydrolase family 13 into subfamilies: towards improved functional annotations of α-amylase-related proteins. Protein Eng. Des. Sel. *19*, 555–562.

Stults, C.L.M., Wade, A.P., and Crouch, S.R. (1987). Immobilized enzyme kinetic study of D-glucose mutarotation by flow injection analysis. Anal. Chem. *59*, 2245–2247.

Swarts, B.M., Holsclaw, C.M., Jewett, J.C., Alber, M., Fox, D.M., Siegrist, M.S., Leary, J.A., Kalscheuer, R., and Bertozzi, C.R. (2012). Probing the mycobacterial trehalome with bioorthogonal chemistry. J. Am. Chem. Soc. *134*, 16123–16126. http://dx.doi.org/10.1021/ja3062419.

Syson, K., Stevenson, C.E., Rejzek, M., Fairhurst, S.A., Nair, A., Bruton, C.J., Field, R.A., Chater, K.F., Lawson, D.M., and Bornemann, S. (2011). Structure of Streptomyces maltosyltransferase GlgE, a homologue of a genetically validated anti-tuberculosis target. J. Biol. Chem. *286*, 38298–38310.

Takayama, K., Wang, C., and Besra, G.S. (2005). Pathway to synthesis and processing of mycolic acids in *Mycobacterium tuberculosis*. Clin. Microbiol. Rev. *18*, 81–101.

Tantanarat, K., Rejzek, M., O'Neill, E., Ruzanski, C., Hill, L., Fairhurst, S.A., Limpaseni, T., and Field, R.A. (2012). An expedient enzymatic route to isomeric 2-, 3- and 6-monodeoxy-monofluoro-maltose derivatives. Carbohydr. Res. *358*, 12–18.

Tewari, Y.B., and Goldberg, R.N. (1991). Thermodynamics of hydrolysis of disaccharides. Lactulose, alpha-D-melibiose, palatinose, D-trehalose, D-turanose and 3-o-beta-D-galactopyranosyl-D-arabinose. Biophys. Chem. *40*, 59–67.

Tewari, Y.B., Lang, B.E., Decker, S.R., and Goldberg, R.N. (2008). Thermodynamics of the hydrolysis reactions of 1,4-β-D-xylobiose, 1,4-β-D-xylotriose, D-cellobiose and D-maltose. J. Chem. Thermodyn. *40*, 1517–1526.

Tzvetkov, M., Klopprogge, C., Zelder, O., and Liebl, W. (2003). Genetic dissection of trehalose biosynthesis in *Corynebacterium glutamicum*: inactivation of trehalose production leads to impaired growth and an altered cell wall lipid composition. Microbiology *149*, 1659–1673.

Wang, J., Elchert, B., Hui, Y., Takemoto, J.Y., Bensaci, M., Wennergren, J., Chang, H., Rai, R., and Chang, C.W.T. (2004). Synthesis of trehalose-based compounds and their inhibitory activities against *Mycobacterium smegmatis*. Bioorg. Med. Chem. *12*, 6397–6413.

Withers, S.G., Rupitz, K., and Street, I.P. (1988). 2-Deoxy-2-fluoro-D-glycosyl fluorides. A new class of specific mechanism-based glycosidase inhibitors. J. Biol. Chem. *263*, 7929–7932.

Wolf, A., Krämer, R., and Morbach, S. (2003). Three pathways for trehalose metabolism in *Corynebacterium glutamicum* ATCC13032 and their significance in response to osmotic stress. Mol. Microbiol. *49*, 1119–1134.

Woodruff, P.J., Carlson, B.L., Siridechadilok, B., Pratt, M.R., Senaratne, R.H., Mougous, J.D., Riley, L.W., Williams, S.J., and Bertozzi, C.R. (2004). Trehalose is required for growth of *Mycobacterium smegmatis*. J. Biol. Chem. *279*, 28835–28843.

Zhang, R., Pan, Y.T., He, S.M., Lam, M., Brayer, G.D., Elbein, A.D., and Withers, S.G. (2011). Mechanistic analysis of trehalose synthase from *Mycobacterium smegmatis*. J. Biol. Chem. *286*, 35601–35609.